National Park Service
U.S. Department of the Interior

Natural Resource Stewardship and Science

Landbird Population Trends in Parks of the Sierra Nevada Network

2011–2019 Synthesis

Natural Resource Report NPS/SIEN/NRR—2022/2402



ON THE COVER

Green-tailed Towhee, one of several species estimated to have increased in density during 2011-2019 breeding periods across parks of the Sierra Nevada Inventory and Monitoring Network.

Photo by: Charles Gates, Flickr, CC BY 2.0

Landbird Population Trends in Parks of the Sierra Nevada Network

2011–2019 Synthesis

Natural Resource Report NPS/SIEN/NRR—2022/2402

Chris Ray,[1] Robert L. Wilkerson,[1] Rodney B. Siegel,[1] Mandy L. Holmgren,[1] and Sylvia A. Haultain[2]

[1]The Institute for Bird Populations
P.O. Box 518
Petaluma, CA 94953

[2]Sierra Nevada Network
Sequoia and Kings Canyon National Parks
47050 Generals Highway
Three Rivers, California 93271

June 2022

U.S. Department of the Interior
National Park Service
Natural Resource Stewardship and Science
Fort Collins, Colorado

The National Park Service, Natural Resource Stewardship and Science office in Fort Collins, Colorado, publishes a range of reports that address natural resource topics. These reports are of interest and applicability to a broad audience in the National Park Service and others in natural resource management, including scientists, conservation and environmental constituencies, and the public.

The Natural Resource Report Series is used to disseminate comprehensive information and analysis about natural resources and related topics concerning lands managed by the National Park Service. The series supports the advancement of science, informed decision-making, and the achievement of the National Park Service mission. The series also provides a forum for presenting more lengthy results that may not be accepted by publications with page limitations.

All manuscripts in the series receive the appropriate level of peer review to ensure that the information is scientifically credible and technically accurate.

Views, statements, findings, conclusions, recommendations, and data in this report do not necessarily reflect views and policies of the National Park Service, U.S. Department of the Interior. Mention of trade names or commercial products does not constitute endorsement or recommendation for use by the U.S. Government.

This report is available in digital format from the Sierra Nevada Network Inventory and Monitoring Program and the Natural Resource Publications Management website. If you have difficulty accessing information in this publication, particularly if using assistive technology, please email irma@nps.gov.

Please cite this publication as:

Ray, C., R. L. Wilkerson, R. B. Siegel, M. L. Holmgren, and S. A. Haultain. 2022. Landbird population trends in parks of the Sierra Nevada Network: 2011–2019 synthesis. Natural Resource Report NPS/SIEN/NRR—2022/2402. National Park Service, Fort Collins, Colorado. https://doi.org/10.36967/nrr-2293643.

NPS 963/181584, June 2022

Contents

Page

Figures....iv

Tables....viii

Appendices....xi

Executive Summary....xii

Acknowledgments....xiii

Introduction....1

Methods....3

Sampling frame....3

Survey and habitat covariates....5

Analyses....6

Results and Discussion....11

Climatic variation during the monitoring period....20

Fitted models....21

Trends by park and elevational stratum....31

Notes on model development....50

Covariates of abundance....51

Covariates of detection....60

Agreement with other studies of trends in bird abundance....64

Conclusion....66

Literature cited....67

Figures

Page

Figure 1. Maintained routes (trails and roads, thin lines) in Sequoia and Kings Canyon National Parks (SEKI) and Yosemite National Park (YOSE), overlaid by bird point-count stations (crosses) and the sampling frame (shaded bands) in each park. 4

Figure 2. Number of birds detected, by species and park, over the monitoring period. 19

Figure 3a. Time-lagged anomalies in precipitation-as-snow (*PAS*) for each point-count station in Sequoia and Kings Canyon National Parks (SEKI) and Yosemite National Park (YOSE). 20

Figure 3b. Time-lagged anomalies in mean spring temperature (*MST*) for each point-count station in Sequoia and Kings Canyon National Parks (SEKI) and Yosemite National Park (YOSE). 21

Figure 4a. Population density estimates for Mountain Quail, Hairy Woodpecker, Northern Flicker, Olive-sided Flycatcher, Western Wood-Pewee, Dusky Flycatcher, Warbling Vireo and Steller's Jay, derived using a hierarchical analysis of point counts from Devils Postpile National Monument. 28

Figure 4b. Population density estimates for Clark's Nutcracker, Mountain Chickadee, Golden-crowned Kinglet, Red-breasted Nuthatch, Brown Creeper, House Wren, Townsend's Solitaire and American Robin, derived using a hierarchical analysis of point counts from Devils Postpile National Monument. 29

Figure 4c. Population density estimates for Cassin's Finch, Fox Sparrow, Dark-eyed Junco, Song Sparrow, Green-tailed Towhee, MacGillivray's Warbler, Yellow-rumped Warbler and Wilson's Warbler, derived using a hierarchical analysis of point counts from Devils Postpile National Monument. 30

Figure 4d. Population density estimates for Western Tanager, derived using a hierarchical analysis of point counts from Devils Postpile National Monument. 31

Figure 5a. Population density estimates by park for Mountain Quail, Sooty Grouse, Anna's Hummingbird, Rufous Hummingbird, Acorn Woodpecker, Williamson's Sapsucker, Red-breasted Sapsucker and Hairy Woodpecker, derived using a hierarchical analysis of point counts from Sequoia and Kings Canyon National Parks (SEKI) and Yosemite National Park (YOSE). 32

Figure 5b. Population density estimates by park for White-headed Woodpecker, Northern Flicker, Pileated Woodpecker, Olive-sided Flycatcher, Western Wood-Pewee, Hammond's Flycatcher, Dusky Flycatcher and Pacific-slope Flycatcher, derived using a hierarchical analysis of point counts from Sequoia and Kings Canyon National Parks (SEKI) and Yosemite National Park (YOSE). 33

Figures (continued)

Page

Figure 5c. Population density estimates by park for Cassin's Vireo, Warbling Vireo, Steller's Jay, Clark's Nutcracker, Common Raven, Mountain Chickadee, Wrentit, and Golden-crowned Kinglet, derived using a hierarchical analysis of point counts from Sequoia and Kings Canyon National Parks (SEKI) and Yosemite National Park (YOSE).....34

Figure 5d. Population density estimates by park for Ruby-crowned Kinglet, Red-breasted Nuthatch, White-breasted Nuthatch, Brown Creeper, Rock Wren, Canyon Wren, House Wren and Pacific Wren, derived using a hierarchical analysis of point counts from Sequoia and Kings Canyon National Parks (SEKI) and Yosemite National Park (YOSE).....35

Figure 5e. Population density estimates by park for Bewick's Wren, Mountain Bluebird, Townsend's Solitaire, Hermit Thrush, American Robin, American Pipit, Gray-crowned Rosy-Finch and Purple Finch, derived using a hierarchical analysis of point counts from Sequoia and Kings Canyon National Parks (SEKI) and Yosemite National Park (YOSE).....36

Figure 5f. Population density estimates by park for Cassin's Finch, Pine Siskin, Chipping Sparrow, Fox Sparrow, Dark-eyed Junco, White-crowned Sparrow, Song Sparrow and Lincoln's Sparrow, derived using a hierarchical analysis of point counts from Sequoia and Kings Canyon National Parks (SEKI) and Yosemite National Park (YOSE). 37

Figure 5g. Population density estimates by park for Green-tailed Towhee, Spotted Towhee, Red-winged Blackbird, Orange-crowned Warbler, Nashville Warbler, MacGillivray's Warbler, Yellow Warbler and Yellow-rumped Warbler, derived using a hierarchical analysis of point counts from Sequoia and Kings Canyon National Parks (SEKI) and Yosemite National Park (YOSE).....38

Figure 5h. Population density estimates by park for Black-throated Gray Warbler, Hermit Warbler, Wilson's Warbler, Western Tanager, Black-headed Grosbeak and Lazuli Bunting, derived using a hierarchical analysis of point counts from Sequoia and Kings Canyon National Parks (SEKI) and Yosemite National Park (YOSE).....39

Figure 6a. Population density estimates by elevational stratum for Mountain Quail, Sooty Grouse, Anna's Hummingbird, Rufous Hummingbird, Acorn Woodpecker, Williamson's Sapsucker, Red-breasted Sapsucker and Hairy Woodpecker, derived using a hierarchical analysis of point counts from Sequoia and Kings Canyon National Parks and Yosemite National Park. 40

Figure 6b. Population density estimates by elevational stratum for White-headed Woodpecker, Northern Flicker, Pileated Woodpecker, Olive-sided Flycatcher, Western Wood-Pewee, Hammond's Flycatcher, Dusky Flycatcher and Pacific-slope Flycatcher, derived using a hierarchical analysis of point counts from Sequoia and Kings Canyon National Parks and Yosemite National Park.....41

Figures (continued)

Page

Figure 6c. Population density estimates by elevational stratum for Cassin's Vireo, Warbling Vireo, Steller's Jay, Clark's Nutcracker, Common Raven, Mountain Chickadee, Wrentit and Golden-crowned Kinglet, derived using a hierarchical analysis of point counts from Sequoia and Kings Canyon National Parks and Yosemite National Park. 42

Figure 6d. Population density estimates by elevational stratum for Ruby-crowned Kinglet, Red-breasted Nuthatch, White-breasted Nuthatch, Brown Creeper, Rock Wren, Canyon Wren, House Wren and Pacific Wren, derived using a hierarchical analysis of point counts from Sequoia and Kings Canyon National Parks and Yosemite National Park. 43

Figure 6e. Population density estimates by elevational stratum for Bewick's Wren, Mountain Bluebird, Townsend's Solitaire, Hermit Thrush, American Robin, American Pipit, Gray-crowned Rosy-Finch and Purple Finch, derived using a hierarchical analysis of point counts from Sequoia and Kings Canyon National Parks and Yosemite National Park. 44

Figure 6f. Population density estimates by elevational stratum for Cassin's Finch, Pine Siskin, Chipping Sparrow, Fox Sparrow, Dark-eyed Junco, White-crowned Sparrow, Song Sparrow and Lincoln's Sparrow, derived using a hierarchical analysis of point counts from Sequoia and Kings Canyon National Parks and Yosemite National Park. 45

Figure 6g. Population density estimates by elevational stratum for Green-tailed Towhee, Spotted Towhee, Red-winged Blackbird, Orange-crowned Warbler, Nashville Warbler, MacGillivray's Warbler, Yellow Warbler and Yellow-rumped Warbler, derived using a hierarchical analysis of point counts from Sequoia and Kings Canyon National Parks and Yosemite National Park. 46

Figure 6h. Population density estimates by elevational stratum for Black-throated Gray Warbler, Hermit Warbler, Wilson's Warbler, Western Tanager, Black-headed Grosbeak and Lazuli Bunting, derived using a hierarchical analysis of point counts from Sequoia and Kings Canyon National Parks and Yosemite National Park. 47

Figure 7. Effects of *year* in hierarchical models of avian abundance based on breeding-season point counts conducted annually during 2011–2014 and 2016–2019. 52

Figure 8. Linear and nonlinear effects of elevation (*elev*) in hierarchical models of avian abundance based on breeding-season point counts conducted annually during 2011–2014 and 2016–2019. 54

Figure 9. Effects of lag-1 anomalies in precipitation-as-snow (*PAS*) in hierarchical models of avian abundance based on breeding-season point counts conducted annually during 2011–2014 and 2016–2019. 56

Figures (continued)

Page

Figure 10. Nonlinear effects of lag-1 anomalies in precipitation-as-snow (PAS^2) in hierarchical models of avian abundance based on breeding-season point counts conducted annually during 2011–2014 and 2016–2019. 57

Figure 11. Effects of lag-1 anomalies in mean spring temperature (*MST*) in hierarchical models of avian abundance based on breeding-season point counts conducted annually during 2011–2014 and 2016–2019. 59

Figure 12. Probabilities of availability for detection (p_a, squares) and detection (p_d, dots) from hierarchical models of avian abundance based on breeding-season point counts conducted annually in Devils Postpile National Monument during 2011–2014 and 2016–2019. 60

Figure 13. Probabilities of availability for detection (p_a, squares) and detection (p_d, dots) from hierarchical models of avian abundance based on breeding-season point counts conducted annually across Sequoia and Kings Canyon National Parks and Yosemite National Park during 2011–2014 and 2016–2019. 61

Figure 14. Effects of day (β_{day}) and hour (β_{hour}) on bird availability, and effects of cover (β_{cover}) and noise (β_{noise}) on bird detection in hierarchical models of avian abundance based on breeding-season point counts conducted annually across Sequoia and Kings Canyon National Parks and Yosemite National Park during 2011–2014 and 2016–2019. 63

Tables

Page

Table 1. Areas and elevations of strata surveyed in Devils Postpile National Monument (DEPO), Sequoia and Kings Canyon National Parks (SEKI) and Yosemite National Park (YOSE). 5

Table 2. Survey effort by year and park. 11

Table 3. Frequencies of detection during 2011–2019 for (a) single-species groups of various sizes, and (b) total counts of all birds (regardless of species) during a single point-count. 12

Table 4. Counts for 134 bird species detected at least once during 2011–2019 point-count surveys across Devils Postpile National Monument (DEPO), Sequoia and Kings Canyon National Parks (SEKI) and Yosemite National Park (YOSE). 13

Table 5. Model covariates for 62 species analyzed in Sequoia and Kings Canyon National Parks (SEKI) and Yosemite National Park (YOSE). 22

Table 6. Model covariates for 25 species analyzed in Devils Postpile National Monument (DEPO). 26

Table A1-1. Output files generated by script4trendAnalysis-synthesis-sm-pk.R, exemplified using an analysis of Western Tanager (WETA) in Devils Postpile National Monument (DEPO). 73

Table A1-2. Contents of the first few rows of a comma-separated file used as input for the data-harvesting scripts. 74

Table A1-3. Scripts used to generate figures in the current report. 75

Table A1-4. Scripts used to generate tables in the current report. 75

Table A2-1. Full species list and park-specific record type for each of 166 bird species detected during 2011–2019 across three parks of the Sierra Nevada Inventory and Monitoring Network: Devils Postpile National Monument (DEPO), Sequoia and Kings Canyon National Parks (SEKI) and Yosemite National Park (YOSE). 76

Table A6-1. Derived estimates of mean population density, and fixed effects of *year* (β_{year}) from hierarchical models of abundance based on avian point-count data collected annually during 2011–2014 and 2016–2019 in Devils Postpile National Monument. 103

Tables (continued)

Page

Table A6-2. Derived estimates of mean population density, and fixed effects of *year* (β_{year}) and *park* (β_{park}) on abundance, from hierarchical models of avian point-count data collected annually during 2011–2014 and 2016–2019 in Sequoia and Kings Canyon National Parks (SEKI) and Yosemite National Park (YOSE). 105

Table A7-1. Estimates of year-by-park (β_{YP}) and year-by-elevation (β_{YE}) interaction effects from hierarchical models of avian point-count data collected annually during 2011–2014 and 2016–2019 in Sequoia and Kings Canyon National Parks (SEKI) and Yosemite National Park (YOSE). 108

Table A7-2. Estimates of park-by-elevation (β_{PE}) and park-by-elevation-by-year (β_{PEY}) interaction effects from hierarchical models of avian point-count data collected annually during 2011–2014 and 2016–2019 in Sequoia and Kings Canyon National Parks (SEKI) and Yosemite National Park (YOSE). 111

Table A8-1. Estimates of linear and nonlinear effects of elevation (β_{elev} and β_{elev^2}), two of several covariates in hierarchical models of avian population density based on point-count data collected annually during 2011–2014 and 2016–2019 in Sequoia and Kings Canyon National Parks and Yosemite National Park. 114

Table A9-1. Estimates of linear and nonlinear effects of precipitation-as-snow (β_{PAS} and β_{PAS^2}) and linear effects of mean spring temperature (β_{MST}), three of several covariates in hierarchical models of avian population density based on breeding-season point-count data collected annually during 2011–2014 and 2016–2019 in Devils Postpile National Monument. 117

Table A9-2. Estimates of linear and nonlinear effects of precipitation-as-snow (β_{PAS} and β_{PAS^2}) and linear effects of mean spring temperature (β_{MST}), three of several covariates in hierarchical models of avian population density based on breeding-season point-count data collected annually during 2011–2014 and 2016–2019 in Sequoia and Kings Canyon National Parks and Yosemite National Park. 119

Table A10-1. Probabilities of availability for detection (p_a) and detection (p_d), and metrics of fit (Bayesian p-values for sub-models of availability and detection) from hierarchical models of breeding-season avian point-count data collected annually during 2011–2014 and 2016–2019 in Devils Postpile National Monument (DEPO). 122

Table A10-2. Probabilities of availability for detection (p_a) and detection (p_d), and metrics of fit (Bayesian p-values for sub-models of availability and detection) from hierarchical models of breeding-season avian point-count data collected annually during 2011–2014 and 2016–2019 in Sequoia and Kings Canyon National Parks and Yosemite National Park. 124

Tables (continued)

Page

Table A11-1. Effects of day (β_{day}) and hour (β_{hour}) on bird availability for detection, and effects of cover (β_{cover}) and noise (β_{noise}) on bird detection in hierarchical models of avian population density based on breeding-season point counts conducted annually across Sequoia and Kings Canyon National Parks and Yosemite National Park during 2011–2014 and 2016–2019. 127

Table A12-1. Detection-distance parameters by species in Devils Postpile National Monument (DEPO), including the percent of recorded distances discarded (D%) from the tail of the observed detection-distance distribution prior to fitting a half-normal density to the data, the maximum detection distance (d_{max}) in the remaining sample, the effective area (Area) over which density was estimated around each point-count station, and the fitted estimate (mean and 95% credible interval) of the shape parameter of the half-normal detection-distance function ($\sigma_{half\text{-}norm}$). 131

Table A12-2. Detection-distance parameters by species in Sequoia and Kings Canyon National Parks and Yosemite National Park, including the percent of recorded distances discarded (D%) from the tail of the observed detection-distance distribution prior to fitting a half-normal density to the data, the maximum detection distance (d_{max}) in the remaining sample, the effective area (Area) over which density was estimated around each point-count station, and the fitted estimate (mean and 95% credible interval) of the shape parameter of the half-normal detection-distance function ($\sigma_{half\text{-}norm}$). 133

Table A13-1. Independent estimates of population growth based on Breeding Bird Survey (BBS) data, for species with *negative* population growth ($\lambda_G < 1$ in Appendix 5) in the current study of Sequoia and Kings Canyon National Parks (SEKI) and Yosemite National Park (YOSE). 136

Table A13-2. Independent estimates of population growth based on Breeding Bird Survey (BBS) data, for species with *positive* population growth ($\lambda_G > 1$ in Appendix 5) in the current study of Sequoia and Kings Canyon National Parks (SEKI) and Yosemite National Park (YOSE). 137

Appendices

Page

Appendix 1. Procedures for synthesis of SIEN landbird trends....72

Appendix 2. Species list by park and record type....76

Appendix 3. Climate in Devils Postpile National Monument....87

Appendix 4. Counts by species, park and elevation....88

Appendix 5. Average population growth at the largest scale of analysis....94

Appendix 6. Parameter estimates: effects of year and park on abundance and derived population density....103

Appendix 7. Parameter estimates: interaction effects on abundance involving year, park and elevation....108

Appendix 8. Parameter estimates: effects of elevation on abundance in the larger parks....114

Appendix 9. Parameter estimates: effects of lagged precipitation and temperature on abundance....117

Appendix 10. Parameter estimates: availability and detection....122

Appendix 11. Parameter estimates: effects of survey timing and habitat conditions on detection....127

Appendix 12. Parameter estimates: detection distance....131

Appendix 13. Breeding Bird Survey trend estimates for species trending in the Sierra Nevada Network....136

Executive Summary

Long-term monitoring of landbird populations within the National Park Service (NPS) Sierra Nevada Inventory and Monitoring Network (SIEN) began in 2011, with the goal of detecting trends to inform the conservation and management of landbirds and their habitats. Here, we used 2011–2019 monitoring data from 2408 point-count stations to analyze landbird population trends in several SIEN parks: Devils Postpile National Monument, Sequoia and Kings Canyon National Parks and Yosemite National Park. Survey crews detected 166 species within these parks during the monitoring period, including 134 detected during formal counts and 32 detected during other crew activities.

Point-count data, which included information on potential covariates of abundance as well as distance and time to detection of each bird, were combined in a Bayesian hierarchical modeling framework to derive trends in population density for 62 species with sufficient counts to support these models. The number of species declining in density over the monitoring period (up to ten species) was more than matched by the number increasing in density over the same period (up to 14 species). Most populations varied directly with spring temperature and almost half varied inversely with precipitation-as-snow. These relationships, combined with a series of dry winters and mild spring temperatures in these parks, might have helped stabilize landbird densities during the monitoring period. Population density also varied with elevation for many species, but evidence was mixed for temporal trends in population density with elevation.

These results align with previous analyses of similar point-count data from national parks in the Pacific Northwest's North Coast and Cascades Network which suggested that landbird populations within parks might be exhibiting more positive population trends than those reported for the surrounding region. A qualitative comparison of our results for SIEN parks with California-wide results from the Breeding Bird Survey suggests that several species have fared better in these parks than across the state over the past decade. Our results also suggest reduced snow cover may play an important role in the recent, perhaps ephemeral, stability of landbirds within Sierra Nevada national parks. The timing of snow melt might affect breeding site success and bird densities in the following year, such that recent warming and snow drought has led to higher recruitment in some populations. If the depth and duration of snow cover continues to decline, however, negative impacts of drought on primary productivity and breeding habitat quality could lead eventually to negative effects on avian abundance. Indeed, for most species we found a negative effect of year on abundance, indicating an underlying temporal decline that was not completely ameliorated by the apparently favorable climate during recent years in these parks. Another cause for concern is an apparent disparity in trends between parks: negative trends in population growth were observed predominantly in Sequoia and Kings Canyon National Parks, the southernmost parks in this analysis.

Parks with a range of relatively natural habitats distributed at a variety of elevations might offer refuge for landbird species sensitive to changes in climate. Although we did not find strong evidence that bird density is shifting by elevation within these parks over the past decade, our study design is stratified by elevation to facilitate estimation of any future elevational response in landbird densities, and to infer distributional shifts from differential changes in density across elevational strata.

Acknowledgments

This analysis was funded by the National Park Service (NPS) under Agreement P15AC00468, with additional in-kind support from the NPS Sierra Nevada Inventory and Monitoring Network (SIEN), The Institute for Bird Populations (IBP), Devils Postpile National Monument, Sequoia and Kings Canyon National Parks, and Yosemite National Park. Data for the analyses were collected and managed by the SIEN under the auspices of its Landbird Monitoring Project and Cooperative Agreement with IBP. We thank dozens of highly trained field technicians who collected data, Sarah Stock and Tyler Coleman for field-crew support, and Alex Eddy for providing logistical and data management support that made this analysis possible. We also thank external reviewers Richard Camp and Matthew Johnson for providing comments that improved this report. Any use of trade, firm, or product names is for descriptive purposes only and does not imply endorsement by the U.S. Government.

This report is Contribution Number 714 of The Institute for Bird Populations.



The population density of Rock Wren appeared stable but responded to variation in snowpack across the breeding seasons of 2011–2019, a pattern shared by many bird species analyzed in this study.
COURTESY GARY LINDQUIST

Introduction

Avian monitoring is part of a suite of monitoring activities adopted by the National Park Service (NPS) to track 'vital signs' related to NPS resources (Fancy et al. 2009, Weber et al. 2009). Landbird population trends can serve as vital signs of terrestrial ecosystem change because many landbirds occupy relatively high trophic positions and provide important ecological functions such as seed dispersal and insect control. Within our National Parks, landbird populations should be less impacted by many of the anthropogenic processes local to non-park landscapes (Simons et al. 1999), while still being impacted by global processes such as climate change. Thus, monitoring landbird trends in National Parks should help us infer responses to climate and other stressors related to global change. Vital signs monitoring is especially urgent in mountain parks, because montane habitats are among those most immediately susceptible to effects of climate change (IPCC 2013, 2014). In 2011, the NPS Sierra Nevada Inventory and Monitoring Network began monitoring landbird populations in three mountain parks of the southern Sierra Nevada, under a peer-reviewed protocol (Siegel et al. 2010) designed in coordination with other resource monitoring networks.

National Parks in the Sierra Nevada Network (SIEN) can serve as reference sites for assessing the effects of land-use and land-cover changes on bird populations throughout the Sierra Nevada, while also offering refuge to bird species dependent on late-successional forests, undeveloped montane wetlands and riparian zones, and other important bird habitats that are less common outside the parks (Silsbee and Peterson 1991, Siegel et al. 2010). However, bird populations within the SIEN parks might also face numerous stressors related to changing abiotic conditions and biotic communities. Monitoring the effects of those stressors is necessary to reveal problems before they become more difficult to address, and also to provide insight on actions park managers might take to manage park resources. The NPS has identified seven major ecological stressors as the greatest threats to natural resources of the SIEN parks and the central/southern Sierra Nevada: anthropogenic climate change, altered fire regimes, air pollution, habitat loss and fragmentation, non-native species, novel diseases and human-use impacts (Steel et al. 2012). Each of these ecological stressors might pose a quantifiable threat to bird populations in these parks.

Climate change is likely the most serious of these threats to bird populations in the parks (Steel et al. 2012), in part because of its capacity to aggravate several of the other threats. Siegel et al. (2014) identified 17 bird species (generally associated with aquatic systems or high-elevation habitats) likely to be most vulnerable to climate change in the region, but also concluded that many species associated with xeric Sierra habitats, particularly in the foothills, might actually expand their ranges in the Sierra Nevada during the coming years. For the greater Sierra Nevada bioregion in which the SIEN parks are situated, climate models rather uniformly project warming temperatures, but vary more with respect to changes in the magnitude and even direction of changes projected in precipitation and other moisture metrics (Cayan et al. 2008, Thorne et al. 2015). Regardless of whether overall precipitation amounts will change greatly, warming is expected to result in more precipitation falling as rain rather than snow (Hayhoe et al. 2004) as well as substantial reductions in spring snowpack as runoff continues to initiate earlier in warmer years (Knowles and Cayan 2002, Dettinger et al. 2004). The magnitude of the reduction in snowpack and increases in winter runoff are

expected to vary substantially across elevations and subregions (Dettinger et al. 2004, Maurer et al. 2007), but will boost winter flooding while reducing spring and summer streamflow across the region (Knowles and Cayan 2002, Hayhoe et al. 2004). Throughout the 21st century, climate change is projected to decrease the area of montane and subalpine conifer forest in the Sierra Nevada, and increase the extent of grasslands and mixed oak/pine woodlands and forests (Lenihan et al. 2003, PRBO Conservation Science 2011). Evidence is mounting that the distribution of many bird species in the Sierra Nevada is already changing in response to changes in climate (Tingley et al. 2009, 2012; Tingley and Beissinger 2013, Siegel et al. 2014).

In this time of substantial change, the primary goal of long-term avian monitoring in the SIEN is to assess park-level and Network-wide trends in bird population density and to use surveys of the Network's diverse habitats and broad habitat gradients to infer the drivers of trends in abundance by species. A synthesis of landbird monitoring results from the SIEN should provide information to inform future decisions on important management issues, including fire management, meadow restoration, the effects of introduced species, visitor impacts, and steps needed to improve population resilience in the context of climate change (Steel et al. 2012), by providing substantial insight into trends relevant to terrestrial ecosystems in the Sierra Nevada. Here, we use point-count analysis to estimate trends in abundance and derive time-series of population density for 62 species at park and Network scales. We explore lagged effects of precipitation and temperature on the annual abundance of each species, and effects of survey conditions on species detection. Applying a unified framework for trend analysis at local and regional scales, this synthesis extends landbird monitoring results summarized in several peer-reviewed publications from this region.



Avian trends during 2011–2019 estimated for Sequoia and Kings Canyon National Parks included a three-fold decline in Wrentit density during the breeding season. Photo by Andy Reago and Chrissy McClaren, Flickr, CC BY 2.0.

Methods

With the goal of monitoring population trends in multiple species (Siegel et al. 2010), point counts are conducted during the annual breeding season within three SIEN preserves (hereafter 'parks'): Devils Postpile National Monument (DEPO), Sequoia and Kings Canyon National Parks (SEKI—two parks managed as one unit) and Yosemite National Park (YOSE). Each park is surveyed in four out of every five years, with the fifth year reserved for analysis of results. To minimize variability due to seasonal processes, surveys are timed to coincide with the annual peak in birdsong and other breeding activities for most species. In each year during 2011–2014 and 2016–2019, all surveys were conducted between May 20 and July 31, and points at lower elevations were targeted for survey earlier in the season than points at higher elevations, to better track peak breeding season by elevation. To minimize annual variability related to the observation process, The Institute for Bird Populations (IBP) recruits qualified observers who must attend a three-week training session and pass an examination demonstrating proficiency in bird identification skills prior to conducting surveys. The survey design for each park is detailed in Siegel et al. (2010), and relevant details from a comparable design can be drawn from Saracco et al. (2014) and Ray et al. (2017 a, b).

Sampling frame

The sampling frame for DEPO includes the entire park, with point-count stations (hereafter, stations) distributed at nearly regular intervals throughout the frame. Stations in DEPO range in elevation from 2220 m to 2481 m. In contrast, SEKI and YOSE stations are linked along transects that originate on maintained travel routes (trails and some roads) and extend 1–2 km into off-trail habitats. During the design phase of this study, the expected extent of off-trail sampling suggested the sampling frame could reasonably be assumed to extend 1.625 km from all maintained travel routes within SEKI and YOSE (Figure 1). Potential transect origins were identified as a set of points spaced every 50 m along these maintained routes. From these points, a spatially dispersed sample of transect origins was selected for each park using the Generalized Random-Tessellation Stratified (GRTS) sampling method (Stevens and Olsen 2004). To ensure adequate sampling across elevations, origins were drawn from three elevational strata (Table 1), defined as low-elevation (<1600 m above sea level in SEKI, <1800 m in YOSE), medium-elevation (1600–3000 m in SEKI, 1800–2750 in YOSE) or high-elevation (>3000 m in SEKI, >2750 in YOSE). The selected definitions of low, medium and high strata in these parks correspond broadly with foothill, montane and alpine/subalpine habitats, respectively. Selected transects were grouped at random into five panels, one "annual" and four "alternating"; the annual and one alternating panel are surveyed each year. Each transect links a set of point-count stations spaced at 250-m intervals, and each half-transect extends away from the trail (at 90 or 45 degrees, in order of preference) or continues along the trail until a departure is feasible. Permanent stations are established along the line of departure except where deviations are required to accommodate obstacles. Any required change in direction after the first off-trail point is accomplished by turning 45 degrees to the right or left (at random) of the current line of travel. Point-count stations ranged in elevation from 831 to 3784 meters above sea level (m asl) during 2011–2019 surveys across the three parks.

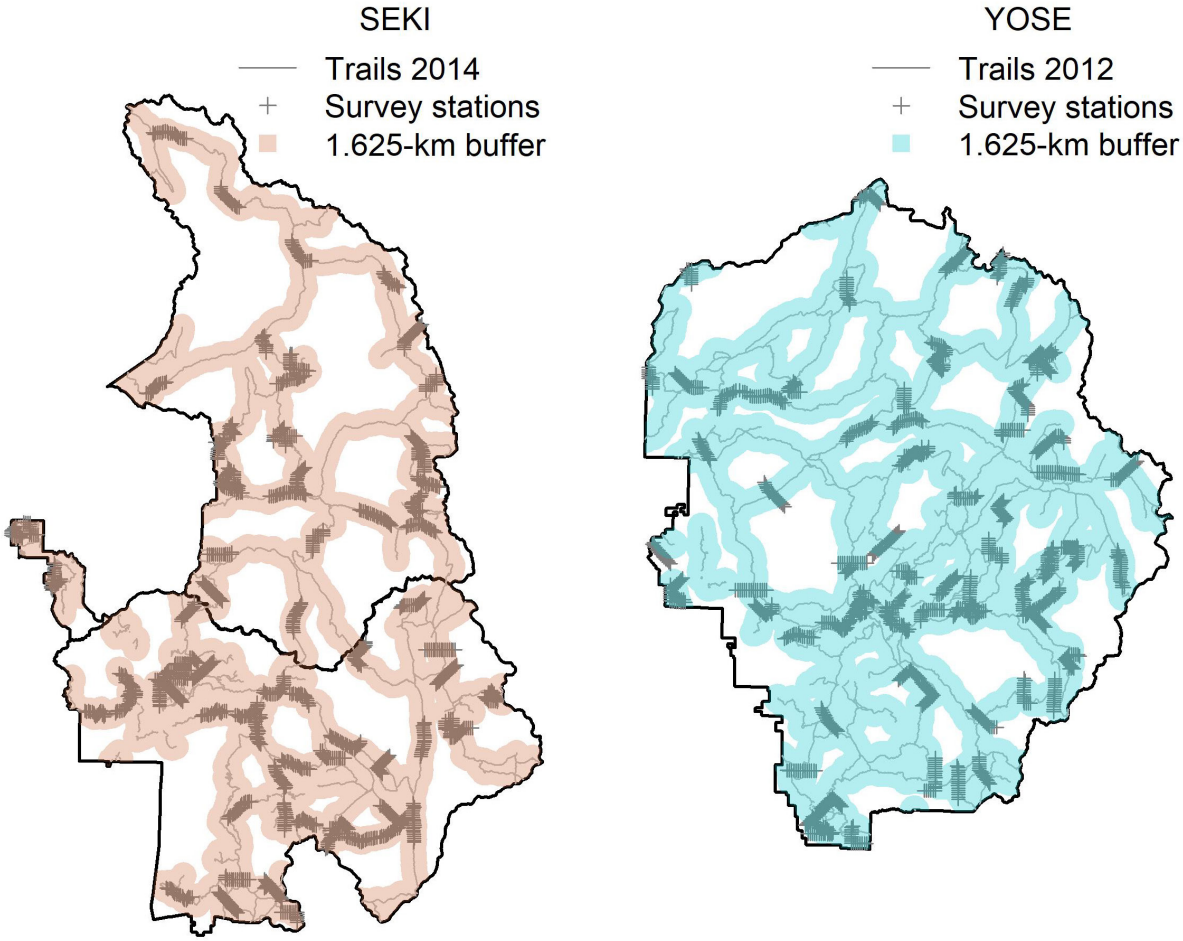


Figure 1. Maintained routes (trails and roads, thin lines) in Sequoia and Kings Canyon National Parks (SEKI) and Yosemite National Park (YOSE), overlaid by bird point-count stations (crosses) and the sampling frame (shaded bands) in each park. Stations are clustered in transects and transects sample from an area extending approximately 1.625 km from maintained routes. The sampling frame included 61% and 71% of total park area in SEKI and YOSE, respectively. In DEPO (not shown), the sampling frame included 100% of the park, given a sampling grid consisting of approximately one station for every 7.7 ha of park area.

Table 1. Areas and elevations of strata surveyed in Devils Postpile National Monument (DEPO), Sequoia and Kings Canyon National Parks (SEKI) and Yosemite National Park (YOSE).

Park / Total area (ha)	Elevational stratum	Stratum area (ha)	Elevational range (m)
DEPO / 323	NA	NA	2200–2250
SEKI / 350,444	High-elevation	69,215	>3000
	Medium-elevation	72,898	1600–3000
	Low-elevation	71,658	<1600
YOSE / 307,407	High-elevation	72,718	>2750
	Medium-elevation	71,007	1800–2750
	Low-elevation	74,534	<1800

Survey and habitat covariates

In each park, all bird species heard or seen during a seven-minute survey are recorded, along with the time-to-detection and distance-to-detection of each bird or of each group of birds acting as a flock, enabling analyses that account for birds present but undetected during each survey (Royle et al. 2004, Alldredge et al. 2007, Amundson et al. 2014). Potential covariates of detection and abundance recorded during surveys include observer, date, survey start time, ambient noise level, vegetation type, presence of forest cover, cover density, point coordinates and group size (number of birds acting as a unit or flock; usually one bird). Potential covariates calculated from a digital elevation model using annual field records of point coordinates include elevation, aspect and slope, where aspect and slope were averaged within 90 m of station coordinates.

We hypothesized that years of heavy snow and cooler spring temperatures could delay initiation of breeding and result in food scarcity early in the nesting season (Hahn et al. 2004, Pereyra 2011, Mathewson et al. 2012), leading to lower recruitment and lagged effects of lower breeding bird abundance in the subsequent year (DeSante 1990). To test this hypothesis, we selected ClimateNA as a source of downscaled climate data for North America (Wang et al. 2016). Using the protocol and code in Appendix 3 of Ray et al. (2017 b), annual data and 1981–2010 normals were accessed from https://www.climatewna.com/. To characterize spring conditions, we selected mean spring temperature (MST, the average daily temperature from March 1 through May 31) and annual precipitation as snow (PAS, millimeters of snow falling between August 1 and July 31). Specifically, we calculated MST and PAS as anomalies, relative to 1981–2010 normals, under the expectation that breeding and recruitment would be inversely related to snowfall and directly related to temperature. For surveys in year t, lag-1 MST was the mean temperature anomaly from March 1 to May 31 of year t-1, and lag-1 PAS was the snowfall anomaly from Aug 1 of year t-2 to July 31 of year t-1. Following Graham (2003), we considered simultaneous effects of these correlated predictors by replacing MST with residual MST (rMST), the residuals of a simple linear regression of MST on PAS.

Analyses

In this synthesis of results from the first nine years of monitoring, we focused on effects of climate, elevation and park (management unit DEPO, SEKI or YOSE) on abundance for species detected frequently enough to support estimates of detection probability and trend. Covariate effects on detection and abundance were estimated for each species, and time-series of population density were derived using a Bayesian hierarchical modeling framework (Kéry and Schaub 2012) as detailed in Ray et al. (2017 a, b). Code and procedures used for generating the analyses in this report are detailed in Appendix 1.

Hierarchical models involve the decomposition of a complex relationship into a series of interdependent sub-models to facilitate understanding and computation as well as to clarify each level of uncertainty in the relationship. A simple example would involve a count of Y individuals from a population of size N and an individual detection probability of p. The hierarchy in this example involves one level at which Y is modeled as a function of N and p, and another level at which p can be modeled, perhaps as a function of potential covariates like observer identity and day of year. Bayesian models allow us to estimate the "posterior" probability density of each parameter value, provided that we supply a "prior" probability density summarizing any prior information about the distribution of values the parameter might take. Bayesian methods require estimation of the joint probability density of all model parameters, a computationally intensive process facilitated by simulation methods such as Markov chain Monte Carlo (MCMC). MCMC can be used to sample from the joint posterior distribution of model parameters by jumping around (almost) randomly in parameter space to test for parameter values that maximize the probability of obtaining the observed data given the proposed model. If we require that the joint probability of obtaining the observed data generally increases as we jump around, then a long series (MCMC chain) of jumps (samples) will eventually put us in the vicinity of the best estimates for each parameter, and plotting a histogram of samples from this vicinity will reveal the shape of each parameter's posterior distribution. We used the JAGS programmable platform (Plummer 2003) to perform MCMC simulation and to provide summaries of the resulting samples, such as a credible interval (CRI) for each parameter estimate. In this report, a 95% CRI refers to a Bayesian credible interval which contains the value of the focal parameter with a subjective probability of 0.95.

For this analysis, we adapted a model developed by Amundson et al. (2014), allowing estimation of 1) components of individual detection, including effects of covariates on probabilities of individual availability and perceptibility, where availability is the probability that a bird will perform a detectable action, like singing, while perceptibility is the probability that observers will perceive that action; 2) the relationship between bird abundance and yearly point-counts, as a function of availability and perceptibility; and 3) spatiotemporal trends in abundance, including effects of climate. Data from multiple count intervals were used to generate individual detection histories modeled within a closed-population framework to characterize availability (Alldredge et al. 2007).

Following Farnsworth et al. (2002), availability was modeled from time-removal data, in which each detection of a unique individual was assigned to one of three count intervals (minutes 0–3:00, 3:01–5:00 or 5:01–7:00), and subsequent detections of the same individual were ignored. Using removal

data allowed us to model availability as a function of q, the per-minute probability of a bird's failure to sing or otherwise be available for detection. In the current analysis, the probability that a bird was present and not available during all three count intervals (totaling seven minutes) was q^7, and availability was $1\text{-}q^7$. Assuming q might vary in space and time, it can be modeled as $\text{logit}(q_{kt}) = \alpha_0 + \sum_x \alpha_x x_{kt}$, where x_{kt} are covariates specific to station k and year t (Amundson et al. 2014).

To characterize effects of distance on perceptibility, we first dropped about 10% of the farthest (and possibly least accurate) detections of each species to obtain the maximum effective detection distance (per Kéry and Royle 2016) and then sorted the remaining detection distances into variable-width bins, equalizing the number of detections in each bin (Amundson et al. 2014). We followed Buckland et al. (2001) in modeling the probability of detecting a bird in distance bin b using the half-normal distribution, which is controlled by shape parameter σ, the decay rate of detections with distance. We then modeled perceptibility as a function of point- and year-specific covariates affecting σ as $\log(\sigma_{kt}) = \log(\sigma_0) + \sum_x \gamma_x x_{kt}$ (Amundson et al. 2014).

We combined these models of q and σ (components of p) with a model of N in an N-mixture or binomial mixture model. N-mixture models typically pair a Poisson model of N (abundance) with a binomial model of Y (count). N-mixture models provide a hierarchical extension of generalized linear models (GLMs), linking multiple GLMs to allow for structure in parameters at each hierarchical level (Royle 2004). For the current analysis, we first modeled the observed count from each station k and year t (Y_{kt}) assuming a binomial distribution with probability of detection $p_{d,kt}$ and conditioned on the number of birds available for detection ($n_{a,kt}$). We then modeled the number of birds available assuming a binomial distribution with probability of availability $p_{a,kt}$ conditioned on the total number of birds (N_{kt}). Finally, we modeled the expected value of N_{kt} assuming a Poisson distribution with mean λ_{kt}, resulting in the following hierarchical model,

$Y_{kt} \sim \text{binomial}(p_{d,kt}, n_{a,kt})$,

$n_{a,kt} \sim \text{binomial}(p_{a,kt}, N_{kt})$, and

$N_{kt} \sim \text{Poisson}(\lambda_{kt})$.

Amundson et al. (2014) developed this approach and demonstrated how to incorporate effects of covariates at each level in the hierarchy by modeling λ, q and σ given that $p_a = f(q)$ and $p_d = f(\sigma)$. We refer below to these models of λ, q and σ as sub-models in the hierarchy.

Preliminary analyses of SIEN landbird data and previous analyses of similar NCCN data (Ray et al. 2017 a) suggested at least 17 candidates as covariates of detection and abundance. Consequently, our 'full model' included each of these 17 candidates as a covariate in sub-models of detection and abundance as follows:

$$\text{logit}(q_{kt}) = \alpha_0 + \alpha_1 day_{k,t} + \alpha_2 hour_{k,t} \quad \text{(Eqn. 1a)}$$

$$\log(\sigma_{kt}) = \log(\sigma_0) + \gamma_1 noise_{k,t} + \gamma_2 cover_{k,t} + \omega_{observer[k,t]} \quad \text{(Eqn. 1b)}$$

$$\log(\lambda_{kt}) = \beta_{0,station[k]} + \beta_1 year_t + \beta_2 park_k + \beta_3 elev_k + \beta_4 elev^2_k \quad \text{(Eqn. 1c)}$$

$$+ \beta_5 year_t\ elev_k + \beta_6\ year_t\ park_k + \beta_7\ park_k\ elev_k + \beta_8\ year_t\ park_k\ elev_k$$

$$+ \beta_9 PAS_{k,t-1} + \beta_{10} PAS^2_{k,t-1} + \beta_{11} rMST_{k,t-1}$$

In the sub-model of bird availability for detection (Eqn. 1a), we allowed for effects of both the *day* and the *hour* that each survey was conducted at station *k* in year *t*. In the sub-model of distance-mediated detection (Eqn. 1b), we included potential effects of *noise* during the survey and vegetative *cover* density (which varied by station and somewhat by year), as well as a random effect of *observer*. The sub-model of expected abundance (Eqn. 1c) featured a random intercept for each station (nested within transect) as well as fixed effects of *year*, *park*, elevation (*elev*), $elev^2$, all interactions between *year*, *park* and *elev*, plus three effects of climate. Climatic influences considered in the full model were linear and quadratic effects of anomalies in precipitation-as-snow (*PAS*) and a linear effect of anomalies in mean spring temperature (*MST*). *PAS* and *MST* were both calculated as anomalies relative to 1981–2010 normals, and both were lagged one year such that *N* in the current year (*t*) might be affected by weather in the preceding year (*t-1*) through presumed effects on recruitment success. Although correlation was low between *year* and each anomaly, correlation between anomalies *PAS* and *MST* was high. We avoided excess covariance among covariates in the full model, and in any reduced model containing both precipitation and temperature effects, by replacing *MST* with *rMST*, the residuals of a simple linear regression of *MST* on *PAS*.

Using the model represented by Eqn. 1, it would be possible to integrate data across all three parks, obtaining park-specific parameter estimates through the action of terms that include a park effect. However, that approach was not appropriate in the current analysis for several reasons related to absolute park size. DEPO is smaller than the other two parks by three orders of magnitude (Table 1), so parameter estimates would be dominated by data from the larger parks as the model 'borrows strength' from their larger datasets. Also, elevation varies little across the small extent of DEPO, reducing the relevance of elevation effects in that park. Finally, the spatial structure of surveys in DEPO did not include clustering of point-count stations into transects; instead, stations were more-or-less uniformly distributed throughout the park. In order to include DEPO in the multi-park model, we would need to group its stations into arbitrary transects or combine them all into a single transect, which would constitute by far the largest transect in the study. For these reasons, we integrated data from the two larger parks but modeled data from DEPO separately, using a reduced version of the full model that did not include park or elevation effects. We began each analysis of data from species in DEPO by attempting to fit the following reduced model, adding detection covariates from the full model (Eqn. 1a and 1b) if needed to achieve convergence of parameter estimates and adequate model fit according to posterior predictive checks.

$$\text{logit}(q_{kt}) = \alpha_0 \qquad \text{(Eqn. 2a)}$$

$$\log(\sigma_{kt}) = \log(\sigma_0) \qquad \text{(Eqn. 2b)}$$

$$\log(\lambda_{kt}) = \beta_{0,station[k]} + \beta_1\ year_t + \beta_9\ PAS_{k,t-1} + \beta_{10}\ PAS^2_{k,t-1} + \beta_{11}\ rMST_{k,t-1} \qquad \text{(Eqn. 2c)}$$

In contrast, the amount of data from SEKI was similar to the amount of data from YOSE, and the combined data from one species across these two larger parks was often sufficient to support the full

model (Eqn. 1). For these reasons, we began the analysis of each species in the larger parks by attempting to fit a model with the full set of covariates described in Equation 1, removing covariates as needed to achieve model convergence and adequate model fit. By fitting a single model to data from both parks, we were able to borrow power from the park with higher counts to estimate parameters in the park with lower counts. The higher counts and larger datasets obtained using this approach also supported the estimation of more parameters for each species, allowing us to better assess the many possible effects on species detection and density.

In addition to estimating annual abundance (N) and the coefficients in Eqn. 1 or 2 for each population, we estimated annual population density (N per hectare) as a derived parameter. Density was averaged over all point-count stations within an area (park or elevational stratum) by dividing the sum of N across all stations in the area by the number of stations in the area and the effective area surveyed at each station. Effective area surveyed varied with detection distance for the species. For each species potentially in decline within a park, we also estimated the 9-year time series of total population size (N) within the sampling frame relevant to that park (e.g., within 1.625 km of park trails and roads). For comparison, we also present the time series of raw annual counts corrected for survey effort. Specifically, the raw count for species x in year t, $Ct_{x,t}^{raw}$, was corrected for effort as $Ct_{x,t}^{c} = Ct_{x,t}^{raw}/P_t/M_t$, where P_t was the number of points surveyed and M_t was the number of minutes surveyed per point in year t.

Estimates of N were obtained for all point-count stations, even in years without counts, because the Bayesian modeling framework adopted here is robust to missing data (Kéry and Royle 2016). We exploited this feature to model data from every point-count station that was surveyed at least once during the monitoring period, with the exception of stations within transects that have been officially retired from this study (one transect in SEKI and three in YOSE, all retired before 2013). Although data from retired transects could have been included in the current analysis, that approach could render this analysis less comparable with future analyses of these data, which might be less likely to include transects retired early in this study. Finally, because retired transects were located near currently active transects, their exclusion did not affect the scope of inference for either park.

We limited the influence of prior distributions on posterior parameter estimates by assigning only vague priors. For each fixed effect, we assigned a normal prior distribution with mean 0 and precision 0.001, where precision (τ) is the inverse of variance ($\tau = 1/\sigma^2$). For each random effect, precision was assigned a uniform prior ranging from 0 to 10 at the scale of the standard deviation ($1/\tau^{1/2}$). The random observer effect was assigned a normal prior with mean 0, while the random effect of station (nested within transect) was assigned a normal prior with mean $\mu_{transect}$, and $\mu_{transect}$ was assigned a normal prior with mean 0. For σ_0, the intercept of the scale parameter for the half-normal distribution describing decay of detection with distance, we assigned a uniform prior ranging from 0 to 200.

Models were fitted using JAGS version 4.3.0 (Plummer 2003) called remotely from R version 4.1.0 (R Core Team 2021) using the package jagsUI (Kellner 2015). For each fitted parameter, we drew posterior estimates from three Markov chains of 40,000–80,000 samples each, after thinning by 1 in 10 and discarding the first 10,000–20,000 samples. Continuous covariates were standardized (mean-

centered and divided by standard deviation) to facilitate convergence of parameter estimates and interpretation of relative effects. Years 2011–2019 were coded as 1–9.

Convergence of parameter estimates was assessed using the Gelman-Rubin R-hat statistic and visual inspection of MCMC summaries provided by JAGS. Adequate fit was achieved when all parameter estimates converged and, in addition, Bayesian p-values for both sub-models of detection (p_a and p_d) were between 0.2 and 0.8 (Amundson et al. 2014, 2018). If adequate fit could not be achieved by altering the set of covariates in a model, we attempted to reduce unmodeled heterogeneity by limiting the scope of inference to one park and/or a subset of elevational strata. Using this protocol, we were able to maximize the number of focal parameters estimated for each species.

The analytical approach adopted here is suited to situations in which each point-count station is surveyed once within the breeding season (Amundson et al. 2014). We adopted this approach because the scale and topography of our sampling frame combined to preclude multiple visits within the short breeding season, given the monitoring resources available. It is important to keep in mind that single-visit studies cannot estimate variation in detection probability throughout the breeding season (Schmidt et al. 2013, Mizel et al. 2017). However, this issue should be considered in light of our estimates of the magnitude of detection probability and effects of *day* on detection.

Results and Discussion

From 2011 to 2019, we completed 6,678 point-count surveys (Table 2) at 2,408 unique point-count stations distributed throughout the monitored parks (42 stations in DEPO, 1,192 in SEKI and 1,174 in YOSE). The number of stations surveyed along each transect during 2011–2019 was 15.15±0.20 (mean±SE), with a range of 4–25. Stations in the larger parks were arranged in 144 transects, 72 in SEKI and 72 in YOSE (excluding four transects that were retired by 2012 and were not included in the analyses presented here). Each station was surveyed from one to eight times, depending on its park and survey-design-panel membership, and 1,903 stations were surveyed more than once, including 42 in DEPO, 885 in SEKI and 976 in YOSE. Stations that were surveyed eight times were on the annual panel of transects in each park. Stations on alternating panels in the larger parks were mostly surveyed twice during 2011–2019 (e.g., in 2011 and 2016, or in 2012 and 2017, etc.). Stations surveyed only once tended to be on the distal ends of transects in the larger parks, farthest from trails. Taking a Bayesian approach allowed us to incorporate these solitary counts, improving estimates of population density at the outer limits of our sampling frame.

Table 2. Survey effort by year and park. Number of point-count surveys completed during 2011–2019 at each park in the SIEN landbird monitoring project.

	Number of point-count surveys completed			
Year	**DEPO**	**SEKI**	**YOSE**	**Total**
2011	42	339 [a]	345 [a]	726
2012	42	427 [a]	409 [a]	878
2013	42	445	419	906
2014	42	437	434	913
2015	–	–	–	–
2016	42	380	422	844
2017	42	394	392	828
2018	42	428	389	859
2019	42	286	396	724
Total	***336***	***3136***	***3206***	***6678***

[a] Additional point-count stations along one transect in SEKI and three in YOSE were retired after 2011 or 2012, and data from these four transects were omitted from all summaries and tables in this report.

We conducted 336 point counts in DEPO, 3,136 in SEKI and 3,206 in YOSE, including 2,109 at high elevations, 3,224 at medium elevations and 1,345 at low elevations (Table 1). The habitat types most often recorded at each station were Sierra Mixed Conifer (31%), Lodgepole Pine (20%) and Subalpine Conifer (13%). Across these counts, we recorded 73,734 individual birds, not counting a few duplicate records of individuals detected at more than one station. Individual birds accounted for

97.18% (71,653) of all detections (Table 3), while larger groups or flocks accounted for 2.82% (2,081). Counts of zero (no birds detected) occurred in 1.32% (88) of all point-count surveys.

Table 3. Frequencies of detection during 2011–2019 [a] for (a) single-species groups of various sizes, and (b) total counts of all birds (regardless of species) during a single point-count.

(a) Single-species group size	Frequency	(b) Number of birds detected per count	Frequency	Number of birds detected per count	Frequency
1	71,653	0	88	22	94
2	101	1	173	23	74
3	84	2	241	24	51
4	47	3	229	25	40
5	37	4	298	26	45
6	23	5	369	27	22
7	12	6	360	28	17
8	11	7	404	29	13
9	12	8	395	30	8
10	7	9	374	31	9
11	3	10	372	32	5
12	7	11	422	33	1
13	4	12	405	35	4
14	1	13	363	36	4
15	8	14	349	37	3
16	2	15	341	39	2
17	1	16	252	40	3
18	1	17	246	42	2
19	2	18	199	44	1
20	1	19	152	49	1
23	1	20	130	50	1
25	4	21	115	57	1
26	1	–	–	–	–
30	2	–	–	–	–
41	1	–	–	–	–

[a] This table includes birds not identified to species (n = 898 of 73,734).

Table 3 (continued). Frequencies of detection during 2011–2019[a] for (a) single-species groups of various sizes, and (b) total counts of all birds (regardless of species) during a single point-count.

(a) Single-species group size	Frequency	(b) Number of birds detected per count	Frequency	Number of birds detected per count	Frequency
43	1	–	–	–	–
45	1	–	–	–	–

[a] This table includes birds not identified to species (n = 898 of 73,734).

Including only unique detections of birds identified to species, there were 72,833 birds detected during point counts across the three parks, including 3725 birds in DEPO, 34,996 in SEKI and 34,112 in YOSE. The number of birds per count was similar across parks, at 11.26±0.23 (mean±SE) in DEPO, 11.31±0.12 in SEKI, 10.75±0.11 in YOSE and 11.04±08 overall. Birds detected during point counts represented 134 bird species (Table 4). Dark-eyed Junco was the most frequently detected species, with 5,922 individuals detected across these parks during the monitoring period. We also detected more than 1,000 individuals each of 20 additional species, including (in descending order of detections) Mountain Chickadee, Yellow-rumped Warbler, Steller's Jay, Red-breasted Nuthatch, Western Tanager, Fox Sparrow, Dusky Flycatcher, Western Wood-Pewee, American Robin, Nashville Warbler, Golden-crowned Kinglet, Cassin's Finch, Mountain Quail, Brown Creeper, Clark's Nutcracker, Black-headed Grosbeak, Warbling Vireo, Hermit Warbler, Hermit Thrush and MacGillivray's Warbler.

Table 4. Counts for 134 bird species detected at least once during 2011–2019 point-count surveys across Devils Postpile National Monument (DEPO), Sequoia and Kings Canyon National Parks (SEKI) and Yosemite National Park (YOSE). Species are listed in taxonomic order (Chesser et al. 2021).

Code	Common Name	Scientific Name	DEPO	SEKI	YOSE	Total
CANG	Canada Goose	*Branta canadensis*	0	0	4	4
MALL	Mallard	*Anas platyrhynchos*	1	12	30	43
BUFF	Bufflehead	*Bucephala albeola*	0	0	1	1
COME	Common Merganser	*Mergus merganser*	0	0	12	12
MOUQ	Mountain Quail	*Oreortyx pictus*	89	750	947	1786
CAQU	California Quail	*Callipepla californica*	0	7	9	16
WTPT	White-tailed Ptarmigan	*Lagopus leucura*	0	6	2	8
SOGR	Sooty Grouse	*Dendragapus fuliginosus*	1	127	54	182
PBGR	Pied-billed Grebe	*Podilymbus podiceps*	0	0	2	2
BTPI	Band-tailed Pigeon	*Patagioenas fasciata*	1	51	23	75
MODO	Mourning Dove	*Zenaida macroura*	0	24	17	41

Table 4 (continued). Counts for 134 bird species detected at least once during 2011–2019 point-count surveys across Devils Postpile National Monument (DEPO), Sequoia and Kings Canyon National Parks (SEKI) and Yosemite National Park (YOSE). Species are listed in taxonomic order (Chesser et al. 2021).

Code	Common Name	Scientific Name	DEPO	SEKI	YOSE	Total
CONI	Common Nighthawk	*Chordeiles minor*	0	1	0	1
COPO	Common Poorwill	*Phalaenoptilus nuttallii*	0	0	1	1
BLSW	Black Swift	*Cypseloides niger*	0	60	9	69
VASW	Vaux's Swift	*Chaetura vauxi*	0	23	4	27
WTSW	White-throated Swift	*Aeronautes saxatalis*	0	180	726	906
ANHU	Anna's Hummingbird	*Calypte anna*	12	102	76	190
CAHU	Calliope Hummingbird	*Selasphorus calliope*	3	31	20	54
RUHU	Rufous Hummingbird	*Selasphorus rufus*	14	87	24	125
VIRA	Virginia Rail	*Rallus limicola*	0	0	2	2
SPSA	Spotted Sandpiper	*Actitis macularius*	8	21	33	62
CAGU	California Gull	*Larus californicus*	0	2	1	3
TUVU	Turkey Vulture	*Cathartes aura*	0	0	6	6
OSPR	Osprey	*Pandion haliaetus*	0	0	8	8
GOEA	Golden Eagle	*Aquila chrysaetos*	0	1	1	2
SSHA	Sharp-shinned Hawk	*Accipiter striatus*	0	5	2	7
COHA	Cooper's Hawk	*Accipiter cooperii*	0	2	2	4
NOGO	Northern Goshawk	*Accipiter gentilis*	1	6	7	14
BAEA	Bald Eagle	*Haliaeetus leucocephalus*	0	1	0	1
RSHA	Red-shouldered Hawk	*Buteo lineatus*	0	1	1	2
RTHA	Red-tailed Hawk	*Buteo jamaicensis*	2	13	13	28
FLOW	Flammulated Owl	*Psiloscops flammeolus*	0	1	0	1
GHOW	Great Horned Owl	*Bubo virginianus*	1	0	0	1
NOPO	Northern Pygmy-Owl	*Glaucidium gnoma*	1	26	7	34
SPOW	Spotted Owl	*Strix occidentalis*	0	3	1	4
BEKI	Belted Kingfisher	*Megaceryle alcyon*	1	3	1	5
ACWO	Acorn Woodpecker	*Melanerpes formicivorus*	0	53	195	248
WISA	Williamson's Sapsucker	*Sphyrapicus thyroideus*	9	104	179	292
RBSA	Red-breasted Sapsucker	*Sphyrapicus ruber*	29	175	136	340
BBWO	Black-backed Woodpecker	*Picoides arcticus*	2	0	35	37

Table 4 (continued). Counts for 134 bird species detected at least once during 2011–2019 point-count surveys across Devils Postpile National Monument (DEPO), Sequoia and Kings Canyon National Parks (SEKI) and Yosemite National Park (YOSE). Species are listed in taxonomic order (Chesser et al. 2021).

Code	Common Name	Scientific Name	DEPO	SEKI	YOSE	Total
DOWO	Downy Woodpecker	*Dryobates pubescens*	1	2	16	19
NUWO	Nuttall's Woodpecker	*Dryobates nuttallii*	0	1	5	6
HAWO	Hairy Woodpecker	*Dryobates villosus*	62	272	334	668
WHWO	White-headed Woodpecker	*Dryobates albolarvatus*	24	380	350	754
NOFL	Northern Flicker	*Colaptes auratus*	40	484	463	987
PIWO	Pileated Woodpecker	*Dryocopus pileatus*	1	140	184	325
AMKE	American Kestrel	*Falco sparverius*	2	4	5	11
PEFA	Peregrine Falcon	*Falco peregrinus*	0	1	1	2
ATFL	Ash-throated Flycatcher	*Myiarchus cinerascens*	0	16	9	25
WEKI	Western Kingbird	*Tyrannus verticalis*	0	0	1	1
OSFL	Olive-sided Flycatcher	*Contopus cooperi*	126	335	303	764
WEWP	Western Wood-Pewee	*Contopus sordidulus*	285	970	794	2049
HAFL	Hammond's Flycatcher	*Empidonax hammondii*	2	248	156	406
DUFL	Dusky Flycatcher	*Empidonax oberholseri*	115	885	1266	2266
PSFL	Pacific-slope Flycatcher	*Empidonax difficilis*	1	176	141	318
BLPH	Black Phoebe	*Sayornis nigricans*	1	5	12	18
HUVI	Hutton's Vireo	*Vireo huttoni*	0	12	19	31
CAVI	Cassin's Vireo	*Vireo cassinii*	6	211	569	786
WAVI	Warbling Vireo	*Vireo gilvus*	108	779	536	1423
STJA	Steller's Jay	*Cyanocitta stelleri*	199	1809	1509	3517
CASJ	California Scrub-Jay	*Aphelocoma californica*	0	41	29	70
CLNU	Clark's Nutcracker	*Nucifraga columbiana*	43	811	827	1681
AMCR	American Crow	*Corvus brachyrhynchos*	0	3	0	3
CORA	Common Raven	*Corvus corax*	5	205	233	443
MOCH	Mountain Chickadee	*Poecile gambeli*	261	2567	2231	5059
CBCH	Chestnut-backed Chickadee	*Poecile rufescens*	0	0	16	16
OATI	Oak Titmouse	*Baeolophus inornatus*	0	11	14	25
HOLA	Horned Lark	*Eremophila alpestris*	0	0	1	1
TRES	Tree Swallow	*Tachycineta bicolor*	5	1	0	6

Table 4 (continued). Counts for 134 bird species detected at least once during 2011–2019 point-count surveys across Devils Postpile National Monument (DEPO), Sequoia and Kings Canyon National Parks (SEKI) and Yosemite National Park (YOSE). Species are listed in taxonomic order (Chesser et al. 2021).

Code	Common Name	Scientific Name	DEPO	SEKI	YOSE	Total
VGSW	Violet-green Swallow	*Tachycineta thalassina*	50	21	83	154
NRWS	Northern Rough-winged Swallow	*Stelgidopteryx serripennis*	2	0	16	18
CLSW	Cliff Swallow	*Petrochelidon pyrrhonota*	2	0	2	4
BUSH	Bushtit	*Psaltriparus minimus*	0	37	45	82
WREN	Wrentit	*Chamaea fasciata*	0	160	57	217
GCKI	Golden-crowned Kinglet	*Regulus satrapa*	37	1096	774	1907
RCKI	Ruby-crowned Kinglet	*Corthylio calendula*	2	106	90	198
RBNU	Red-breasted Nuthatch	*Sitta canadensis*	82	1749	1343	3174
WBNU	White-breasted Nuthatch	*Sitta carolinensis*	34	142	170	346
PYNU	Pygmy Nuthatch	*Sitta pygmaea*	2	24	35	61
BRCR	Brown Creeper	*Certhia americana*	48	799	836	1683
BGGN	Blue-gray Gnatcatcher	*Polioptila caerulea*	0	32	42	74
ROWR	Rock Wren	*Salpinctes obsoletus*	12	190	108	310
CANW	Canyon Wren	*Catherpes mexicanus*	0	24	118	142
HOWR	House Wren	*Troglodytes aedon*	43	201	114	358
PAWR	Pacific Wren	*Troglodytes pacificus*	0	125	74	199
BEWR	Bewick's Wren	*Thryomanes bewickii*	0	44	65	109
CATH	California Thrasher	*Toxostoma redivivum*	0	1	0	1
AMDI	American Dipper	*Cinclus mexicanus*	3	5	6	14
WEBL	Western Bluebird	*Sialia mexicana*	0	42	24	66
MOBL	Mountain Bluebird	*Sialia currucoides*	31	103	65	199
TOSO	Townsend's Solitaire	*Myadestes townsendi*	35	311	339	685
SWTH	Swainson's Thrush	*Catharus ustulatus*	0	0	3	3
HETH	Hermit Thrush	*Catharus guttatus*	4	627	749	1380
AMRO	American Robin	*Turdus migratorius*	104	882	1061	2047
AMPI	American Pipit	*Anthus rubescens*	0	237	17	254
EVGR	Evening Grosbeak	*Coccothraustes vespertinus*	1	1	10	12
PIGR	Pine Grosbeak	*Pinicola enucleator*	3	12	39	54
GCRF	Gray-crowned Rosy-Finch	*Leucosticte tephrocotis*	0	465	48	513

Table 4 (continued). Counts for 134 bird species detected at least once during 2011–2019 point-count surveys across Devils Postpile National Monument (DEPO), Sequoia and Kings Canyon National Parks (SEKI) and Yosemite National Park (YOSE). Species are listed in taxonomic order (Chesser et al. 2021).

Code	Common Name	Scientific Name	DEPO	SEKI	YOSE	Total
HOFI	House Finch	*Haemorhous mexicanus*	2	1	0	3
PUFI	Purple Finch	*Haemorhous purpureus*	5	244	96	345
CAFI	Cassin's Finch	*Haemorhous cassinii*	135	681	1089	1905
RECR	Red Crossbill	*Loxia curvirostra*	6	136	191	333
PISI	Pine Siskin	*Spinus pinus*	28	356	512	896
LEGO	Lesser Goldfinch	*Spinus psaltria*	9	17	37	63
LAGO	Lawrence's Goldfinch	*Spinus lawrencei*	0	41	0	41
CHSP	Chipping Sparrow	*Spizella passerina*	18	80	311	409
BCSP	Black-chinned Sparrow	*Spizella atrogularis*	0	0	4	4
BRSP	Brewer's Sparrow	*Spizella breweri*	0	0	7	7
FOSP	Fox Sparrow	*Passerella iliaca*	459	1405	1033	2897
DEJU	Dark-eyed Junco	*Junco hyemalis*	322	2832	2768	5922
WCSP	White-crowned Sparrow	*Zonotrichia leucophrys*	4	316	281	601
SAVS	Savannah Sparrow	*Passerculus sandwichensis*	0	0	1	1
SOSP	Song Sparrow	*Melospiza melodia*	46	80	220	346
LISP	Lincoln's Sparrow	*Melospiza lincolnii*	22	228	131	381
CALT	California Towhee	*Melozone crissalis*	0	9	2	11
RCSP	Rufous-crowned Sparrow	*Aimophila ruficeps*	0	0	10	10
GTTO	Green-tailed Towhee	*Pipilo chlorurus*	111	304	276	691
SPTO	Spotted Towhee	*Pipilo maculatus*	4	569	391	964
BUOR	Bullock's Oriole	*Icterus bullockii*	0	1	26	27
RWBL	Red-winged Blackbird	*Agelaius phoeniceus*	0	27	251	278
BHCO	Brown-headed Cowbird	*Molothrus ater*	10	24	53	87
BRBL	Brewer's Blackbird	*Euphagus cyanocephalus*	20	55	59	134
OCWA	Orange-crowned Warbler	*Leiothlypis celata*	8	86	20	114
NAWA	Nashville Warbler	*Leiothlypis ruficapilla*	15	1063	935	2013
MGWA	MacGillivray's Warbler	*Geothlypis tolmiei*	68	803	481	1352
YEWA	Yellow Warbler	*Setophaga petechia*	14	33	115	162
YRWA	Yellow-rumped Warbler	*Setophaga coronata*	253	2309	2258	4820

Table 4 (continued). Counts for 134 bird species detected at least once during 2011–2019 point-count surveys across Devils Postpile National Monument (DEPO), Sequoia and Kings Canyon National Parks (SEKI) and Yosemite National Park (YOSE). Species are listed in taxonomic order (Chesser et al. 2021).

Code	Common Name	Scientific Name	DEPO	SEKI	YOSE	Total
BTYW	Black-throated Gray Warbler	*Setophaga nigrescens*	0	231	326	557
TOWA	Townsend's Warbler	*Setophaga townsendi*	0	0	5	5
HEWA	Hermit Warbler	*Setophaga occidentalis*	1	492	906	1399
WIWA	Wilson's Warbler	*Cardellina pusilla*	51	247	174	472
WETA	Western Tanager	*Piranga ludoviciana*	147	1681	1170	2998
BHGR	Black-headed Grosbeak	*Pheucticus melanocephalus*	2	619	816	1437
LAZB	Lazuli Bunting	*Passerina amoena*	8	343	209	560

Species detected more than 100 times each (those named in Figure 2) numbered 66, while 68 additional species (combined as “Other” in Figure 2) were detected less than 100 times each during the monitoring period. Species detected only rarely (from one to nine times across all three parks during the monitoring period) included Canada Goose, Bufflehead, White-tailed Ptarmigan, Pied-billed Grebe, Common Nighthawk, Common Poorwill, Virginia Rail, California Gull, Turkey Vulture, Osprey, Golden Eagle, Sharp-shinned Hawk, Cooper's Hawk, Bald Eagle, Red-shouldered Hawk, Flammulated Owl, Great Horned Owl, Spotted Owl, Belted Kingfisher, Nuttall's Woodpecker, Peregrine Falcon, Western Kingbird, American Crow, Horned Lark, Tree Swallow, Cliff Swallow, California Thrasher, Swainson's Thrush, House Finch, Black-chinned Sparrow, Brewer's Sparrow, Savannah Sparrow, and Townsend's Warbler.

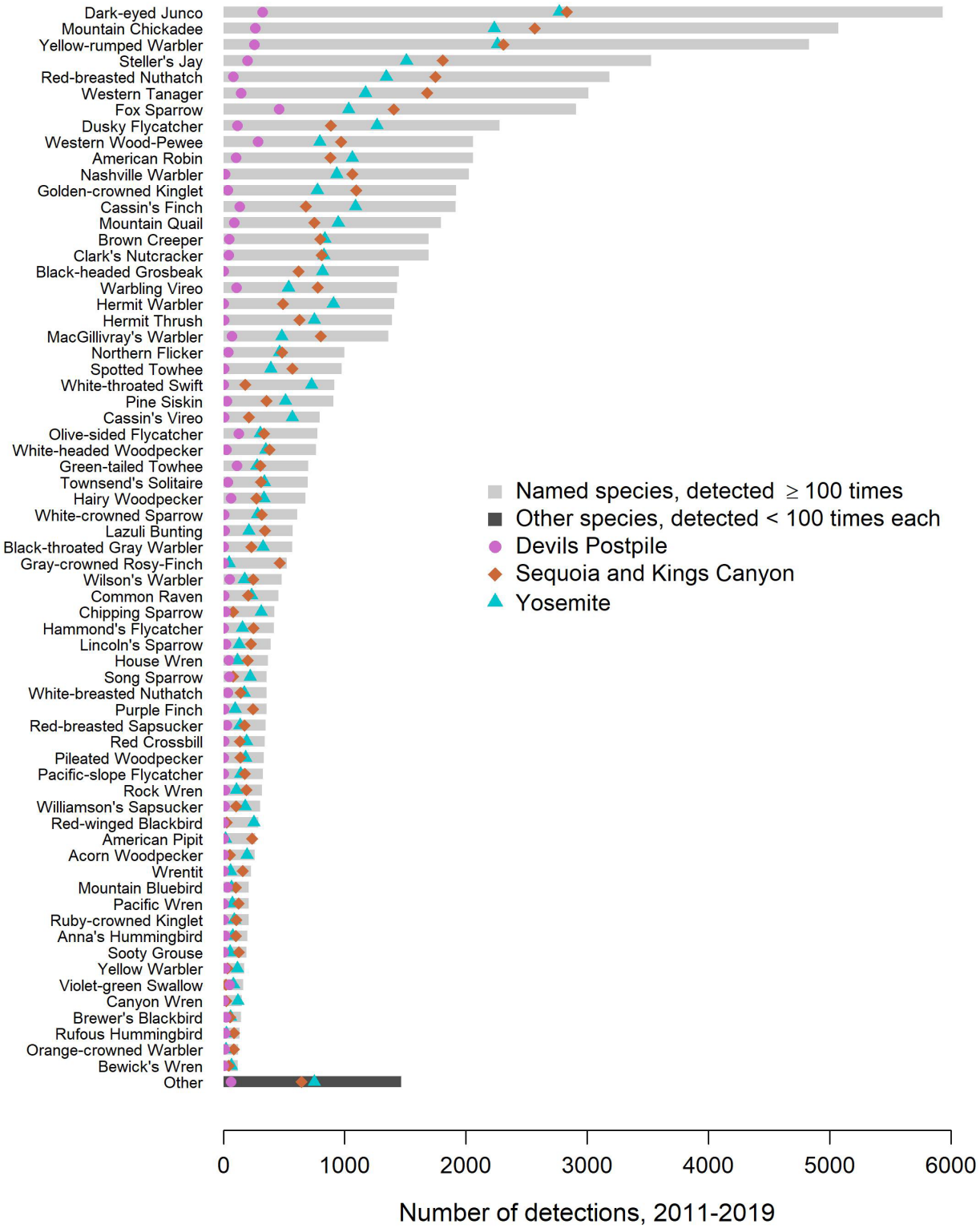


Figure 2. Number of birds detected, by species and park, over the monitoring period. Quantitative data for each species, including the rarer species combined as “Other” in this plot, appear in Table 4.

Additional species detected by survey crews during activities other than point counts brought the total number of species detected to 166. See Appendix 2 for the full species list from each park, and the type of record (point count or other) associated with each species' detection.

Climatic variation during the monitoring period

There was clear variation across the monitoring period in our metrics of spring conditions. In Figure 3, both climate metrics are lagged one year to allow for demographic response in year *t* to breeding habitat conditions in year *t*-1. The annual anomaly in precipitation-as-snow (*PAS*) first declined and later increased during the monitoring period (Figure 3a), while the annual anomaly in mean spring temperature (*MST*) exhibited an opposing pattern (Figure 3b). The magnitude of this variation was widely reported in the literature as unprecedented (Margulis et al. 2016), and the patterns observed were common to all three parks (see Appendix 3 for climate summaries from DEPO). In addition to the temporal variation observed, time-averaged values of *PAS* during 2011–2019 were somewhat lower than 1981–2010 normals, while time-averaged values of *MST* were higher than 1981–2010 normals (Figure 3b). Thus, snows were lighter and springs were warmer during the monitoring period relative to the long-term average in these parks. Comparisons among parks further suggest that SEKI experienced the lightest snowpacks and warmest springs in this study.

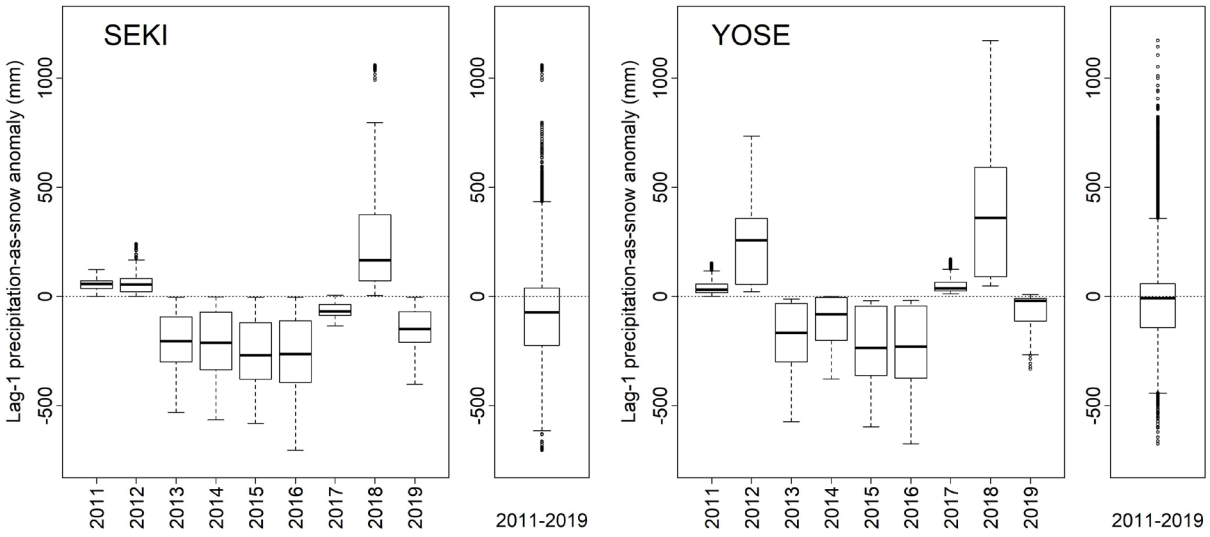


Figure 3a. Time-lagged anomalies in precipitation-as-snow (*PAS*) for each point-count station in Sequoia and Kings Canyon National Parks (SEKI) and Yosemite National Park (YOSE). Annual and time-averaged anomalies (left- and right-hand panels for each park) are expressed here as the deviation from 1981–2010 normals for data from August 1st of year t-1 to July 31st of year t and are further lagged one year to serve as a potential covariate of demographic response to breeding habitat conditions. Each boxplot indicates the median (thick horizontal line), interquartile range (box), and range of the data (whiskers), excepting outliers (dots) >1.5 times the interquartile range. See Figure A2-1 for similar *PAS* data from Devils Postpile National Monument.

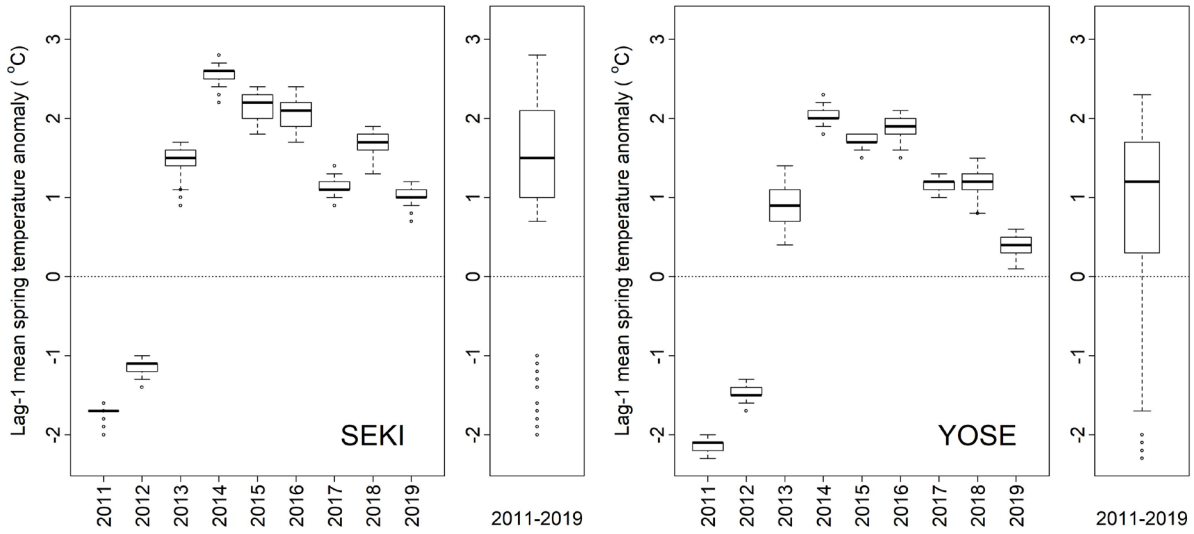


Figure 3b. Time-lagged anomalies in mean spring temperature (*MST*) for each point-count station in Sequoia and Kings Canyon National Parks (SEKI) and Yosemite National Park (YOSE). Annual and time-averaged anomalies (left- and right-hand panels for each park) are expressed here as the deviation from 1981–2010 normals for data from March 1st to May 31st, lagged by one year to serve as a potential covariate of demographic response to breeding habitat conditions. Each boxplot indicates the median (thick horizontal line), interquartile range (box), and range of the data (whiskers), excepting outliers (dots) >1.5 times the interquartile range. See Figure A2-2 for similar *MST* data from Devils Postpile National Monument.

Fitted models

Models of temporal trend in abundance, corrected for variation in detection rates, were fitted successfully to data on 62 of the species detected in SEKI and YOSE (Table 5) and 25 species in DEPO (Table 6). All species that were detected more than 100 times across SEKI and YOSE during the monitoring period supported our relatively parameter-rich models, with the exception of four species often observed in flocks (White-throated Swift, Violet-green Swallow, Red Crossbill and Brewer's Blackbird), which we did not model because flocking species do not meet the assumptions of the models considered here. On the other hand, we were able to fit a reduced model to several populations in DEPO from species detected fewer than 100 times, including Mountain Quail (89 detections), Hairy Woodpecker (62), Northern Flicker (40), Clark's Nutcracker (43), Golden-crowned Kinglet (37), Red-breasted nuthatch (82), Brown Creeper (48), House Wren (43), Townsend's Solitaire (35), Song Sparrow (46), MacGillivray's Warbler (68) and Wilson's Warbler (51). Restricting the analysis of DEPO populations to within that relatively small park allowed us to estimate trends based on a smaller sample size, probably because there was less unexplained spatial heterogeneity in the data across this small park. In the larger parks, we often achieved convergence for models of the less common species by reducing the spatial scale of model scope. Data from species with just over 100 detections across SEKI and YOSE might not support a model of trend across both parks, but often supported a model of trend in the park in which the species was more frequent. The same pattern held across elevational strata. For this reason, we were not able to generate model fits for all parks and elevational strata for every species analyzed.

Table 5. Model covariates for 62 species analyzed in Sequoia and Kings Canyon National Parks (SEKI) and Yosemite National Park (YOSE) (see Table 4 for species codes). Each model included the indicated covariates (+) from Equation 1 and a random effect on abundance of station nested within transect (not shown). Potential covariates in the sub-model of availability were *day* of year and *hour* of day. Potential covariates in the sub-model of detection (gray shading) were *cover* density, ambient *noise* and *observer* (a random effect). Potential covariates of abundance were *year* (*Y*), *park* (*P*), elevation (*elev, E*) and their interactions; a quadratic effect of elevation (E^2); a precipitation-as-snow (*PAS*) anomaly and its quadratic effect (PAS^2); and a mean-spring-temperature (*MST*) anomaly or (to avoid covariance in models with *PAS*) the residual of a regression of *MST* on *PAS* (*rMST*). Anomalies were calculated relative to 1981–2010 normals and lagged −1 year.

Species code	*day*	*hour*	*cover*	*noise*	*obser-ver*	*year (Y)*	*park (P)*	*elev (E)*	*Y×E*	*Y×P*	*P×E*	*P×E×Y*	E^2	*PAS*	PAS^2	*(r)MST*
MOUQ	+	–	+	+	+	+	+	+	+	+	+	+	+	+	+	+
SOGR	–	–	–	+	+	+	+	+	+	+	+	+	+	–	–	+
ANHU	–	–	+	–	+	+	–	+	–	–	–	–	–	+	–	+
RUHU	+	+	–	+	–	+	+	+	–	+	–	–	–	+	–	+
ACWO	+	+	–	–	+	+	+	+	–	–	–	–	–	–	–	+
WISA	+	+	+	+	+	+	+	+	+	+	+	+	+	–	–	+
RBSA	+	+	+	+	+	+	+	+	+	+	+	+	+	–	–	+
HAWO	+	–	+	+	+	+	+	+	+	+	+	+	+	+	+	+
WHWO	+	+	–	+	+	+	–	+	+	–	–	–	+	+	+	+
NOFL	+	–	+	+	+	+	+	+	+	+	+	+	+	+	+	+
PIWO	+	+	+	+	+	+	+	+	+	+	+	+	+	–	–	+
OSFL	+	–	+	+	+	+	+	+	+	+	+	+	+	+	+	+
WEWP	+	+	+	+	+	+	+	+	+	+	+	+	+	+	+	+
HAFL	+	–	–	+	+	+	+	+	+	+	+	+	+	+	+	–
DUFL	–	+	+	+	+	+	+	+	+	–	–	–	+	+	–	+
PSFL	–	–	–	–	+	+	+	–	–	+	–	–	–	–	–	+
CAVI	+	+	+	+	+	+	+	+	+	+	+	+	+	+	+	+

Table 5 (continued). Model covariates for 62 species analyzed in Sequoia and Kings Canyon National Parks (SEKI) and Yosemite National Park (YOSE) (see Table 4 for species codes). Each model included the indicated covariates (+) from Equation 1 and a random effect on abundance of station nested within transect (not shown). Potential covariates in the sub-model of availability were day of year and hour of day. Potential covariates in the sub-model of detection (gray shading) were cover density, ambient noise and observer (a random effect). Potential covariates of abundance were *year* (*Y*), *park* (*P*), elevation (*elev, E*) and their interactions; a quadratic effect of elevation (E^2); a precipitation-as-snow (*PAS*) anomaly and its quadratic effect (PAS^2); and a mean-spring-temperature (*MST*) anomaly or (to avoid covariance in models with *PAS*) the residual of a regression of *MST* on *PAS* (*rMST*). Anomalies were calculated relative to 1981–2010 normals and lagged −1 year.

Species code	*day*	*hour*	*cover*	*noise*	*obser-ver*	*year (Y)*	*park (P)*	*elev (E)*	*Y×E*	*Y×P*	*P×E*	*P×E×Y*	E^2	*PAS*	PAS^2	*(r)MST*
WAVI	–	+	+	+	+	+	+	+	+	+	+	+	+	–	–	+
STJA	+	–	–	+	+	+	+	+	+	+	+	+	+	–	–	+
CLNU	+	–	+	+	+	+	+	+	+	–	–	–	–	+	+	+
CORA	+	+	+	+	+	+	+	+	+	+	+	+	+	+	+	+
MOCH	+	+	–	+	+	+	+	+	+	–	–	–	+	+	+	+
WREN	–	–	–	+	+	+	+	+	+	+	–	–	–	+	–	+
GCKI	–	+	+	+	+	+	+	+	+	+	+	+	+	+	+	+
RCKI	–	–	–	+	+	+	+	+	+	+	+	+	–	+	–	–
RBNU	+	–	–	+	+	+	+	+	–	–	+	–	+	+	–	+
WBNU	–	–	–	–	+	+	+	+	+	+	+	+	–	–	–	+
BRCR	–	+	+	+	+	+	+	+	+	+	+	+	+	+	+	+
ROWR	–	–	–	–	+	+	+	–	–	+	–	–	–	+	–	+
CANW	+	–	–	–	+	+	+	–	–	–	–	–	–	–	–	–
HOWR	–	–	–	+	+	+	+	+	+	+	+	+	–	–	–	+
PAWR	–	–	–	–	+	+	+	–	–	+	–	–	–	–	–	–
BEWR	+	+	–	–	+	+	+	+	–	–	–	–	–	–	–	+
MOBL	–	–	–	+	–	+	+	–	–	–	–	–	–	–	–	–

Table 5 (continued). Model covariates for 62 species analyzed in Sequoia and Kings Canyon National Parks (SEKI) and Yosemite National Park (YOSE) (see Table 4 for species codes). Each model included the indicated covariates (+) from Equation 1 and a random effect on abundance of station nested within transect (not shown). Potential covariates in the sub-model of availability were day of year and hour of day. Potential covariates in the sub-model of detection (gray shading) were cover density, ambient noise and observer (a random effect). Potential covariates of abundance were *year* (*Y*), *park* (*P*), elevation (*elev, E*) and their interactions; a quadratic effect of elevation (E^2); a precipitation-as-snow (*PAS*) anomaly and its quadratic effect (PAS^2); and a mean-spring-temperature (*MST*) anomaly or (to avoid covariance in models with *PAS*) the residual of a regression of *MST* on *PAS* (*rMST*). Anomalies were calculated relative to 1981–2010 normals and lagged −1 year.

Species code	*day*	*hour*	*cover*	*noise*	*observer*	*year (Y)*	*park (P)*	*elev (E)*	*Y×E*	*Y×P*	*P×E*	*P×E×Y*	E^2	*PAS*	PAS^2	*(r)MST*
TOSO	+	–	+	+	+	+	+	+	+	+	+	+	+	+	–	+
HETH	+	–	+	+	+	+	+	+	+	+	+	+	+	+	+	+
AMRO	–	+	+	+	+	+	+	+	+	+	+	+	+	+	+	–
AMPI	–	–	–	+	–	+	+	+	+	+	+	+	–	+	–	+
GCRF	+	–	–	–	+	+	+	+	–	–	–	–	–	+	+	+
PUFI	–	–	–	–	+	+	+	+	+	–	–	–	–	+	–	–
CAFI	–	+	+	+	+	+	+	+	+	+	+	+	+	+	–	+
PISI	+	–	+	+	+	+	+	+	–	–	–	–	+	–	–	+
CHSP	–	+	+	+	+	+	+	+	+	+	+	+	+	+	+	+
FOSP	+	+	+	+	+	+	+	+	+	+	+	+	+	+	+	+
DEJU	+	+	–	+	+	+	+	+	+	+	+	+	+	+	+	+
WCSP	+	–	+	+	+	+	+	+	+	–	–	–	–	+	+	+
SOSP	–	–	+	+	+	+	+	+	+	+	+	+	+	–	–	–
LISP	–	+	+	+	+	+	+	+	+	+	+	+	+	+	+	+
GTTO	+	+	+	+	+	+	+	+	+	+	+	+	+	+	+	+
SPTO	–	–	+	+	+	+	+	+	+	+	+	+	+	–	–	+
RWBL	–	–	–	–	+	+	–	–	–	–	–	–	–	+	–	+

Table 5 (continued). Model covariates for 62 species analyzed in Sequoia and Kings Canyon National Parks (SEKI) and Yosemite National Park (YOSE) (see Table 4 for species codes). Each model included the indicated covariates (+) from Equation 1 and a random effect on abundance of station nested within transect (not shown). Potential covariates in the sub-model of availability were day of year and hour of day. Potential covariates in the sub-model of detection (gray shading) were cover density, ambient noise and observer (a random effect). Potential covariates of abundance were *year* (*Y*), *park* (*P*), elevation (*elev, E*) and their interactions; a quadratic effect of elevation (E^2); a precipitation-as-snow (*PAS*) anomaly and its quadratic effect (PAS^2); and a mean-spring-temperature (*MST*) anomaly or (to avoid covariance in models with *PAS*) the residual of a regression of *MST* on *PAS* (*rMST*). Anomalies were calculated relative to 1981–2010 normals and lagged −1 year.

Species code	*day*	*hour*	*cover*	*noise*	*obser-ver*	*year (Y)*	*park (P)*	*elev (E)*	*Y×E*	*Y×P*	*P×E*	*P×E×Y*	E^2	*PAS*	PAS^2	*(r)MST*
OCWA	+	+	–	+	+	+	+	+	+	–	–	–	–	–	–	–
NAWA	+	+	+	+	+	+	+	+	+	–	–	–	+	+	–	+
MGWA	+	–	+	+	+	+	+	+	+	+	+	+	+	+	+	+
YEWA	–	–	–	–	+	+	–	+	+	–	–	–	–	+	+	+
YRWA	–	–	+	+	+	+	+	+	+	–	–	–	+	+	–	+
BTYW	+	–	+	+	+	+	+	+	+	+	+	+	+	–	–	+
HEWA	+	–	+	+	+	+	+	+	+	+	+	+	+	+	+	+
WIWA	+	–	+	+	+	+	+	+	+	+	+	+	+	+	+	+
WETA	+	+	–	+	+	+	+	+	+	–	–	–	+	+	–	+
BHGR	+	–	+	+	+	+	+	+	+	+	+	+	+	+	+	+
LAZB	+	+	+	+	+	+	+	+	+	+	+	+	+	+	+	+

Table 6. Model covariates for 25 species analyzed in Devils Postpile National Monument (DEPO) (see Table 4 for species codes). Each model included the indicated covariates (+) from Equation 2 and a random effect of station on abundance (not shown). Potential covariates in the sub-model of availability were *day* of year and *hour* of day. Potential covariates in the sub-model of detection (gray shading) were *cover* density, ambient *noise* and *observer* (a random effect). Potential covariates of abundance were *year* and anomalies in precipitation-as-snow (*PAS*) and mean spring temperature (*MST*) or (to avoid covariance in models with *PAS*) the residual of a regression of *MST* on *PAS* (*rMST*). Anomalies were calculated relative to 1981–2010 normals and lagged −1 year.

Species code	*day*	*hour*	*cover*	*noise*	*observer*	*year*	*PAS*	PAS^2	*rMST*
MOUQ	–	–	–	–	–	+	+	+	+
HAWO	–	–	–	–	–	+	+	+	+
NOFL	–	–	–	–	–	+	+	+	+
OSFL	–	–	–	–	–	+	+	+	+
WEWP	+	+	+	+	+	+	+	+	+
DUFL	+	+	+	+	+	+	+	+	+
WAVI	–	–	–	–	–	+	+	+	+
STJA	–	–	–	–	–	+	+	+	+
CLNU	–	–	–	–	–	+	+	+	+
MOCH	–	–	+	+	+	+	+	+	+
GCKI	–	–	–	–	–	+	+	+	+
RBNU	–	–	–	–	–	+	+	+	+
BRCR	–	–	–	–	–	+	+	+	+
HOWR	–	–	–	–	–	+	+	+	+
TOSO	–	–	–	–	–	+	+	+	+
AMRO	–	–	–	–	–	+	+	+	+
CAFI	–	–	–	–	–	+	+	+	+
FOSP	–	–	–	–	+	+	+	+	+
DEJU	–	–	–	–	–	+	+	+	+
SOSP	–	–	–	–	–	+	+	+	+
GTTO	–	–	–	–	–	+	+	+	+
MGWA	–	–	–	–	–	+	+	+	+
YRWA	–	–	–	+	+	+	+	+	+
WIWA	–	–	–	–	–	+	+	+	+
WETA	–	–	–	–	–	+	+	+	+

The covariates included in each species' final model varied according to our model-fitting approach, as described in Methods. Briefly, each model of combined SEKI and YOSE data (Table 5) began with the full model based on 17 covariates (Eqn. 1) and, if the fit of this full model was not adequate, covariates with lower support were dropped until we achieved adequate model fit or until it appeared that model scope required adjustment. Using this protocol, we were able to maximize the number of focal parameters estimated for each species. Across the 62 species-specific models from these parks (Table 5), the average number of covariates included in each model was 11.5 (range 3–16), and the mean number of species-specific coefficients estimated for each covariate was 45 (range 26–62). In contrast, each model of DEPO data (Table 6) began with a reduced model based on four of our focal covariates (Eqn. 2c) and, if model fit was not adequate, covariates of detection were added in attempts to improve model fit. Using this protocol we were able to retain all four focal covariates in the sub-model of abundance for each of the 25 species analyzed in DEPO (Table 6). Note that detection was modeled in every case, but modeling covariates of detection was not necessary to achieve adequate fit for most of our DEPO models.

Temporal trends in population density during the breeding season, according to the final models for each species, are shown in Figures 4–6. Beginning with temporal trends in DEPO, we found strong evidence for a decline in density for only one of 25 species analyzed, countered by strong evidence for an increase in density for five species. By 2019, the density of MacGillivray's Warbler had fallen to less than half its estimate for 2011 (Figure 4c), while densities of Dusky Flycatcher, Steller's Jay, House Wren, American Robin and Green-tailed Towhee all rose during the same period.

We summarized the temporal trend in density in terms of population growth, widely termed lambda and symbolized λ. To differentiate lambdas symbolizing population growth from those symbolizing expected abundance (Eqn. 1c and 2c), we introduce alternative subscripts. Figure 4 displays two metrics of λ, both derived from results of the hierarchical model: λ_P is the slope of a Poisson regression through mean annual estimates of population density (λ_t) provided by the hierarchical model, and λ_G is the geometric mean rate of population growth based on all annual estimates of population density. The Poisson regression is provided as a smooth metric of apparent trend and does not account for the actual trajectory of the population or the full distribution of annual abundance estimates generated by the hierarchical model. In contrast, the geometric mean lambda was derived from estimates of population size generated during the stochastic simulations required for model fit and faithfully reflects the trajectory of, and uncertainty in, those estimates. Note that the value of λ_G tends to be greater than the value of λ_P whenever population size begins below the curve and ends above the curve, and conversely. In some cases, the geometric mean growth rate is less than 1 while the smoothed growth rate (which assumes independence in sequential values of annual mean density) is greater than 1, and conversely. The geometric mean growth rate is a more suitable metric of trend for time series with serial correlation and processes involving compound growth. Therefore, we note support for the apparent trend based only on support for positive or negative geometric growth ($\lambda_G > 1$ or $\lambda_G < 1$, respectively), and we use an asterisk on λ_G and a solid curve to indicate that the credible interval for λ_G did not overlap zero.

Although interannual variation in population density was apparent, the vast majority of species analyzed in DEPO appeared stable during 2011–2019. There were no supported trends in density during the monitoring period for 19 of 25 species analyzed in this monument (Figure 4).

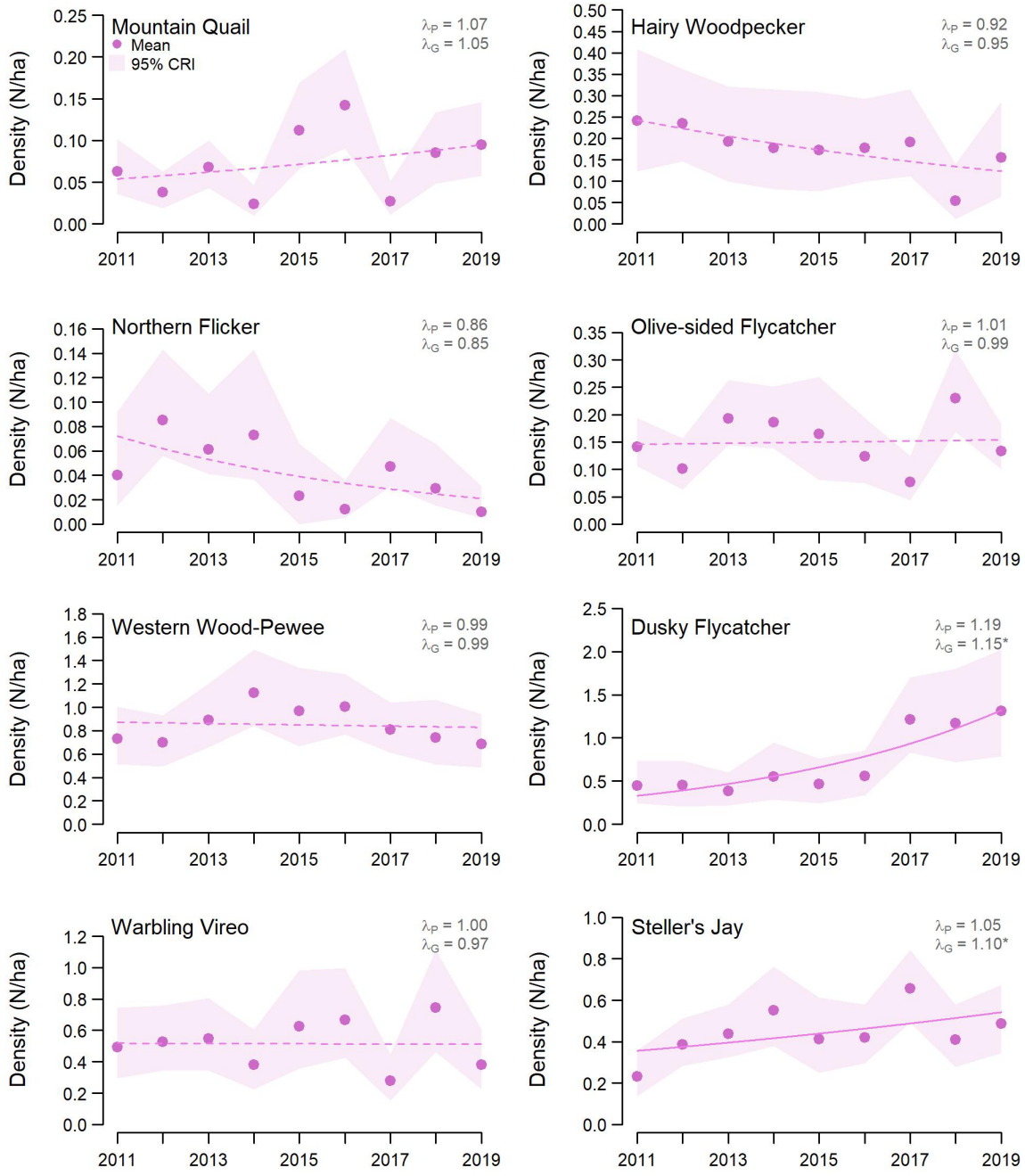


Figure 4a. Population density estimates for Mountain Quail, Hairy Woodpecker, Northern Flicker, Olive-sided Flycatcher, Western Wood-Pewee, Dusky Flycatcher, Warbling Vireo and Steller's Jay, derived using a hierarchical analysis of point counts from Devils Postpile National Monument. Smoothed trends (curves) and both smoothed (λ_P) and geometric mean (λ_G) population growth rates are shown (λ>1 indicates positive growth). Solid curves and asterisks indicate strongly supported trends for which the 95% credible interval (CRI) on λ_G did not overlap 1.

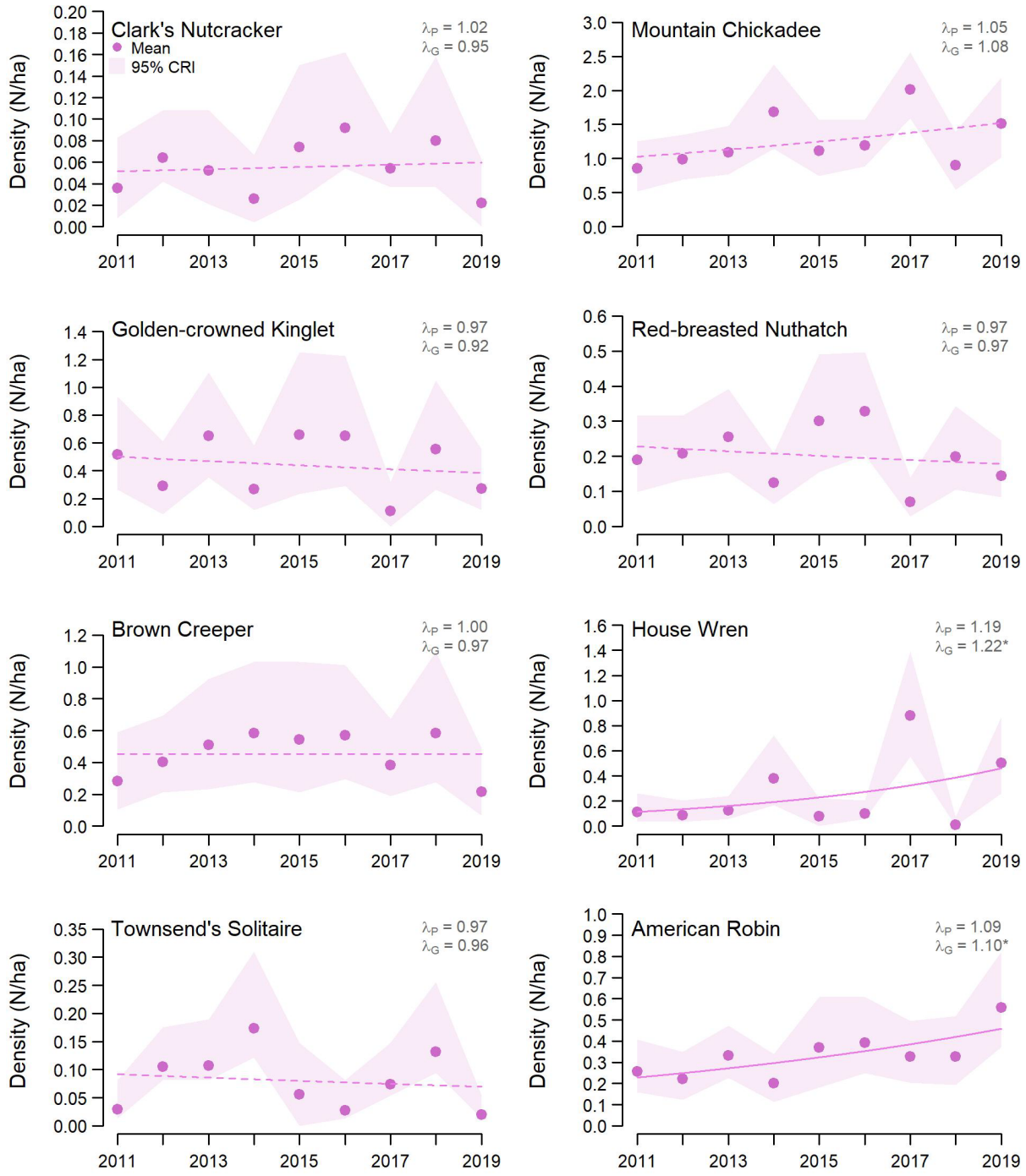


Figure 4b. Population density estimates for Clark's Nutcracker, Mountain Chickadee, Golden-crowned Kinglet, Red-breasted Nuthatch, Brown Creeper, House Wren, Townsend's Solitaire and American Robin, derived using a hierarchical analysis of point counts from Devils Postpile National Monument. Smoothed trends (curves) and both smoothed (λ_P) and geometric mean (λ_G) population growth rates are shown (λ>1 indicates positive growth). Solid curves and asterisks indicate strongly supported trends for which the 95% credible interval (CRI) on λ_G did not overlap 1.

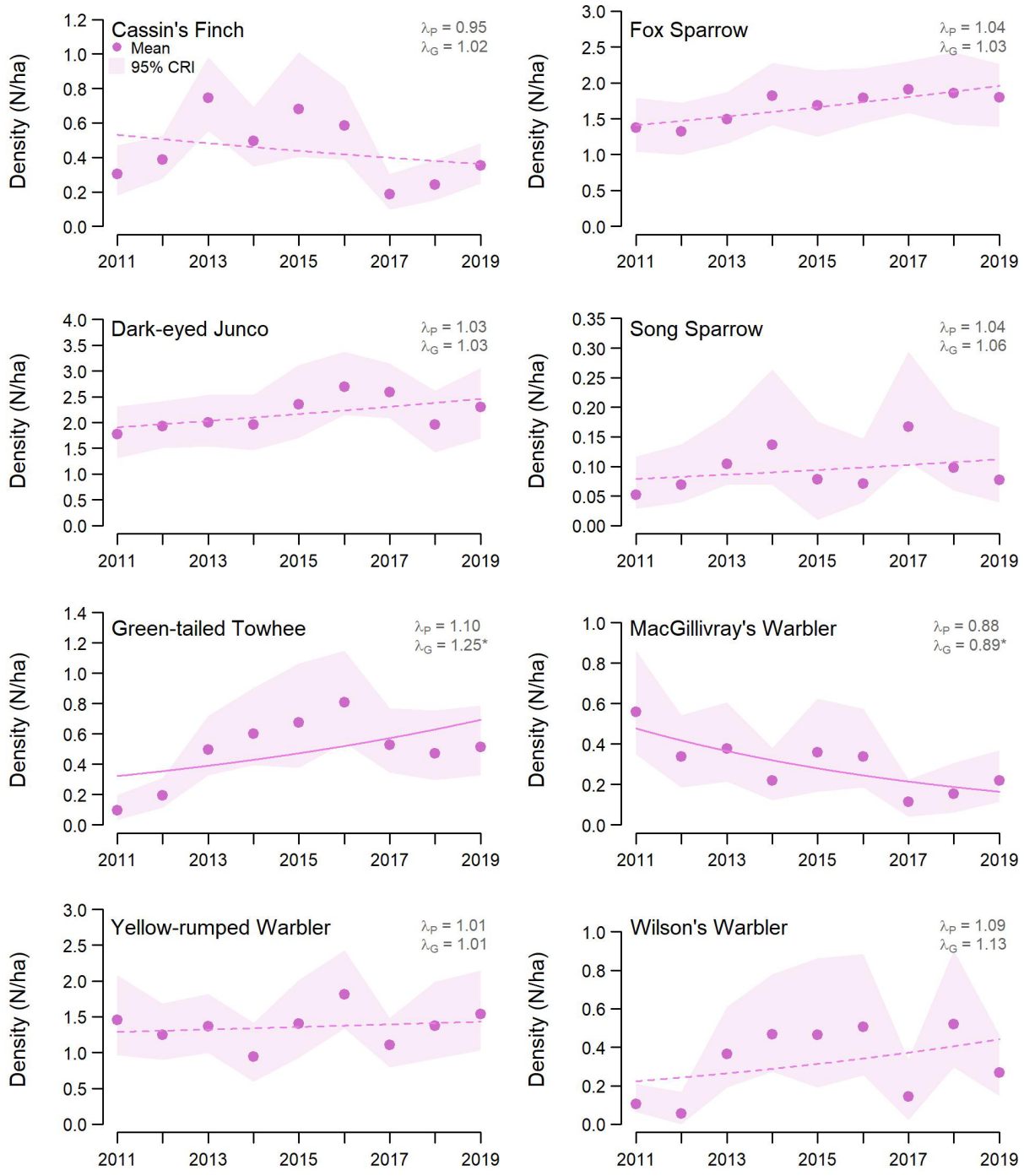


Figure 4c. Population density estimates for Cassin's Finch, Fox Sparrow, Dark-eyed Junco, Song Sparrow, Green-tailed Towhee, MacGillivray's Warbler, Yellow-rumped Warbler and Wilson's Warbler, derived using a hierarchical analysis of point counts from Devils Postpile National Monument. Smoothed trends (curves) and both smoothed (λ_P) and geometric mean (λ_G) population growth rates are shown (λ>1 indicates positive growth). Solid curves and asterisks indicate strongly supported trends for which the 95% credible interval (CRI) on λ_G did not overlap 1.

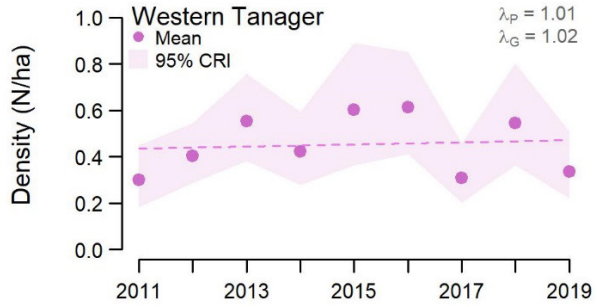


Figure 4d. Population density estimates for Western Tanager, derived using a hierarchical analysis of point counts from Devils Postpile National Monument. Smoothed trends (curves) and both smoothed (λ_P) and geometric mean (λ_G) population growth rates are shown (λ>1 indicates positive growth). Solid curves and asterisks indicate strongly supported trends for which the 95% credible interval (CRI) on λ_G did not overlap 1.



Trends in Steller's Jay breeding-season population density were mixed across the Sierra Nevada Inventory and Monitoring Network during 2011–2019. Photo by Bryan Jones, Flickr, CC BY-NC-ND 2.0.

Trends by park and elevational stratum

For 62 species detected frequently enough in SEKI and YOSE to support our models, we derived trends in population density differentiated by park (Figures 5a-h) and by elevational stratum (Figures 6a-h).

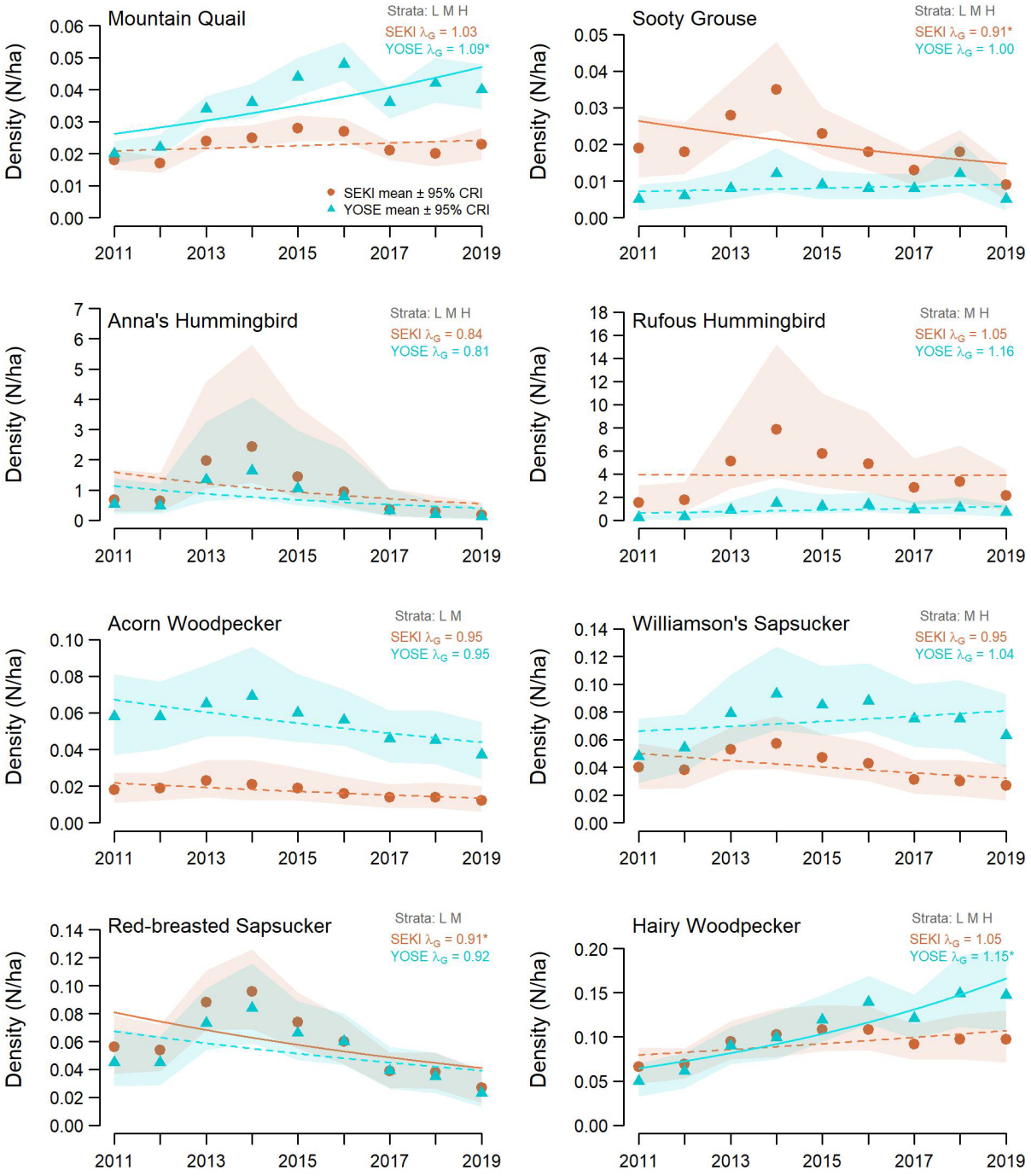


Figure 5a. Population density estimates by park for Mountain Quail, Sooty Grouse, Anna's Hummingbird, Rufous Hummingbird, Acorn Woodpecker, Williamson's Sapsucker, Red-breasted Sapsucker and Hairy Woodpecker, derived using a hierarchical analysis of point counts from Sequoia and Kings Canyon National Parks (SEKI) and Yosemite National Park (YOSE). Strata included in each model are listed as low (L), medium (M) and/or high (H) elevation (Table 1). Smoothed trends in population growth (curves) and geometric mean population growth rates (λ_G values) are reported for each species and park analyzed. Solid curves and asterisks indicate strongly supported trends for which the 95% credible interval on λ_G did not overlap 1. Species are listed in taxonomic order (Table 4).

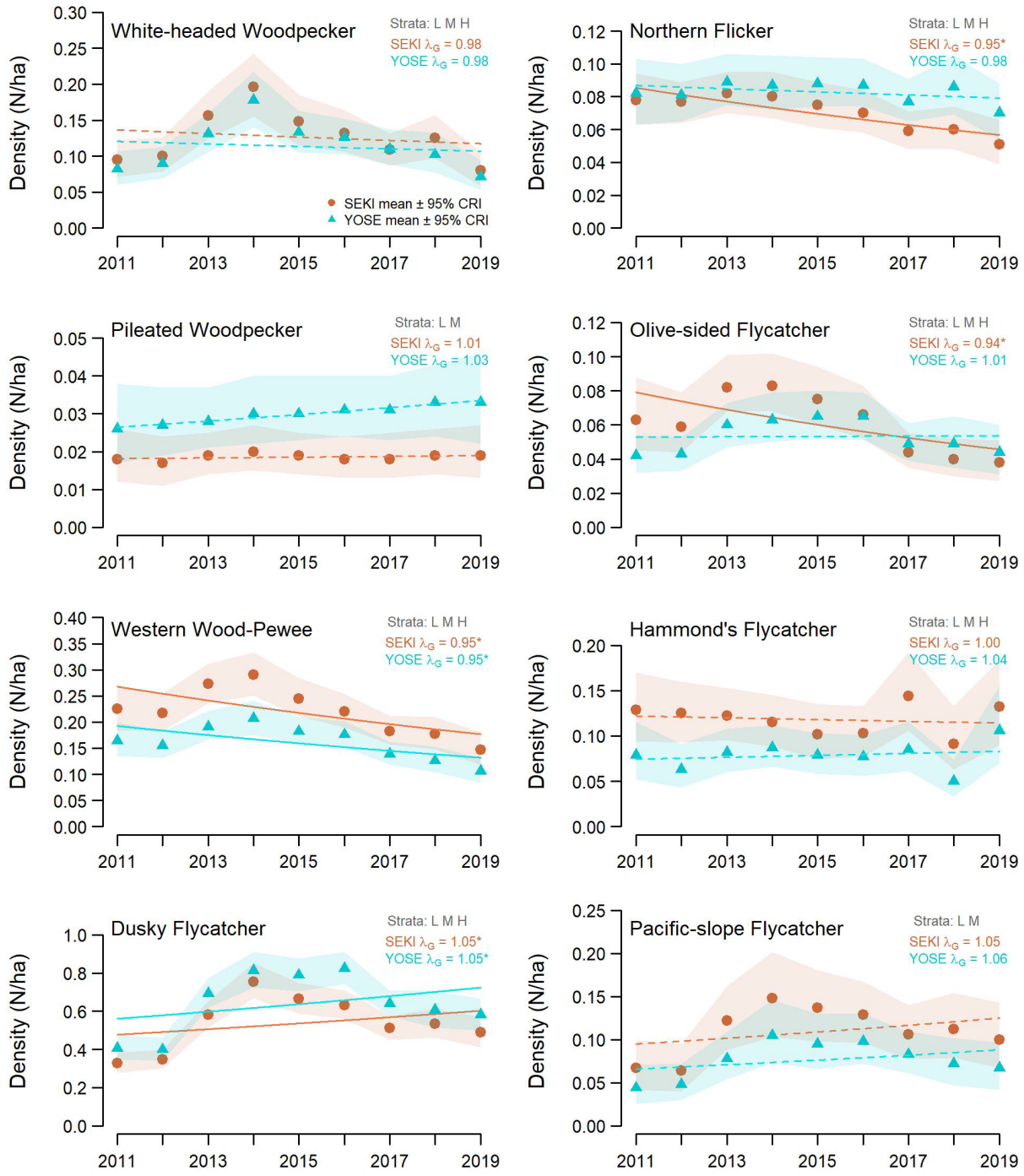


Figure 5b. Population density estimates by park for White-headed Woodpecker, Northern Flicker, Pileated Woodpecker, Olive-sided Flycatcher, Western Wood-Pewee, Hammond's Flycatcher, Dusky Flycatcher and Pacific-slope Flycatcher, derived using a hierarchical analysis of point counts from Sequoia and Kings Canyon National Parks (SEKI) and Yosemite National Park (YOSE). Strata included in each model are listed as low (L), medium (M) and/or high (H) elevation (Table 1). Smoothed trends in population growth (curves) and geometric mean population growth rates (λ_G values) are reported for each species and park analyzed. Solid curves and asterisks indicate strongly supported trends for which the 95% credible interval on λ_G did not overlap 1. Species are listed in taxonomic order (Table 4).

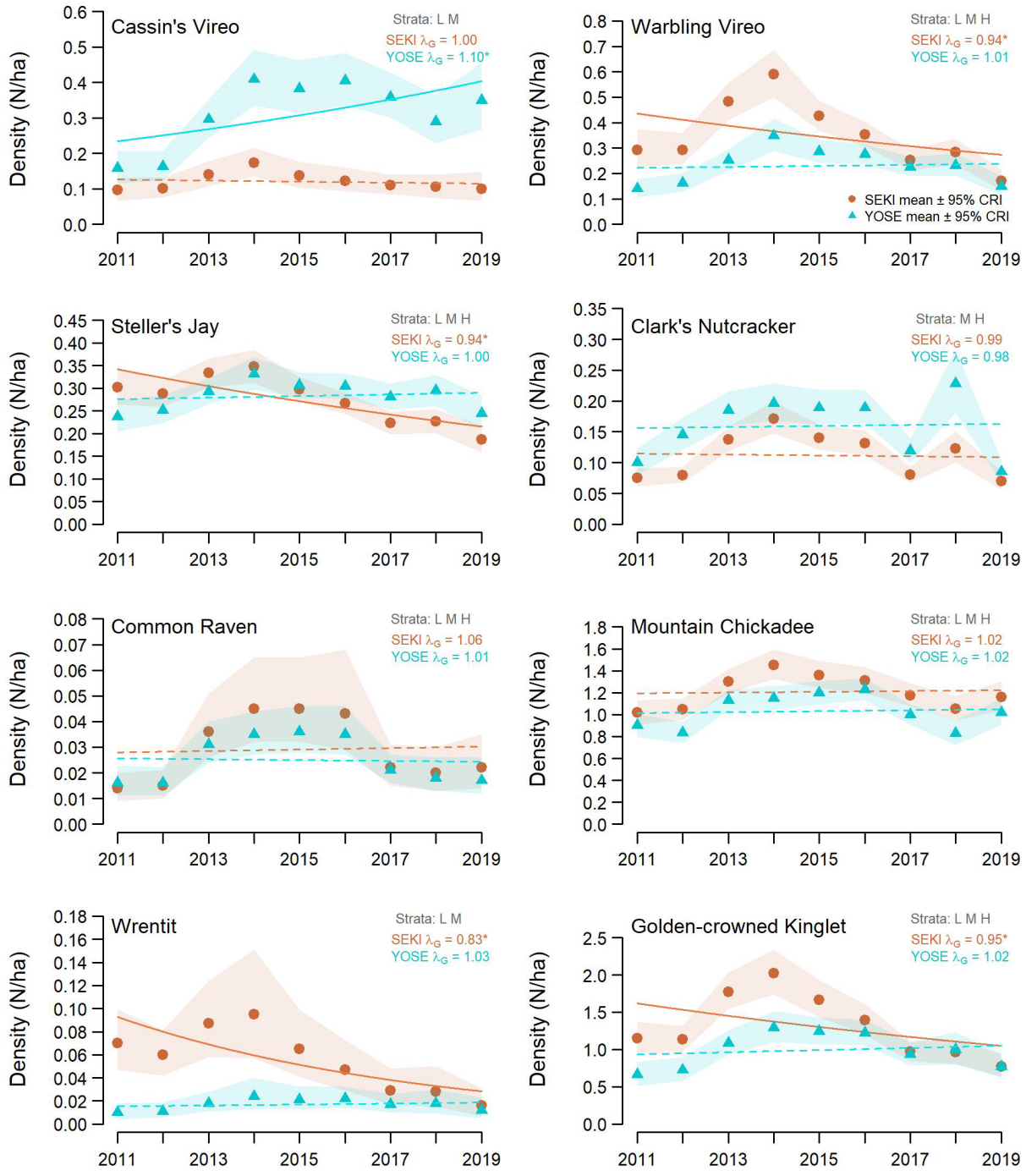


Figure 5c. Population density estimates by park for Cassin's Vireo, Warbling Vireo, Steller's Jay, Clark's Nutcracker, Common Raven, Mountain Chickadee, Wrentit, and Golden-crowned Kinglet, derived using a hierarchical analysis of point counts from Sequoia and Kings Canyon National Parks (SEKI) and Yosemite National Park (YOSE). Strata included in each model are listed as low (L), medium (M) and/or high (H) elevation (Table 1). Smoothed trends in population growth (curves) and geometric mean population growth rates (λ_G values) are reported for each species and park analyzed. Solid curves and asterisks indicate strongly supported trends for which the 95% credible interval on λ_G did not overlap 1. Species are listed in taxonomic order (Table 4).

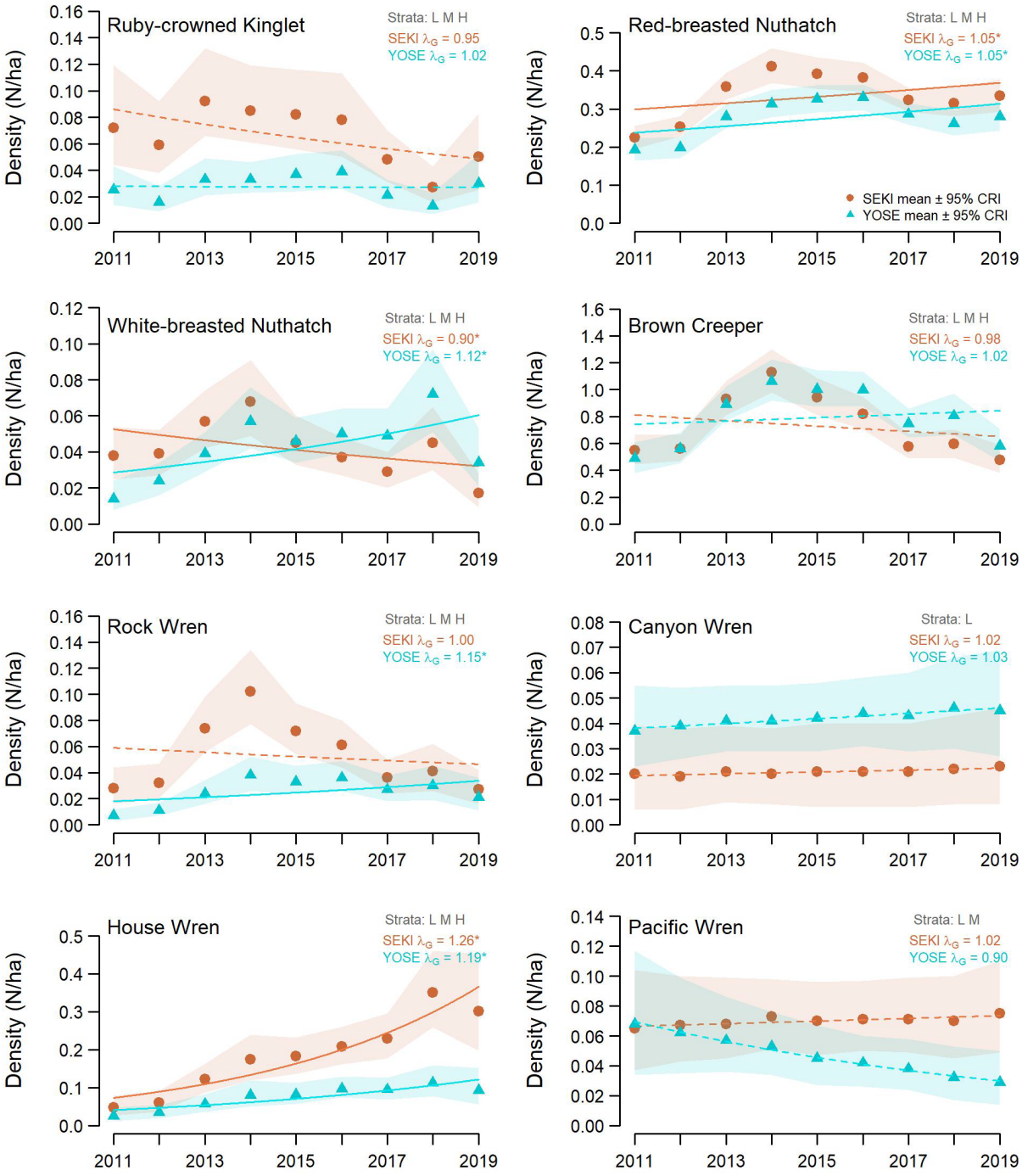


Figure 5d. Population density estimates by park for Ruby-crowned Kinglet, Red-breasted Nuthatch, White-breasted Nuthatch, Brown Creeper, Rock Wren, Canyon Wren, House Wren and Pacific Wren, derived using a hierarchical analysis of point counts from Sequoia and Kings Canyon National Parks (SEKI) and Yosemite National Park (YOSE). Strata included in each model are listed as low (L), medium (M) and/or high (H) elevation (Table 1). Smoothed trends in population growth (curves) and geometric mean population growth rates (λ_G values) are reported for each species and park analyzed. Solid curves and asterisks indicate strongly supported trends for which the 95% credible interval on λ_G did not overlap 1. Species are listed in taxonomic order (Table 4).

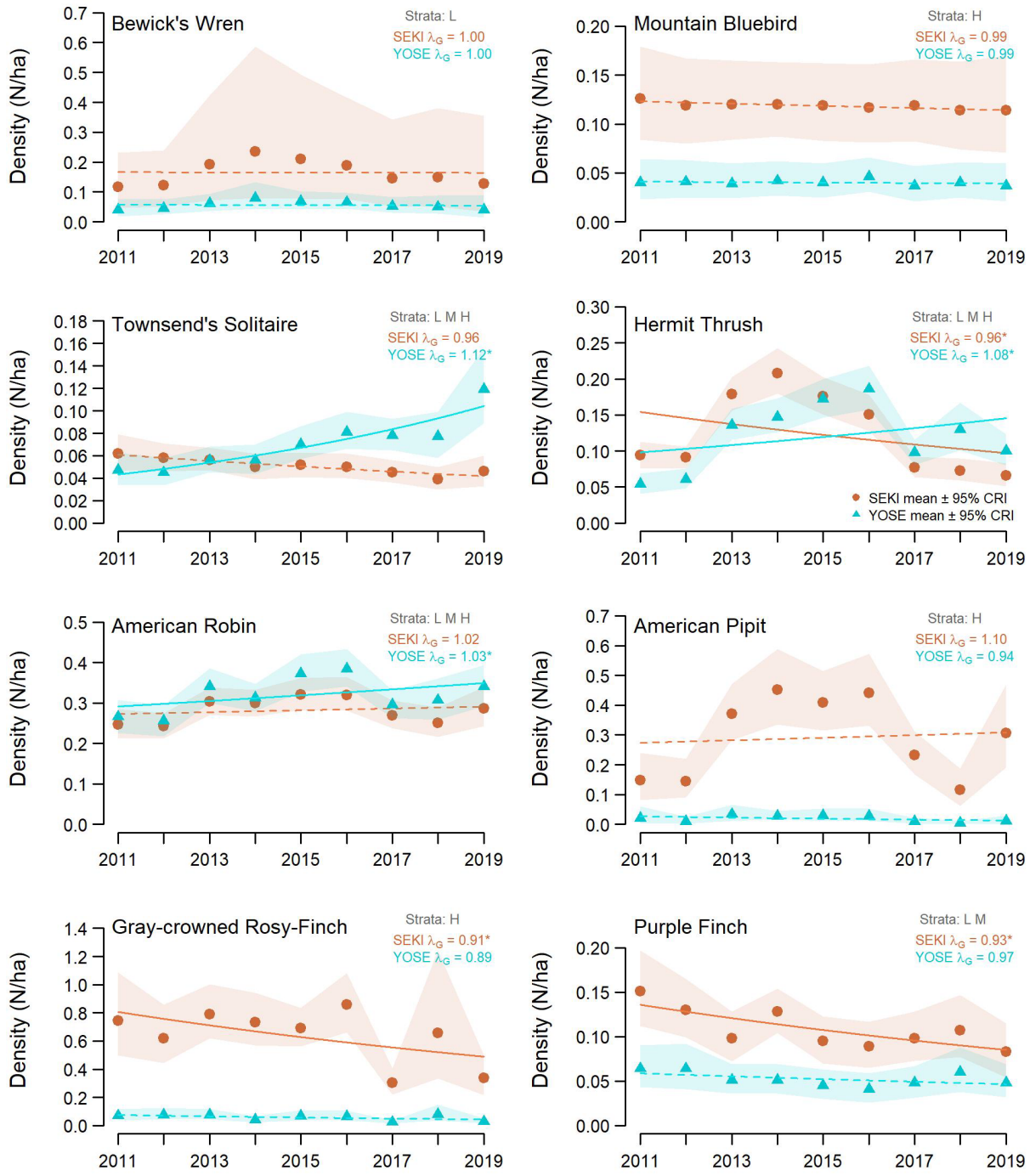


Figure 5e. Population density estimates by park for Bewick's Wren, Mountain Bluebird, Townsend's Solitaire, Hermit Thrush, American Robin, American Pipit, Gray-crowned Rosy-Finch and Purple Finch, derived using a hierarchical analysis of point counts from Sequoia and Kings Canyon National Parks (SEKI) and Yosemite National Park (YOSE). Strata included in each model are listed as low (L), medium (M) and/or high (H) elevation (Table 1). Smoothed trends in population growth (curves) and geometric mean population growth rates (λ_G values) are reported for each species and park analyzed. Solid curves and asterisks indicate strongly supported trends for which the 95% credible interval on λ_G did not overlap 1. Species are listed in taxonomic order (Table 4).

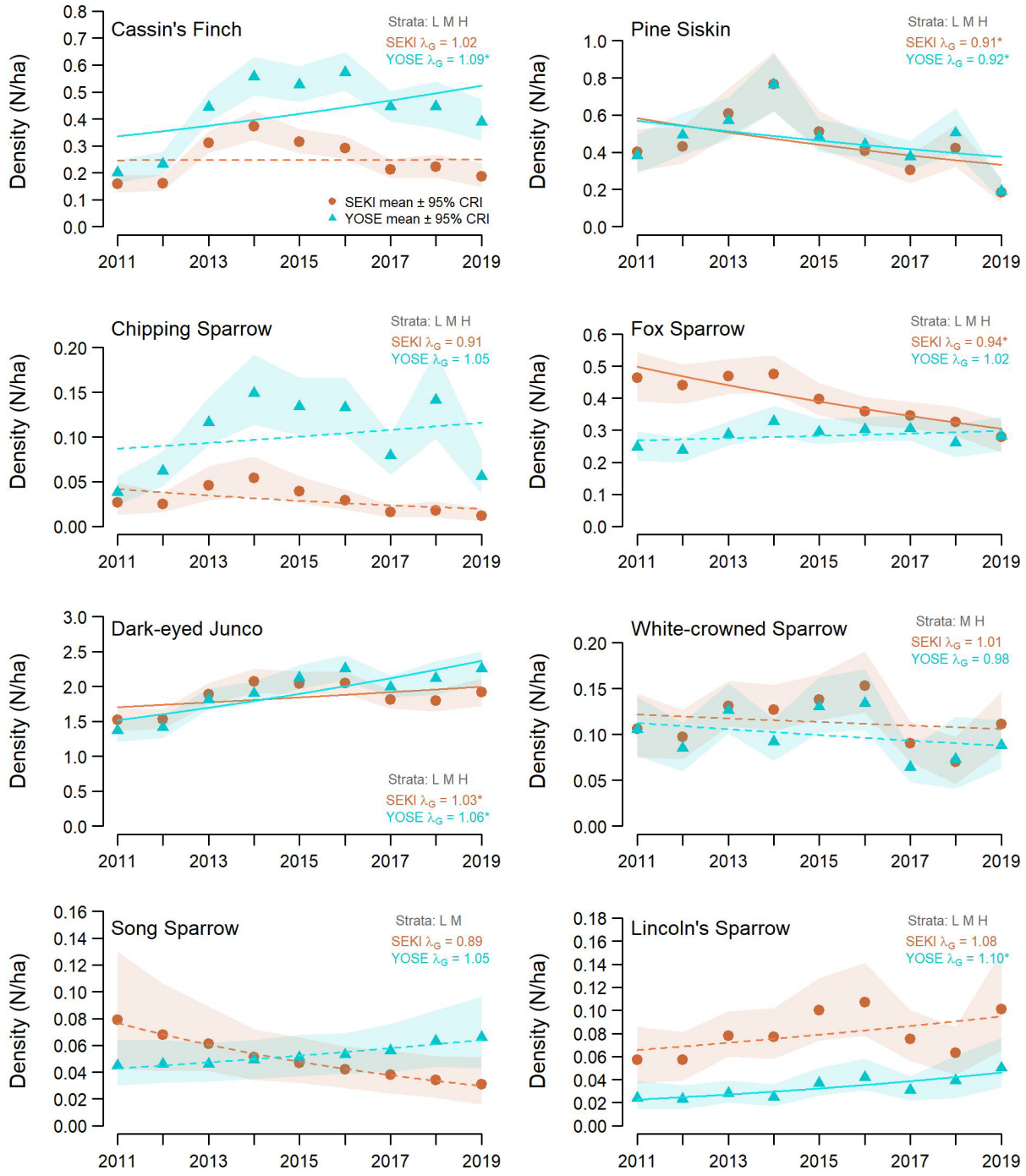


Figure 5f. Population density estimates by park for Cassin's Finch, Pine Siskin, Chipping Sparrow, Fox Sparrow, Dark-eyed Junco, White-crowned Sparrow, Song Sparrow and Lincoln's Sparrow, derived using a hierarchical analysis of point counts from Sequoia and Kings Canyon National Parks (SEKI) and Yosemite National Park (YOSE). Strata included in each model are listed as low (L), medium (M) and/or high (H) elevation (Table 1). Smoothed trends in population growth (curves) and geometric mean population growth rates (λ_G values) are reported for each species and park analyzed. Solid curves and asterisks indicate strongly supported trends for which the 95% credible interval on λ_G did not overlap 1. Species are listed in taxonomic order (Table 4).

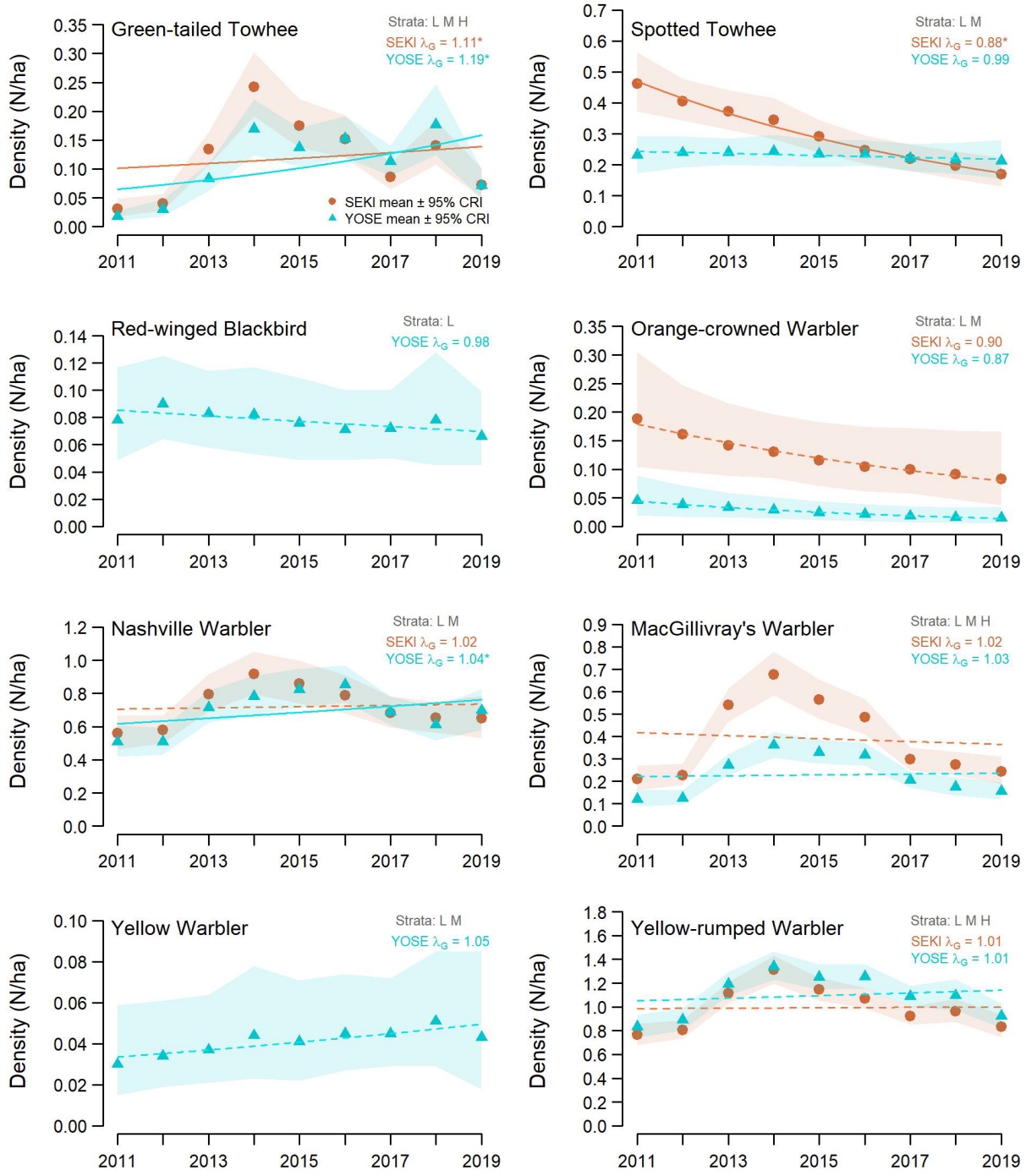


Figure 5g. Population density estimates by park for Green-tailed Towhee, Spotted Towhee, Red-winged Blackbird, Orange-crowned Warbler, Nashville Warbler, MacGillivray's Warbler, Yellow Warbler and Yellow-rumped Warbler, derived using a hierarchical analysis of point counts from Sequoia and Kings Canyon National Parks (SEKI) and Yosemite National Park (YOSE). Strata included in each model are listed as low (L), medium (M) and/or high (H) elevation (Table 1). Smoothed trends in population growth (curves) and geometric mean population growth rates (λ_G values) are reported for each species and park analyzed. Solid curves and asterisks indicate strongly supported trends for which the 95% credible interval on λ_G did not overlap 1. Species are listed in taxonomic order (Table 4).

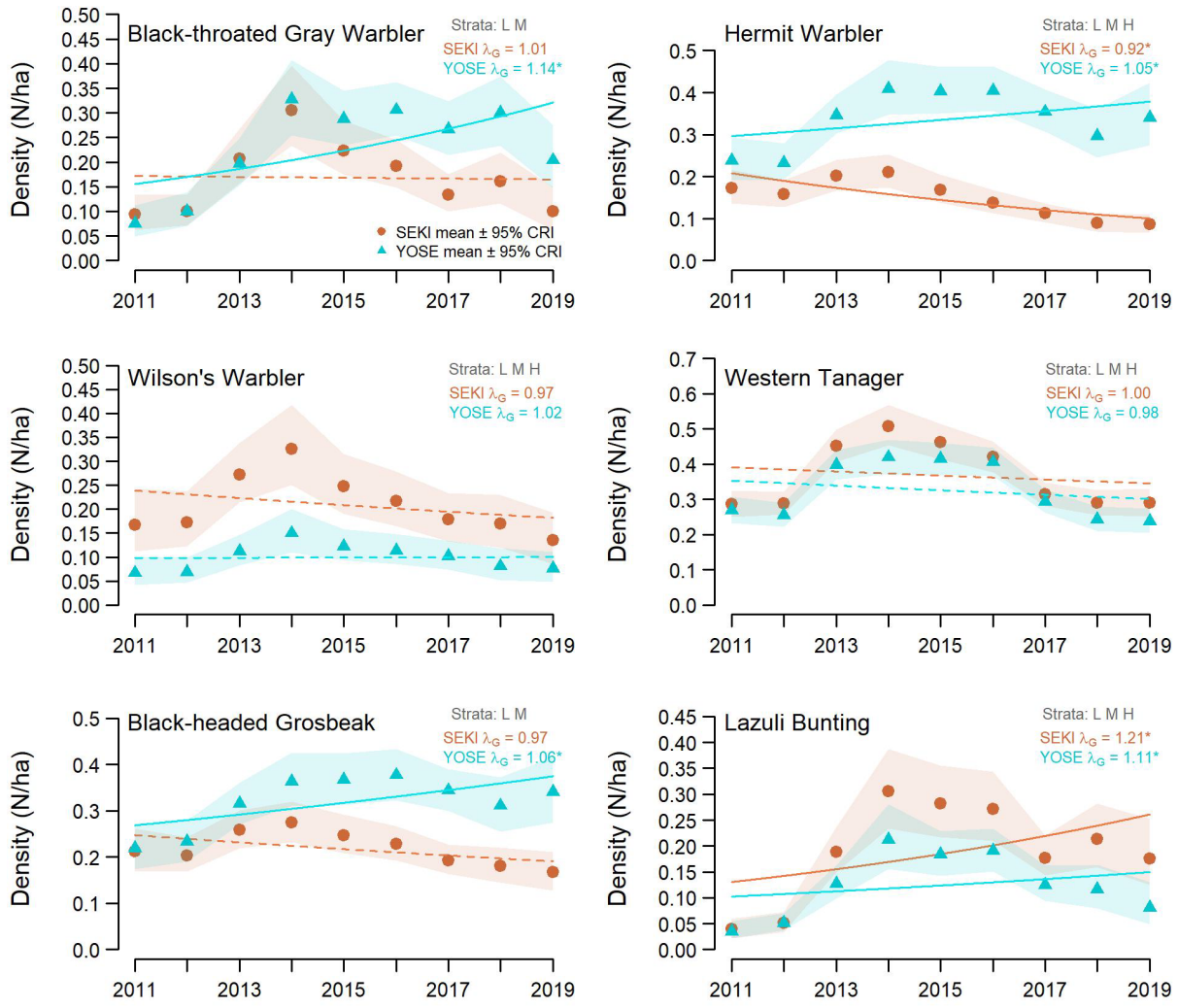


Figure 5h. Population density estimates by park for Black-throated Gray Warbler, Hermit Warbler, Wilson's Warbler, Western Tanager, Black-headed Grosbeak and Lazuli Bunting, derived using a hierarchical analysis of point counts from Sequoia and Kings Canyon National Parks (SEKI) and Yosemite National Park (YOSE). Strata included in each model are listed as low (L), medium (M) and/or high (H) elevation (Table 1). Smoothed trends in population growth (curves) and geometric mean population growth rates (λ_G values) are reported for each species and park analyzed. Solid curves and asterisks indicate strongly supported trends for which the 95% credible interval on λ_G did not overlap 1. Species are listed in taxonomic order (Table 4).

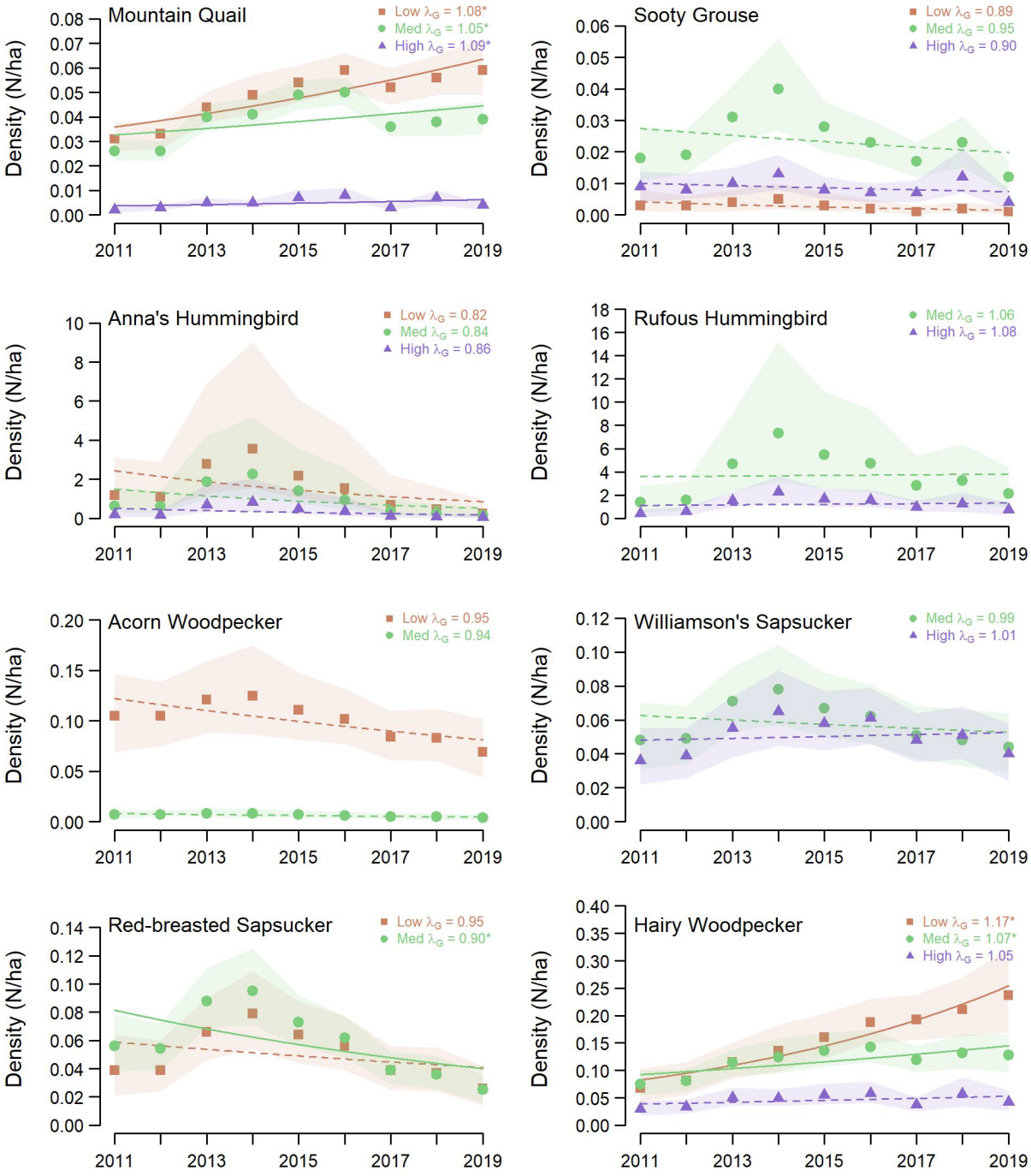


Figure 6a. Population density estimates by elevational stratum for Mountain Quail, Sooty Grouse, Anna's Hummingbird, Rufous Hummingbird, Acorn Woodpecker, Williamson's Sapsucker, Red-breasted Sapsucker and Hairy Woodpecker, derived using a hierarchical analysis of point counts from Sequoia and Kings Canyon National Parks and Yosemite National Park. Smoothed trends in population growth (curves) and geometric mean population growth rates (λ_G values) are reported for each species and stratum analyzed. Solid curves and asterisks indicate strongly supported trends for which the 95% credible interval on λ_G did not overlap 1. Species are listed in taxonomic order (Table 4). Elevational ranges for Low, Medium and High strata differ slightly by park (Table 1).

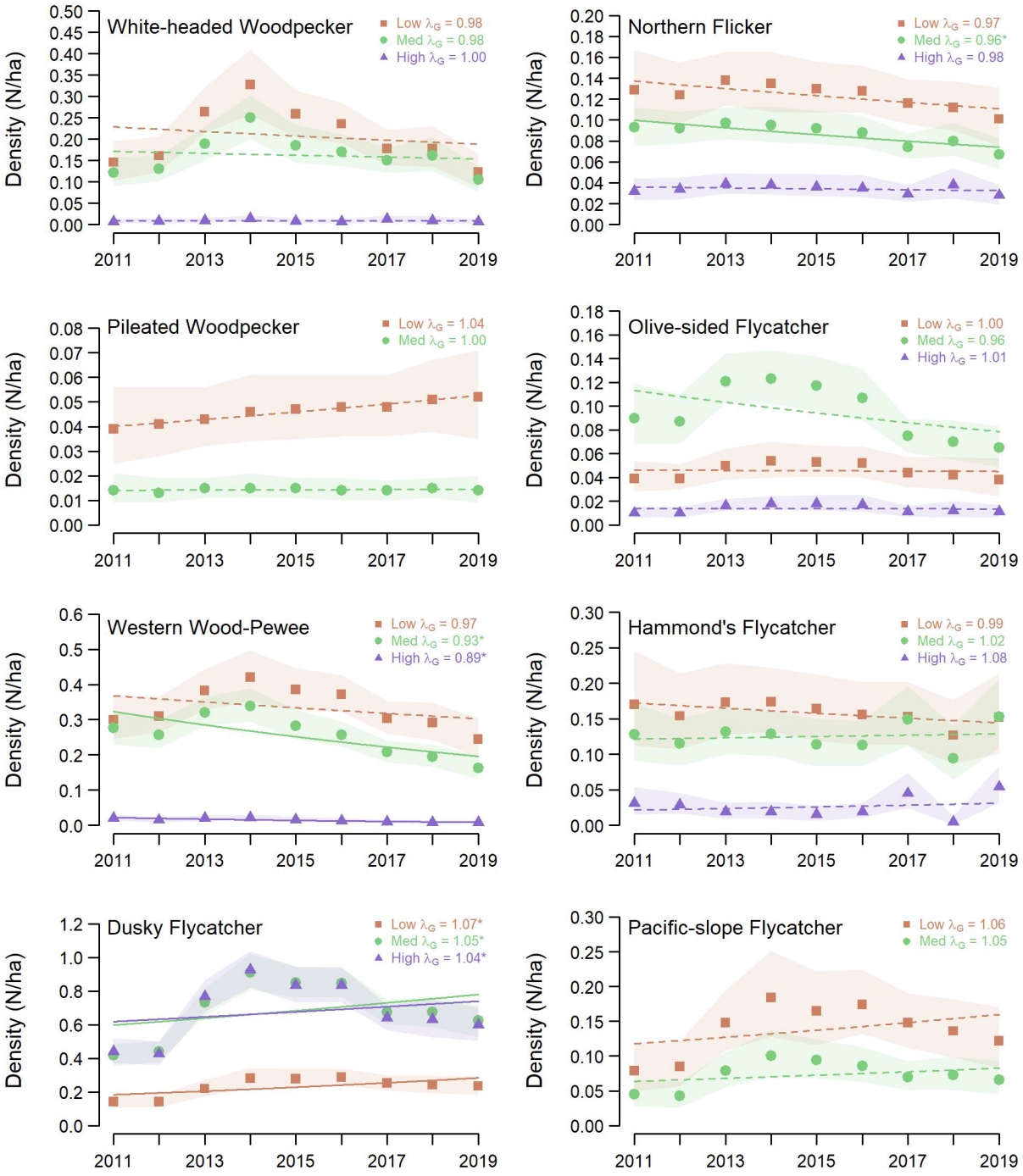


Figure 6b. Population density estimates by elevational stratum for White-headed Woodpecker, Northern Flicker, Pileated Woodpecker, Olive-sided Flycatcher, Western Wood-Pewee, Hammond's Flycatcher, Dusky Flycatcher and Pacific-slope Flycatcher, derived using a hierarchical analysis of point counts from Sequoia and Kings Canyon National Parks and Yosemite National Park. Smoothed trends in population growth (curves) and geometric mean population growth rates (λ_G values) are reported for each species and stratum analyzed. Solid curves and asterisks indicate strongly supported trends for which the 95% credible interval on λ_G did not overlap 1. Species are listed in taxonomic order (Table 4). Elevational ranges for Low, Medium and High strata differ slightly by park (Table 1).

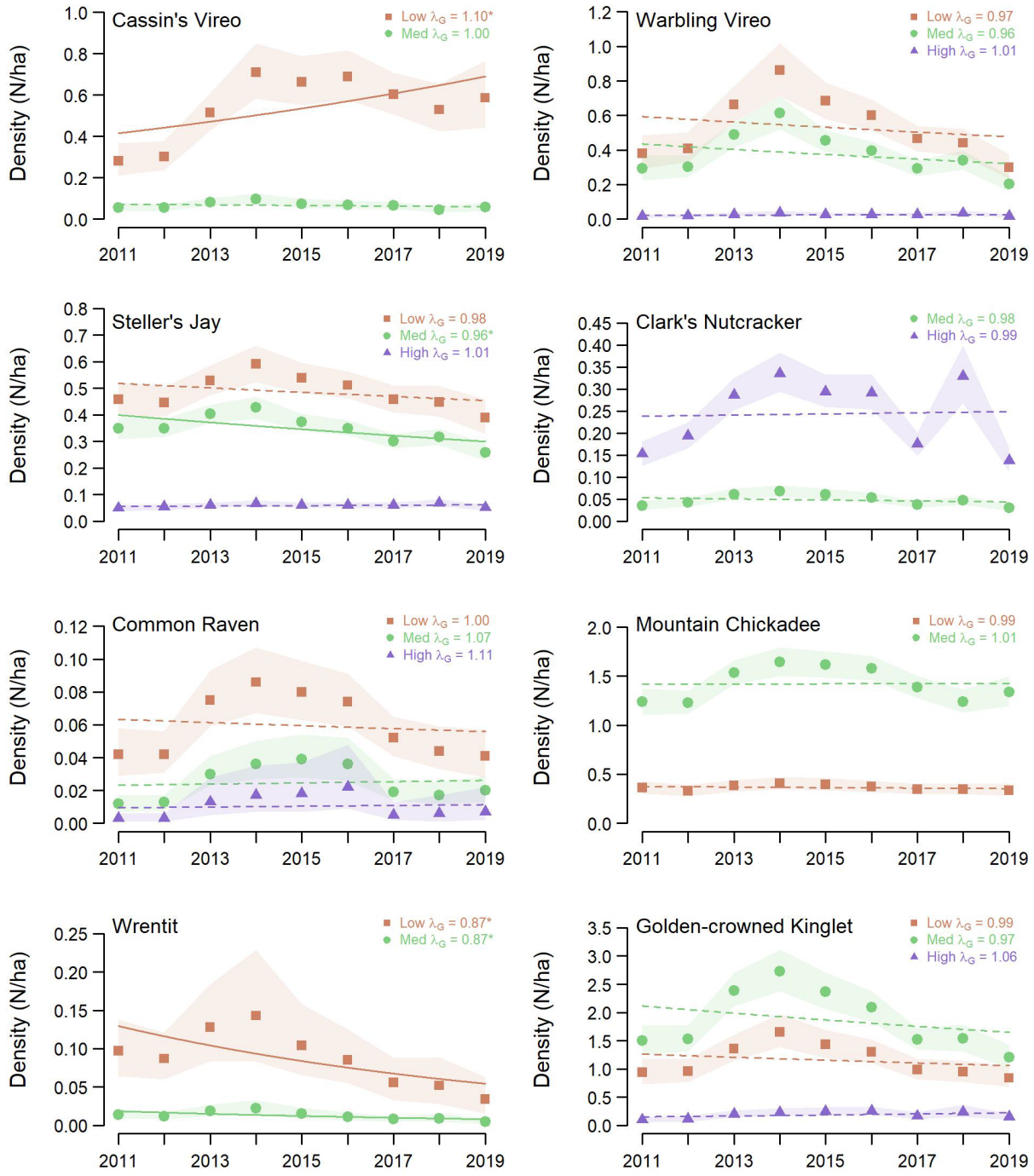


Figure 6c. Population density estimates by elevational stratum for Cassin's Vireo, Warbling Vireo, Steller's Jay, Clark's Nutcracker, Common Raven, Mountain Chickadee, Wrentit and Golden-crowned Kinglet, derived using a hierarchical analysis of point counts from Sequoia and Kings Canyon National Parks and Yosemite National Park. Smoothed trends in population growth (curves) and geometric mean population growth rates (λ_G values) are reported for each species and stratum analyzed. Solid curves and asterisks indicate strongly supported trends for which the 95% credible interval on λ_G did not overlap 1. Species are listed in taxonomic order (Table 4). Elevational ranges for Low, Medium and High strata differ slightly by park (Table 1).

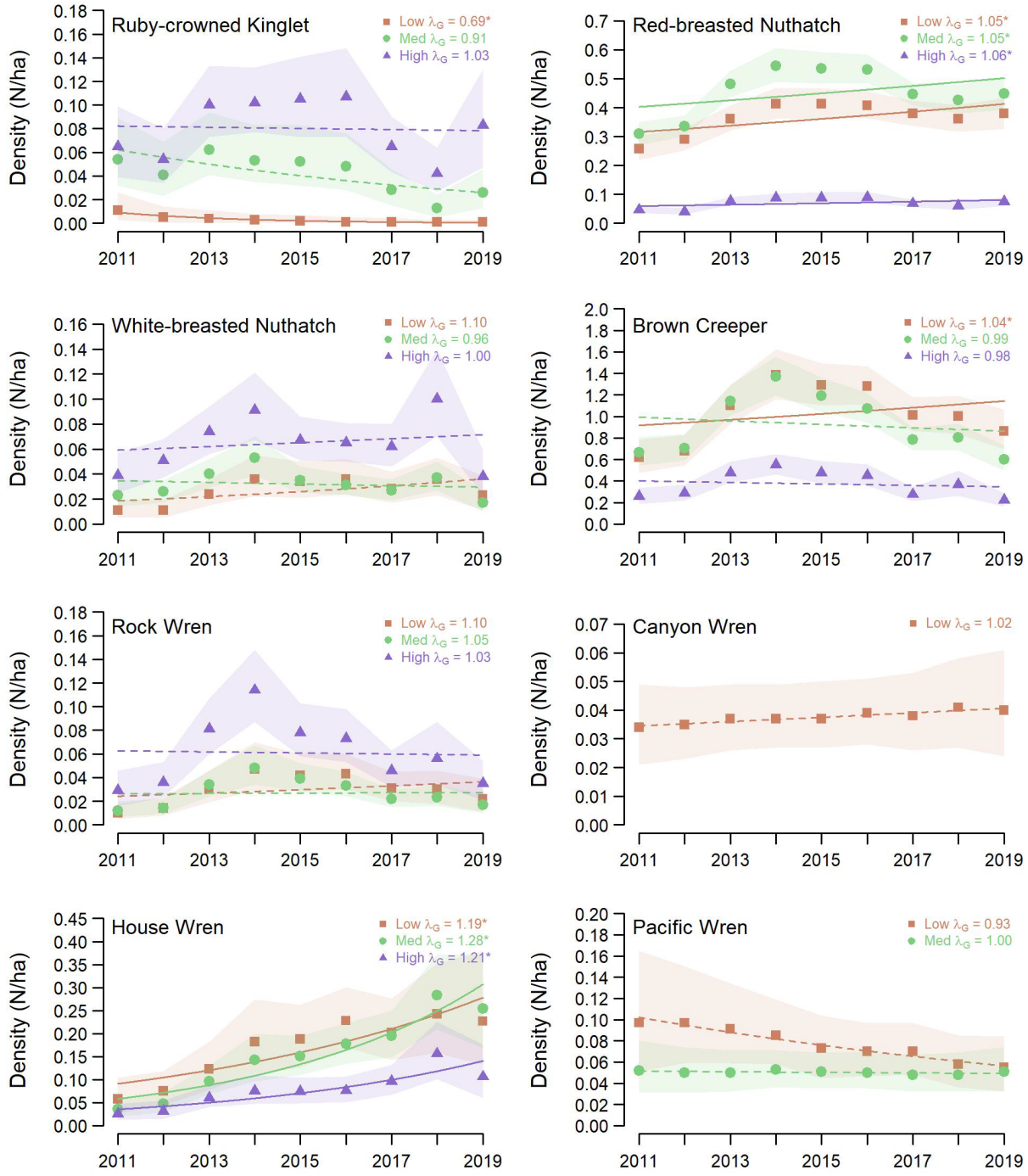


Figure 6d. Population density estimates by elevational stratum for Ruby-crowned Kinglet, Red-breasted Nuthatch, White-breasted Nuthatch, Brown Creeper, Rock Wren, Canyon Wren, House Wren and Pacific Wren, derived using a hierarchical analysis of point counts from Sequoia and Kings Canyon National Parks and Yosemite National Park. Smoothed trends in population growth (curves) and geometric mean population growth rates (λ_G values) are reported for each species and stratum analyzed. Solid curves and asterisks indicate strongly supported trends for which the 95% credible interval on λ_G did not overlap 1. Species are listed in taxonomic order (Table 4). Elevational ranges for Low, Medium and High strata differ slightly by park (Table 1).

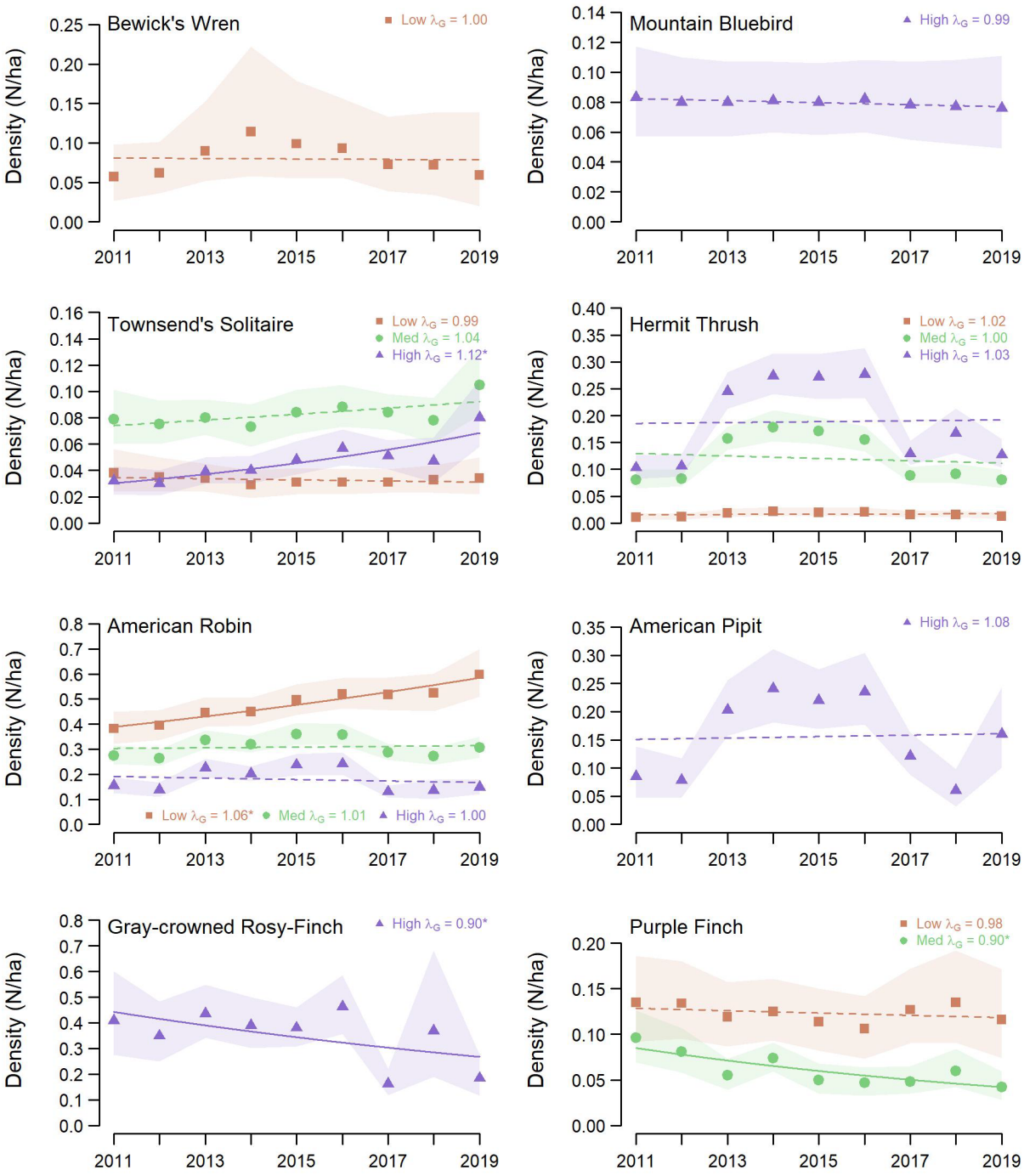


Figure 6e. Population density estimates by elevational stratum for Bewick's Wren, Mountain Bluebird, Townsend's Solitaire, Hermit Thrush, American Robin, American Pipit, Gray-crowned Rosy-Finch and Purple Finch, derived using a hierarchical analysis of point counts from Sequoia and Kings Canyon National Parks and Yosemite National Park. Smoothed trends in population growth (curves) and geometric mean population growth rates (λ_G values) are reported for each species and stratum analyzed. Solid curves and asterisks indicate strongly supported trends for which the 95% credible interval on λ_G did not overlap 1. Species are listed in taxonomic order (Table 4). Elevational ranges for Low, Medium and High strata differ slightly by park (Table 1).

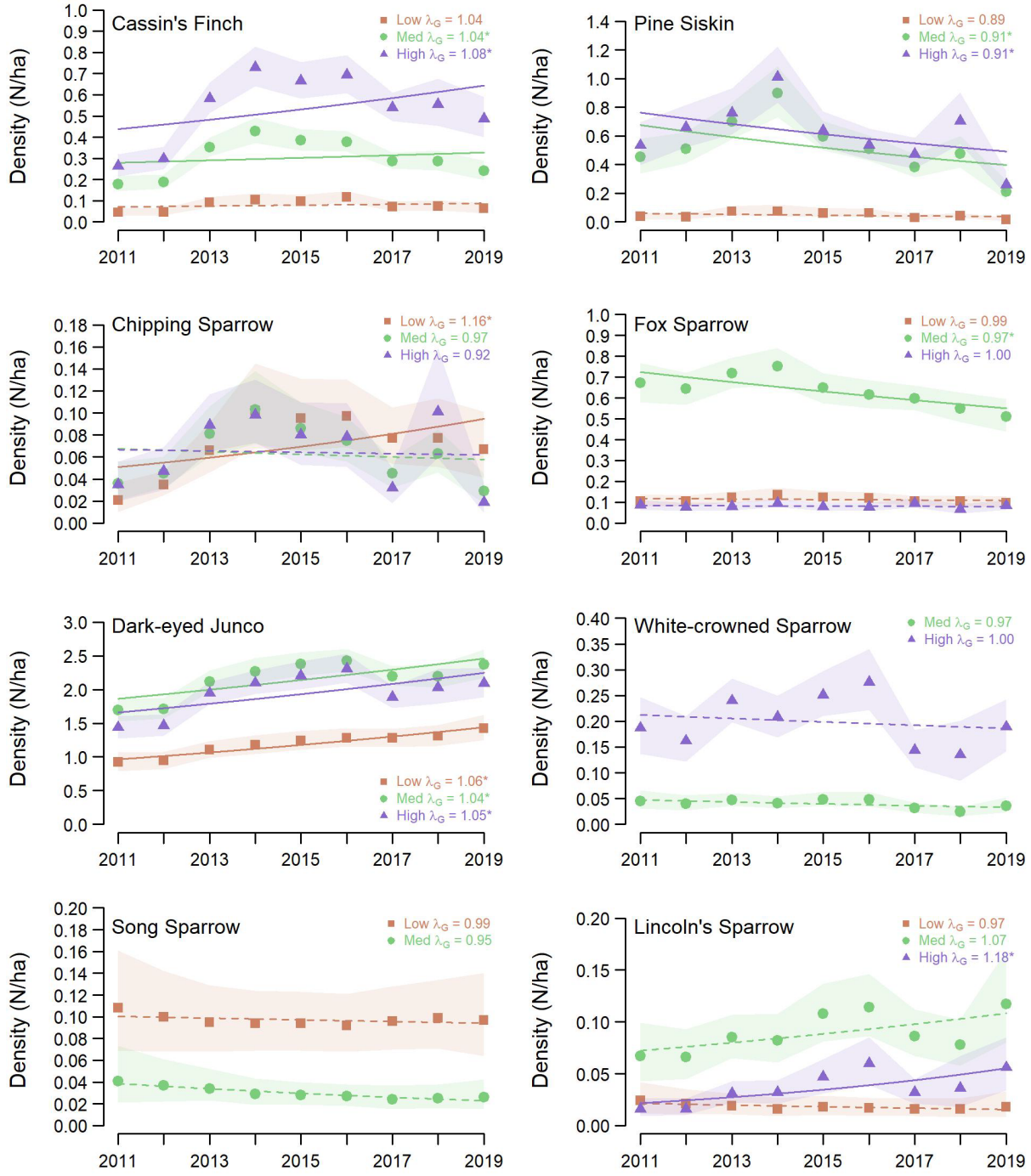


Figure 6f. Population density estimates by elevational stratum for Cassin's Finch, Pine Siskin, Chipping Sparrow, Fox Sparrow, Dark-eyed Junco, White-crowned Sparrow, Song Sparrow and Lincoln's Sparrow, derived using a hierarchical analysis of point counts from Sequoia and Kings Canyon National Parks and Yosemite National Park. Smoothed trends in population growth (curves) and geometric mean population growth rates (λ_G values) are reported for each species and stratum analyzed. Solid curves and asterisks indicate strongly supported trends for which the 95% credible interval on λ_G did not overlap 1. Species are listed in taxonomic order (Table 4). Elevational ranges for Low, Medium and High strata differ slightly by park (Table 1).

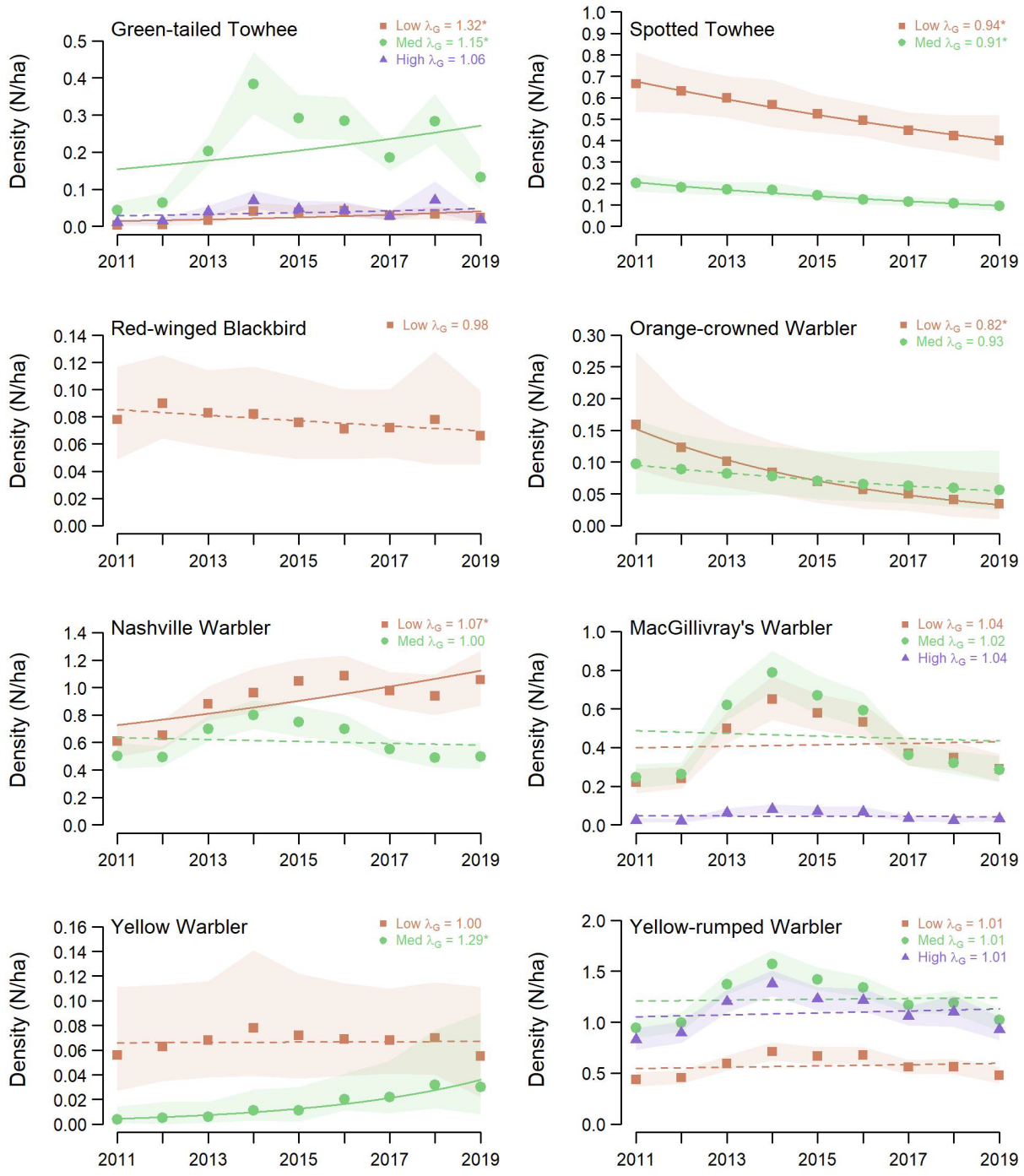


Figure 6g. Population density estimates by elevational stratum for Green-tailed Towhee, Spotted Towhee, Red-winged Blackbird, Orange-crowned Warbler, Nashville Warbler, MacGillivray's Warbler, Yellow Warbler and Yellow-rumped Warbler, derived using a hierarchical analysis of point counts from Sequoia and Kings Canyon National Parks and Yosemite National Park. Smoothed trends in population growth (curves) and geometric mean population growth rates (λ_G values) are reported for each species and stratum analyzed. Solid curves and asterisks indicate strongly supported trends for which the 95% credible interval on λ_G did not overlap 1. Species are listed in taxonomic order (Table 4). Elevational ranges for Low, Medium and High strata differ slightly by park (Table 1).

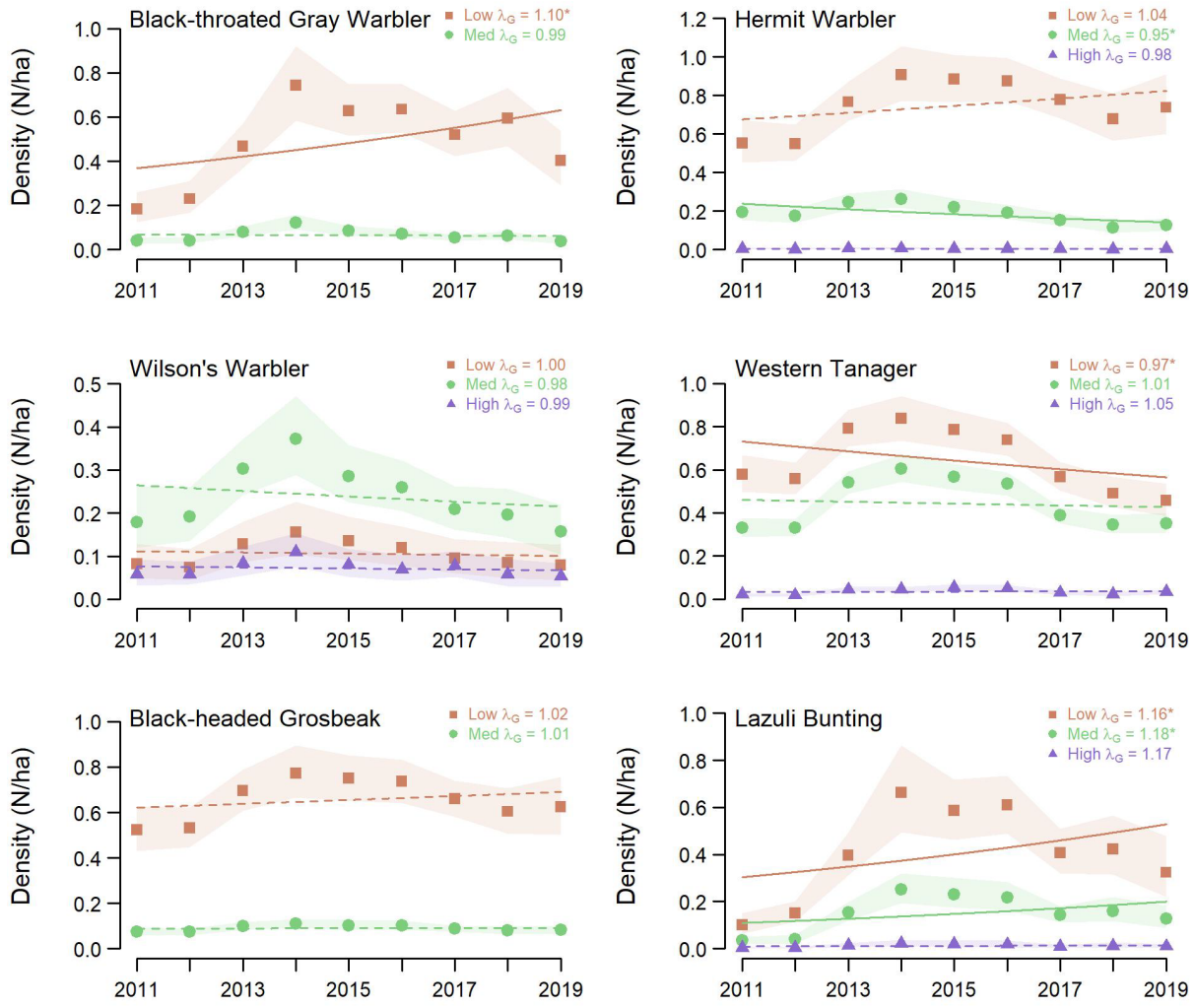


Figure 6h. Population density estimates by elevational stratum for Black-throated Gray Warbler, Hermit Warbler, Wilson's Warbler, Western Tanager, Black-headed Grosbeak and Lazuli Bunting, derived using a hierarchical analysis of point counts from Sequoia and Kings Canyon National Parks and Yosemite National Park. Smoothed trends in population growth (curves) and geometric mean population growth rates (λ_G values) are reported for each species and stratum analyzed. Solid curves and asterisks indicate strongly supported trends for which the 95% credible interval on λ_G did not overlap 1. Species are listed in taxonomic order (Table 4). Elevational ranges for Low, Medium and High strata differ slightly by park (Table 1).

Trends in park-specific (Figures 5a-h) or stratum-specific (Figures 6a-h) population density were derived from the same set of final models (Table 5). Differences in density were often evident by park and by stratum in part because the models generally included park and elevation effects, and also due to other fixed and random effects that allowed summaries of density at the park and stratum level to differ even if park and elevation effects were not modeled.

Model scope, like model parameters, also varied among species in our final models. Some species were rarely or never detected in one park or in one or two elevational strata, suggesting that our scope of inference should be restricted to the park and/or strata used more commonly. Low detections in a park or stratum also tended to interfere with the convergence of parameter estimates. In these cases, we excluded data from the park, stratum or strata where detections were low, and we consider the scope of inference for that population to be reduced to the area for which the model was parameterized. Park-specific trends in Figures 5a-h were based on data from both parks in almost every case, with just two exceptions: we dropped SEKI data from models for Red-winged Blackbird and Yellow Warbler (Figure 5g), which were detected in SEKI just 27 and 33 times, respectively. Our model of Red-winged Blackbird was further restricted to data from YOSE's low-elevation stratum (Table 1), where 240 of 251 individuals were detected. Patterns of effort-corrected detection by park and stratum (Appendix 4) can suggest direct and interaction effects of park, stratum and year on the abundance of each species, and were used to guide model scope and parameter reduction if the fit or convergence of the full model was inadequate. Model scope is indicated in Figure 5 by the park(s) and strata named in the upper right-hand corner of each panel, where 'Strata: L M H' indicates that data from all strata (Low, Medium, and High) were included in the model of population density.

Trends in population density estimated for the larger parks were based on counts from all three elevational strata in the majority (37 of 62) of cases. Species modeled only in the High stratum were Mountain Bluebird, American Pipit and Gray-crowned Rosy Finch, while those modeled only in the Low stratum were Canyon Wren, Bewick's Wren and Red-winged Blackbird. Five species rarely or never detected in the Low stratum were modeled across only Medium and High strata: Rufous Hummingbird, Williamson's Sapsucker, Clark's Nutcracker and White-crowned Sparrow. Fifteen species rarely or never detected in the High stratum were modeled across only Medium and Low strata: Acorn Woodpecker, Red-breasted Sapsucker, Pileated Woodpecker, Pacific-slope Flycatcher, Cassin's Vireo, Wrentit, Pacific Wren, Purple Finch, Song Sparrow, Spotted Towhee, Orange-crowned Warbler, Nashville Warbler, Yellow Warbler, Black-throated Gray Warbler and Black-headed Grosbeak. Counts by park and stratum used in these determinations appear in Appendix 4.

After scoping models appropriately, 45 park-level trends were supported across the monitoring period, including 26 positive and 19 negative trends (Figures 5a-h). Support for each trend was determined by the 95% credible interval on the geometric mean growth in population density, λ_G, described above as a suitable metric of trend for time series with serial correlation. Smoothed growth curves based on Poisson regression are also shown in Figures 5a-h, as in Figure 4, with solid curves indicating support based on λ_G. The total number of supported trends was similar between SEKI (23) and YOSE (22), but the general direction of trends contrasted between parks, with six positive and 17 negative trends in SEKI as compared with 20 positive and two negative trends in YOSE. Two species exhibited a negative trend in density across both parks: declines in both Western Wood-Pewee and Pine Siskin were supported in models with the broadest scope of inference (applying to both parks and all three elevational strata). Six species exhibited a positive trend across both parks: increasing densities of Dusky Flycatcher, Red-breasted Nuthatch, House Wren, Dark-eyed Junco, Green-tailed Towhee and Lazuli Bunting were all supported in models with the broadest scope. Three species

declined in SEKI while increasing in YOSE: White-breasted Nuthatch, Hermit Thrush and Hermit Warbler exhibited contrasting trends across parks in models with the broadest scope. The remaining 51 species exhibited a supported trend in only one park (23) or in neither park (28). Thus, in nearly half of the species analyzed, park-level trends in population density were not supported.

Trends in population density supported at the level of each elevational stratum (Figures 6a-h) were more often increasing (32) than decreasing (17), and increasing trends were more common in Low (14) than in Medium (10) or High strata (8), while decreasing trends were more common in Medium (10) than Low (5) or High strata (2). Stratum-level trends were summarized across both parks for each species analyzed, except the YOSE-specific trends for Red-winged Blackbird and Yellow Warbler.

Of the 62 species analyzed, 30 exhibited no supported trend in any elevational stratum; 21 exhibited a supported trend in just one stratum (10 species with positive and 11 with negative trends); six exhibited supported trends in each of two strata (three species with paired positive and three with paired negative trends); and five species exhibited supported trends in all three strata (Mountain Quail, Dusky Flycatcher, Red-breasted Nuthatch, House Wren and Dark-eyed Junco). No species exhibited support for trends that differed in direction across strata (positive growth in one stratum and negative in another). Of 27 species with supported trends in just one or two strata, model scope was limited to those strata in three cases (Wrentit, Gray-crowned Rosy Finch and Spotted Towhee), and in two of those cases the species declined across all strata analyzed: Gray-crowned Rosy Finch in the High stratum (Figure 6e) and Spotted Towhee in Medium and Low strata (Figure 6g).

For the two species declining in density across both parks, stratum-level declines were supported in two of three strata; however, Western Wood-Pewee decline was not supported in the stratum in which it achieved highest population density (Figure 6b), while declines in Pine Siskin included both strata with higher population density (Figure 6f). For the six species increasing in density across both parks, four were also increasing across all three elevational strata (Dusky Flycatcher, Red-breasted Nuthatch, House Wren and Dark-eyed Junco), and two (Green-tailed Towhee and Lazuli Bunting) were increasing in two of three strata, including strata associated with higher population densities.

Park-specific or stratum-specific trends can dominate the overall trend in population growth, depending on the relative strength of trends and population size within each park or stratum. When estimates of population density were summarized at the largest scale in this analysis (across all strata in both large parks), negative trends were supported for 10 species and positive trends were supported for 14 species (Appendix 5). Species declining at this scale were Red-breasted Sapsucker, Western Wood-Pewee, Steller's Jay, Wrentit, Gray-crowned Rosy Finch, Purple Finch, Pine Siskin, Fox Sparrow, Spotted Towhee and Orange-crowned Warbler, while species increasing at this scale were Mountain Quail, Hairy Woodpecker, Dusky Flycatcher, Cassin's Vireo, Red-breasted Nuthatch, House Wren, Townsend's Solitaire, American Robin, Cassin's Finch, Dark-eyed Junco, Lincoln's Sparrow, Green-tailed Towhee, Black-throated Gray Warbler and Lazuli Bunting. Regardless of the scale of our analysis, more species were increasing than decreasing during 2011–2019. However, more declines were revealed by summarizing estimates across strata and parks, illustrating how stronger trends in one area can dominate weaker trends in another. For example, while 10 species

declined at the largest scale of analysis, just two species declined across both SEKI and YOSE based on park-specific trends (Western Wood-Pewee and Pine Siskin), and again just two species declined across all species-relevant elevational strata in the analysis based on stratum-specific trends (Gray-crowned Rosy Finch and Spotted Towhee). Note that trends shown in Appendix 5 were derived from the same final models as those in Figures 5a-h and 6a-h.

Notes on model development

The trends in Figures 4–6 (and Appendix 5) represent only the final models fitted to data for each species in each park and stratum. Especially in the larger parks, additional models were fitted to the data for many species during development of the final models. To explore effects on model fit and convergence of parameter estimates, we added fixed effects of slope, aspect and forest presence to the sub-model of abundance; added fixed or random effects of year, day and forest presence to detection sub-models; and dropped the random effect of observer. The only appreciable improvements we discovered are outlined here. One improvement involved models for Song Sparrow in the larger parks, which had failed to converge even when the detection model fit well and even after reducing the scope of inference to Low and Medium strata where most Song Sparrows were detected. Climate-related covariates of the sub-model of abundance, as described in Table 5, appeared to have no effect in preliminary models for this species, and there remained a source of variation in abundance not addressed by the full model. Reviewing the covariates at hand, we noticed a strong relationship between slope and Song Sparrow count. Adding slope as an effect on abundance successfully modeled the excess variation, allowing all parameter estimates to converge and revealing effects of climate not previously evident. There was a negative relationship between Song Sparrow count and slope (steepness of terrain within 90 m of the count station), which translated into a negative effect of slope on Song Sparrow abundance in our hierarchical model. Slope was also related to count in many other species we analyzed; however, no other species required the addition of slope to the full or reduced model (Table 5) in order to achieve convergence of parameter estimates. In general, the full model addressed most sources of variation in species counts, and variation involving non-focal, so-called ‘nuisance’ effects was reduced by survey design. Effects of day and hour were minimized by conducting surveys during peak days and hours of conspicuous breeding behavior, and observer effects were minimized through training. For most populations in the larger parks, model fit was adequate when a random observer effect was included in the detection model. We tested this formula in several cases by removing the observer effect, with mostly poor results except in the case of Rufous Hummingbird. Hummingbird detection is often facilitated by their attraction to observers, and perhaps this behavior negated any observer effect on detection of this species. Note, however, that a random observer effect was retained in our model for Anna’s Hummingbird (Table 5). In general, including a random observer effect essentially introduced a year effect on detection due to substantial annual turnover in observers. We modeled detection as a function of multiple variables whenever possible, to reduce our chances of finding spurious trends in abundance that might be due to temporal variation in detection. Overall, however, addition and exclusion of model parameters had relatively small effects on model fit. Much larger improvements were often gained by adjusting model scope to avoid ‘fitting the noise’ in areas with low detections. Finally, it is important to note that when the full model failed to fit we at least assessed the stability of parameter estimates across ‘distinct’ models, defined here as those that differed by more than one

parameter. We have presented results here only from models with adequate fit or from those resulting in similar density estimates and trends across multiple distinct models.

Covariates of abundance

Despite the predominance of positive trends in population density estimated for these parks (Figures 4–6 and Appendix 5), the fixed effect of *year* was often negative in our models, and was overwhelmingly negative in models fitted to data from the larger parks (Appendix 6). Although negative effects of *year* were only slightly more common than positive ones in DEPO (Figure 7, left-hand panel), in the larger parks 55 of 62 *year* effects were negative, and over half (36) of those negative effects were supported (Figure 7, right-hand panel). No positive effects of *year* were supported for any species in our analyses of combined data from the larger parks (Table A6-2). However, the full effect of *year* was spread across several interaction effects (Table 5), including at least one that compensated somewhat for the negative effects of *year* alone: although both *year* and *park* effects were mainly negative (Appendix 6), *year*-by-*park* effects were mainly positive (Appendix 7). The positive effect of the *year*-by-*park* interaction highlighted the tendency for population densities in YOSE (coded as *park* = 2) to increase during the monitoring period, often beginning lower and ending higher than densities in SEKI (*park* = 1), a pattern that was well-supported for 19 species (Figure 5, Table A7-1). Thus, the negative effects of both *year* and *park* were curbed somewhat by their interaction effect.

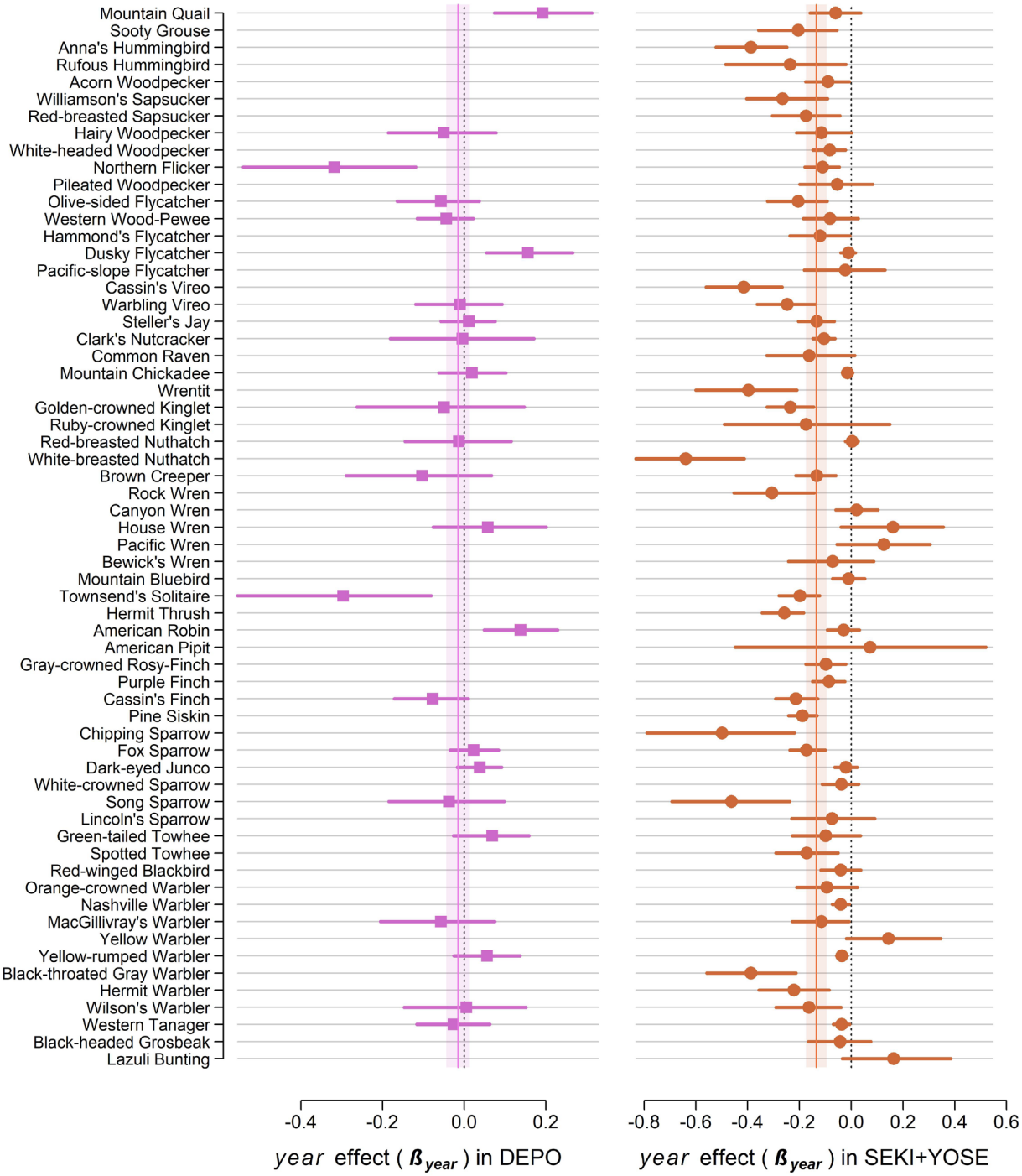


Figure 7. Effects of *year* in hierarchical models of avian abundance based on breeding-season point counts conducted annually during 2011–2014 and 2016–2019. Years 2011–2019 were coded as 1–9 in multiple-regression sub-models of abundance (Tables 5 and 6). Means and 95% credible intervals are shown for the coefficient of *year* from data on each of 25 species surveyed in Devils Postpile National Monument (DEPO, squares) and 62 species surveyed across Sequoia and Kings Canyon National Parks and Yosemite National Park (SEKI+YOSE, dots). Solid vertical lines and shading indicate grand means and 95% confidence intervals for effects across species. Species are listed in taxonomic order (Table 4).

Although data from a majority (37) of the species analyzed in the larger parks supported the estimation of all interaction effects considered in the full model (Table 5), there was only weak support for two of the four interactions (Appendix A7). The *year*-by-*elev* effect on abundance was supported for only 12 species, with three positive and nine negative effects (Table A7-1), suggesting little evidence that trends in population density varied by elevation in any concerted way across these taxa. The three-way interaction of *park*, *elev* and *year* was supported by even fewer populations, including just six positive effects and one negative effect (Table A7-2). In contrast, there was support across 19 species for the uniformly positive *year*-by-*park* interaction mentioned above, and support across 24 species for a mainly negative *park*-by-*elev* effect (Table A7-2) that suggested lower densities for some species at higher elevations in YOSE relative to other areas surveyed.

Both linear and nonlinear effects of elevation were supported for many species across the larger parks (Figure 8, Appendix 8). Positive effects of *elev* were supported for 14 species, while negative effects were supported for 21 species, suggesting that abundance increased with elevation for nearly one-quarter of the species analyzed and declined with elevation for over one-third of the species analyzed. Although there were more negative than positive effects of *elev*, positive effects tended to be larger, such that the grand mean effect of *elev* across species was centered on zero (Figure 8). Quadratic effects of elevation were supported for nearly two-thirds (39) of the species analyzed, and all of these effects were negative (Figure 8, Table A8-1), suggesting that densities peaked at some intermediate elevation for many of these species.

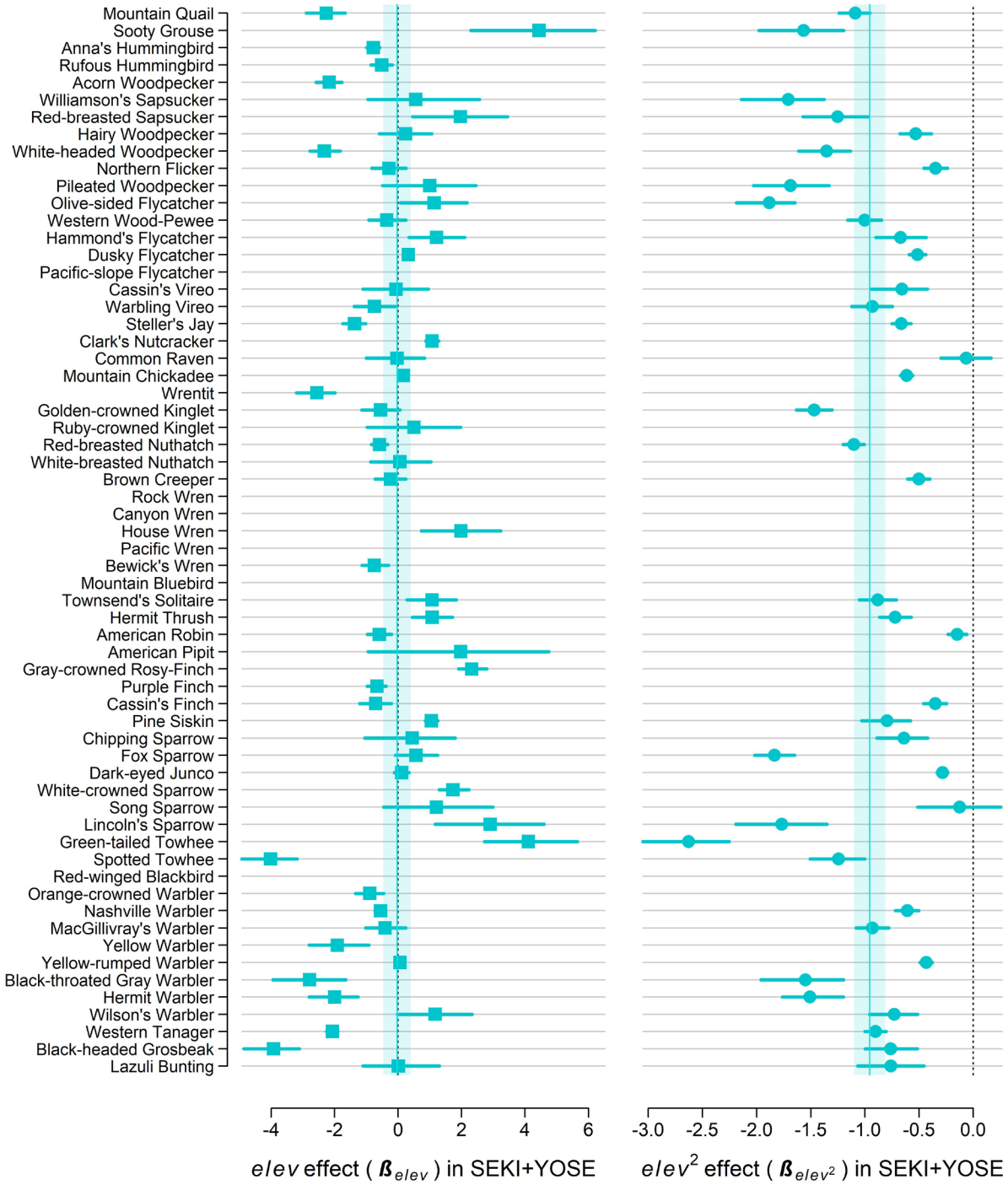


Figure 8. Linear and nonlinear effects of elevation (*elev*) in hierarchical models of avian abundance based on breeding-season point counts conducted annually during 2011–2014 and 2016–2019. Elevation was standardized in multiple-regression sub-models of abundance (Table 5). Means and 95% credible intervals are shown for the coefficient of *elev* (squares) and $elev^2$ (dots) from data on each of 62 species surveyed across Sequoia and Kings Canyon National Parks (SEKI) and Yosemite National Park (YOSE). Solid vertical lines and shading indicate grand means and 95% confidence intervals for effects across species. Species are listed in taxonomic order (Table 4).

The effect of precipitation-as-snow (*PAS*) was overwhelmingly negative in our models (Figure 9, Appendix 9), indicating that abundance was lower in years following higher-than-average snowfall. Although this pattern was most evident in the larger parks (Figure 9, right-hand panel), it was also clear even in the smaller samples from DEPO (Figure 9, left-hand panel; Table A9-1), and helps explain the many positive trends in population density during the monitoring period, when snowfall was generally lower than the long-term average (Figure 3). We found no support for a positive effect of *PAS* on abundance for any species except Purple Finch in the larger parks (Table A9-2). Quadratic effects of precipitation-as-snow, however, were mixed (Figure 10, Appendix 9). While effects of PAS^2 were supported for many of the populations we analyzed, the combined number and magnitude of positive and negative effects across species were similar enough that the grand mean effect of PAS^2 centered on zero regardless of park (Figure 10). Negative effects of PAS^2 would suggest that abundance is highest after years with intermediate amounts of snowfall. Positive effects of PAS^2 most likely suggest that abundance is highest after low-snowfall years, similar to the linear effect of *PAS*, but that the decline in abundance with snowfall levels off with higher snowfall. Populations with support for positive effects of PAS^2 were Mountain Quail and Clark's Nutcracker in both DEPO and the larger parks; Warbling Vireo, Golden-crowned Kinglet, Red-breasted Nuthatch, Yellow-rumped Warbler and Western Tanager in DEPO; and Hermit Thrush, American Robin, Gray-crowned Rosy Finch, Chipping Sparrow, White-crowned Sparrow and Lincoln's Sparrow in the larger parks. Populations with support for negative effects of PAS^2 were Steller's Jay, Mountain Chickadee and especially House Wren in DEPO; and Hammond's Flycatcher, Cassin's Vireo, Fox Sparrow and Hermit Warbler in models of combined data from SEKI and YOSE (Tables A9-1 and A9-2). Together, these results suggest reduced snow cover may play an important role in the recent—and perhaps ephemeral—stability of landbirds within Sierra Nevada national parks. Earlier snowmelt might allow earlier access to breeding habitats by more birds, perhaps increasing productivity and subsequent density of breeding bird populations during surveys in the following year. An additional possibility is that late-lasting snow correlates with early-season adverse weather that might result in widespread nest failures, especially for cup-nesting species, again affecting breeding site selection and bird densities in the following year.

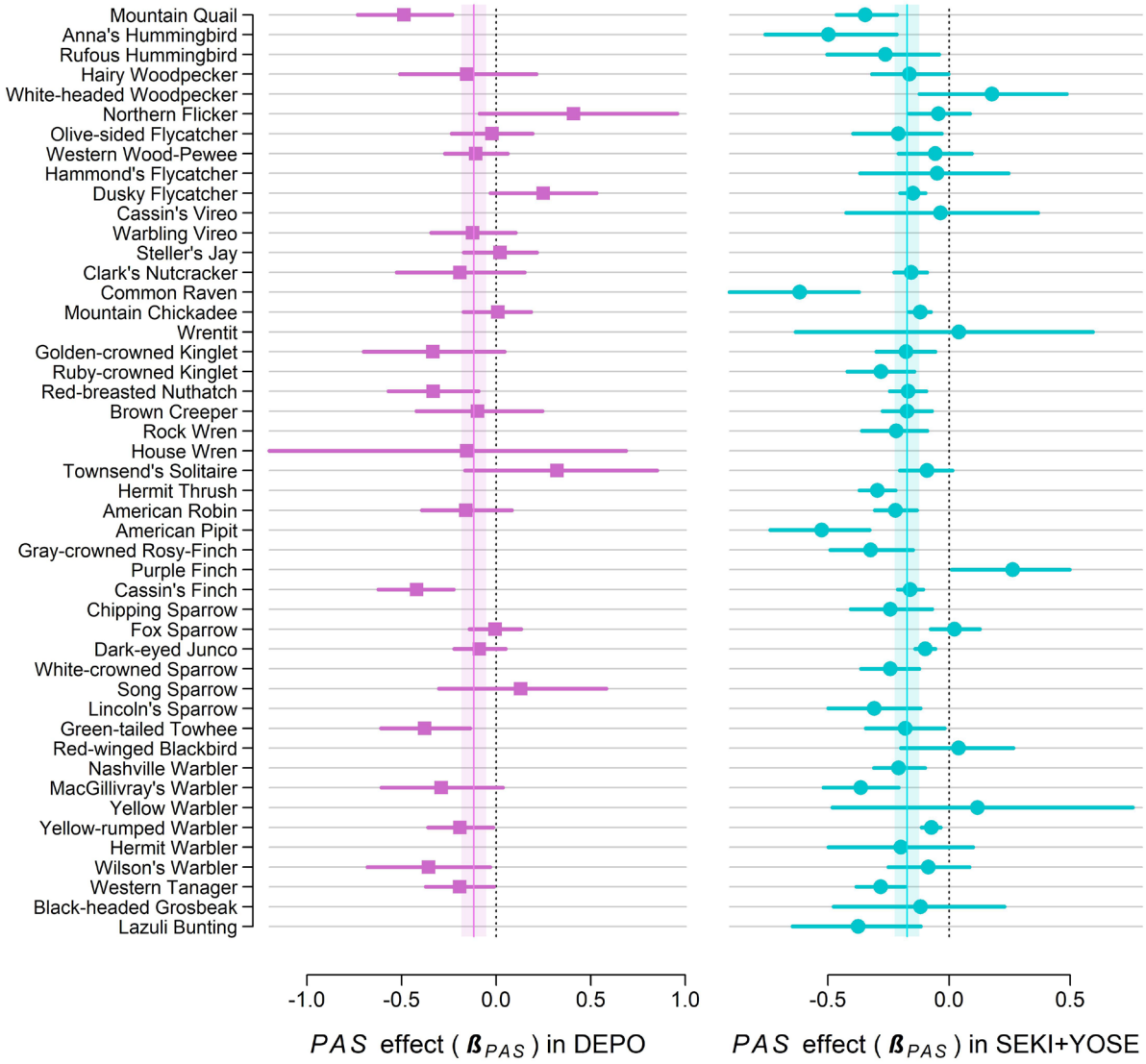


Figure 9. Effects of lag-1 anomalies in precipitation-as-snow (*PAS*) in hierarchical models of avian abundance based on breeding-season point counts conducted annually during 2011–2014 and 2016–2019. *PAS* was standardized in multiple-regression sub-models of abundance (Tables 5 and 6). Means and 95% credible intervals are shown for the coefficient of *PAS* from data on each of 25 species surveyed in Devils Postpile National Monument (DEPO, squares) and 47 species surveyed across Sequoia and Kings Canyon National Parks and Yosemite National Park (SEKI+YOSE, dots). Solid vertical lines and shading indicate grand means and 95% confidence intervals for effects across species. Species are listed in taxonomic order and include only those for which *PAS* was retained in a final model for DEPO and/or SEKI+YOSE (Tables 5 and 6).

Although park and sample sizes differ dramatically between analyses of data from DEPO and the larger parks, it is worth noting whether effects of *PAS* were similar between the two analyses. Models for 18 species included *PAS* as a covariate in both analyses, and in no case did supported effect signs for *PAS* differ between analyses of data from DEPO and the larger parks for the same species (Figure 9, Appendix 9). For 10 of these 18 species, effects of *PAS* were either clearly

negative in both analyses or not supported in either analysis. For each of the other eight species, the effect of *PAS* was clearly negative in one analysis and unsupported in the other.

Effects of PAS^2 followed a similar pattern (Figure 10, Appendix 9). Models for 15 species included PAS^2 as a covariate in both DEPO and larger park analyses, and in no case did supported effect signs differ between analyses for the same species. For 11 of these 15 species, effects of PAS^2 were clearly positive in both analyses or not supported in either analysis. For the remaining four species, effects of PAS^2 were either positive or negative in one analysis and not supported in the other.

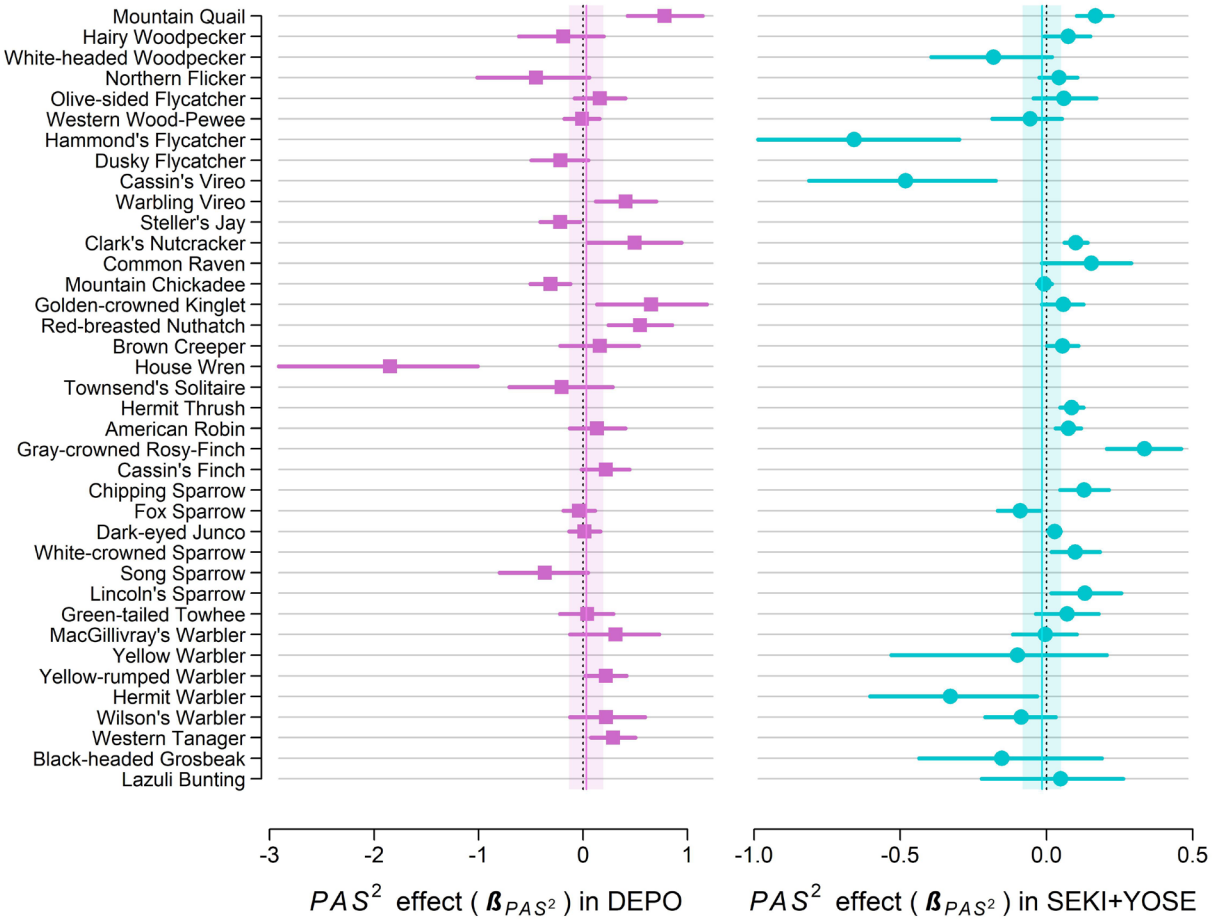


Figure 10. Nonlinear effects of lag-1 anomalies in precipitation-as-snow (PAS^2) in hierarchical models of avian abundance based on breeding-season point counts conducted annually during 2011–2014 and 2016–2019. PAS^2 appeared in multiple-regression sub-models of abundance (Tables 5 and 6). Means and 95% credible intervals are shown for the coefficient of PAS^2 from data on each of 25 species surveyed in Devils Postpile National Monument (DEPO, squares) and 38 species surveyed across Sequoia and Kings Canyon National Parks and Yosemite National Park (SEKI+YOSE, dots). Solid vertical lines and shading indicate means and 95% confidence intervals for effects across species. Species are listed in taxonomic order and include only those for which PAS^2 was retained in a final model for DEPO and/or SEKI+YOSE (Tables 5 and 6).

The effect of mean spring temperature (*MST*) or residual *MST* (*rMST*) was overwhelmingly positive in our models (Figure 11, Appendix 9), indicating that abundance was higher in years following higher-than-average spring temperatures. Although this pattern was less definitive in the smaller samples from DEPO (Figure 11, left-hand panel; Table A9-1), it was clear in the larger parks (Figure 11, right-hand panel, Table A9-2), and helps explain the many positive trends in population density during the monitoring period, when mean spring temperature was generally higher than the long-term average (Figure 3). We found no support for a negative effect of *MST* on abundance for any species except a negative effect of *rMST* on Mountain Quail and Yellow-rumped Warbler in DEPO (Table A9-1).

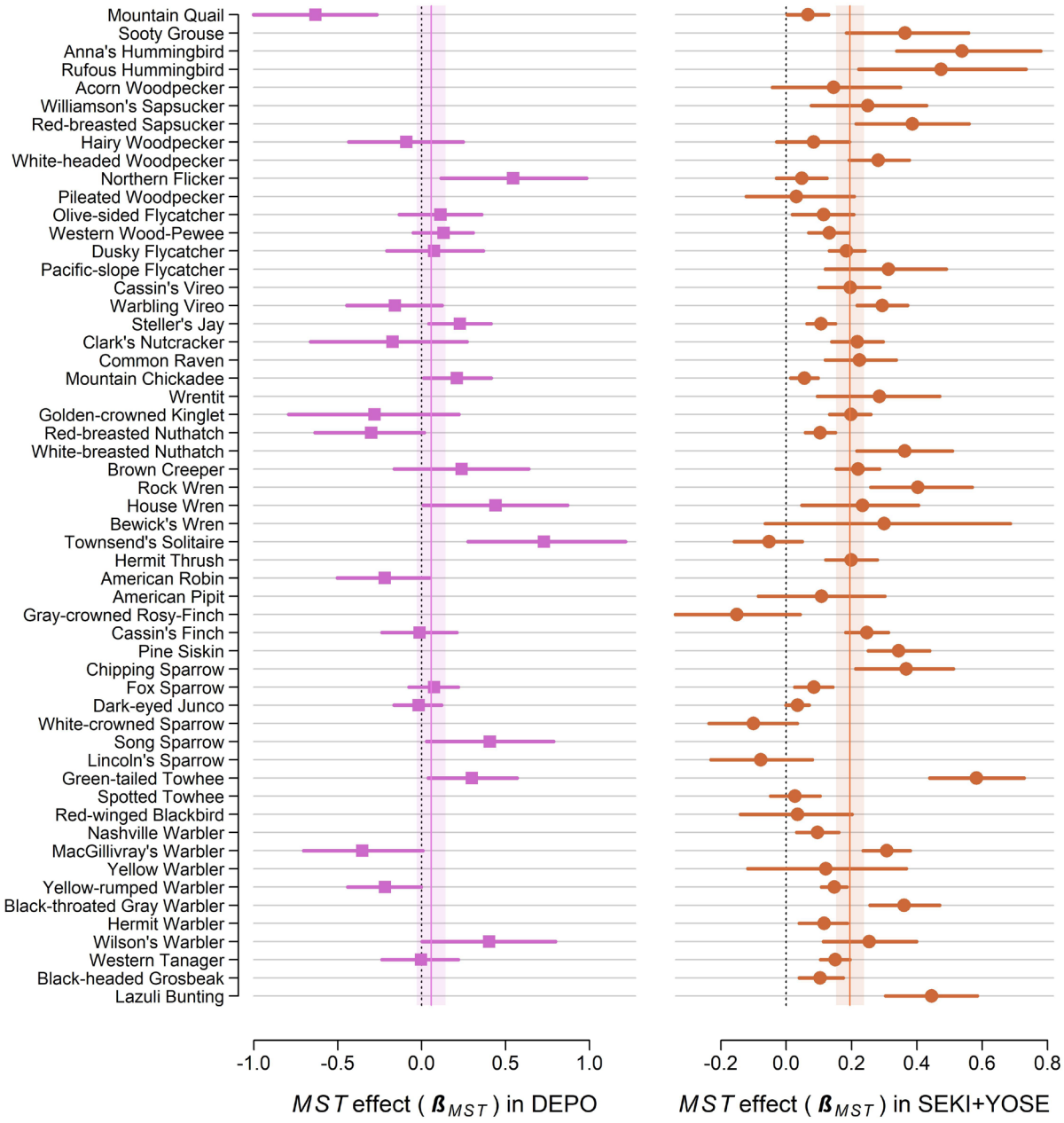


Figure 11. Effects of lag-1 anomalies in mean spring temperature (*MST*) in hierarchical models of avian abundance based on breeding-season point counts conducted annually during 2011–2014 and 2016–2019. *MST* was standardized in multiple-regression sub-models of abundance or (when appearing in sub-models with *PAS*) was replaced by *rMST*, the residuals of a simple linear regression of *MST* on *PAS* (Tables 5 and 6). Means and 95% credible intervals are shown for the coefficient of *MST* from data on each of 25 species surveyed in Devils Postpile National Monument (DEPO, squares) and 55 species surveyed across Sequoia and Kings Canyon National Parks and Yosemite National Park (SEKI+YOSE, dots). Solid vertical lines and shading indicate means and 95% confidence intervals for effects across species. Species are listed in taxonomic order and include only those for which *MST* or *rMST* was retained in a final model for DEPO and/or SEKI+YOSE (Tables 5 and 6).

Covariates of detection

Availability for detection (p_a) was high across all species analyzed, excepting the hummingbirds and perhaps Common Raven and Gray-crowned Rosy Finch (Figures 12 and 13). Detection probability (p_d) averaged just above 0.4 in the smaller park and just above 0.3 across the larger parks.

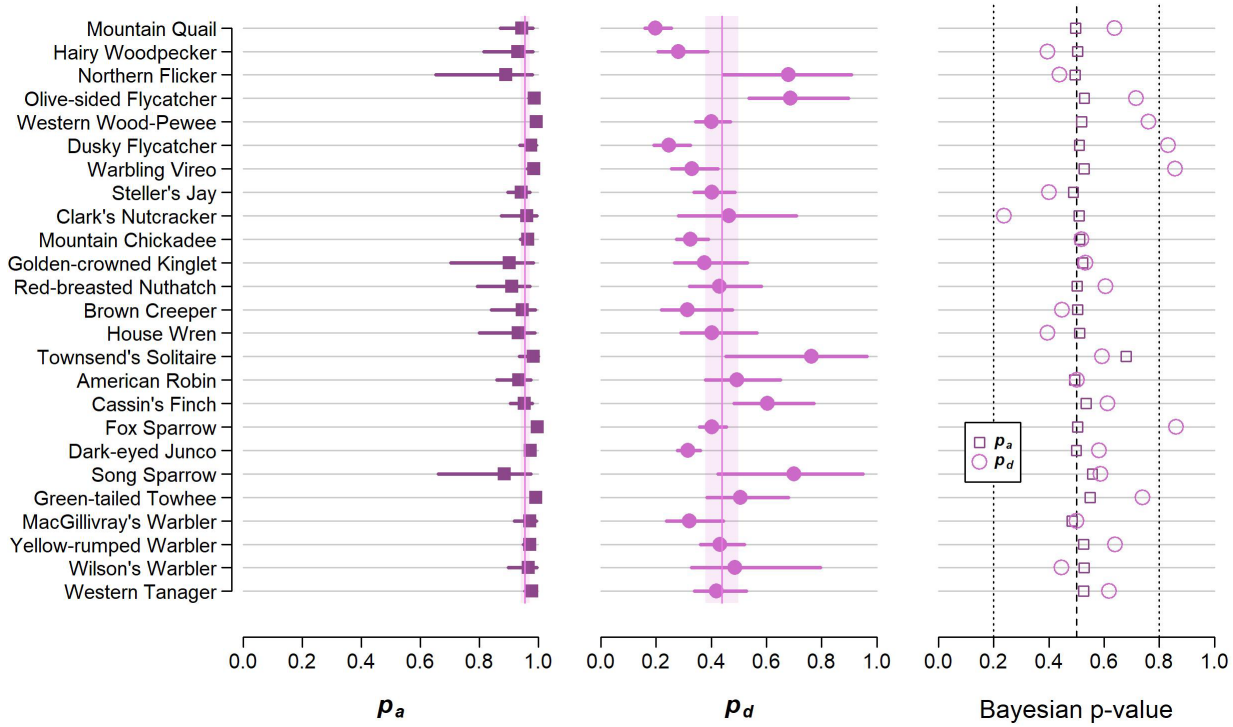


Figure 12. Probabilities of availability for detection (p_a, squares) and detection (p_d, dots) from hierarchical models of avian abundance based on breeding-season point counts conducted annually in Devils Postpile National Monument during 2011–2014 and 2016–2019. Species-specific means and 95% credible intervals are shown for each probability (left-hand panels) and species-specific metrics of model fit (Bayesian p-values) are shown for sub-models generating each probability (right-hand panel). Model fit is adequate for Bayesian p-values between 0.2 and 0.8.

In the final model for each species analyzed in DEPO, as well as each species analyzed in SEKI+YOSE, the sub-model of availability was adequate, each with a Bayesian p-value near 0.5. In contrast, sub-models of detection remained inadequate, with Bayesian p-values less than 0.2 or greater than 0.8, for at least 12% of species in each analysis (Appendix 10). Before detailing the covariates of detection, we discuss these inadequate detection sub-models (hereafter, models).

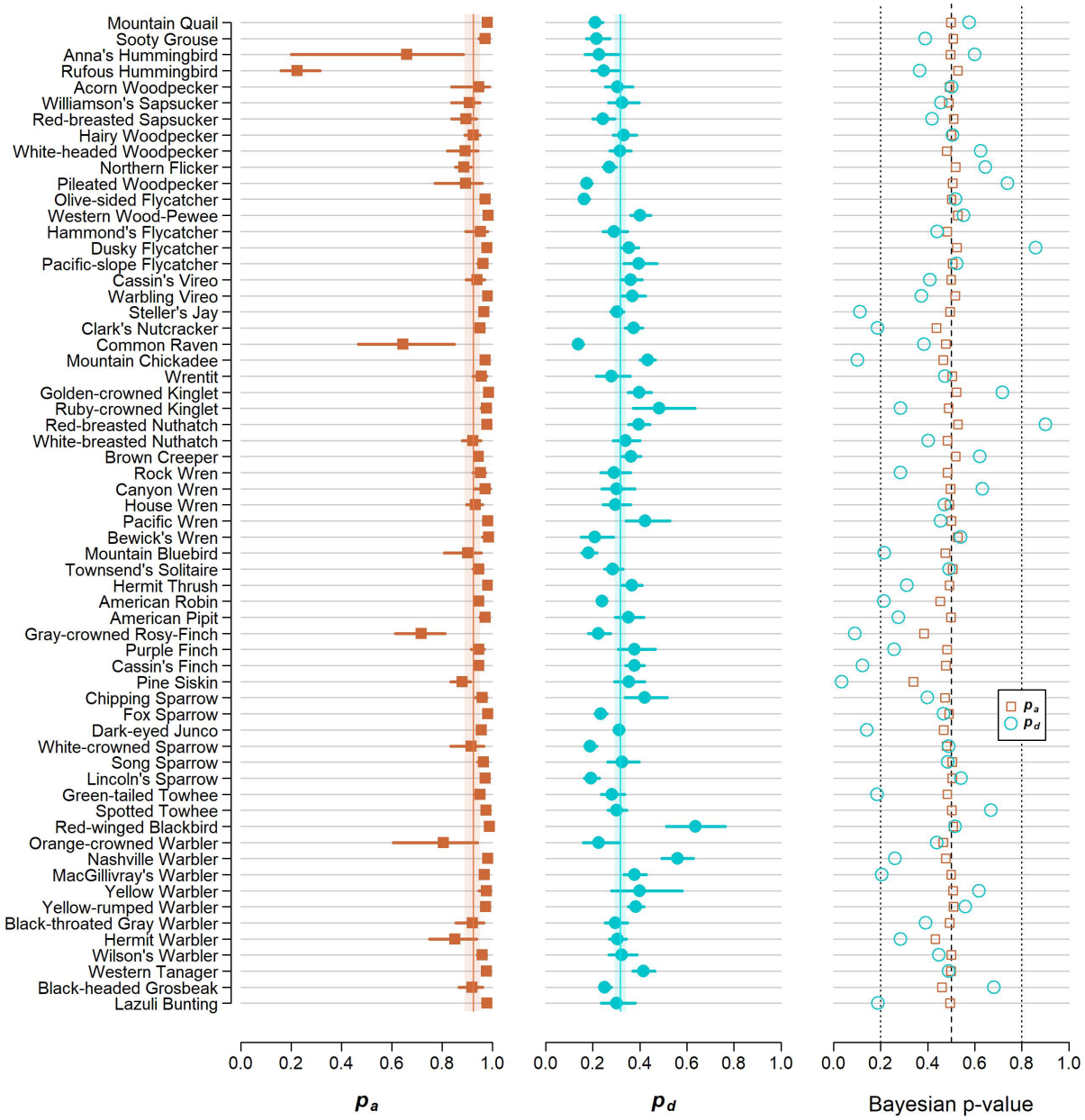


Figure 13. Probabilities of availability for detection (p_a, squares) and detection (p_d, dots) from hierarchical models of avian abundance based on breeding-season point counts conducted annually across Sequoia and Kings Canyon National Parks and Yosemite National Park during 2011–2014 and 2016–2019. Species-specific means and 95% credible intervals are shown for each probability (left-hand panels) and species-specific metrics of model fit (Bayesian p-values) are shown for sub-models generating each probability (right-hand panel). Model fit is adequate for Bayesian p-values between 0.2 and 0.8.

Inadequate detection models were apparent for three of 25 species analyzed in DEPO and eight of 62 species analyzed across SEKI+YOSE (Figures 12 and 13, right-hand panels). Of the three species with clearly inadequate detection models in DEPO, two species (Warbling Vireo and Fox Sparrow) had adequate detection models in the SEKI+YOSE analysis and, for both species, the trends we report here were congruent between DEPO and the adjacent large park, YOSE, suggesting that

inadequate detection models in the DEPO analysis did not bias results from that park. We cannot make the same inference for the third species with an inadequate detection model in DEPO (Dusky Flycatcher) because, for that species, detection models were inadequate in both analyses. However, we estimated positive population trends in every park and stratum for Dusky Flycatcher, and our parameter estimates were stable across alternative models within each analysis. For example, in several distinct models fitted to Dusky Flycatcher data from SEKI+YOSE, mean estimates for a_0 (Eqn. 1a) ranged from 0.763 to 0.770 and mean estimates of β_{hour} ranged from 0.035 to 0.036, while σ_0 (Eqn. 1b) ranged from 31.4 to 31.5 and β_{noise} ranged from −0.076 to −0.080. In the same set of models, β_{year} (Eqn. 1c) ranged from −0.010 to 0.002 and the year effect was not supported in any model for Dusky Flycatcher in SEKI+YOSE (Figure 7, right-hand panel). Despite the stability in parameter estimates across models for this species, it will be important to revisit the detection model for Dusky Flycatcher in any further analyses. Given Bayesian p-values of 0.831 in our DEPO analysis and 0.859 in our SEKI+YOSE analysis, our detection models might be over-fit for this species, and our report of positive trends in Dusky Flycatcher should be considered with caution. Similarly, we suggest a cautious interpretation of results for species with clearly inadequate detection models in the larger parks, including Steller's Jay, Mountain Chickadee, Red-breasted Nuthatch, Gray-crowned Rosy Finch, Cassin's Finch and Pine Siskin. Although three of these species were also modeled in DEPO, where their detection models were adequate, only one exhibited trends that were congruent between DEPO and SEKI+YOSE: Mountain Chickadee appeared stable across all parks and strata, while Red-breasted Nuthatch and Cassin's Finch appeared stable in DEPO (where the detection model was adequate) but increasing in the adjacent park YOSE (where the detection model was inadequate). On the other hand, we found no evidence that the trends we report for these species were caused by trends in detection: for species with poor fit to the detection model we attempted to fit a model with *year* effect on detection rather than abundance, and found no support for that effect.

Our covariates of availability were *day* (of year) and *hour* (of day), while covariates of detection were *observer* identity, *noise* level during the survey, and presence of dense vegetative *cover*. In analyses of DEPO data, where smaller sample sizes supported few parameters in each model, we estimated fixed effects of covariates on availability for only two species (Table 6), and those effects were not supported. Fixed effects of covariates on detection in DEPO were estimated for five species, but the only supported relationship was a negative effect of *noise* on Yellow-rumped Warbler detection. In analyses of SEKI+YOSE data, effects of covariates on availability and detection were estimated for many species (Table 5; Figure 14; Appendix 11). Supported effects of *day* on bird availability for detection were few and mixed, with six species more available earlier in the annual survey period and 10 more available later. This result suggests that the timing of annual surveys currently encompasses the peak of conspicuous breeding-season activities. Effects of *hour* on availability were supported for only eight species, and each of these effects was positive, suggesting that our crews have been arriving at the survey sites early enough to capture the daily peak in conspicuous activities. For seven species, detection was affected negatively by the presence of dense *cover*, and positive effects of *cover* were supported for five species that might have taken advantage of that cover to engage in conspicuous activities. Finally, our analysis of fixed effects on detection showed broad support for a negative effect of *noise*, affecting 44 of 62 species (right-hand panels of

Figure 14 and Table A11-1). Continuing to account for the negative effect of noise using consistent methods will be important for long-term monitoring of birds in these parks.

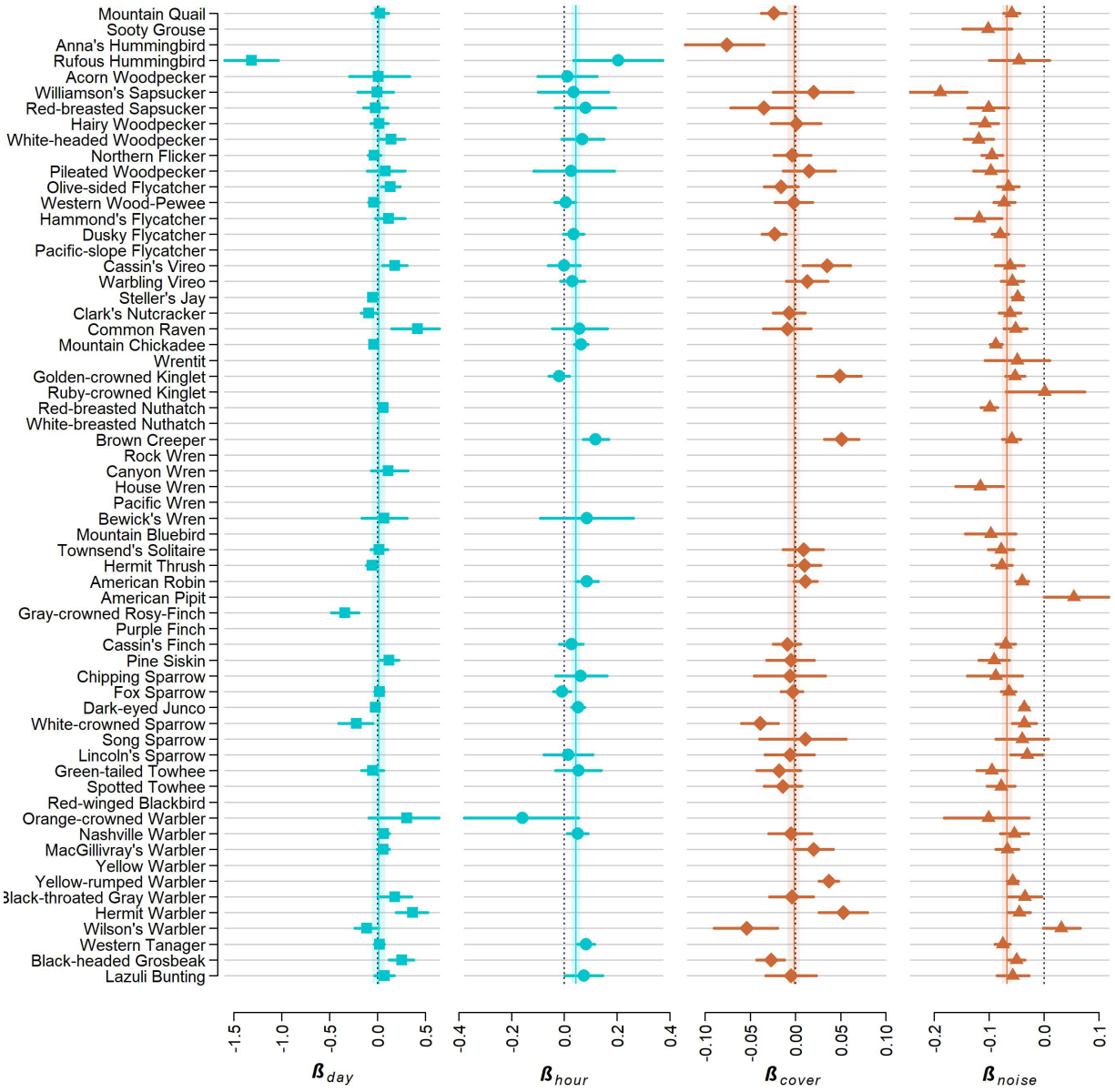


Figure 14. Effects of day (β_{day}) and hour (β_{hour}) on bird availability, and effects of cover (β_{cover}) and noise (β_{noise}) on bird detection in hierarchical models of avian abundance based on breeding-season point counts conducted annually across Sequoia and Kings Canyon National Parks and Yosemite National Park during 2011–2014 and 2016–2019. Means and 95% credible intervals are shown for each of 62 species listed in taxonomic order (Table 4). Solid vertical lines and shading indicate grand means and 95% confidence intervals for effects across species.

In addition to the fixed effects on detection reported above, a random effect of observer was included in 59 of 62 final models in our analysis of data from SEKI+YOSE, and 5 of 25 final models from

DEPO. We included the random effect of observer by default in models based on the large SEKI+YOSE dataset, and we dropped this effect for only three species (Rufous Hummingbird, Mountain Bluebird and American Pipit) because it interfered with model convergence. In contrast, we excluded the observer effect by default in models based on the smaller DEPO dataset, and added this effect for only five species (Western Wood-Pewee, Dusky Flycatcher, Mountain Chickadee, Fox Sparrow and Yellow-rumped Warbler) that were in need of improved fit to the detection sub-model.

Estimates of population density can depend sensitively on how we model the decline in detection with distance from the observer. We first discarded a percentage of the farthest detection distances recorded for each species (mean±SE = 9.83±0.32% of distances in DEPO and 8.54±0.45% of distances in SEKI+YOSE) to avoid undue influence of the small sample of long-distance detections on model fit, and to eliminate any significant correlation between distance- and time-to-detection. The maximum detection distance in the remaining data varied across species from 24 to 346 meters, resulting in effective detection areas that varied from 0.2 to 37.6 hectares, and estimates of σ (the scale parameter of the half-normal detection-distance function) that varied from 8 to 111 (Appendix 12). Although discarding fully 10% of detection distances is a common rule-of-thumb, for some species with relatively low numbers of detections—especially those with low numbers of long-distance detections—we retained a bit more than 90% of recorded distances in order to facilitate model fit, which requires at least some 'tail' on the observed detection-distance distribution. In all but one of these cases, we retained up to 95% of all recorded distances for the given species, after verifying that distance- and time-to-detection remained independent in this expanded sample (ANOVA: $p > 0.05$ in a test for association). The one exception was for detection of Spotted Towhee in the larger parks, which did not decline convincingly with distance unless we retained the entire distribution of estimated detection distances. In this case only, detection distance and time to detection were not independent. This departure from model assumptions might not bias our estimate of trend in this species, but it could certainly bias our estimates of absolute density, despite acceptable fit to the detection sub-model (Figure 13). If additional monitoring does not alter the observed detection-distance distribution for Spotted Towhee, alternative methods for modeling effects of distance on detection should be considered for this species.

Agreement with other studies of trends in bird abundance

Results presented here agree broadly with other analyses of landbird population trends in this region over the past decade, which have noted the relative stability of avian populations as well as evidence for positive population growth in relation to declines in snow cover and higher spring temperatures (Tingley et al. 2012, Ray et al. 2017 a, Ray et al. 2017 b, DeSante and Saracco 2021). However, the identity of species trending in these parks appears to have varied over time and across studies. Of 12 species trending significantly from 1990 to 2006 in a YOSE demographic study (Stock et al. 2010), only two trends were corroborated here: declines in Western Wood-Pewee and Purple Finch have apparently continued through 2019. A 32-year study of breeding activity at a study site near treeline in YOSE (DeSante and Saracco 2021) found that few species were trending from 1978 to 2009, but the three species that trended in that study (Yellow Warbler, Clark's Nutcracker and Chipping Sparrow) were not among those that trended consistently across the SIEN during the period analyzed here. In a 2010–2016 study of drought and tree mortality across the southern Sierra Nevada (Roberts

et al. 2019), avian populations were again determined to be relatively stable in response to these disturbances, with only one of 45 species decreasing over the study period (American Robin) and eight increasing (Nashville Warbler, Golden-crowned Kinglet, Western Wood-Pewee, MacGillivray's Warbler, Hammond's Flycatcher, Wrentit, Yellow Warbler and Dusky Flycatcher).

To provide context for our specific results through a comparison with contemporaneous data from the landscapes surrounding these parks, we turned to the Breeding Bird Survey (BBS) conducted along routes throughout North America for the past several decades (Pardieck et al. 2020). Using *bbsBayes*, a package recently developed for customized analyses of BBS data, we were able to estimate focal population trends for the region and period of interest using an analytical approach similar to the methods applied here (Edwards and Smith 2021). We focused our comparison at two spatial scales: Bird Conservation Region (BCR) 15, which encompasses SEKI and YOSE, and the state of California, which encompasses BCR 15. At each scale, we estimated indices of abundance during 2011–2019 for each of the species that we found to be trending across the two largest SIEN parks (Appendix 5), including ten populations that decreased and 14 that increased over our study period. We found that species with declining abundance in the SIEN generally trended negative in the BBS data as well (Appendix 13). Of the ten populations that decreased in the SIEN, nine showed negative mean growth across BCR 15 (Table A13-1), and five of those declines were supported (the 95% CRIs on trend did not overlap zero for Western Wood-Pewee, Wrentit, Purple Finch, Pine Siskin and Fox Sparrow). Seven of the ten populations that decreased in the SIEN also showed negative mean trends across California, and six of those declines were supported (for Western Wood-Pewee, Wrentit, Purple Finch, Pine Siskin, Fox Sparrow and Orange-crowned Warbler). No species decreasing in the SIEN showed a supported increase in BCR 15 or across California. Furthermore, species increasing in the SIEN often trended negative in the surrounding landscapes (Table A13-2). Nine of 14 species increasing in the SIEN showed negative mean growth in BCR 15, and three of those negative trends were supported (for American Robin, Cassin's Finch and Black-throated Gray Warbler). At the largest scale of comparison, four of 14 species increasing in the SIEN showed negative mean growth across California, and the trend for one of those declining populations (Black-throated Gray Warbler) was supported. In addition, the BBS web page (https://www.mbr-pwrc.usgs.gov/) reported trends in abundance for a number of species that did not trend across SEKI and YOSE in our current analysis. The BBS trends, each analyzed at the scale of BCR 15 and limited to the period 2011–2019, were positive for two species common to our analyses (White-headed Woodpecker and Common Raven) and negative for five species (Rufous Hummingbird, Olive-sided Flycatcher, Mountain Chickadee, Chipping Sparrow and White-crowned Sparrow). Taken together, our comparison of trends in landbird abundance based on SIEN and BBS data suggests that several species have fared better in the parks than in surrounding landscapes over the past decade, similar to results recently reported for protected areas in coastal California (Dettling et al. 2021).

Conclusion

Using a relatively robust framework for analysis of avian monitoring data from three park units in the Sierra Nevada Inventory and Monitoring Network, we estimate that the vast majority of analyzed populations present during the breeding season were stable or increasing between 2011 and 2019. The populations analyzed represent nearly half the species and almost 95% of all birds detected in our surveys, suggesting that the trends we found are quite representative of birds breeding in these parks. Results were fairly similar among elevational strata, with no increase in trends at higher elevations and no stratum-by-year interaction that might indicate a response to recent climate change. However, the majority of declines occurred in Sequoia and Kings Canyon National Parks, the southern-most area in our analysis. Also, we found a clearly negative effect of year on abundance for many of the populations analyzed, a relationship typically associated with declining populations. Yet most populations were increasing or stable over the monitoring period, apparently in response to anomalously low snowfall and high spring temperature. The positive effects of low snowfall and high spring temperature appear to have more than countered any deterioration in abundance that was indexed by year. In general, years of higher breeding-season densities followed years of lower snowfall and higher spring temperatures. Thus, the dramatic depression in snowfall in this region over the monitoring period likely contributed to the favorable trends we found, and many of these populations might be poised to decline in years with more typical snowfall. On the other hand, there are many possible drivers that might explain these complex results. Attention should be given to the potential for shifting phenology in breeding behaviors within a season, which could cause apparent trends (or mask real trends) in data like ours that derive from a single visit to each point-count station during a breeding season. For example, if the trends we observed were due to changes in phenology, we would expect to find effects of day or elevation on abundance. Although we have seen no evidence for effects of day or elevation on abundance in this first synthesis of results from our long-term monitoring plan, the data summarized here provide a wealth of opportunities for further analysis and set the stage for targeted studies of bird species and communities of concern.

Literature cited

Alldredge, M. W., K. H. Pollock, T. R. Simons, J. A. Collazo, and S. A. Shriner. 2007. Time-of-detection method for estimating abundance from point-count surveys. The Auk 124:653.

Amundson, C. L., J. A. Royle, and C. M. Handel. 2014. A hierarchical model combining distance sampling and time removal to estimate detection probability during avian point counts. The Auk 131:476–494.

Amundson, C. L., C. M. Handel, D. R. Ruthrauff, T. L. Tibbitts, and R. E. Gill Jr. 2018. Montane-breeding bird distribution and abundance across national parks of southwestern Alaska. Journal of Fish and Wildlife Management 9:180–207; e1944-687X. DOI:10.3996/062017-JFWM-050.

Buckland, S. T., D. R. Anderson, K. P. Burnham, J. L. Laake, D. L. Borchers, and L. Thomas. 2001. Introduction to distance sampling. Oxford University Press, Oxford, United Kingdom.

Cayan, D. R., E. P. Maurer, M. D. Dettinger, M. Tyree, and K. Hayhoe. 2008. Climate change scenarios for the California region. Climatic Change 87:S21-S42. DOI 10.1007/s10584-007-9377-6.

Chesser, R. T., S. M. Billerman, K. J. Burns, C. Cicero, J. L. Dunn, B. E. Hernández-Baños, A. W. Kratter, I. J. Lovette, N. A. Mason, P. C. Rasmussen, J. V. Remsen, Jr., D. F. Stotz, and K. Winker. 2021. Sixty-second supplement to the American Ornithological Society's Check-list of North American Birds. Ornithology 138:ukab037. DOI 10.1093/ornithology/ukab037.

DeSante, D. F. 1990. The role of recruitment in the dynamics of a Sierran subalpine bird community. American Naturalist 136:429–455.

DeSante, D. F., and J. F. Saracco. 2021. Climate variation drives dynamics and productivity of a subalpine breeding bird community. Ornithological Applications 123:1–16.

Dettling, M. D., K. E. Dybala, D. L. Humple, and T. Gardali. 2021. Protected areas safeguard landbird populations in central coastal California: evidence from long-term population trends. Ornithological Applications 123:1–12. https://doi.org/10.1093/ornithapp/duab035.

Dettinger, M. D., D. R. Cayan, M. K. Meyer, et al. 2004. Simulated hydrologic responses to climate variations and change in the Merced, Carson, and American River basins, Sierra Nevada, California, 1900–2099. Climatic Change 62:283–317. https://doi.org/10.1023/B:CLIM.0000013683.13346.4f.

Edwards, B. P. M., and A. C. Smith. 2021. bbsBayes: An R package for hierarchical Bayesian analysis of North American Breeding Bird Survey data. Journal of Open Research Software, 9:19. https://doi.org/10.5334/jors.329.

Fancy, S. G., J. E. Gross and S. L. Carter. 2009. Monitoring the condition of natural resources in US National Parks. Environmental Monitoring and Assessment 151:161–174.

Farnsworth, G. L., K. H. Pollock, J. D. Nichols, T. R. Simons, J. E. Hines, and J. R. Sauer. 2002. A removal model for estimating detection probabilities from point-count surveys. The Auk 119:414–425.

Graham, M. L. 2003. Confronting multicollinearity in ecological multiple regression. Ecology 84:2809–2815.

Hahn, T. P., K. W. Sockman, C. W. Breuner, and M. L. Morton. 2004. Facultative altitudinal movements by mountain white-crowned sparrows (Zonotrichia leucophrys oriantha) in the Sierra Nevada. The Auk 121:1269–1281.

Hayhoe, K., D. Cayan, C. B. Field, P. C. Frumhoff, E. P. Maurer, N. L. Miller, S. C. Moser, S. H. Schneider, K. N. Cahill, E. E. Cleland, et al. 2004. Emissions pathways, climate change, and impacts on California. Proceedings of the National Academy of Sciences USA 101:12422–12427.

IPCC (Intergovernmental Panel on Climate Change). 2013. Summary for policymakers. Pages 3–29 in: T. F. Stocker, D. Qin, G.-K. Plattner, M. Tignor, S. K. Allen, J. Boschung, A. Nauels, Y. Xia, V. Bex, and P. M. Midgley, editors. Climate change 2013: The physical science basis. Contribution of Working Group I to the Fifth Assessment Report of the Intergovernmental Panel on Climate Change. Cambridge University Press, Cambridge, UK.

IPCC (Intergovernmental Panel on Climate Change). 2014. Summary for policymakers. Pages 1–32 in: C. B. Field, V. R. Barros, D. J. Dokken, K. J. Mach, M. D. Mastrandrea, T. E. Bilir, M. Chatterjee, K. L. Ebi, Y. O. Estrada, R. C. Genova, B. Girma, E. S. Kissel, A. N. Levy, S. MacCracken, P. R. Mastrandrea, and L. L. White, editors. Climate change 2014: Impacts, adaptation, and vulnerability. Part A: Global and Sectoral Aspects. Contribution of Working Group II to the Fifth Assessment Report of the Intergovernmental Panel on Climate Change. Cambridge University Press, Cambridge, UK.

Kellner, K. 2015. jagsUI: a wrapper around 'rjags' to streamline 'JAGS' analyses. R package version 1.3.7. Available online: https://cran.r-project.org/web/packages/jagsUI/index.html.

Kéry, M., and J. A. Royle, editors. 2016. Applied hierarchical modeling in ecology: Analysis of distribution, abundance and species richness in R and BUGS. Volume 1, Prelude and static models. Elsevier, Amsterdam and Boston. xxiv, 783 pp.

Kéry, M., and M. Schaub. 2012. Bayesian population analysis using WinBUGS: A hierarchical perspective. Academic Press, 535 pp.

Knowles, N., and D. R. Cayan. 2002. Potential effects of global warming on the Sacramento/San Joaquin watershed and the San Francisco estuary. Geophysical Research Letters 29:381–384.

Lenihan, J. M., R. Drapek, D. Bachelet, and R. Neilson. 2003. Climate change effects on vegetation distribution, carbon, and fire in California. Ecological Applications 13:1667–1681.

Margulis, S. A., G. Cortés, M. Girotto, L. S. Huning, D. Li, and M. Durand. 2016. Characterizing the extreme 2015 snowpack deficit in the Sierra Nevada (USA) and the implications for drought recovery. Geophysical Research Letters 43:6341–6349. DOI: 10.1002/2016GL068520.

Mathewson, H. A., M. L. Morrison, H. L. Loffland, and P. Brussard. 2012. Ecology of willow flycatchers (*Empidonax traillii*) in the Sierra Nevada, California: Effects of meadow characteristics and weather on demographics. Ornithological Monographs 75:1–32.

Maurer, E. P., I. T. Stewart, C. Bonfils, P. B. Duffy, and D. Cayan. 2007. Detection, attribution, and sensitivity of trends toward earlier streamflow in the Sierra Nevada. Journal of Geophysical Research: Atmospheres 112, D11118. https://doi.org/10.1029/2006JD008088.

Mizel, J. D., J. H. Schmidt, C. L. McIntyre, and M. S. Lindberg. 2017. Subarctic-breeding passerines exhibit phenological resilience to extreme spring conditions. Ecosphere 8(2):e01680. 10.1002/ecs2.1680.

Pardieck, K. L., Ziolkowski Jr., D. J., Lutmerding, M., Aponte, V. I., Hudson, M. A. R. 2020. North American Breeding Bird Survey Dataset 1966 - 2019. U.S. Geological Survey data release. https://doi.org/10.5066/P9J6QUF6.

Pereyra, M. E. 2011. Effects of snow-related environmental variation on breeding schedules and productivity in a high altitude flycatcher (*Empidonax oberholseri*). The Auk 128:746–758.

Plummer, M. 2003. JAGS: A program for analysis of Bayesian graphical models using Gibbs sampling. Pages 1–10 *in*: K. Hornik, F. Leisch, and A. Zeileis, editors. Proceedings of the 3rd International Workshop on Distributed Statistical Computing (DCS2003), March 20–22, Technische Universität, Vienna, Austria.

PRBO Conservation Science. 2011. Projected Effects of Climate Change in California: Ecoregional Summaries Emphasizing Consequences for Wildlife. Version 1.0. http://data.prbo.org/apps/bssc/Climatechange.

R Core Team. 2021. R: A language and environment for statistical computing. R Foundation for Statistical Computing, Vienna, Austria. URL https://www.R-project.org/.

Ray, C., J. F. Saracco, M. L. Holmgren, R. L. Wilkerson, R. B. Siegel, K. J. Jenkins, J. I. Ransom, P. J. Happe, J. R. Boetsch, and M.H. Huff. 2017 a. Recent stability of resident and migratory landbird populations in National Parks of the Pacific Northwest. Ecosphere 8:e01902.

Ray, C., J. Saracco, K. Jenkins, M. Huff, P. Happe, and J. Ransom. 2017 b. Development of a robust analytical framework for assessing landbird population trends, dynamics and relationships with environmental covariates in the North Coast and Cascades Network. Natural Resource Report NPS/NCCN/NRR—2017/1483. National Park Service, Fort Collins, Colorado.

Roberts, L. J., R. Burnett, J. Tietz, and S. Veloz. 2019. Recent drought and tree mortality effects on the avian community in southern Sierra Nevada: A glimpse of the future? Ecological Applications 29:e01848.

Royle, J. A. 2004. *N*-mixture models for estimating population size from spatially replicated counts. Biometrics 60:108–115.

Royle, J. A., D. K. Dawson, and S. Bates. 2004. Modeling abundance effects in distance sampling. Ecology 85:1591–1597.

Saracco, J. F., A. L. Holmgren, R. L. Wilkerson, R. B. Siegel, R. C. Kuntz II, K. J. Jenkins, P. J. Happe, J. R. Boetsch, and M. H. Huff. 2014. Landbird trends in National Parks of the North Coast and Cascades Network, 2005–2012. U.S. Geological Survey open-file report 2014–1202.

Schmidt, J. H., C. L. McIntyre, and M. C. MacCluskie. 2013. Accounting for incomplete detection: What are we estimating and how might it affect long-term passerine monitoring programs? Biological Conservation 160:130–139.

Siegel, R. B. 2000. Methods for monitoring landbirds. U.S. Department of Interior National Park Service Technical Report NPS/NRNOCA/NRTR/00-03.

Siegel, R. B., and R. C. Kuntz II. 2009. Designing a landbird monitoring program at North Cascades National Park Service Complex: Summary recommendations from a September 2000 workshop. Natural Resource Report NPS/NCCN/NRR—2009/075. National Park Service. Fort Collins, Colorado.

Siegel, R. B., P. Pyle, J. H. Thorne, A. J. Holguin, C. A. Howell, S. Stock, and M. W. Tingley. 2014. Vulnerability of birds to climate change in California's Sierra Nevada. Avian Conservation and Ecology 9(1):7.

Siegel, R. B., R. L. Wilkerson, and M. Goldin Rose. 2010. Bird monitoring protocol for national parks in the Sierra Nevada Network. Natural Resource Report NPS/SIEN/NRR—2010/231. National Park Service, Fort Collins, Colorado.

Siegel, R. B., R. L. Wilkerson, K. J. Jenkins, R. C. Kuntz II, J. R. Boetsch, J. P. Schaberl, and P. J. Happe. 2007. Landbird monitoring protocol for national parks in the North Coast and Cascades Network. U.S. Geological Survey Techniques and Methods 2-A6. 208 pp.

Siegel, R. B., R. L. Wilkerson, R. C. Kuntz II, J. F. Saracco, and A. L. Holmgren. 2012. Elevation ranges of birds at Mount Rainier National Park, North Cascades National Park Service Complex, and Olympic National Park. The Northwestern Naturalist 93:23–39.

Silsbee, G. G., and D. L. Peterson. 1991. Designing and implementing comprehensive long-term inventory and monitoring programs for National Park System lands. Natural Resources Report NPS/NRUW/NRR-91/04, Denver, Colorado.

Simons, T. R., K. N. Rabenold, D. A. Buehler, J. A. Collazo, and K. E. Fransreb. 1999. The role of indicator species: Neotropical migratory song birds. Pages 187–208 *in*: J. D. Peine, editor. Ecosystem management for sustainability: Principles and practices illustrated by a regional biosphere reserve cooperative. Lewis, New York, New York.

Steel, Z. L., M. L. Bond, R. B. Siegel, and P. Pyle. 2012. "Avifauna of Sierra Nevada Network parks: Assessing distribution, abundance, stressors, and conservation opportunities for 145 bird species". Natural Resource Report NPS/SIEN/NRR—2012/506. National Park Service, Fort Collins, Colorado.

Stevens, D. L., and A. R. Olsen. 2004. Spatially balanced sampling of natural resources. Journal of the American Statistical Association 99:262–278.

Thorne, J. H., R. M. Boynton, L. E. Flint, and A. L. Flint. 2015. The magnitude and spatial patterns of historicaland future hydrologic change in California's watersheds. Ecosphere 6(2):24.

Tingley, M. W., and S. R. Beissinger. 2013. Cryptic loss of montane avian richness and high community turnover over 100 years. Ecology 94:598–609.

Tingley, M. W., M. S. Koo, C. Moritz, A. Rush, and S. R. Beissinger. 2012. The push and pull of climate change causes heterogeneous shifts in avian elevational ranges. Global Change Biology 18:3279–3290.

Tingley, M. W., W. B. Monahan, S. R. Beissinger, and C. Moritz. 2009. Birds track their Grinnellian niche through a century of climate change. Proceedings of the National Academy of Sciences USA 106:19637–19643.

Wang, T., Hamann, A. Spittlehouse, D., and C. Carroll. 2016. Locally downscaled and spatially customizable climate data for historical and future periods for North America. PLoS ONE 11(6):e0156720. doi:10.1371/journal.pone.0156720.

Weber, S., A. Woodward, and J. Freilich. 2009. North Coast and Cascades Network vital signs monitoring report (2005). Natural Resource Report NPS/NCCN/NRR—2009/098. National Park Service, Fort Collins, Colorado.

Appendix 1. Procedures for synthesis of SIEN landbird trends

The synthesis provided in this report can be replicated in future analyses of SIEN landbird monitoring data using a suite of scripts linked directly to the SIEN landbird monitoring database. Procedures for applying these scripts in sequence to reproduce these analyses and graphics are provided here, with some reference to Ray et al. (2017 b), which provides instruction on how to access monitoring and climate data and conduct trend analyses. Each script is fully annotated and can easily accommodate application to data from different periods of time. In every script, we used "***" to flag any lines of code that might require minor revision when altering the focal dataset. All scripts were written in the open-access programming language R (R Core Team 2021), and scripts for estimating trends in population density also include code written in JAGS (Plummer 2003), using the interface package jagsUI (Kellner 2015) to call JAGS from R.

Data preparation

Data recorded during each point-count survey, and data describing each point-count station or site, are accessed using two queries as detailed in Section 3.1 of Ray et al. (2017 b). For the current synthesis, output from these two queries were pre-processed for trend analysis using `script4processingQueryData-synthesis.R`, which writes the pre-processed data to two comma-delimited (.csv) files, `sien.survey.data.2011to2019.csv` and `sien.site.data.2011to2019.csv`. This data-processing script will require minimal revision to reflect the focal period targeted for analyses, such as altering the range of years designated in the output file names. In this and all other scripts described here, lines of code requiring review and possible revision can be located quickly by searching for comments containing "`***`".

Using `sien.climateNA.pts.csv` as a query, downscaled climate data can be accessed from ClimateWNA according to the procedure detailed in Appendix 3 of Ray et al. (2017 b). This procedure involves using `script4climateNAdata.R` in order to 1) re-format `sien.climateNA.pts.csv` as required by ClimateNA, 2) select the climate variables desired for analysis from the large number of variables downloaded by default from ClimateNA, 3) explore the focal climate data and 4) format the downloaded data as input for trend analysis. The output from `script4climateNAdata.R` is an input file for the trend analysis (e.g., `sien.climate.anoms…csv`, where the ellipsis indicates the focal time period) as well as several graphics summarizing focal climate variables (e.g., Figures 1–3 in the current synthesis).

Trend analysis

Trend analysis procedures are detailed in Ray et al. (2017 a, b). A final data-step prior to fitting trends is the creation of an input file for the fitting script, created using `script4pt-ct-data-plotting-and-binning…R`. This script also plots many relationships in the effort-corrected data to guide model development for each species. Input file names are of the form `DEJU.all.all.wClim.wNAs.csv`, where the first and second 'all' indicate that data from all years and all parks are included in this file, 'wClim' indicates climate covariates are included for

each station-year, and 'wNAs' indicates the data are padded with NAs for all station-years in which surveys were not conducted. Trends across the two larger parks, SEKI and YOSE, are analyzed in a single model, fitted using `script4pt-ct-trend-analysis-SEKI-YOSE.R.`, which is similar to the script presented in Appendix 4 of Ray et al. (2017 b). Trends in DEPO are fitted using `script4pt-ct-trend-analysis-DEPO.R`. Each of these scripts fits the full models presented in Eqns. 1 and 2 of the current synthesis, but each also includes comments marked "`***`" to indicate the few lines of code that might require alteration to accommodate other model variants, such as those with other covariates of abundance (e.g., slope) or covariates of detection (e.g., forest).

Harvesting output from trend analyses

Output from each `script4pt-ct-trend-analysis…R` consists of several species-specific files (Table A1-1) as well as several files (e.g., `pt-yr-plots1.pdf`) that are not species-specific because they summarize data at the point-count level, such as: the number of point-counts completed by park, year, day-of-year, hour, observer and elevational stratum; the number of point-counts completed in each cover class; the distribution of noise levels during counts; the distribution of counts by elevation, slope and aspect; and (for larger parks) the association across counts between park and observer or noise. Most of these outputs are also represented in some way within a single text file summarizing model parameters, fitted parameter estimates and statistics related to model fit and convergence. This key text file, hereafter "the output file," is generally named for the focal species, model type (covariates) and/or park: e.g., `FOSPout...txt` is the output file for a fitted model of Fox Sparrow trends. Table A1-1 describes the .txt output file and each additional output file from an application of `script4pt-ct-trend-analysis…R`.

Table A1-1. Output files generated by script4trendAnalysis-synthesis-sm-pk.R, exemplified using an analysis of Western Tanager (WETA) in Devils Postpile National Monument (DEPO).

Example output file	Contents
WETAoutDEPO.txt	Model parameters, parameter estimates, fit and convergence statistics
WETAoutDEPOMODEL.jagsUI	Model specification including priors and covariates of abundance/detection
WETAoutDEPOChains.pdf	Diagnostic plots of posterior distributions for estimated model parameters
WETAoutDEPO.fitStats…pdf	Discrepancy plots and fit statistics for the sub-models of species detection
WETAoutDEPO.plots1.pdf	Plots and statistics relating raw count to park and elevational stratum [a]
WETAoutDEPO.plots2.pdf	Raw count distribution and Poisson regression of count on day/hour/noise
WETAoutDEPO.plots3.pdf	Plots of unadjusted and effort-adjusted raw counts per station by year
WETAoutDEPO.plots4.pdf	Poisson regression of effort-adjusted raw count on year
WETAoutDEPO.plots5.pdf	Plots/statistics relating count or occupancy to cover, elevation and slope
WETAoutDEPO.plots6.pdf	Plots/Poisson regressions relating count to aspect and climate covariates
WETAoutDEPO.plots7.pdf	Histograms of detection distance and detection distance-class

[a] Additional plots and statistics are generated in analyses involving multiple parks.

Table A1-1 (continued). Output files generated by script4trendAnalysis-synthesis-sm-pk.R, exemplified using an analysis of Western Tanager (WETA) in Devils Postpile National Monument (DEPO).

Example output file	Contents
WETAoutDEPO.plots8.pdf	Plots/statistics relating detection interval and distance to select covariates
WETAoutDEPO.plots9.pdf	Plot of detections by count interval; ANOVAs for interval × distance/hour
WETA.all.DEPOwClim.csv	Group size (0, 1, …) and covariates for every focal species (non)detection
WETA.all.DEPO…wNAs.csv	Same as above but padded with NAs for all station-years not surveyed

[a] Additional plots and statistics are generated in analyses involving multiple parks.

Data can be harvested from a set of output files—specifically the .txt output file for each of a set of modeled species—using a `script4tabulating-jags-output.R` and a `script4harvesting-model-results.R`. Each script takes as input a comma-separated "species-list" file (`spList...csv`) containing a column of species code names and a column of associated output files, as exemplified in Table A1-2. The `spList...csv` should contain a list of output files that are comparable among species in terms of model type: i.e., it should list the best basic model for each species in a given park, or the best climate model for each species in a park. However, the details of each species' model might vary somewhat. For example, covariates of detection were allowed to vary among species in the current synthesis, as would be expected also in future analyses.

For the larger parks, the data-harvesting script further takes its cue from the name of the `spList…csv` file to narrow the harvest to trends specific to the named park. For example, if the output file for a species that breeds in the mountain parks includes a park-specific trend for each park, only the YOSE trend will be harvested if the species-list file is named `spListYOSE-bestClimModels.R`.

Table A1-2. Contents of the first few rows of a comma-separated file used as input for the data-harvesting scripts. The file in this example was named spListDEPO-bestModels.csv and contained all the preferred output files from analyses of species occurring in Devils Postpile National Monument.

Species	Output file
WAVI	WAVIoutDEPObins3aug.txt
AMRO	AMROoutDEPObins3aug.txt
MOUQ	MOUQoutDEPObins3aug.txt
RBNU	RBNUoutDEPObins3aug.txt

The data-harvesting scripts first create a new set of comma-separated files, each containing the table of results for a given species in the species-list file. For example, `AMROoutDEPObins3aug.txt` is stripped of header and footer to generate a new file, `AMROoutDEPObins3aug.table.csv`,

which contains only a table of all estimated parameters and fit metrics and their associated means, quantiles and convergence statistics. Some of the subsequent code in the data-harvesting script accesses specific data from this new set of tables to collect the data needed for summary plots and tables in the synthesis: population trends, effects of covariates, and derived population densities. Additional code in the data-harvesting script returns to the output (`.txt`) files to harvest model parameters in the header or footer, such as the maximum detection distance and the percent of detection distances censored to avoid sampling error in the tail of the detection-distance distribution and to meet assumptions of independence between detection interval and distance.

Plotting and tabulating output from trend analyses

Key figures contained in the current synthesis can be reproduced using the scripts named in Table A1-3, while tables can be reproduced using those in Table A1-4. Most of these scripts require a "`spList…csv`" file to identify the set of species summarized by each figure or table. Despite the similarity in plots and tables that summarize results from DEPO vs. the larger parks, separate scripts were usually developed for each, to simplify the code within each script for dealing with the unique features of their results.

Table A1-3. Scripts used to generate figures in the current report.

Figure-generating script	Figure(s)	Figure contents
script4calculating-stratum-areas.R	1	Park boundaries, trails, roads and point-count stations grouped into transects
script4sien-data-summary-figs.R	2, A4-1	Counts by species and park
script4plotting-effort-adjusted-counts.R	A4-2	Counts by species, park and elevational stratum
script4climateNAdata.R	3, A3-1	Annual PAS and MST anomalies by park
script4plotting-density-est-by-yr.R	4–6, A5	Population density trends over time by park unit(s) or elevational stratum
script4fig-param-ests-SIEN.R	7–11	Parameter estimates for coefficients of model covariates by species and park unit(s)

Table A1-4. Scripts used to generate tables in the current report.

Table-generating script	Table(s)	Table contents
script4calculating-stratum-areas.R	1	Sampling frame areas by stratum
script4sien-data-summaries.R	2–4, A2	Survey effort by year and park unit; frequencies of each group-size and count; frequencies of species by park
script4tabulating-jags-model-specs.R	5–6	List of covariates in final models for each species analyzed
script4harvesting-model-results.R	A6-A11	Parameter estimates for coefficients of model covariates

Appendix 2. Species list by park and record type

Table A2-1. Full species list and park-specific record type for each of 166 bird species detected during 2011–2019 across three parks of the Sierra Nevada Inventory and Monitoring Network: Devils Postpile National Monument (DEPO), Sequoia and Kings Canyon National Parks (SEKI) and Yosemite National Park (YOSE). Records were derived from point-counts (count) or, for species never detected during counts, from observations recorded by survey crews at times other than formal counts (other).

Species	DEPO count	DEPO other	SEKI count	SEKI other	YOSE count	YOSE other
Canada Goose, *Branta canadensis*	–	–	–	–	X	–
Wood Duck, *Aix sponsa*	–	–	–	–	–	X
Mallard, *Anas platyrhynchos*	X	–	X	–	X	–
Bufflehead, *Bucephala albeola*	–	–	–	–	X	–
Common Merganser, *Mergus merganser*	–	X	–	X	X	–
Mountain Quail, *Oreortyx pictus*	X	–	X	–	X	–
California Quail, *Callipepla californica*	–	–	X	–	X	–
Wild Turkey, *Meleagris gallopavo*	–	–	–	–	–	X
White-tailed Ptarmigan, *Lagopus leucura*	–	–	X	–	X	–
Sooty Grouse, *Dendragapus fuliginosus*	X	–	X	–	X	–
Pied-billed Grebe, *Podilymbus podiceps*	–	–	–	–	X	–
Eared Grebe, *Podiceps nigricollis*	–	–	–	–	–	X
Clark's Grebe, *Aechmophorus clarkii*	–	–	–	–	–	X
Band-tailed Pigeon, *Patagioenas fasciata*	X	–	X	–	X	–
Eurasian Collared-Dove, *Streptopelia decaocto*	–	–	–	X	–	–

Table A2-1 (continued). Full species list and park-specific record type for each of 166 bird species detected during 2011–2019 across three parks of the Sierra Nevada Inventory and Monitoring Network: Devils Postpile National Monument (DEPO), Sequoia and Kings Canyon National Parks (SEKI) and Yosemite National Park (YOSE). Records were derived from point-counts (count) or, for species never detected during counts, from observations recorded by survey crews at times other than formal counts (other).

Species	DEPO count	DEPO other	SEKI count	SEKI other	YOSE count	YOSE other
Mourning Dove, *Zenaida macroura*	–	X	X	–	X	–
Common Nighthawk, *Chordeiles minor*	–	–	X	–	–	X
Common Poorwill, *Phalaenoptilus nuttallii*	–	–	–	–	X	–
Black Swift, *Cypseloides niger*	–	–	X	–	X	–
Vaux's Swift, *Chaetura vauxi*	–	X	X	–	X	–
White-throated Swift, *Aeronautes saxatalis*	–	X	X	–	X	–
Anna's Hummingbird, *Calypte anna*	X	–	X	–	X	–
Calliope Hummingbird, *Selasphorus calliope*	X	–	X	–	X	–
Rufous Hummingbird, *Selasphorus rufus*	X	–	X	–	X	–
Allen's Hummingbird, *Selasphorus sasin*	–	–	–	–	–	X
Virginia Rail, *Rallus limicola*	–	–	–	–	X	–
Sora, *Porzana carolina*	–	–	–	–	–	X
American Coot, *Fulica americana*	–	–	–	X	–	–
Killdeer, *Charadrius vociferus*	–	–	–	X	–	–
Least Sandpiper, *Calidris minutilla*	–	–	–	X	–	–
Spotted Sandpiper, *Actitis macularius*	X	–	X	–	X	–

Table A2-1 (continued). Full species list and park-specific record type for each of 166 bird species detected during 2011–2019 across three parks of the Sierra Nevada Inventory and Monitoring Network: Devils Postpile National Monument (DEPO), Sequoia and Kings Canyon National Parks (SEKI) and Yosemite National Park (YOSE). Records were derived from point-counts (count) or, for species never detected during counts, from observations recorded by survey crews at times other than formal counts (other).

Species	DEPO count	DEPO other	SEKI count	SEKI other	YOSE count	YOSE other
California Gull, *Larus californicus*	–	–	X	–	X	–
Double-crested Cormorant, *Nannopterum auritum*	–	–	–	–	–	X
Great Blue Heron, *Ardea herodias*	–	–	–	X	–	X
Turkey Vulture, *Cathartes aura*	–	–	–	X	X	–
Osprey, *Pandion haliaetus*	–	–	–	–	X	–
Golden Eagle, *Aquila chrysaetos*	–	–	X	–	X	–
Sharp-shinned Hawk, *Accipiter striatus*	–	–	X	–	X	–
Cooper's Hawk, *Accipiter cooperii*	–	–	X	–	X	–
Northern Goshawk, *Accipiter gentilis*	X	–	X	–	X	–
Bald Eagle, *Haliaeetus leucocephalus*	–	–	X	–	–	X
Red-shouldered Hawk, *Buteo lineatus*	–	–	X	–	X	–
Red-tailed Hawk, *Buteo jamaicensis*	X	–	X	–	X	–
Barn Owl, *Tyto alba*	–	–	–	X	–	–
Flammulated Owl, *Psiloscops flammeolus*	–	–	X	–	–	X
Western Screech-Owl, *Megascops kennicottii*	–	–	–	X	–	X
Great Horned Owl, *Bubo virginianus*	X	–	–	X	–	X

Table A2-1 (continued). Full species list and park-specific record type for each of 166 bird species detected during 2011–2019 across three parks of the Sierra Nevada Inventory and Monitoring Network: Devils Postpile National Monument (DEPO), Sequoia and Kings Canyon National Parks (SEKI) and Yosemite National Park (YOSE). Records were derived from point-counts (count) or, for species never detected during counts, from observations recorded by survey crews at times other than formal counts (other).

Species	DEPO count	DEPO other	SEKI count	SEKI other	YOSE count	YOSE other
Northern Pygmy-Owl, *Glaucidium gnoma*	X	–	X	–	X	–
Spotted Owl, *Strix occidentalis*	–	–	X	–	X	–
Great Gray Owl, *Strix nebulosa*	–	–	–	–	–	X
Northern Saw-whet Owl, *Aegolius acadicus*	–	–	–	X	–	X
Belted Kingfisher, *Megaceryle alcyon*	X	–	X	–	X	–
Acorn Woodpecker, *Melanerpes formicivorus*	–	–	X	–	X	–
Williamson's Sapsucker, *Sphyrapicus thyroideus*	X	–	X	–	X	–
Red-breasted Sapsucker, *Sphyrapicus ruber*	X	–	X	–	X	–
Black-backed Woodpecker, *Picoides arcticus*	X	–	–	X	X	–
Downy Woodpecker, *Dryobates pubescens*	X	–	X	–	X	–
Nuttall's Woodpecker, *Dryobates nuttallii*	–	–	X	–	X	–
Hairy Woodpecker, *Dryobates villosus*	X	–	X	–	X	–
White-headed Woodpecker, *Dryobates albolarvatus*	X	–	X	–	X	–
Northern Flicker, *Colaptes auratus*	X	–	X	–	X	–
Pileated Woodpecker, *Dryocopus pileatus*	X	–	X	–	X	–
American Kestrel, *Falco sparverius*	X	–	X	–	X	–

Table A2-1 (continued). Full species list and park-specific record type for each of 166 bird species detected during 2011–2019 across three parks of the Sierra Nevada Inventory and Monitoring Network: Devils Postpile National Monument (DEPO), Sequoia and Kings Canyon National Parks (SEKI) and Yosemite National Park (YOSE). Records were derived from point-counts (count) or, for species never detected during counts, from observations recorded by survey crews at times other than formal counts (other).

Species	DEPO count	DEPO other	SEKI count	SEKI other	YOSE count	YOSE other
Peregrine Falcon, *Falco peregrinus*	–	–	X	–	X	–
Prairie Falcon, *Falco mexicanus*	–	–	–	X	–	X
Ash-throated Flycatcher, *Myiarchus cinerascens*	–	–	X	–	X	–
Western Kingbird, *Tyrannus verticalis*	–	–	–	X	X	–
Olive-sided Flycatcher, *Contopus cooperi*	X	–	X	–	X	–
Western Wood-Pewee, *Contopus sordidulus*	X	–	X	–	X	–
Willow Flycatcher, *Empidonax traillii*	–	–	–	–	–	X
Hammond's Flycatcher, *Empidonax hammondii*	X	–	X	–	X	–
Gray Flycatcher, *Empidonax wrightii*	–	–	–	–	–	X
Dusky Flycatcher, *Empidonax oberholseri*	X	–	X	–	X	–
Pacific-slope Flycatcher, *Empidonax difficilis*	X	–	X	–	X	–
Black Phoebe, *Sayornis nigricans*	X	–	X	–	X	–
Say's Phoebe, *Sayornis saya*	–	–	–	–	–	X
Vermilion Flycatcher, *Pyrocephalus rubinus*	–	–	–	X	–	–
Hutton's Vireo, *Vireo huttoni*	–	–	X	–	X	–
Cassin's Vireo, *Vireo cassinii*	X	–	X	–	X	–

Table A2-1 (continued). Full species list and park-specific record type for each of 166 bird species detected during 2011–2019 across three parks of the Sierra Nevada Inventory and Monitoring Network: Devils Postpile National Monument (DEPO), Sequoia and Kings Canyon National Parks (SEKI) and Yosemite National Park (YOSE). Records were derived from point-counts (count) or, for species never detected during counts, from observations recorded by survey crews at times other than formal counts (other).

Species	DEPO count	DEPO other	SEKI count	SEKI other	YOSE count	YOSE other
Warbling Vireo, *Vireo gilvus*	X	–	X	–	X	–
Steller's Jay, *Cyanocitta stelleri*	X	–	X	–	X	–
California Scrub-Jay, *Aphelocoma californica*	–	–	X	–	X	–
Clark's Nutcracker, *Nucifraga columbiana*	X	–	X	–	X	–
American Crow, *Corvus brachyrhynchos*	–	–	X	–	–	–
Common Raven, *Corvus corax*	X	–	X	–	X	–
Mountain Chickadee, *Poecile gambeli*	X	–	X	–	X	–
Chestnut-backed Chickadee, *Poecile rufescens*	–	–	–	–	X	–
Oak Titmouse, *Baeolophus inornatus*	–	–	X	–	X	–
Horned Lark, *Eremophila alpestris*	–	–	–	X	X	–
Tree Swallow, *Tachycineta bicolor*	X	–	X	–	–	X
Violet-green Swallow, *Tachycineta thalassina*	X	–	X	–	X	–
Northern Rough-winged Swallow, *Stelgidopteryx serripennis*	X	–	–	X	X	–
Purple Martin, *Progne subis*	–	–	–	X	–	–
Barn Swallow, *Hirundo rustica*	–	–	–	–	–	X
Cliff Swallow, *Petrochelidon pyrrhonota*	X	–	–	X	X	–

Table A2-1 (continued). Full species list and park-specific record type for each of 166 bird species detected during 2011–2019 across three parks of the Sierra Nevada Inventory and Monitoring Network: Devils Postpile National Monument (DEPO), Sequoia and Kings Canyon National Parks (SEKI) and Yosemite National Park (YOSE). Records were derived from point-counts (count) or, for species never detected during counts, from observations recorded by survey crews at times other than formal counts (other).

Species	DEPO count	DEPO other	SEKI count	SEKI other	YOSE count	YOSE other
Bushtit, *Psaltriparus minimus*	–	X	X	–	X	–
Wrentit, *Chamaea fasciata*	–	–	X	–	X	–
Golden-crowned Kinglet, *Regulus satrapa*	X	–	X	–	X	–
Ruby-crowned Kinglet, *Corthylio calendula*	X	–	X	–	X	–
Cedar Waxwing, *Bombycilla cedrorum*	–	–	–	–	–	X
Phainopepla, *Phainopepla nitens*	–	–	–	X	–	–
Red-breasted Nuthatch, *Sitta canadensis*	X	–	X	–	X	–
White-breasted Nuthatch, *Sitta carolinensis*	X	–	X	–	X	–
Pygmy Nuthatch, *Sitta pygmaea*	X	–	X	–	X	–
Brown Creeper, *Certhia americana*	X	–	X	–	X	–
Blue-gray Gnatcatcher, *Polioptila caerulea*	–	X	X	–	X	–
Rock Wren, *Salpinctes obsoletus*	X	–	X	–	X	–
Canyon Wren, *Catherpes mexicanus*	–	–	X	–	X	–
House Wren, *Troglodytes aedon*	X	–	X	–	X	–
Pacific Wren, *Troglodytes pacificus*	–	–	X	–	X	–
Bewick's Wren, *Thryomanes bewickii*	–	–	X	–	X	–

Table A2-1 (continued). Full species list and park-specific record type for each of 166 bird species detected during 2011–2019 across three parks of the Sierra Nevada Inventory and Monitoring Network: Devils Postpile National Monument (DEPO), Sequoia and Kings Canyon National Parks (SEKI) and Yosemite National Park (YOSE). Records were derived from point-counts (count) or, for species never detected during counts, from observations recorded by survey crews at times other than formal counts (other).

Species	DEPO count	DEPO other	SEKI count	SEKI other	YOSE count	YOSE other
California Thrasher, *Toxostoma redivivum*	–	–	X	–	–	X
European Starling, *Sturnus vulgaris*	–	–	–	X	–	X
American Dipper, *Cinclus mexicanus*	X	–	X	–	X	–
Western Bluebird, *Sialia mexicana*	–	–	X	–	X	–
Mountain Bluebird, *Sialia currucoides*	X	–	X	–	X	–
Townsend's Solitaire, *Myadestes townsendi*	X	–	X	–	X	–
Swainson's Thrush, *Catharus ustulatus*	–	–	–	–	X	–
Hermit Thrush, *Catharus guttatus*	X	–	X	–	X	–
American Robin, *Turdus migratorius*	X	–	X	–	X	–
House Sparrow, *Passer domesticus*	–	–	–	X	–	X
American Pipit, *Anthus rubescens*	–	–	X	–	X	–
Evening Grosbeak, *Coccothraustes vespertinus*	X	–	X	–	X	–
Pine Grosbeak, *Pinicola enucleator*	X	–	X	–	X	–
Gray-crowned Rosy-Finch, *Leucosticte tephrocotis*	–	–	X	–	X	–
House Finch, *Haemorhous mexicanus*	X	–	X	–	–	–
Purple Finch, *Haemorhous purpureus*	X	–	X	–	X	–

Table A2-1 (continued). Full species list and park-specific record type for each of 166 bird species detected during 2011–2019 across three parks of the Sierra Nevada Inventory and Monitoring Network: Devils Postpile National Monument (DEPO), Sequoia and Kings Canyon National Parks (SEKI) and Yosemite National Park (YOSE). Records were derived from point-counts (count) or, for species never detected during counts, from observations recorded by survey crews at times other than formal counts (other).

Species	DEPO count	DEPO other	SEKI count	SEKI other	YOSE count	YOSE other
Cassin's Finch, *Haemorhous cassinii*	X	–	X	–	X	–
Red Crossbill, *Loxia curvirostra*	X	–	X	–	X	–
Pine Siskin, *Spinus pinus*	X	–	X	–	X	–
Lesser Goldfinch, *Spinus psaltria*	X	–	X	–	X	–
Lawrence's Goldfinch, *Spinus lawrencei*	–	–	X	–	–	X
Black-throated Sparrow, *Amphispiza bilineata*	–	–	–	X	–	X
Lark Sparrow, *Chondestes grammacus*	–	–	–	X	–	X
Chipping Sparrow, *Spizella passerina*	X	–	X	–	X	–
Black-chinned Sparrow, *Spizella atrogularis*	–	–	–	–	X	–
Brewer's Sparrow, *Spizella breweri*	–	–	–	–	X	–
Fox Sparrow, *Passerella iliaca*	X	–	X	–	X	–
Dark-eyed Junco, *Junco hyemalis*	X	–	X	–	X	–
White-crowned Sparrow, *Zonotrichia leucophrys*	X	–	X	–	X	–
Golden-crowned Sparrow, *Zonotrichia atricapilla*	–	–	–	X	–	X
Savannah Sparrow, *Passerculus sandwichensis*	–	–	–	–	X	–
Song Sparrow, *Melospiza melodia*	X	–	X	–	X	–

Table A2-1 (continued). Full species list and park-specific record type for each of 166 bird species detected during 2011–2019 across three parks of the Sierra Nevada Inventory and Monitoring Network: Devils Postpile National Monument (DEPO), Sequoia and Kings Canyon National Parks (SEKI) and Yosemite National Park (YOSE). Records were derived from point-counts (count) or, for species never detected during counts, from observations recorded by survey crews at times other than formal counts (other).

Species	DEPO count	DEPO other	SEKI count	SEKI other	YOSE count	YOSE other
Lincoln's Sparrow, *Melospiza lincolnii*	X	–	X	–	X	–
California Towhee, *Melozone crissalis*	–	–	X	–	X	–
Rufous-crowned Sparrow, *Aimophila ruficeps*	–	–	–	X	X	–
Green-tailed Towhee, *Pipilo chlorurus*	X	–	X	–	X	–
Spotted Towhee, *Pipilo maculatus*	X	–	X	–	X	–
Bullock's Oriole, *Icterus bullockii*	–	–	X	–	X	–
Red-winged Blackbird, *Agelaius phoeniceus*	–	–	X	–	X	–
Brown-headed Cowbird, *Molothrus ater*	X	–	X	–	X	–
Brewer's Blackbird, *Euphagus cyanocephalus*	X	–	X	–	X	–
Great-tailed Grackle, *Quiscalus mexicanus*	–	–	–	X	–	X
Orange-crowned Warbler, *Leiothlypis celata*	X	–	X	–	X	–
Nashville Warbler, *Leiothlypis ruficapilla*	X	–	X	–	X	–
MacGillivray's Warbler, *Geothlypis tolmiei*	X	–	X	–	X	–
Common Yellowthroat, *Geothlypis trichas*	–	–	–	–	–	X
Yellow Warbler, *Setophaga petechia*	X	–	X	–	X	–
Yellow-rumped Warbler, *Setophaga coronata*	X	–	X	–	X	–

Table A2-1 (continued). Full species list and park-specific record type for each of 166 bird species detected during 2011–2019 across three parks of the Sierra Nevada Inventory and Monitoring Network: Devils Postpile National Monument (DEPO), Sequoia and Kings Canyon National Parks (SEKI) and Yosemite National Park (YOSE). Records were derived from point-counts (count) or, for species never detected during counts, from observations recorded by survey crews at times other than formal counts (other).

Species	DEPO count	DEPO other	SEKI count	SEKI other	YOSE count	YOSE other
Black-throated Gray Warbler, *Setophaga nigrescens*	–	–	X	–	X	–
Townsend's Warbler, *Setophaga townsendi*	–	–	–	X	X	–
Hermit Warbler, *Setophaga occidentalis*	X	–	X	–	X	–
Wilson's Warbler, *Cardellina pusilla*	X	–	X	–	X	–
Western Tanager, *Piranga ludoviciana*	X	–	X	–	X	–
Black-headed Grosbeak, *Pheucticus melanocephalus*	X	–	X	–	X	–
Lazuli Bunting, *Passerina amoena*	X	–	X	–	X	–

Appendix 3. Climate in Devils Postpile National Monument

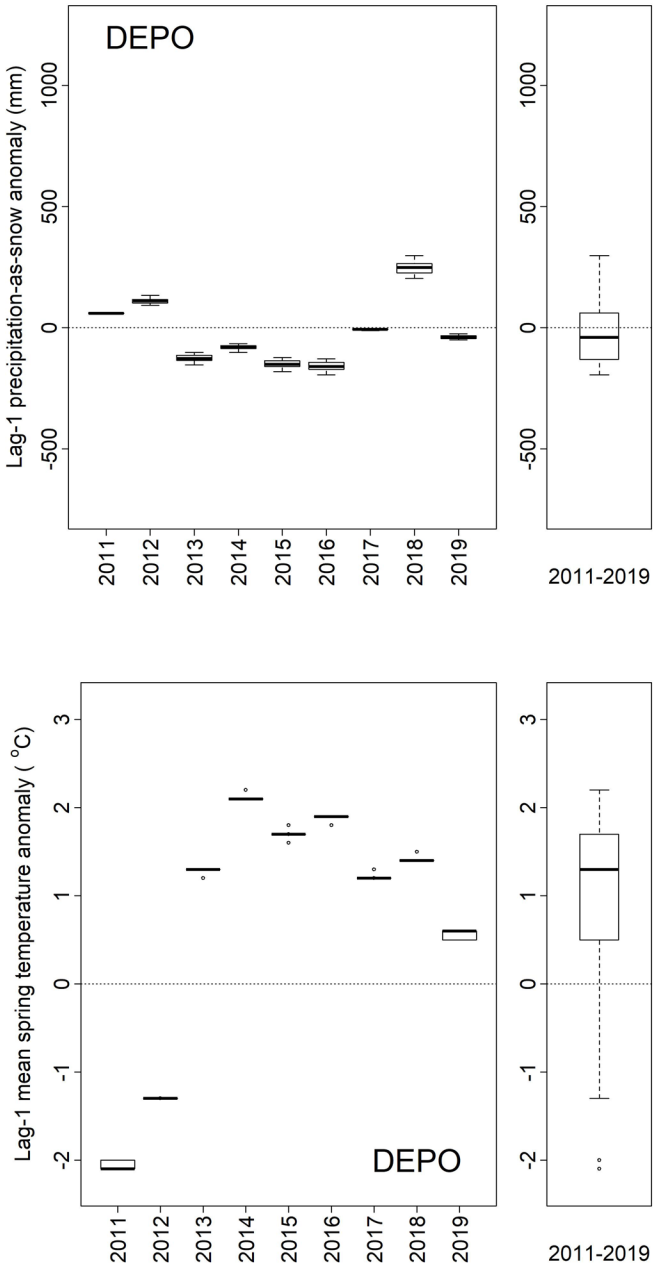


Figure A3-1. Time-lagged anomalies in precipitation-as-snow (*PAS*) for each point-count station in Devils Postpile National Monument (DEPO). Annual and time-averaged anomalies are shown in left- and right-hand panels for each climate metric. *PAS* is expressed here as the deviation from 1981–2010 normals for data from August 1st of year *t*-1 to July 31st of year *t* and are further lagged one year to serve as a potential covariate of demographic response to breeding habitat conditions. *MST* is expressed here as the deviation from 1981–2010 normals for data from March 1st to May 31st, again lagged by one year. Each boxplot indicates the median (thick horizontal line), interquartile range (box), and range of the data (whiskers), excepting outliers (dots) >1.5 times the interquartile range.

Appendix 4. Counts by species, park and elevation

Effort-adjusted counts of species are shown for Devils Postpile National Monument in Figure A4-1 and for Sequoia and Kings Canyon and Yosemite National Parks in Figures A4-2a through A4-2e.

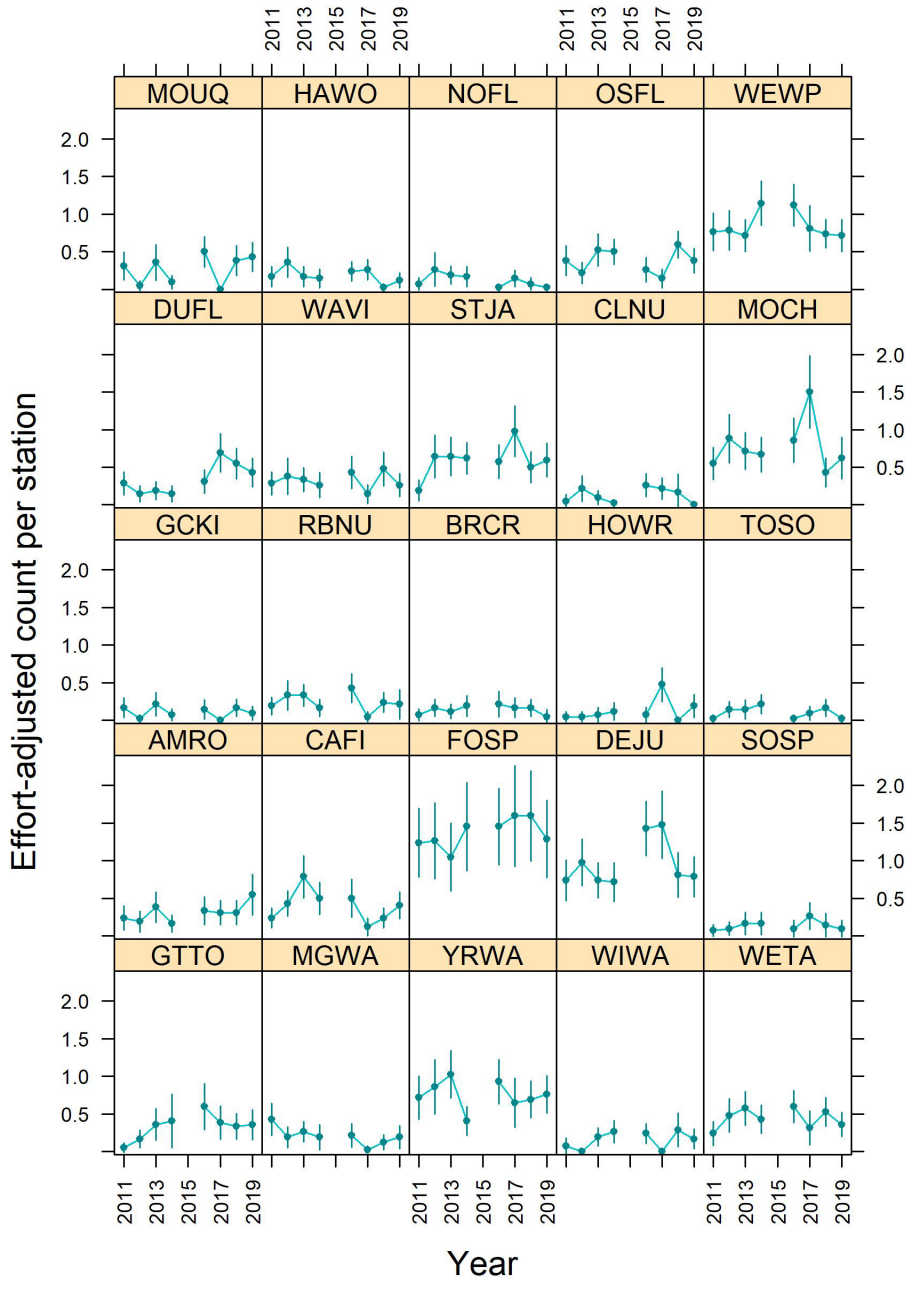


Figure A4-1. Effort-adjusted count per station for 25 species analyzed in Devils Postpile National Monument. Species appear in taxonomical order, and species abbreviations are defined in Table 4 of the main text. Vertical lines represent approximate 95% confidence intervals based on count variation across stations. Counts were conducted annually from 2011 to 2014 and 2016 to 2019.

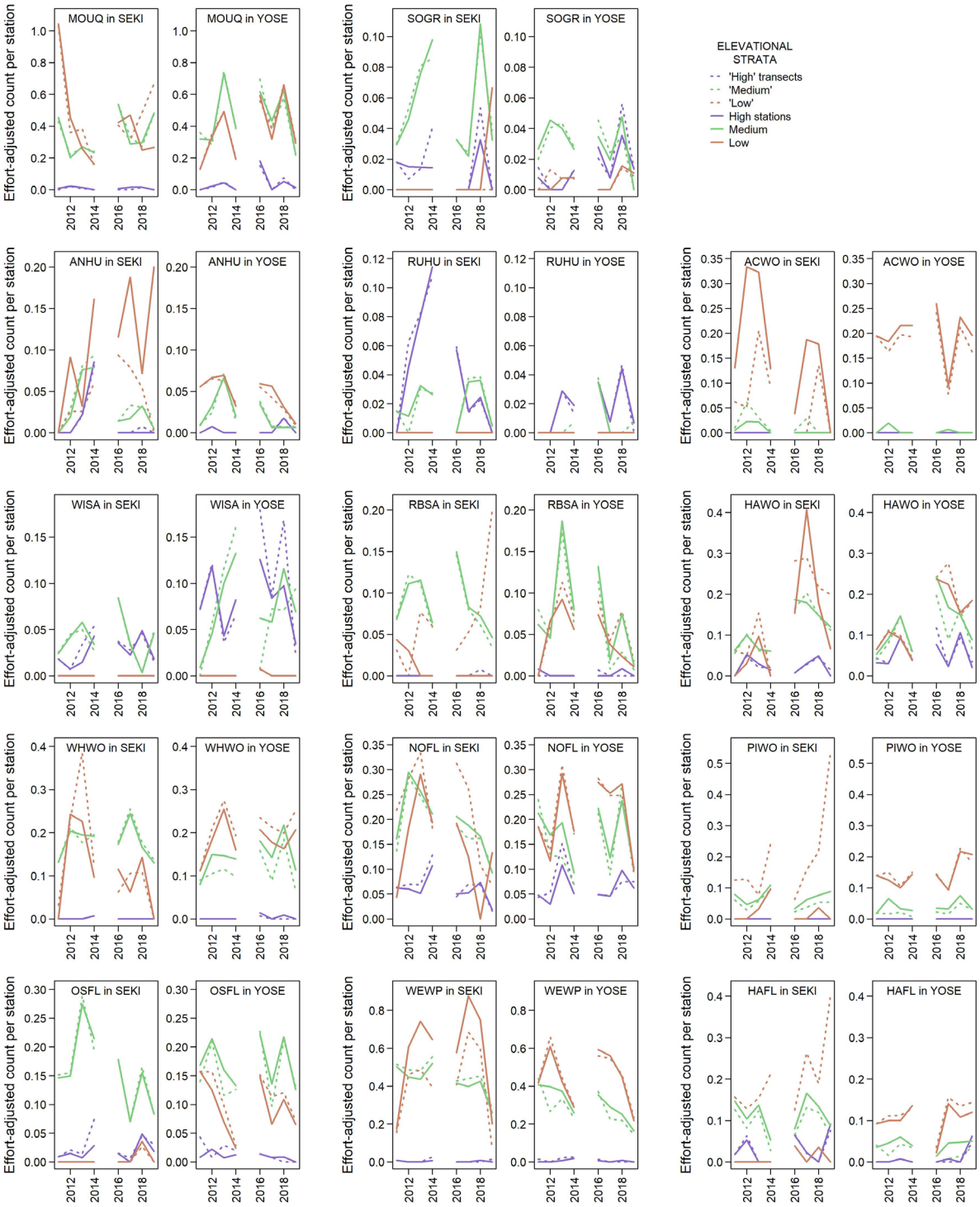


Figure A4-2a. Effort-adjusted counts for 14 of 62 species analyzed in Sequoia and Kings Canyon National Parks (SEKI) and Yosemite National Park (YOSE). Species appear in taxonomical order, and species abbreviations are defined in Table 4 of the main text. Using the elevational stratum definitions in Table 1 of the main text, counts by design stratum (dashed lines) were based on the elevation of each transect origin, while counts by realized stratum (solid lines) were based on the elevation of each station. Counts were conducted annually from 2011 to 2014 and 2016 to 2019.

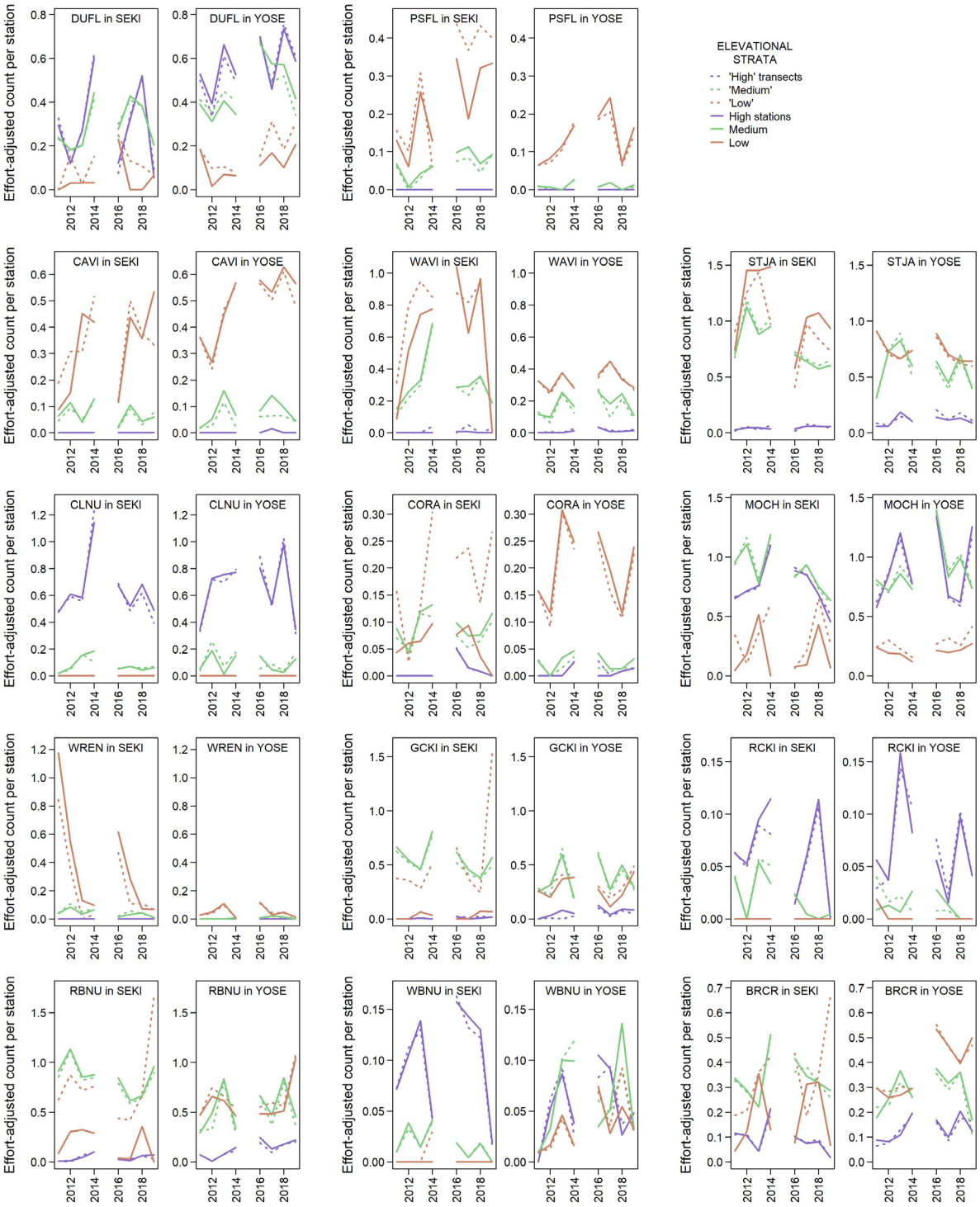


Figure A4-2b. Effort-adjusted counts for 14 of 62 species analyzed in Sequoia and Kings Canyon National Parks (SEKI) and Yosemite National Park (YOSE). Species appear in taxonomical order, and species abbreviations are defined in Table 4 of the main text. Using the elevational stratum definitions in Table 1 of the main text, counts by design stratum (dashed lines) were based on the elevation of each transect origin, while counts by realized stratum (solid lines) were based on the elevation of each station. Counts were conducted annually from 2011 to 2014 and 2016 to 2019.

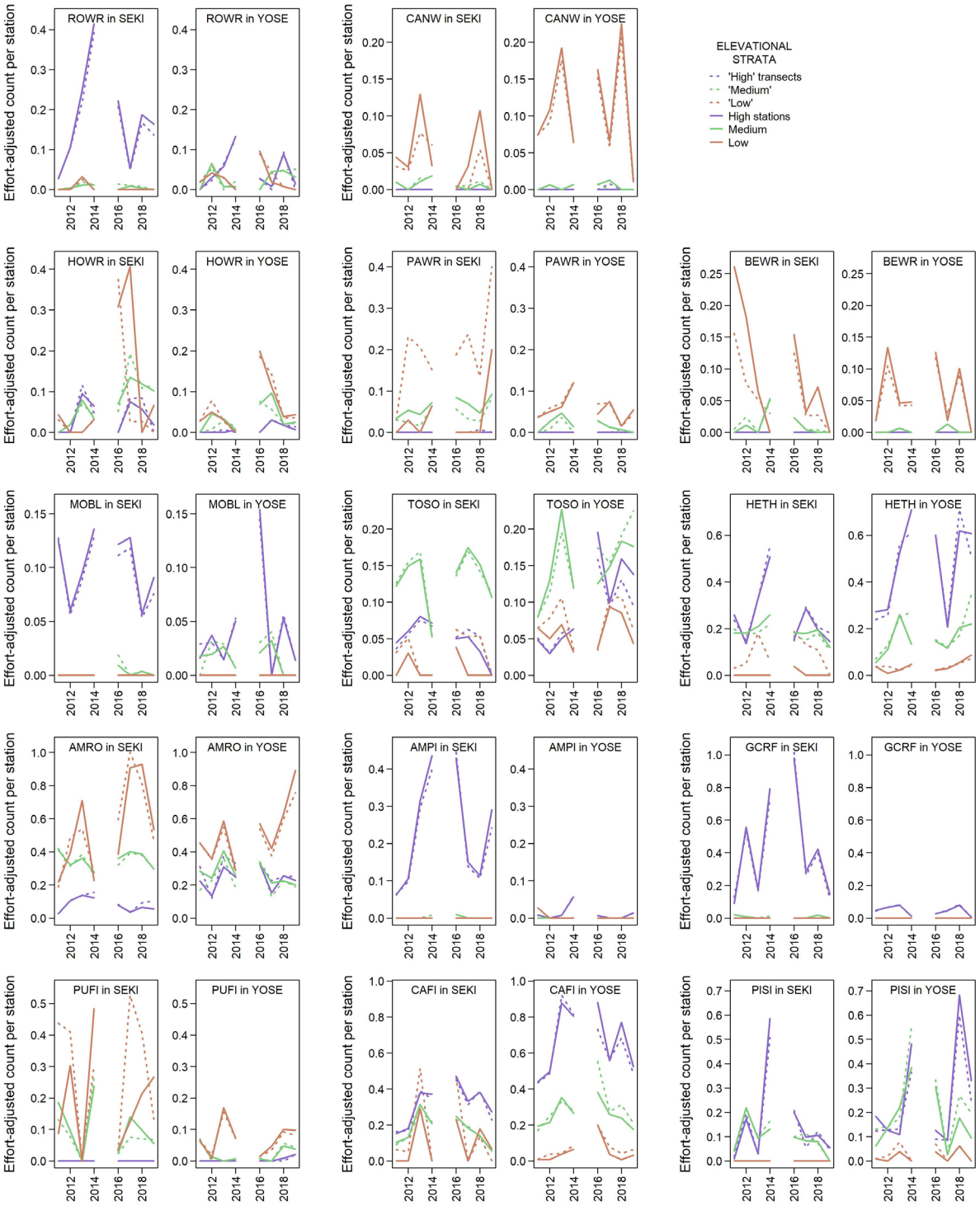


Figure A4-2c. Effort-adjusted counts for 14 of 62 species analyzed in Sequoia and Kings Canyon National Parks (SEKI) and Yosemite National Park (YOSE). Species appear in taxonomical order, and species abbreviations are defined in Table 4 of the main text. Using the elevational stratum definitions in Table 1 of the main text, counts by design stratum (dashed lines) were based on the elevation of each transect origin, while counts by realized stratum (solid lines) were based on the elevation of each station. Counts were conducted annually from 2011 to 2014 and 2016 to 2019.

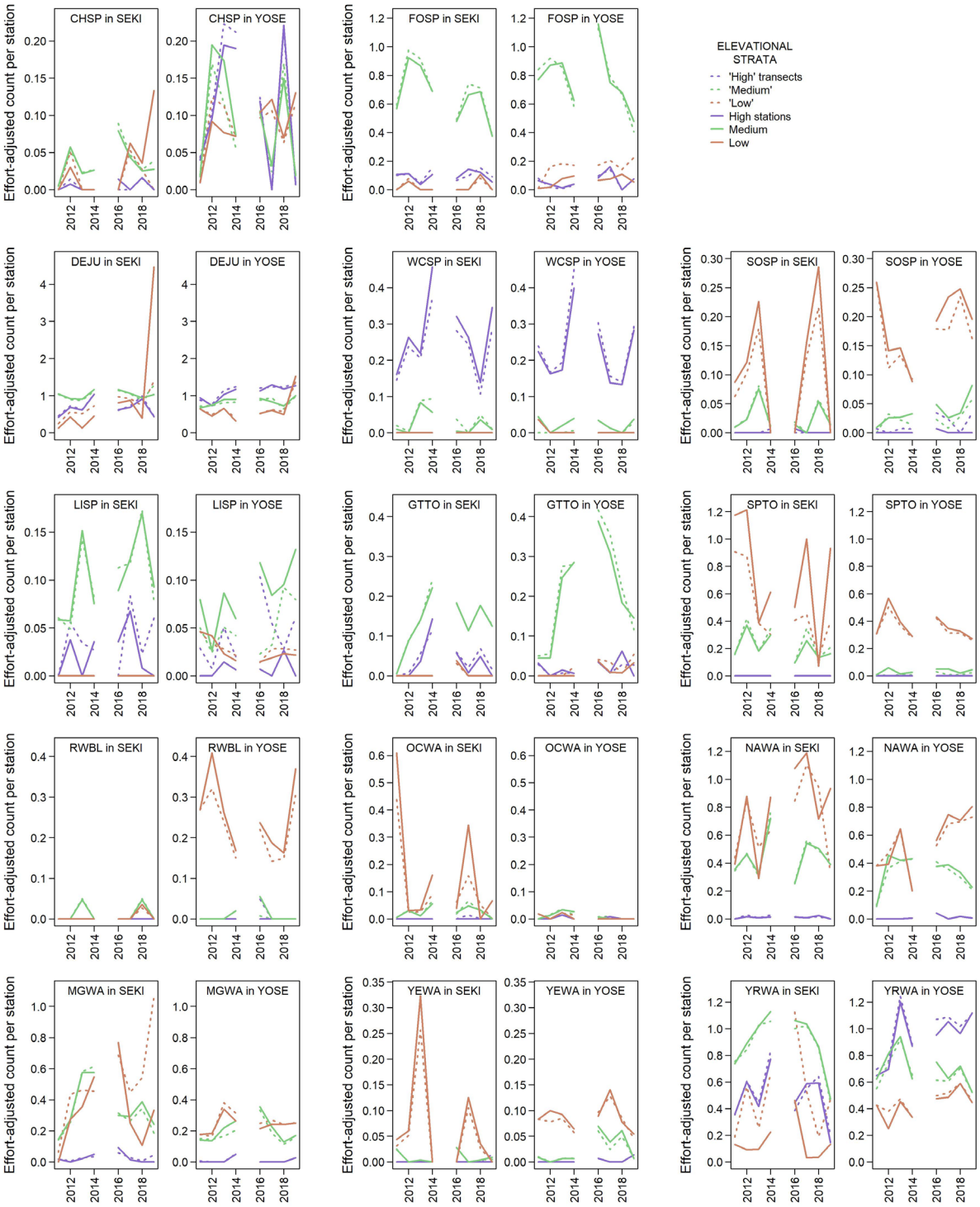


Figure A4-2d. Effort-adjusted counts for 14 of 62 species analyzed in Sequoia and Kings Canyon National Parks (SEKI) and Yosemite National Park (YOSE). Species appear in taxonomical order, and species abbreviations are defined in Table 4 of the main text. Using the elevational stratum definitions in Table 1 of the main text, counts by design stratum (dashed lines) were based on the elevation of each transect origin, while counts by realized stratum (solid lines) were based on the elevation of each station. Counts were conducted annually from 2011 to 2014 and 2016 to 2019.

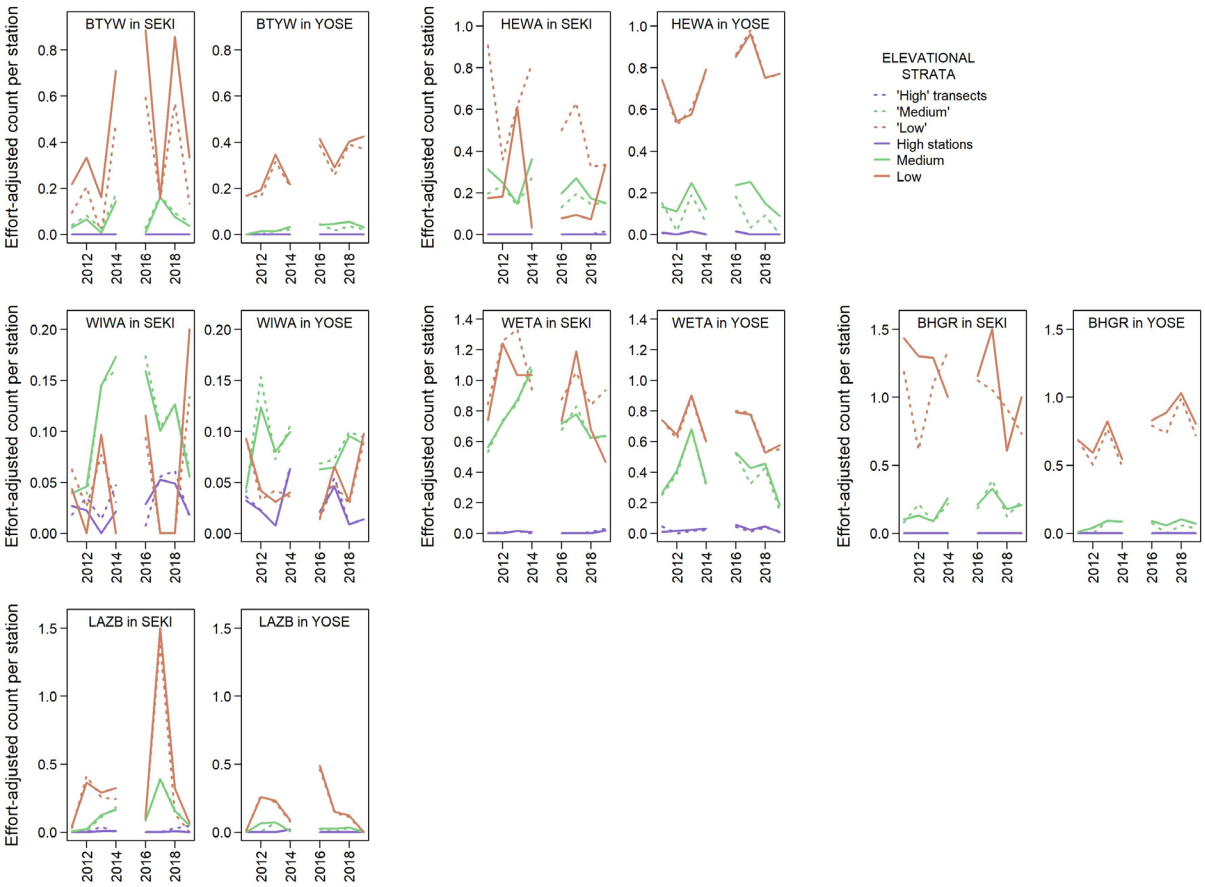


Figure A4-2e. Effort-adjusted counts for six of 62 species analyzed in Sequoia and Kings Canyon National Parks (SEKI) and Yosemite National Park (YOSE). Species appear in taxonomical order, and species abbreviations are defined in Table 4 of the main text. Using the elevational stratum definitions in Table 1 of the main text, counts by design stratum (dashed lines) were based on the elevation of each transect origin, while counts by realized stratum (solid lines) were based on the elevation of each station. Counts were conducted annually from 2011 to 2014 and 2016 to 2019.

Appendix 5. Average population growth at the largest scale of analysis

Temporal trends in avian population density estimated from hierarchical models of breeding-season point-count data collected during 2011–2019 and combined across two park units in the Sierra Nevada Inventory and Monitoring Network, Sequoia and Kings Canyon National Parks (SEKI) and Yosemite National Park (YOSE). The trend in population density combined across both parks is presented for each of 62 species (Figures A5-1a through A5-1h, beginning on the next page). For each species, we report the elevational strata considered in the model, including High, Medium and/or Low elevations as defined in Table 1 of the main text, as well as two metrics of population growth: 1) a smoothed growth curve based on Poisson regression through our estimates of annual mean density and characterized by λ_P, the mean regression coefficient; and 2) the geometric mean rate of growth in population density, λ_G, accounting for the full range of estimates generated by the hierarchical model and serial correlation in those estimates. Support for each trend in population density is determined by the 95% credible interval (CRI) on λ_G, indicated by an asterisk and a solid regression curve when the CRI on λ_G did not overlap zero.

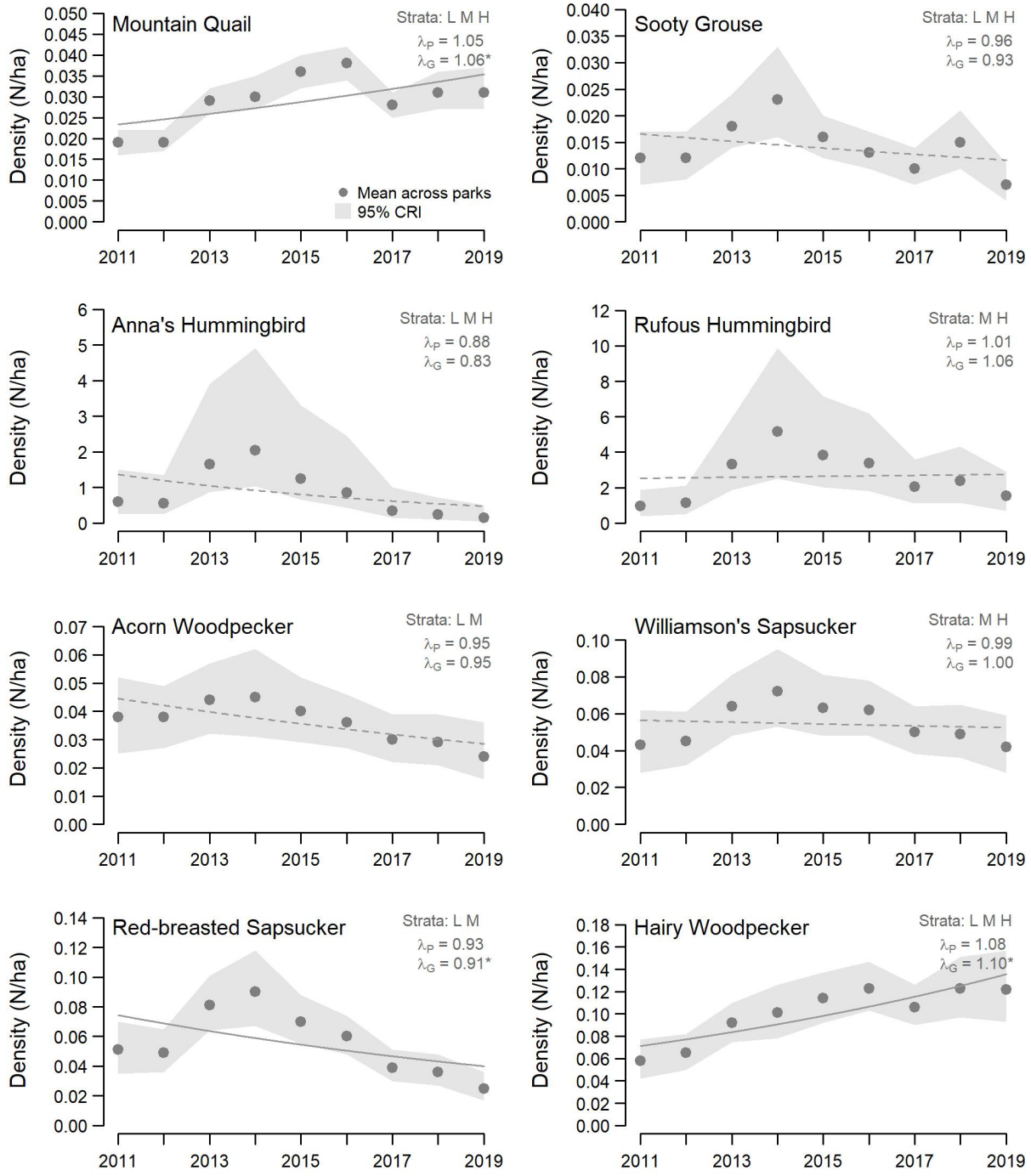


Figure A5-1a. Network-level density estimates for Mountain Quail, Sooty Grouse, Anna's Hummingbird, Rufous Hummingbird, Acorn Woodpecker, Williamson's Sapsucker, Red-breasted Sapsucker and Hairy Woodpecker, derived using a hierarchical analysis of point counts from low (L), medium (M) and/or high (H) elevation strata in Sequoia and Kings Canyon National Parks and Yosemite National Park (Table 1). Smoothed trends (curves) and both smoothed (λ_P) and geometric mean (λ_G) population growth rates are shown. Solid curves and asterisks indicate strongly supported trends for which the 95% credible interval (CRI) on λ_G did not overlap 1. Species are listed in taxonomic order (Table 4).

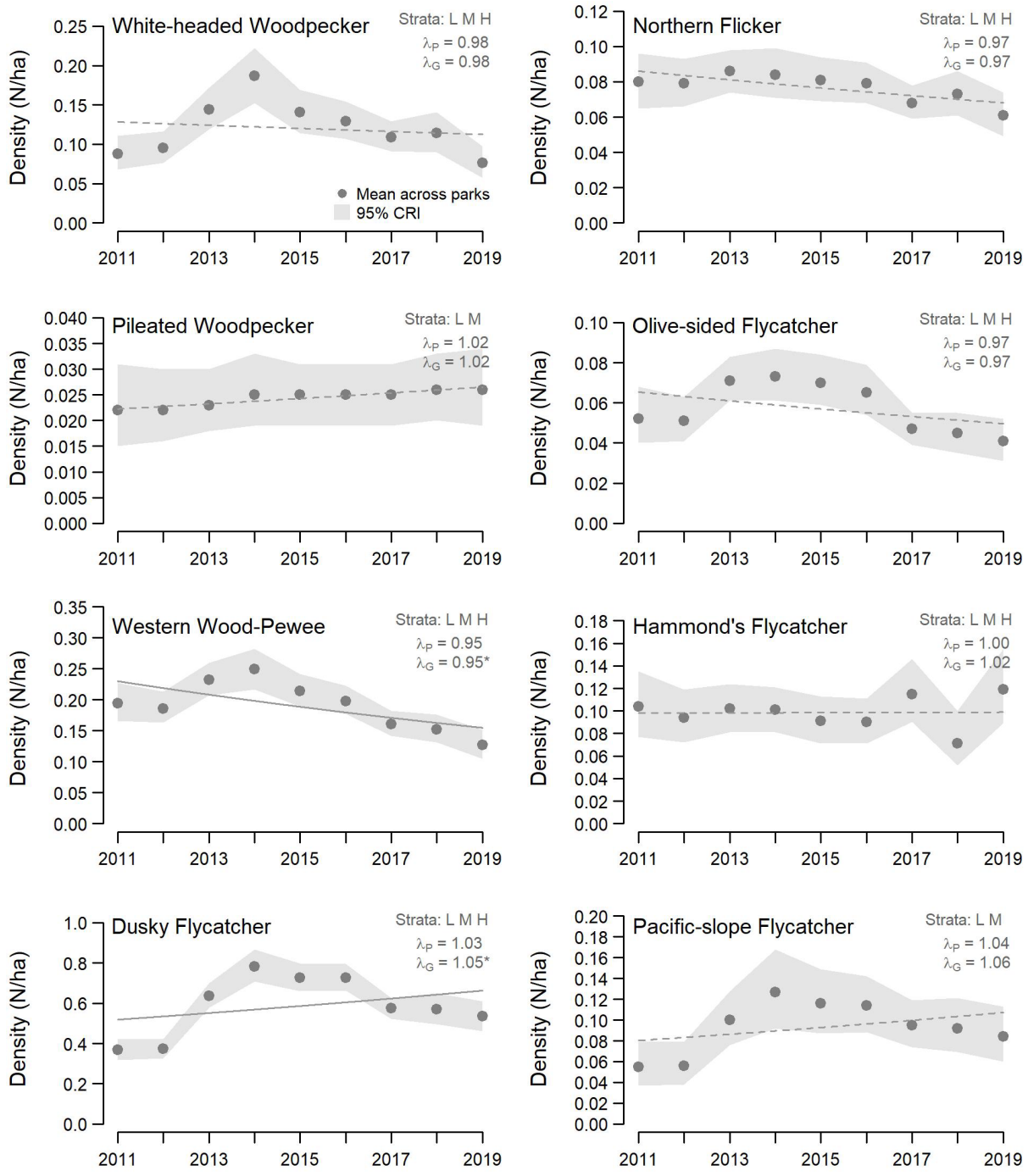


Figure A5-1b. Network-level density estimates for White-headed Woodpecker, Northern Flicker, Pileated Woodpecker, Olive-sided Flycatcher, Western Wood-Pewee, Hammond's Flycatcher, Dusky Flycatcher and Pacific-slope Flycatcher, derived using a hierarchical analysis of point counts from low (L), medium (M) and/or high (H) elevation strata in Sequoia and Kings Canyon National Parks and Yosemite National Park (Table 1). Smoothed trends (curves) and both smoothed (λ_P) and geometric mean (λ_G) population growth rates are shown. Solid curves and asterisks indicate strongly supported trends for which the 95% credible interval (CRI) on λ_G did not overlap 1. Species are listed in taxonomic order (Table 4).

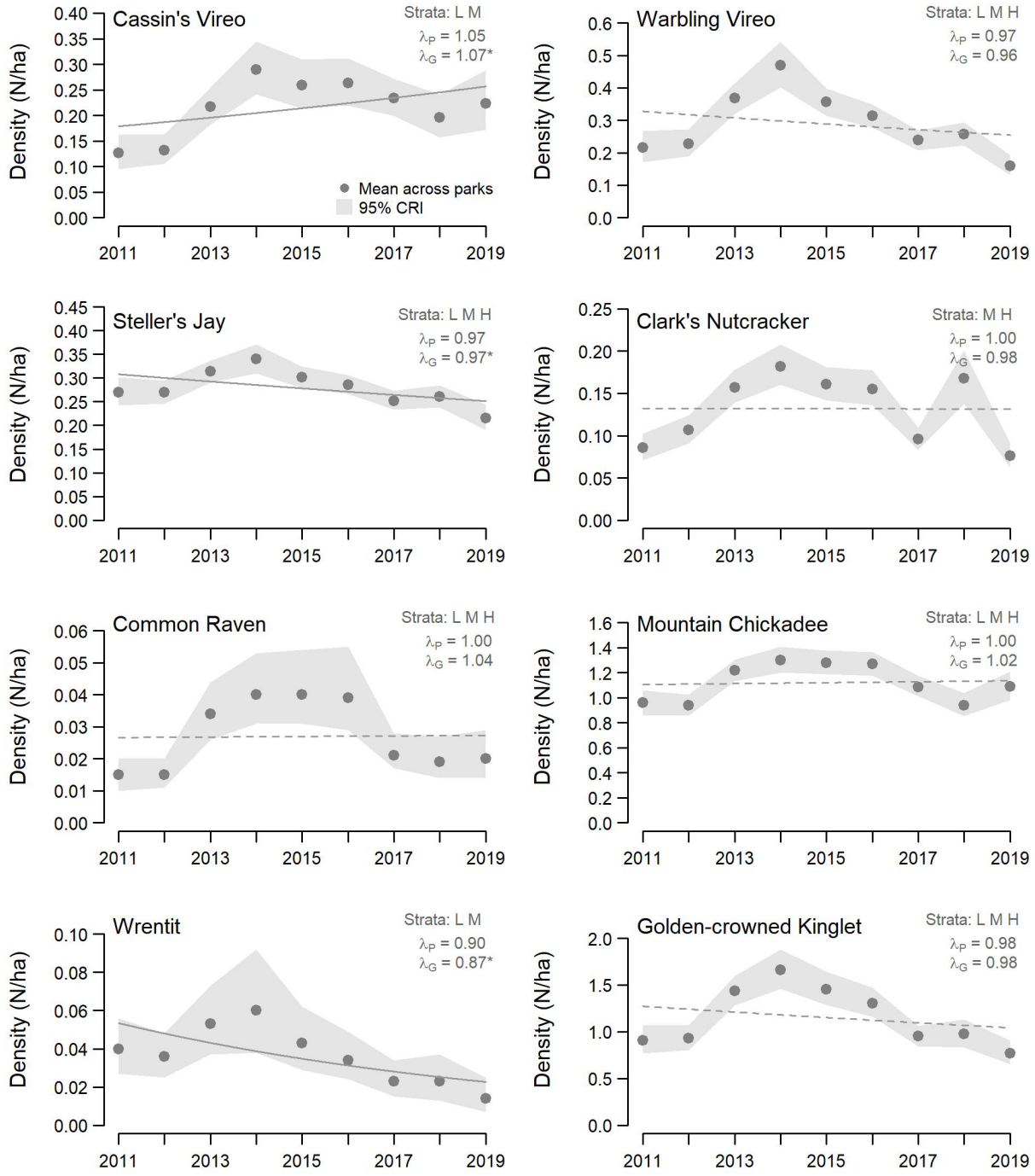


Figure A5-1c. Network-level density estimates for Cassin's Vireo, Warbling Vireo, Steller's Jay, Clark's Nutcracker, Common Raven, Mountain Chickadee, Wrentit and Golden-crowned Kinglet, derived using a hierarchical analysis of point counts from low (L), medium (M) and/or high (H) elevation strata in Sequoia and Kings Canyon National Parks and Yosemite National Park (Table 1). Smoothed trends (curves) and both smoothed (λ_P) and geometric mean (λ_G) population growth rates are shown. Solid curves and asterisks indicate strongly supported trends for which the 95% credible interval (CRI) on λ_G did not overlap 1. Species are listed in taxonomic order (Table 4).

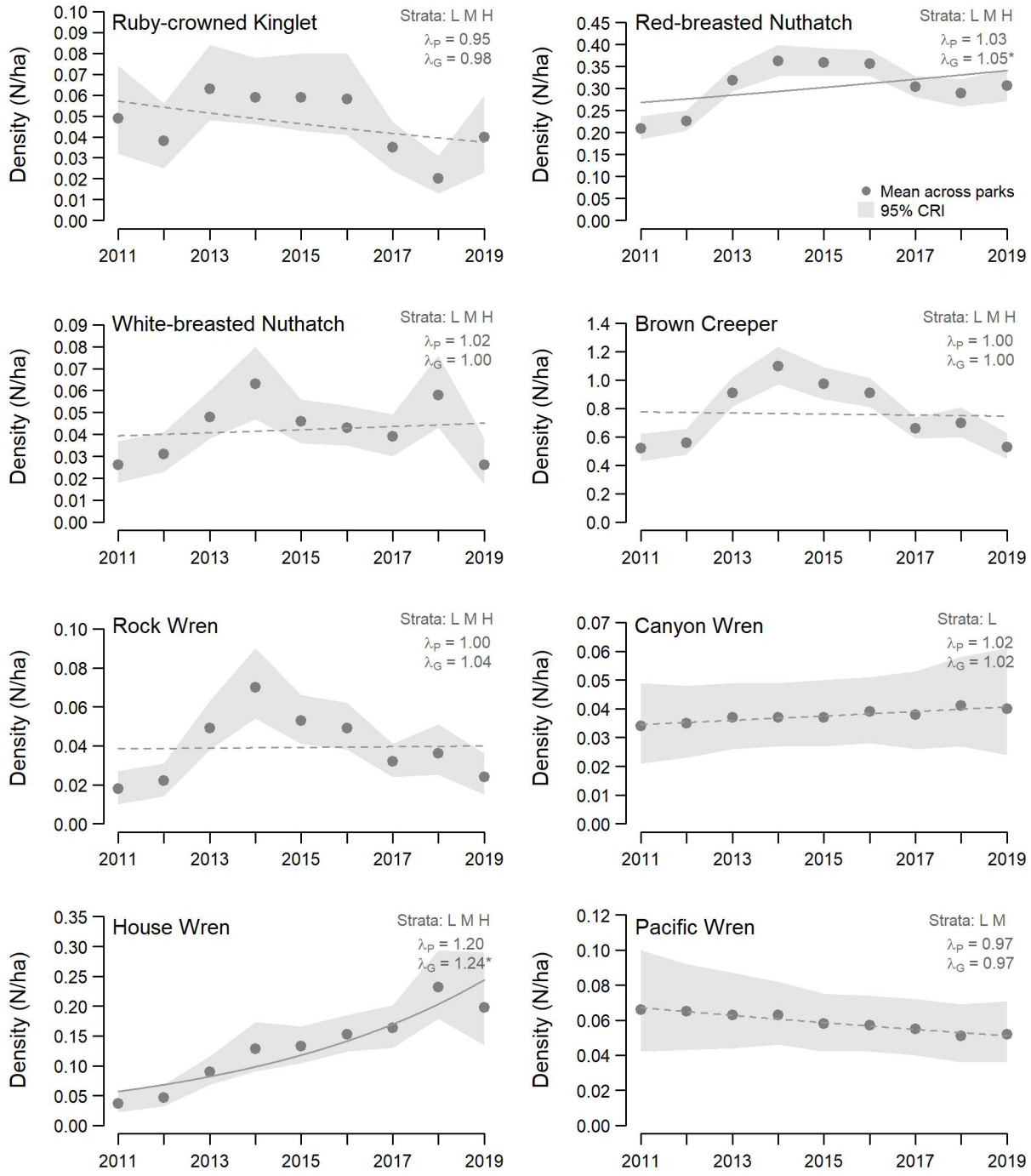


Figure A5-1d. Network-level density estimates for Ruby-crowned Kinglet, Red-breasted Nuthatch, White-breasted Nuthatch, Brown Creeper, Rock Wren, Canyon Wren, House Wren and Pacific Wren, derived using a hierarchical analysis of point counts from low (L), medium (M) and/or high (H) elevation strata in Sequoia and Kings Canyon National Parks and Yosemite National Park (Table 1). Smoothed trends (curves) and both smoothed (λ_P) and geometric mean (λ_G) population growth rates are shown. Solid curves and asterisks indicate strongly supported trends for which the 95% credible interval (CRI) on λ_G did not overlap 1. Species are listed in taxonomic order (Table 4).

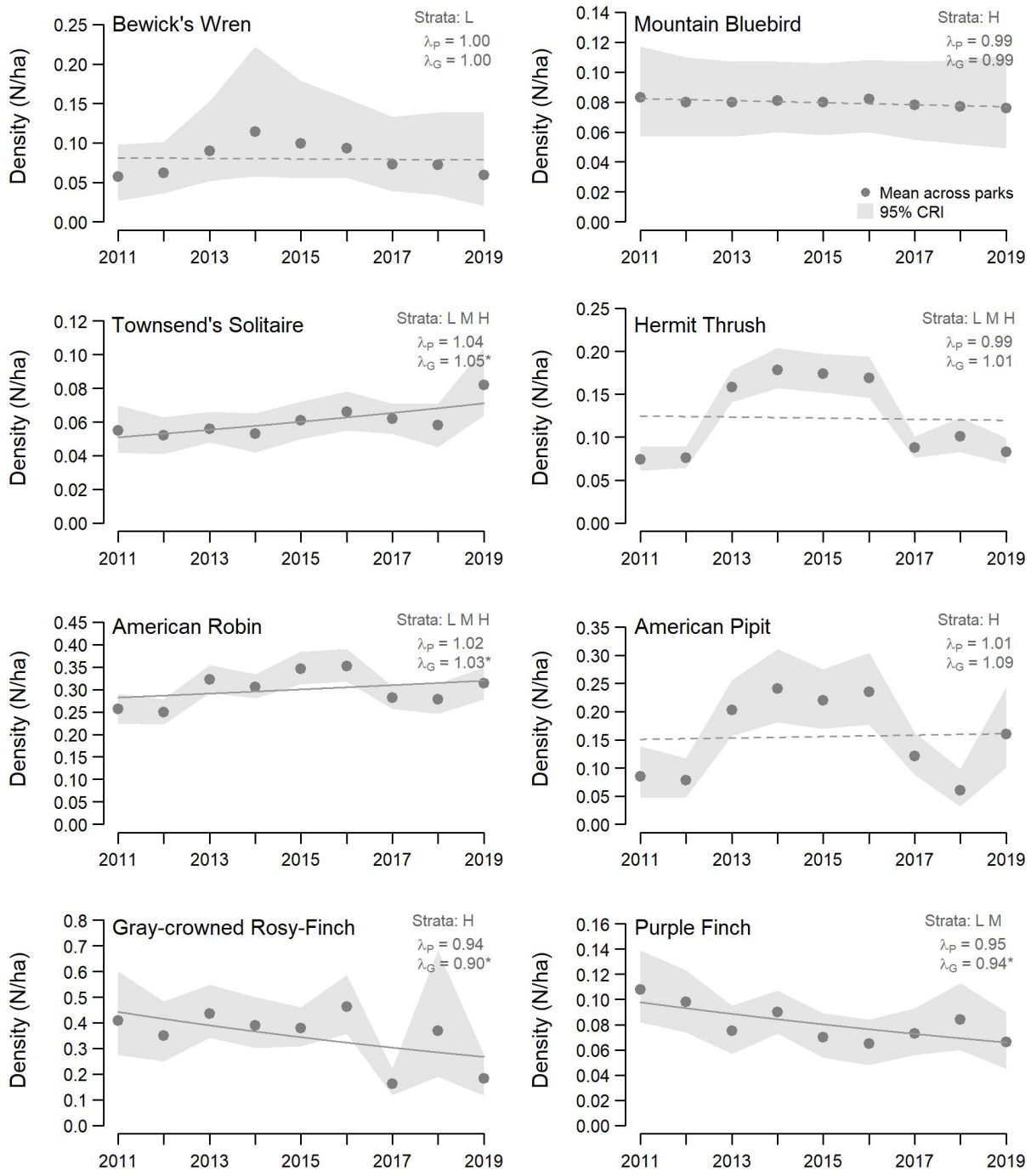


Figure A5-1e. Network-level density estimates for Bewick's Wren, Mountain Bluebird, Townsend's Solitaire, Hermit Thrush, American Robin, American Pipit, Gray-crowned Rosy-Finch and Purple Finch, derived using a hierarchical analysis of point counts from low (L), medium (M) and/or high (H) elevation strata in Sequoia and Kings Canyon National Parks and Yosemite National Park (Table 1). Smoothed trends (curves) and both smoothed (λ_P) and geometric mean (λ_G) population growth rates are shown. Solid curves and asterisks indicate strongly supported trends for which the 95% credible interval (CRI) on λ_G did not overlap 1. Species are listed in taxonomic order (Table 4).

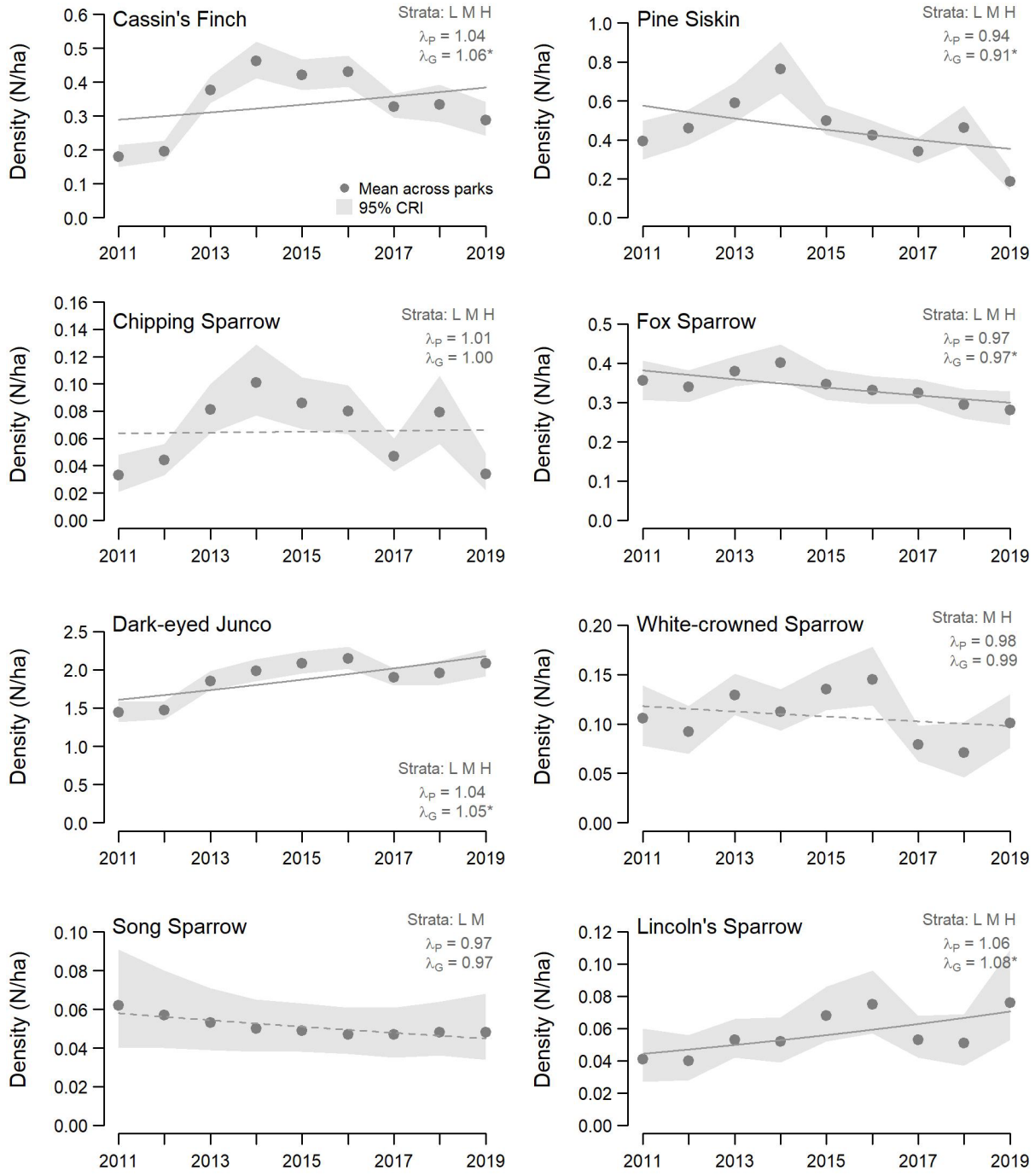


Figure A5-1f. Network-level density estimates for Cassin's Finch, Pine Siskin, Chipping Sparrow, Fox Sparrow, Dark-eyed Junco, White-crowned Sparrow, Song Sparrow and Lincoln's Sparrow, derived using a hierarchical analysis of point counts from low (L), medium (M) and/or high (H) elevation strata in Sequoia and Kings Canyon National Parks and Yosemite National Park (Table 1). Smoothed trends (curves) and both smoothed (λ_P) and geometric mean (λ_G) population growth rates are shown. Solid curves and asterisks indicate strongly supported trends for which the 95% credible interval (CRI) on λ_G did not overlap 1. Species are listed in taxonomic order (Table 4).

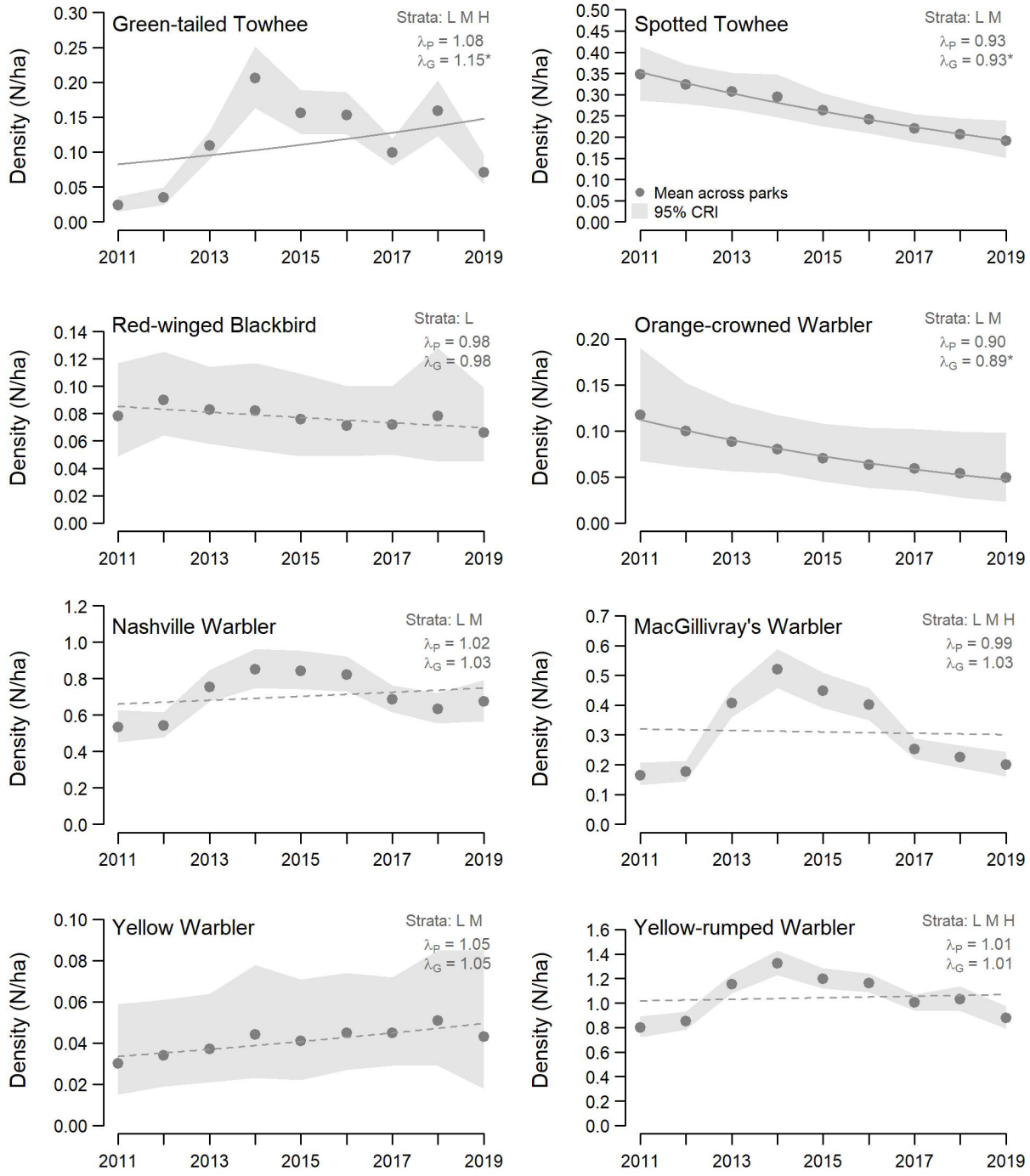


Figure A5-1g. Network-level density estimates for Green-tailed Towhee, Spotted Towhee, Red-winged Blackbird, Orange-crowned Warbler, Nashville Warbler, MacGillivray's Warbler, Yellow Warbler and Yellow-rumped Warbler, derived using a hierarchical analysis of point counts from low (L), medium (M) and/or high (H) elevation strata in Sequoia and Kings Canyon National Parks and Yosemite National Park (Table 1). Smoothed trends (curves) and both smoothed (λ_P) and geometric mean (λ_G) population growth rates are shown. Solid curves and asterisks indicate strongly supported trends for which the 95% credible interval (CRI) on λ_G did not overlap 1. Species are listed in taxonomic order (Table 4).

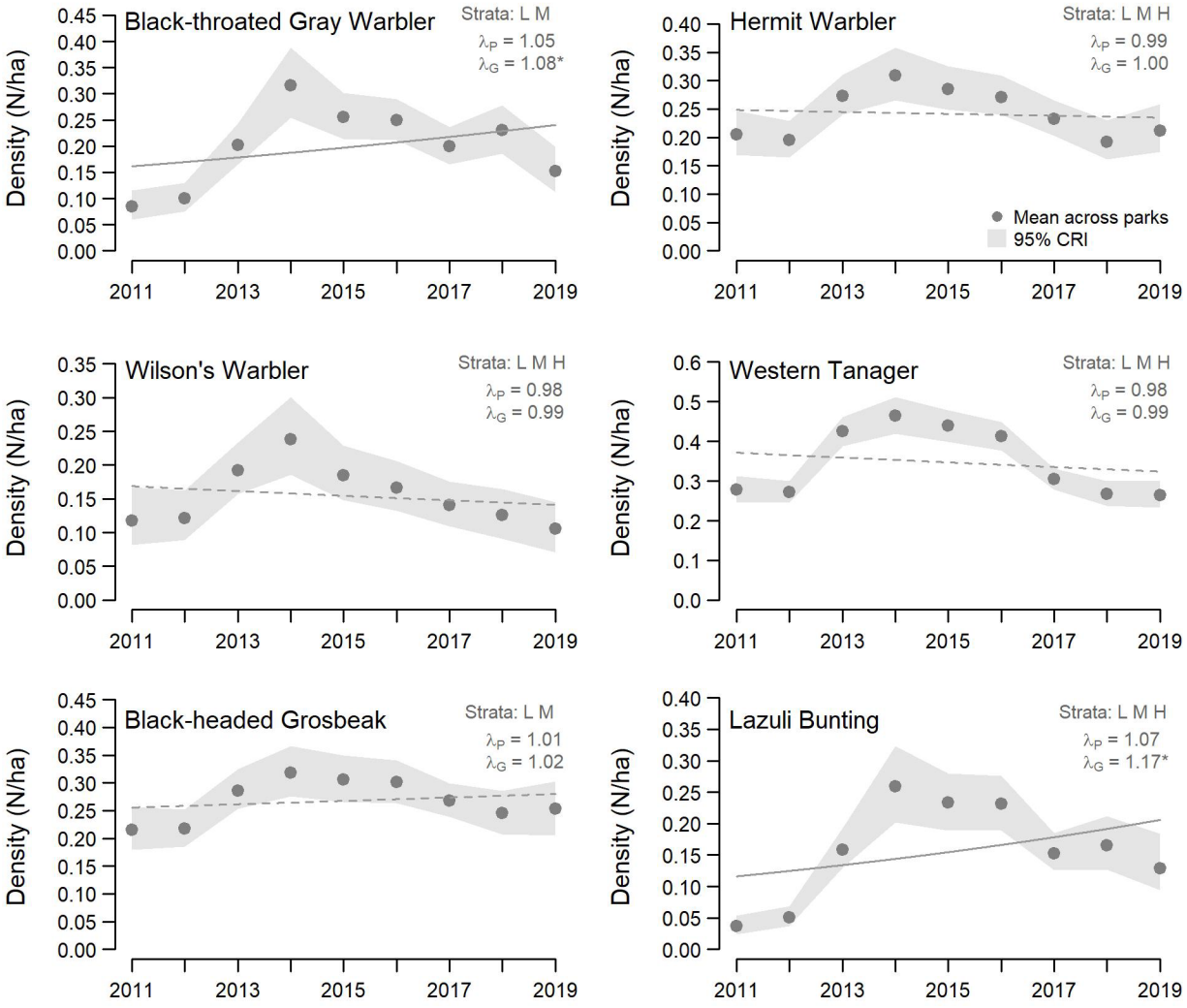


Figure A5-1h. Network-level density estimates for Black-throated Gray Warbler, Hermit Warbler, Wilson's Warbler, Western Tanager, Black-headed Grosbeak and Lazuli Bunting, derived using a hierarchical analysis of point counts from low (L), medium (M) and/or high (H) elevation strata in Sequoia and Kings Canyon National Parks and Yosemite National Park (Table 1). Smoothed trends (curves) and both smoothed (λ_P) and geometric mean (λ_G) population growth rates are shown. Solid curves and asterisks indicate strongly supported trends for which the 95% credible interval (CRI) on λ_G did not overlap 1. Species are listed in taxonomic order (Table 4).

Appendix 6. Parameter estimates: effects of year and park on abundance and derived population density

Derived estimates of mean population density are presented for Devils Postpile National Monument (Table A6-1) and for Sequoia and Kings Canyon National Parks and Yosemite National Park (Table A6-2).

Table A6-1. Derived estimates of mean population density, and fixed effects of year (β_{year}) from hierarchical models of abundance based on avian point-count data collected annually during 2011–2014 and 2016–2019 in Devils Postpile National Monument. The 25 species analyzed are listed in taxonomic order. Values of *year* (2011–2019) were coded as 1–9. For each β_{year} with asterisk (also shown in bold italics), the 95% credible interval (CRI) on the mean did not overlap zero, indicating strong support for the effect.

	Population density		β_{year}	
Species	**Mean**	**95% CRI**	**Mean**	**95% CRI**
Mountain Quail	0.084	(0.058, 0.116)	***0.192*** [a]	(0.074, 0.313)
Hairy Woodpecker	0.167	(0.106, 0.242)	−0.050	(−0.186, 0.078)
Northern Flicker	0.036	(0.023, 0.063)	***−0.318*** [a]	(−0.541, −0.119)
Olive-sided Flycatcher	0.143	(0.105, 0.188)	−0.057	(−0.164, 0.037)
Western Wood-Pewee	0.808	(0.675, 0.968)	−0.044	(−0.115, 0.022)
Dusky Flycatcher	0.944	(0682, 1.288)	***0.156*** [a]	(0.055, 0.266)
Warbling Vireo	0.508	(0.361, 0.678)	−0.010	(−0.119, 0.093)
Steller's Jay	0.450	(0.353, 0.565)	0.011	(−0.057, 0.076)
Clark's Nutcracker	0.055	(0.030, 0.092)	−0.004	(−0.181, 0.171)
Mountain Chickadee	1.291	(1.056, 1.577)	0.019	(−0.062, 0.102)
Golden-crowned Kinglet	0.414	(0.246, 0.649)	−0.049	(−0.263, 0.147)
Red-breasted Nuthatch	0.192	(0.127, 0.276)	−0.013	(−0.145, 0.115)
Brown Creeper	0.417	(0.241, 0.649)	−0.103	(−0.289, 0.067)
House Wren	0.287	(0.178, 0.456)	0.058	(−0.076, 0.201)
Townsend's Solitaire	0.070	(0.047, 0.120)	***−0.297*** [a]	(−0.555, −0.081)
American Robin	0.380	(0.256, 0.527)	***0.138*** [a]	(0.049, 0.229)
Cassin's Finch	0.396	(0.291, 0.510)	−0.077	(−0.171, 0.010)
Fox Sparrow	1.713	(1.482, 1.960)	0.023	(−0.034, 0.084)
Dark-eyed Junco	2.228	(1.855, 2.652)	0.038	(−0.017, 0.092)
Song Sparrow	0.093	(0.057, 0.163)	−0.037	(−0.184, 0.098)

Table A6-1 (continued). Derived estimates of mean population density, and fixed effects of year (β_{year}) from hierarchical models of abundance based on avian point-count data collected annually during 2011–2014 and 2016–2019 in Devils Postpile National Monument. The 25 species analyzed are listed in taxonomic order. Values of year (2011–2019) were coded as 1–9. For each β_{year} with asterisk (also shown in bold italics), the 95% credible interval (CRI) on the mean did not overlap zero, indicating strong support for the effect.

	Population density		β_{year}	
Species	**Mean**	**95% CRI**	**Mean**	**95% CRI**
Green-tailed Towhee	0.485	(0.341, 0.663)	0.069	(−0.026, 0.159)
MacGillivray's Warbler	0.273	(0.181, 0.387)	−0.057	(−0.205, 0.075)
Yellow-rumped Warbler	1.352	(1.085, 1.651)	0.056	(−0.025, 0.137)
Wilson's Warbler	0.304	(0.170, 0.467)	0.005	(−0.147, 0.151)
Western Tanager	0.433	(0.321, 0.569)	−0.026	(−0.116, 0.063)

Table A6-2. Derived estimates of mean population density, and fixed effects of *year* (β_{year}) and *park* (β_{park}) on abundance, from hierarchical models of avian point-count data collected annually during 2011–2014 and 2016–2019 in Sequoia and Kings Canyon National Parks (SEKI) and Yosemite National Park (YOSE). The 62 species analyzed are listed in taxonomic order. Values of *year* (2011–2019) were coded as 1–9, and *park* was coded as 1 for SEKI and 2 for YOSE. For each β with asterisk (also shown in bold italics), the 95% credible interval (CRI) on the mean did not overlap zero, indicating strong support for the effect. Missing values appear where effects were removed from models to improve fit or promote the convergence of other parameter estimates.

	Population density		β_{year}		β_{park}	
Species	**Mean**	**95% CRI**	**Mean**	**95% CRI**	**Mean**	**95% CRI**
Mountain Quail	0.029	(0.027, 0.031)	−0.060	(−0.159, 0.037)	−0.159	(−0.412, 0.087)
Sooty Grouse	0.014	(0.011, 0.018)	***−0.205*** [a]	(−0.358, −0.055)	***−0.974*** [a]	(−1.452, −0.571)
Anna's Hummingbird	0.854	(0.475, 2.132)	***−0.387*** [a]	(−0.522, −0.249)	–	–
Rufous Hummingbird	2.642	(1.486, 4.672)	***−0.236*** [a]	(−0.485, −0.020)	***−1.550*** [a]	(−2.361, −0.808)
Acorn Woodpecker	0.036	(0.029, 0.043)	***−0.090*** [a]	(−0.176, −0.007)	***−2.927*** [a]	(−4.131, −1.868)
Williamson's Sapsucker	0.054	(0.044, 0.066)	***−0.265*** [a]	(−0.404, −0.091)	***−0.566*** [a]	(−0.850, −0.268)
Red-breasted Sapsucker	0.056	(0.046, 0.067)	***−0.174*** [a]	(−0.304, −0.044)	−0.097	(−0.424, 0.216)
Hairy Woodpecker	0.101	(0.087, 0.115)	−0.115	(−0.212, 0.001)	***−0.781*** [a]	(−1.031, −0.564)
White-headed Woodpecker	0.120	(0.105, 0.137)	***−0.083*** [a]	(−0.148, −0.022)	–	–
Northern Flicker	0.077	(0.069, 0.085)	***−0.110*** [a]	(−0.179, −0.046)	***−0.305*** [a]	(−0.482, −0.135)
Pileated Woodpecker	0.024	(0.020, 0.030)	−0.054	(−0.199, 0.083)	***−0.708*** [a]	(−1.086, −0.324)
Olive-sided Flycatcher	0.057	(0.051, 0.064)	***−0.205*** [a]	(−0.323, −0.093)	−0.021	(−0.334, 0.288)
Western Wood-Pewee	0.190	(0.175, 0.208)	−0.082	(−0.185, 0.027)	−0.253	(−0.542, 0.011)
Hammond's Flycatcher	0.099	(0.082, 0.116)	***−0.120*** [a]	(−0.237, −0.005)	***−1.656*** [a]	(−2.090, −1.314)
Dusky Flycatcher	0.588	(0.548, 0.628)	−0.010	(−0.040, 0.016)	***0.123*** [a]	(0.003, 0.244)
Pacific-slope Flycatcher	0.093	(0.076, 0.112)	−0.023	(−0.181, 0.130)	***−1.965*** [a]	(−2.560, −1.434)
Cassin's Vireo	0.216	(0.191, 0.244)	***−0.415*** [a]	(−0.560, −0.267)	***−0.697*** [a]	(−1.024, −0.392)
Warbling Vireo	0.290	(0.259, 0.318)	***−0.247*** [a]	(−0.363, −0.137)	***−0.658*** [a]	(−1.006, −0.313)
Steller's Jay	0.279	(0.263, 0.295)	***−0.133*** [a]	(−0.204, −0.065)	***0.255*** [a]	(0.019, 0.462)
Clark's Nutcracker	0.132	(0.120, 0.144)	***−0.105*** [a]	(−0.148, −0.063)	−0.197	(−0.534, 0.224)
Common Raven	0.027	(0.022, 0.034)	−0.162	(−0.326, 0.014)	***−1.370*** [a]	(−1.856, −0.937)
Mountain Chickadee	1.121	(1.067, 1.178)	−0.014	(−0.034, 0.006)	0.346	(−0.023, 0.559)
Wrentit	0.036	(0.027, 0.048)	***−0.397*** [a]	(−0.600, −0.210)	***−3.084*** [a]	(−3.920, −2.324)
Golden-crowned Kinglet	1.155	(1.064, 1.251)	***−0.235*** [a]	(−0.325, −0.145)	−0.140	(−0.417, 0.102)
Ruby-crowned Kinglet	0.047	(0.033, 0.066)	−0.174	(−0.490, 0.149)	***−2.624*** [a]	(−3.202, −1.984)
Red-breasted Nuthatch	0.304	(0.287, 0.323)	0.004	(−0.022, 0.027)	0.118	(−0.061, 0.277)

Table A6-2 (continued). Derived estimates of mean population density, and fixed effects of *year* (β_{year}) and *park* (β_{park}) on abundance, from hierarchical models of avian point-count data collected annually during 2011–2014 and 2016–2019 in Sequoia and Kings Canyon National Parks (SEKI) and Yosemite National Park (YOSE). The 62 species analyzed are listed in taxonomic order. Values of year (2011–2019) were coded as 1–9, and park was coded as 1 for SEKI and 2 for YOSE. For each β with asterisk (also shown in bold italics), the 95% credible interval (CRI) on the mean did not overlap zero, indicating strong support for the effect. Missing values appear where effects were removed from models to improve fit or promote the convergence of other parameter estimates.

	Population density		β_{year}		β_{park}	
Species	**Mean**	**95% CRI**	**Mean**	**95% CRI**	**Mean**	**95% CRI**
White-breasted Nuthatch	0.042	(0.035, 0.051)	***−0.639*** [a]	(−0.832, −0.413)	***−1.354*** [a]	(−1.701, −1.023)
Brown Creeper	0.761	(0.705, 0.826)	***−0.133*** [a]	(−0.214, −0.059)	0.010	(−0.170, 0.175)
Rock Wren	0.039	(0.032, 0.048)	***−0.306*** [a]	(−0.453, −0.143)	***−1.978*** [a]	(−2.390, −1.576)
Canyon Wren	0.037	(0.028, 0.049)	0.021	(−0.059, 0.103)	0.709	(−1.140, 2.851)
House Wren	0.131	(0.108, 0.157)	0.161	(−0.039, 0.356)	***−3.195*** [a]	(−3.857, −2.629)
Pacific Wren	0.059	(0.044, 0.074)	0.126	(−0.055, 0.305)	***−2.687*** [a]	(−3.586, −1.818)
Bewick's Wren	0.080	(0.053, 0.128)	−0.071	(−0.242, 0.087)	***−1.851*** [a]	(−3.498, −0.914)
Mountain Bluebird	0.080	(0.060, 0.104)	−0.010	(−0.072, 0.052)	−1.015	(−1.628, 0.109)
Townsend's Solitaire	0.060	(0.054, 0.068)	***−0.198*** [a]	(−0.279, −0.122)	***−0.542*** [a]	(−0.737, −0.353)
Hermit Thrush	0.122	(0.111, 0.134)	***−0.258*** [a]	(−0.344, −0.184)	***−0.344*** [a]	(−0.528, −0.164)
American Robin	0.301	(0.280, 0.322)	−0.029	(−0.092, 0.032)	−0.026	(−0.162, 0.106)
American Pipit	0.156	(0.125, 0.191)	0.073	(−0.448, 0.521)	***2.971*** [a]	(0.594, 4.871)
Gray-crowned Rosy-Finch	0.349	(0.286, 0.425)	***−0.097*** [a]	(−0.175, −0.021)	−0.582	(−1.610, 0.965)
Purple Finch	0.081	(0.066, 0.096)	***−0.086*** [a]	(−0.149, −0.025)	***−1.489*** [a]	(−1.837, −1.143)
Cassin's Finch	0.335	(0.309, 0.363)	***−0.213*** [a]	(−0.292, −0.129)	−0.151	(−0.307, 0.011)
Pine Siskin	0.458	(0.397, 0.524)	***−0.188*** [a]	(−0.242, −0.132)	***−0.375*** [a]	(−0.655, −0.098)
Chipping Sparrow	0.065	(0.055, 0.075)	***−0.499*** [a]	(−0.789, −0.219)	***−0.927*** [a]	(−1.346, −0.536)
Fox Sparrow	0.339	(0.317, 0.364)	***−0.173*** [a]	(−0.237, −0.100)	0.147	(−0.250, 0.448)
Dark-eyed Junco	1.880	(1.798, 1.969)	−0.020	(−0.064, 0.023)	***0.422*** [a]	(0.187, 0.604)
White-crowned Sparrow	0.108	(0.095, 0.123)	−0.038	(−0.112, 0.029)	***−1.358*** [a]	(−2.049, −0.744)
Song Sparrow	0.051	(0.041, 0.065)	***−0.463*** [a]	(−0.693, −0.238)	***−3.315*** [a]	(−4.203, −1.886)
Lincoln's Sparrow	0.057	(0.048, 0.067)	−0.074	(−0.230, 0.091)	***−2.213*** [a]	(−2.760, −1.691)
Green-tailed Towhee	0.112	(0.097, 0.128)	−0.098	(−0.227, 0.036)	***−0.760*** [a]	(−1.113, −0.423)
Spotted Towhee	0.266	(0.240, 0.294)	***−0.172*** [a]	(−0.291, −0.051)	***−1.017*** [a]	(−1.350, −0.707)
Red-winged Blackbird	0.077	(0.061, 0.097)	−0.040	(−0.117, 0.037)	–	–
Orange-crowned Warbler	0.075	(0.050, 0.112)	−0.094	(−0.211, 0.024)	***−2.016*** [a]	(−2.703, −1.279)

Table A6-2 (continued). Derived estimates of mean population density, and fixed effects of *year* (β_{year}) and *park* (β_{park}) on abundance, from hierarchical models of avian point-count data collected annually during 2011–2014 and 2016–2019 in Sequoia and Kings Canyon National Parks (SEKI) and Yosemite National Park (YOSE). The 62 species analyzed are listed in taxonomic order. Values of year (2011–2019) were coded as 1–9, and park was coded as 1 for SEKI and 2 for YOSE. For each β with asterisk (also shown in bold italics), the 95% credible interval (CRI) on the mean did not overlap zero, indicating strong support for the effect. Missing values appear where effects were removed from models to improve fit or promote the convergence of other parameter estimates.

	Population density		β_{year}		β_{park}	
Species	**Mean**	**95% CRI**	**Mean**	**95% CRI**	**Mean**	**95% CRI**
Nashville Warbler	0.704	(0.651, 0.766)	***−0.040*** [a]	(−0.073, −0.007)	−0.007	(−0.207, 0.213)
MacGillivray's Warbler	0.310	(0.284, 0.338)	***−0.115*** [a]	(−0.227, −0.008)	***−0.430*** [a]	(−0.688, −0.185)
Yellow Warbler	0.041	(0.023, 0.072)	0.144	(−0.019, 0.347)	–	–
Yellow-rumped Warbler	1.044	(0.997, 1.096)	***−0.036*** [a]	(−0.057, −0.015)	***0.581*** [a]	(0.462, 0.697)
Black-throated Gray Warbler	0.199	(0.172, 0.227)	***−0.387*** [a]	(−0.558, −0.213)	***−1.930*** [a]	(−2.356, −1.556)
Hermit Warbler	0.242	(0.220, 0.267)	***−0.221*** [a]	(−0.356, −0.085)	***−0.670*** [a]	(−0.961, −0.384)
Wilson's Warbler	0.155	(0.133, 0.181)	***−0.163*** [a]	(−0.291, −0.039)	***−1.223*** [a]	(−1.551, −0.909)
Western Tanager	0.348	(0.324, 0.370)	***−0.037*** [a]	(−0.069, −0.006)	0.028	(−0.126, 0.185)
Black-headed Grosbeak	0.268	(0.246, 0.291)	−0.043	(−0.165, 0.076)	***−0.783*** [a]	(−1.123, −0.443)
Lazuli Bunting	0.157	(0.136, 0.180)	0.164	(−0.034, 0.385)	***−2.163*** [a]	(−2.728, −1.598)

Appendix 7. Parameter estimates: interaction effects on abundance involving year, park and elevation

Estimates of interaction effects involving year, park, and elevation for Sequoia and Kings Canyon National Parks and Yosemite National Park are presented in Tables A7-1 and A7-2.

Table A7-1. Estimates of year-by-park (β_{YP}) and year-by-elevation (β_{YE}) interaction effects from hierarchical models of avian point-count data collected annually during 2011–2014 and 2016–2019 in Sequoia and Kings Canyon National Parks (SEKI) and Yosemite National Park (YOSE). The 62 species analyzed are listed in taxonomic order. Prior to modeling, year (2011–2019) was coded as 1–9; park was coded as 1 for SEKI, 2 for YOSE; and elevation was standardized. For each β with asterisk (also shown in bold italics), the 95% credible interval (CRI) on the mean did not overlap zero, indicating strong support for the effect. Missing values appear where these effects were removed from models to improve fit or promote the convergence of other parameter estimates.

	β_{YP}		β_{YE}	
Species	**Mean**	**95% CRI**	**Mean**	**95% CRI**
Mountain Quail	0.051	(−0.006, 0.108)	0.016	(−0.088, 0.125)
Sooty Grouse	0.053	(−0.049, 0.166)	***−0.605*** [a]	(−0.903, −0.227)
Anna's Hummingbird	–	–	–	–
Rufous Hummingbird	0.119	(−0.057, 0.295)	–	–
Acorn Woodpecker	–	–	–	–
Williamson's Sapsucker	***0.124*** [a]	(0.024, 0.204)	0.242	(−0.114, 0.525)
Red-breasted Sapsucker	−0.004	(−0.095, 0.084)	−0.163	(−0.429, 0.101)
Hairy Woodpecker	***0.100*** [a]	(0.027, 0.160)	***−0.159*** [a]	(−0.298, −0.018)
White-headed Woodpecker	–	–	0.025	(−0.028, 0.076)
Northern Flicker	0.042	(−0.003, 0.087)	0.005	(−0.094, 0.112)
Pileated Woodpecker	0.033	(−0.066, 0.139)	−0.145	(−0.398, 0.117)
Olive-sided Flycatcher	***0.086*** [a]	(0.010, 0.172)	0.155	(−0.028, 0.354)
Western Wood-Pewee	−0.032	(−0.107, 0.038)	−0.032	(−0.127, 0.067)
Hammond's Flycatcher	***0.118*** [a]	(0.031, 0.213)	−0.093	(−0.228, 0.051)
Dusky Flycatcher	–	–	−0.014	(−0.036, 0.008)
Pacific-slope Flycatcher	0.003	(−0.094, 0.097)	–	–
Cassin's Vireo	***0.227*** [a]	(0.138, 0.312)	***−0.314*** [a]	(−0.519, −0.127)
Warbling Vireo	***0.103*** [a]	(0.027, 0.180)	0.008	(−0.098, 0.109)
Steller's Jay	***0.054*** [a]	(0.012, 0.098)	0.054	(−0.008, 0.115)
Clark's Nutcracker	–	–	0.018	(−0.013, 0.050)

Table A7-1 (continued). Estimates of year-by-park (β_{YP}) and year-by-elevation (β_{YE}) interaction effects from hierarchical models of avian point-count data collected annually during 2011–2014 and 2016–2019 in Sequoia and Kings Canyon National Parks (SEKI) and Yosemite National Park (YOSE). The 62 species analyzed are listed in taxonomic order. Prior to modeling, year (2011–2019) was coded as 1–9; park was coded as 1 for SEKI, 2 for YOSE; and elevation was standardized. For each β with asterisk (also shown in bold italics), the 95% credible interval (CRI) on the mean did not overlap zero, indicating strong support for the effect. Missing values appear where these effects were removed from models to improve fit or promote the convergence of other parameter estimates.

	β_{YP}		β_{YE}	
Species	**Mean**	**95% CRI**	**Mean**	**95% CRI**
Common Raven	0.101	(−0.020, 0.219)	−0.108	(−0.278, 0.077)
Mountain Chickadee	–	–	0.013	(−0.001, 0.028)
Wrentit	***0.234*** [a]	(0.092, 0.385)	0.093	(−0.009, 0.220)
Golden-crowned Kinglet	***0.111*** [a]	(0.057, 0.171)	−0.058	(−0.158, 0.042)
Ruby-crowned Kinglet	−0.009	(−0.241, 0.220)	−0.062	(−0.410, 0.234)
Red-breasted Nuthatch	–	–	–	–
White-breasted Nuthatch	–	–	–	–
Brown Creeper	0.033	(−0.015, 0.082)	−0.018	(−0.100, 0.067)
Rock Wren	***0.159*** [a]	(0.048, 0.265)	–	–
Canyon Wren	–	–	–	–
House Wren	0.012	(−0.129, 0.158)	***−0.194*** [a]	(−0.374, −0.019)
Pacific Wren	−0.114	(−0.237, 0.013)	–	–
Bewick's Wren	–	–	–	–
Mountain Bluebird	–	–	–	–
Townsend's Solitaire	***0.164*** [a]	(0.114, 0.215)	−0.115	(−0.246, 0.017)
Hermit Thrush	***0.126*** [a]	(0.078, 0.176)	−0.037	(−0.130, 0.059)
American Robin	0.016	(−0.023, 0.056)	−0.060	(−0.126, 0.005)
American Pipit	−0.090	(−0.432, 0.270)	0.108	(−0.368, 0.574)
Gray-crowned Rosy-Finch	–	–	–	–
Purple Finch	–	–	***−0.058*** [a]	(−0.113, −0.003)
Cassin's Finch	***0.110*** [a]	(0.062, 0.158)	***0.149*** [a]	(0.066, 0.230)
Pine Siskin	–	–	–	–
Chipping Sparrow	***0.202*** [a]	(0.062, 0.349)	***−0.278*** [a]	(−0.558, −0.013)
Fox Sparrow	***0.087*** [a]	(0.042, 0.129)	−0.032	(−0.129, 0.067)
Dark-eyed Junco	***0.033*** [a]	(0.007, 0.059)	***−0.049*** [a]	(−0.085, −0.011)

Table A7-1 (continued). Estimates of year-by-park (β_{YP}) and year-by-elevation (β_{YE}) interaction effects from hierarchical models of avian point-count data collected annually during 2011–2014 and 2016–2019 in Sequoia and Kings Canyon National Parks (SEKI) and Yosemite National Park (YOSE). The 62 species analyzed are listed in taxonomic order. Prior to modeling, year (2011–2019) was coded as 1–9; park was coded as 1 for SEKI, 2 for YOSE; and elevation was standardized. For each β with asterisk (also shown in bold italics), the 95% credible interval (CRI) on the mean did not overlap zero, indicating strong support for the effect. Missing values appear where these effects were removed from models to improve fit or promote the convergence of other parameter estimates.

	β_{YP}		β_{YE}	
Species	**Mean**	**95% CRI**	**Mean**	**95% CRI**
White-crowned Sparrow	–	–	0.032	(−0.027, 0.088)
Song Sparrow	***0.346*** [a]	(0.180, 0.519)	−0.084	(−0.318, 0.156)
Lincoln's Sparrow	***0.120*** [a]	(0.016, 0.220)	−0.040	(−0.243, 0.157)
Green-tailed Towhee	0.047	(−0.047, 0.130)	***−0.272*** [a]	(−0.496, −0.046)
Spotted Towhee	0.090	(−0.009, 0.180)	0.097	(−0.056, 0.253)
Red-winged Blackbird	–	–	–	–
Orange-crowned Warbler	–	–	0.081	(−0.006, 0.170)
Nashville Warbler	–	–	***−0.065*** [a]	(−0.092, −0.039)
MacGillivray's Warbler	0.015	(−0.063, 0.092)	0.029	(−0.079, 0.135)
Yellow Warbler	–	–	***0.166*** [a]	(0.047, 0.313)
Yellow-rumped Warbler	–	–	0.000	(−0.015, 0.014)
Black-throated Gray Warbler	***0.216*** [a]	(0.106, 0.327)	−0.146	(−0.360, 0.065)
Hermit Warbler	0.083	(−0.006, 0.168)	0.054	(−0.091, 0.201)
Wilson's Warbler	0.052	(−0.033, 0.135)	0.027	(−0.153, 0.209)
Western Tanager	–	–	***0.033*** [a]	(0.009, 0.057)
Black-headed Grosbeak	0.060	(−0.023, 0.140)	0.124	(−0.014, 0.259)
Lazuli Bunting	−0.153	(−0.331, 0.007)	0.014	(−0.172, 0.221)

Table A7-2. Estimates of park-by-elevation (β_{PE}) and park-by-elevation-by-year (β_{PEY}) interaction effects from hierarchical models of avian point-count data collected annually during 2011–2014 and 2016–2019 in Sequoia and Kings Canyon National Parks (SEKI) and Yosemite National Park (YOSE). The 62 species analyzed are listed in taxonomic order. Prior to modeling, year (2011–2019) was coded as 1–9; park was coded as 1 for SEKI, 2 for YOSE; and elevation was standardized. For each β with asterisk (also shown in bold italics), the 95% credible interval (CRI) on the mean did not overlap zero, indicating strong support for the effect. Missing values appear where these effects were removed from models to improve fit or promote the convergence of other parameter estimates.

	β_{PE}		β_{PEY}	
Species	**Mean**	**95% CRI**	**Mean**	**95% CRI**
Mountain Quail	0.214	(−0.128, 0.566)	−0.019	(−0.082, 0.041)
Sooty Grouse	***−3.027*** [a]	(−4.271, −1.606)	***0.411*** [a]	(0.150, 0.622)
Anna's Hummingbird	–	–	–	–
Rufous Hummingbird	–	–	–	–
Acorn Woodpecker	–	–	–	–
Williamson's Sapsucker	−0.381	(−1.589, 0.671)	−0.141	(−0.321, 0.073)
Red-breasted Sapsucker	***−1.408*** [a]	(−2.364, −0.449)	0.066	(−0.101, 0.224)
Hairy Woodpecker	***−0.524*** [a]	(−1.030, −0.041)	0.064	(−0.018, 0.146)
White-headed Woodpecker	–	–	–	–
Northern Flicker	−0.328	(−0.657, 0.004)	0.001	(−0.061, 0.061)
Pileated Woodpecker	***−1.979*** [a]	(−2.914, −1.070)	0.066	(−0.085, 0.213)
Olive-sided Flycatcher	***−1.660*** [a]	(−2.305, −1.005)	−0.078	(−0.204, 0.030)
Western Wood-Pewee	***−0.833*** [a]	(−1.203, −0.471)	−0.010	(−0.073, 0.048)
Hammond's Flycatcher	***−1.618*** [a]	(−2.302, −0.961)	***0.100*** [a]	(0.007, 0.192)
Dusky Flycatcher	–	–	–	–
Pacific-slope Flycatcher	–	–	–	–
Cassin's Vireo	***−0.949*** [a]	(−1.534, −0.376)	***0.159*** [a]	(0.058, 0.268)
Warbling Vireo	***−0.844*** [a]	(−1.298, −0.412)	0.013	(−0.052, 0.079)
Steller's Jay	−0.026	(−0.243, 0.204)	−0.025	(−0.062, 0.013)
Clark's Nutcracker	–	–	–	–
Common Raven	***−0.909*** [a]	(−1.432, −0.351)	0.095	(−0.011, 0.194)
Mountain Chickadee	–	–	–	–
Wrentit	–	–	–	–
Golden-crowned Kinglet	***−0.821*** [a]	(−1.214, −0.437)	0.058	(−0.003, 0.120)
Ruby-crowned Kinglet	0.175	(−0.784, 1.199)	0.175	(−0.057, 0.422)

Table A7-2 (continued). Estimates of park-by-elevation (β_{PE}) and park-by-elevation-by-year (β_{PEY}) interaction effects from hierarchical models of avian point-count data collected annually during 2011–2014 and 2016–2019 in Sequoia and Kings Canyon National Parks (SEKI) and Yosemite National Park (YOSE). The 62 species analyzed are listed in taxonomic order. Prior to modeling, year (2011–2019) was coded as 1–9; park was coded as 1 for SEKI, 2 for YOSE; and elevation was standardized. For each β with asterisk (also shown in bold italics), the 95% credible interval (CRI) on the mean did not overlap zero, indicating strong support for the effect. Missing values appear where these effects were removed from models to improve fit or promote the convergence of other parameter estimates.

	β_{PE}		β_{PEY}	
Species	**Mean**	**95% CRI**	**Mean**	**95% CRI**
Red-breasted Nuthatch	***−0.498*** [a]	(−0.666, −0.335)	–	–
White-breasted Nuthatch	–	–	–	–
Brown Creeper	−0.244	(−0.545, 0.051)	−0.007	(−0.057, 0.044)
Rock Wren	–	–	–	–
Canyon Wren	–	–	–	–
House Wren	***−1.721*** [a]	(−2.669, −0.772)	***0.140*** [a]	(0.016, 0.268)
Pacific Wren	–	–	–	–
Bewick's Wren	–	–	–	–
Mountain Bluebird	–	–	–	–
Townsend's Solitaire	***−0.982*** [a]	(−1.464, −0.461)	***0.110*** [a]	(0.026, 0.192)
Hermit Thrush	−0.193	(−0.633, 0.233)	0.023	(−0.041, 0.090)
American Robin	0.091	(−0.141, 0.319)	0.016	(−0.022, 0.054)
American Pipit	0.589	(−1.926, 3.188)	−0.100	(−0.498, 0.356)
Gray-crowned Rosy-Finch	–	–	–	–
Purple Finch	–	–	–	–
Cassin's Finch	***0.835*** [a]	(0.492, 1.178)	***−0.079*** [a]	(−0.133, −0.025)
Pine Siskin	–	–	–	–
Chipping Sparrow	−0.248	(−1.010, 0.555)	0.093	(−0.050, 0.243)
Fox Sparrow	***−0.934*** [a]	(−1.395, −0.498)	0.035	(−0.031, 0.101)
Dark-eyed Junco	−0.055	(−0.204, 0.096)	***0.027*** [a]	(0.004, 0.050)
White-crowned Sparrow	–	–	–	–
Song Sparrow	***−1.928*** [a]	(−3.138, −0.746)	0.109	(−0.042, 0.255)
Lincoln's Sparrow	***−2.781*** [a]	(−3.883, −1.635)	0.088	(−0.044, 0.218)
Green-tailed Towhee	***−2.821*** [a]	(−3.828, −1.851)	0.104	(−0.051, 0.254)
Spotted Towhee	0.496	(−0.001, 0.999)	−0.033	(−0.136, 0.063)

Table A7-2 (continued). Estimates of park-by-elevation (β_{PE}) and park-by-elevation-by-year (β_{PEY}) interaction effects from hierarchical models of avian point-count data collected annually during 2011–2014 and 2016–2019 in Sequoia and Kings Canyon National Parks (SEKI) and Yosemite National Park (YOSE). The 62 species analyzed are listed in taxonomic order. Prior to modeling, year (2011–2019) was coded as 1–9; park was coded as 1 for SEKI, 2 for YOSE; and elevation was standardized. For each β with asterisk (also shown in bold italics), the 95% credible interval (CRI) on the mean did not overlap zero, indicating strong support for the effect. Missing values appear where these effects were removed from models to improve fit or promote the convergence of other parameter estimates.

	β_{PE}		β_{PEY}	
Species	**Mean**	**95% CRI**	**Mean**	**95% CRI**
Red-winged Blackbird	–	–	–	–
Orange-crowned Warbler	–	–	–	–
Nashville Warbler	–	–	–	–
MacGillivray's Warbler	***−0.755*** [a]	(−1.162, −0.371)	−0.022	(−0.092, 0.047)
Yellow Warbler	–	–	–	–
Yellow-rumped Warbler	–	–	–	–
Black-throated Gray Warbler	***−0.918*** [a]	(−1.580, −0.312)	0.082	(−0.036, 0.201)
Hermit Warbler	***−0.729*** [a]	(−1.174, −0.280)	−0.050	(−0.136, 0.032)
Wilson's Warbler	***−1.179*** [a]	(−1.913, −0.442)	−0.008	(−0.116, 0.102)
Western Tanager	–	–	–	–
Black-headed Grosbeak	0.440	(−0.025, 0.921)	−0.039	(−0.116, 0.039)
Lazuli Bunting	***−1.329*** [a]	(−2.212, −0.543)	−0.044	(−0.190, 0.096)

Appendix 8. Parameter estimates: effects of elevation on abundance in the larger parks

Table A8-1. Estimates of linear and nonlinear effects of elevation (β_{elev} and β_{elev^2}), two of several covariates in hierarchical models of avian population density based on point-count data collected annually during 2011–2014 and 2016–2019 in Sequoia and Kings Canyon National Parks and Yosemite National Park. The species analyzed are listed in taxonomic order. For each β with asterisk (also shown in bold italics), the 95% credible interval (CRI) on the mean did not overlap zero, indicating strong support for this effect. Missing values appear where these effects were removed from models to improve fit or promote the convergence of other parameter estimates.

	β_{elev}		β_{elev^2}	
Species	**Mean**	**95% CRI**	**Mean**	**95% CRI**
Mountain Quail	***−2.263*** [a]	(−2.888, −1.671)	***−1.089*** [a]	(−1.239, −0.954)
Sooty Grouse	4.445	(2.290, 6.215)	***−1.566*** [a]	(−1.978, −1.196)
Anna's Hummingbird	***−0.779*** [a]	(−0.992, −0.575)	–	–
Rufous Hummingbird	***−0.516*** [a]	(−0.858, −0.182)	–	–
Acorn Woodpecker	***−2.171*** [a]	(−2.582, −1.770)	–	–
Williamson's Sapsucker	0.556	(−0.953, 2.572)	***−1.708*** [a]	(−2.141, −1.376)
Red-breasted Sapsucker	***1.968*** [a]	(0.457, 3.451)	***−1.251*** [a]	(−1.573, −0.968)
Hairy Woodpecker	0.241	(−0.588, 1.059)	***−0.531*** [a]	(−0.678, −0.386)
White-headed Woodpecker	***−2.321*** [a]	(−2.779, −1.822)	***−1.353*** [a]	(−1.612, −1.133)
Northern Flicker	−0.286	(−0.829, 0.254)	***−0.348*** [a]	(−0.457, −0.238)
Pileated Woodpecker	0.997	(−0.491, 2.452)	***−1.688*** [a]	(−2.029, −1.332)
Olive-sided Flycatcher	***1.139*** [a]	(0.072, 2.177)	***−1.882*** [a]	(−2.187, −1.646)
Western Wood-Pewee	−0.355	(−0.925, 0.242)	***−1.002*** [a]	(−1.158, −0.848)
Hammond's Flycatcher	***1.215*** [a]	(0.342, 2.099)	***−0.671*** [a]	(−0.900, −0.435)
Dusky Flycatcher	***0.324*** [a]	(0.181, 0.463)	***−0.515*** [a]	(−0.593, −0.438)
Pacific-slope Flycatcher	–	–	–	–
Cassin's Vireo	−0.061	(−1.107, 0.953)	***−0.659*** [a]	(−0.943, −0.424)
Warbling Vireo	***−0.745*** [a]	(−1.381, −0.090)	***−0.931*** [a]	(−1.122, −0.747)
Steller's Jay	***−1.371*** [a]	(−1.739, −1.019)	***−0.665*** [a]	(−0.751, −0.576)
Clark's Nutcracker	***1.074*** [a]	(0.873, 1.284)	–	–
Common Raven	−0.033	(−0.999, 0.834)	−0.065	(−0.298, 0.163)
Mountain Chickadee	***0.169*** [a]	(0.079, 0.261)	***−0.616*** [a]	(−0.673, −0.558)

Table A8-1 (continued). Estimates of linear and nonlinear effects of elevation (β_{elev} and β_{elev^2}), two of several covariates in hierarchical models of avian population density based on point-count data collected annually during 2011–2014 and 2016–2019 in Sequoia and Kings Canyon National Parks and Yosemite National Park. The species analyzed are listed in taxonomic order. For each β with asterisk (also shown in bold italics), the 95% credible interval (CRI) on the mean did not overlap zero, indicating strong support for this effect. Missing values appear where these effects were removed from models to improve fit or promote the convergence of other parameter estimates.

	β_{elev}		β_{elev^2}	
Species	**Mean**	**95% CRI**	**Mean**	**95% CRI**
Wrentit	***−2.561*** [a]	(−3.202, −1.990)	–	–
Golden-crowned Kinglet	−0.552	(−1.141, 0.061)	***−1.468*** [a]	(−1.633, −1.305)
Ruby-crowned Kinglet	0.505	(−0.975, 1.973)	–	–
Red-breasted Nuthatch	***−0.583*** [a]	(−0.841, −0.325)	***−1.102*** [a]	(−1.202, −1.007)
White-breasted Nuthatch	0.059	(−0.864, 1.033)	–	–
Brown Creeper	−0.237	(−0.723, 0.247)	***−0.502*** [a]	(−0.606, −0.400)
Rock Wren	–	–	–	–
Canyon Wren	–	–	–	–
House Wren	***1.982*** [a]	(0.733, 3.236)	–	–
Pacific Wren	–	–	–	–
Bewick's Wren	***−0.747*** [a]	(−1.135, −0.300)	–	–
Mountain Bluebird	–	–	–	–
Townsend's Solitaire	***1.072*** [a]	(0.280, 1.839)	***−0.882*** [a]	(−1.052, −0.711)
Hermit Thrush	***1.075*** [a]	(0.452, 1.714)	***−0.722*** [a]	(−0.865, −0.573)
American Robin	***−0.588*** [a]	(−0.964, −0.204)	***−0.148*** [a]	(−0.234, −0.060)
American Pipit	1.974	(−0.943, 4.753)	–	–
Gray-crowned Rosy-Finch	***2.325*** [a]	(1.911, 2.794)	–	–
Purple Finch	***−0.663*** [a]	(−0.969, −0.376)	–	–
Cassin's Finch	***−0.705*** [a]	(−1.212, −0.208)	***−0.351*** [a]	(−0.459, −0.246)
Pine Siskin	***1.053*** [a]	(0.855, 1.256)	***−0.796*** [a]	(−1.030, −0.579)
Chipping Sparrow	0.449	(−1.053, 1.804)	***−0.641*** [a]	(−0.889, −0.422)
Fox Sparrow	0.563	(−0.083, 1.247)	***−1.834*** [a]	(−2.018, −1.649)
Dark-eyed Junco	0.116	(−0.120, 0.348)	***−0.285*** [a]	(−0.335, −0.234)
White-crowned Sparrow	***1.730*** [a]	(1.300, 2.238)	–	–
Song Sparrow	1.207	(−0.450, 2.986)	−0.125	(−0.513, 0.254)

Table A8-1 (continued). Estimates of linear and nonlinear effects of elevation (β_{elev} and β_{elev^2}), two of several covariates in hierarchical models of avian population density based on point-count data collected annually during 2011–2014 and 2016–2019 in Sequoia and Kings Canyon National Parks and Yosemite National Park. The species analyzed are listed in taxonomic order. For each β with asterisk (also shown in bold italics), the 95% credible interval (CRI) on the mean did not overlap zero, indicating strong support for this effect. Missing values appear where these effects were removed from models to improve fit or promote the convergence of other parameter estimates.

	β_{elev}		β_{elev^2}	
Species	**Mean**	**95% CRI**	**Mean**	**95% CRI**
Lincoln's Sparrow	***2.904*** [a]	(1.166, 4.601)	***−1.768*** [a]	(−2.192, −1.349)
Green-tailed Towhee	***4.110*** [a]	(2.724, 5.652)	***−2.627*** [a]	(−3.050, −2.254)
Spotted Towhee	***−4.021*** [a]	(−4.921, −3.183)	***−1.243*** [a]	(−1.505, −1.003)
Red-winged Blackbird	–	–	–	–
Orange-crowned Warbler	***−0.891*** [a]	(−1.341, −0.451)	–	–
Nashville Warbler	***−0.553*** [a]	(−0.729, −0.387)	***−0.609*** [a]	(−0.719, −0.502)
MacGillivray's Warbler	−0.407	(−1.020, 0.246)	***−0.931*** [a]	(−1.082, −0.779)
Yellow Warbler	***−1.914*** [a]	(−2.808, −0.925)	–	–
Yellow-rumped Warbler	0.065	(−0.025, 0.153)	***−0.434*** [a]	(−0.492, −0.377)
Black-throated Gray Warbler	***−2.788*** [a]	(−3.940, −1.648)	***−1.549*** [a]	(−1.960, −1.197)
Hermit Warbler	***−1.999*** [a]	(−2.806, −1.261)	***−1.509*** [a]	(−1.763, −1.197)
Wilson's Warbler	1.168	(−0.020, 2.335)	***−0.730*** [a]	(−0.958, −0.513)
Western Tanager	***−2.070*** [a]	(−2.257, −1.899)	***−0.903*** [a]	(−1.000, −0.805)
Black-headed Grosbeak	***−3.926*** [a]	(−4.864, −3.114)	***−0.762*** [a]	(−0.997, −0.515)
Lazuli Bunting	0.010	(−1.108, 1.304)	***−0.760*** [a]	(−1.066, −0.454)

Appendix 9. Parameter estimates: effects of lagged precipitation and temperature on abundance

Linear and non-linear effects of precipitation-as-snow and linear effects of mean spring temperature are presented for Devils Postpile National Monument (Table A9-1) and for Sequoia and Kings Canyon National Parks and Yosemite National Park (Table A9-2).

Table A9-1. Estimates of linear and nonlinear effects of precipitation-as-snow (β_{PAS} and β_{PAS^2}) and linear effects of mean spring temperature (β_{MST}), three of several covariates in hierarchical models of avian population density based on breeding-season point-count data collected annually during 2011–2014 and 2016–2019 in Devils Postpile National Monument. The 25 species analyzed are listed in taxonomic order. Each covariate represents a standardized climatic anomaly (relative to 1981–2010 normals), lagged by one year to model the demographic response to conditions in the previous breeding season. For each β with asterisk (also shown in bold italics), the 95% credible interval (CRI) on the mean did not overlap zero, indicating strong support for the effect. Missing values appear where these effects were removed from models to improve fit or promote the convergence of other parameter estimates.

	β_{PAS}		β_{PAS^2}		β_{MST}	
Species	**Mean**	**95% CRI**	**Mean**	**95% CRI**	**Mean**	**95% CRI**
Mountain Quail	***−0.487*** [a]	(−0.732, −0.232)	***0.779*** [a]	(0.427, 1.143)	***−0.632*** [a]	(−1.001, −0.267)
Hairy Woodpecker	−0.156	(−0.509, 0.214)	−0.191	(−0.614, 0.196)	−0.091	(−0.435, 0.248)
Northern Flicker	0.409	(−0.088, 0.957)	−0.452	(−1.013, 0.061)	***0.545*** [a]	(0.115, 0.984)
Olive-sided Flycatcher	−0.022	(−0.235, 0.193)	0.161	(−0.082, 0.406)	0.112	(−0.134, 0.359)
Western Wood-Pewee	−0.108	(−0.271, 0.061)	−0.010	(−0.181, 0.158)	0.131	(−0.050, 0.308)
Dusky Flycatcher	0.249	(−0.030, 0.531)	−0.217	(−0.496, 0.049)	0.074	(−0.207, 0.369)
Warbling Vireo	−0.124	(−0.344, 0.104)	***0.407*** [a]	(0.123, 0.701)	−0.159	(−0.446, 0.122)
Steller's Jay	0.021	(−0.171, 0.216)	***−0.218*** [a]	(−0.409, −0.029)	***0.229*** [a]	(0.044, 0.414)
Clark's Nutcracker	−0.191	(−0.525, 0.151)	***0.494*** [a]	(0.041, 0.942)	−0.173	(−0.662, 0.271)
Mountain Chickadee	0.009	(−0.173, 0.185)	***−0.312*** [a]	(−0.505, −0.121)	***0.210*** [a]	(0.012, 0.415)
Golden-crowned Kinglet	−0.334	(−0.700, 0.045)	***0.650*** [a]	(0.133, 1.184)	−0.281	(−0.793, 0.223)
Red-breasted Nuthatch	***−0.333*** [a]	(−0.569, −0.093)	***0.546*** [a]	(0.242, 0.851)	−0.300	(−0.636, 0.017)
Brown Creeper	−0.098	(−0.421, 0.245)	0.160	(−0.219, 0.534)	0.238	(−0.163, 0.639)
House Wren	−0.156	(−1.198, 0.687)	***−1.847*** [a]	(−2.912, −1.008)	***0.441*** [a]	(0.009, 0.871)
Townsend's Solitaire	0.321	(−0.164, 0.851)	−0.207	(−0.706, 0.285)	***0.729*** [a]	(0.276, 1.215)
American Robin	−0.160	(−0.393, 0.084)	0.133	(−0.128, 0.405)	−0.220	(−0.503, 0.048)
Cassin's Finch	***−0.420*** [a]	(−0.622, −0.225)	0.218	(−0.014, 0.444)	−0.012	(−0.237, 0.210)
Fox Sparrow	−0.006	(−0.141, 0.133)	−0.039	(−0.187, 0.113)	0.075	(−0.076, 0.219)

Table A9-1 (continued). Estimates of linear and nonlinear effects of precipitation-as-snow (β_{PAS} and β_{PAS}^2) and linear effects of mean spring temperature (βMST), three of several covariates in hierarchical models of avian population density based on breeding-season point-count data collected annually during 2011–2014 and 2016–2019 in Devils Postpile National Monument. The 25 species analyzed are listed in taxonomic order. Each covariate represents a standardized climatic anomaly (relative to 1981–2010 normals), lagged by one year to model the demographic response to conditions in the previous breeding season. For each β with asterisk (also shown in bold italics), the 95% credible interval (CRI) on the mean did not overlap zero, indicating strong support for the effect. Missing values appear where these effects were removed from models to improve fit or promote the convergence of other parameter estimates.

	β_{PAS}		β_{PAS}^2		β_{MST}	
Species	**Mean**	**95% CRI**	**Mean**	**95% CRI**	**Mean**	**95% CRI**
Dark-eyed Junco	−0.089	(−0.222, 0.050)	0.013	(−0.133, 0.165)	−0.017	(−0.164, 0.120)
Song Sparrow	0.130	(−0.302, 0.583)	−0.365	(−0.800, 0.048)	***0.407*** [a]	(0.029, 0.787)
Green-tailed Towhee	***−0.378*** [a]	(−0.609, −0.137)	0.038	(−0.221, 0.289)	***0.299*** [a]	(0.039, 0.569)
MacGillivray's Warbler	−0.290	(−0.606, 0.035)	0.309	(−0.126, 0.729)	−0.354	(−0.703, 0.008)
Yellow-rumped Warbler	***−0.191*** [a]	(−0.360, −0.015)	***0.217*** [a]	(0.021, 0.415)	***−0.218*** [a]	(−0.441, −0.002)
Wilson's Warbler	***−0.357*** [a]	(−0.680, −0.032)	0.220	(−0.127, 0.595)	***0.402*** [a]	(0.003, 0.799)
Western Tanager	***−0.193*** [a]	(−0.372, −0.011)	***0.288*** [a]	(0.076, 0.501)	−0.004	(−0.236, 0.218)

Table A9-2. Estimates of linear and nonlinear effects of precipitation-as-snow (β_{PAS} and β_{PAS^2}) and linear effects of mean spring temperature (β_{MST}), three of several covariates in hierarchical models of avian population density based on breeding-season point-count data collected annually during 2011–2014 and 2016–2019 in Sequoia and Kings Canyon National Parks and Yosemite National Park. The 62 species analyzed are listed in taxonomic order. Each covariate represents a standardized climatic anomaly (relative to 1981–2010 normals), lagged by one year to model the demographic response to conditions in the previous breeding season. For each β with asterisk (also shown in bold italics), the 95% credible interval (CRI) on the mean did not overlap zero, indicating strong support for the effect. Missing values appear where these effects were removed from models to improve fit or promote the convergence of other parameter estimates.

	β_{PAS}		β_{PAS^2}		β_{MST}	
Species	**Mean**	**95% CRI**	**Mean**	**95% CRI**	**Mean**	**95% CRI**
Mountain Quail	***−0.346*** [a]	(−0.465, −0.215)	***0.167*** [a]	(0.104, 0.226)	***0.067*** [a]	(0.003, 0.130)
Sooty Grouse	–	–	–	–	***0.364*** [a]	(0.184, 0.558)
Anna's Hummingbird	***−0.498*** [a]	(−0.759, −0.216)	–	–	***0.538*** [a]	(0.338, 0.779)
Rufous Hummingbird	***−0.263*** [a]	(−0.503, −0.041)	–	–	***0.474*** [a]	(0.222, 0.734)
Acorn Woodpecker	–	–	–	–	0.145	(−0.042, 0.350)
Williamson's Sapsucker	–	–	–	–	***0.250*** [a]	(0.077, 0.430)
Red-breasted Sapsucker	–	–	–	–	***0.386*** [a]	(0.214, 0.560)
Hairy Woodpecker	***−0.163*** [a]	(−0.318, −0.002)	0.074	(−0.007, 0.150)	0.084	(−0.029, 0.194)
White-headed Woodpecker	0.177	(−0.122, 0.486)	−0.181	(−0.394, 0.019)	***0.282*** [a]	(0.193, 0.377)
Northern Flicker	−0.044	(−0.165, 0.087)	0.043	(−0.025, 0.105)	0.048	(−0.030, 0.125)
Pileated Woodpecker	–	–	–	–	0.031	(−0.122, 0.208)
Olive-sided Flycatcher	***−0.209*** [a]	(−0.396, −0.030)	0.059	(−0.045, 0.171)	***0.115*** [a]	(0.019, 0.207)
Western Wood-Pewee	−0.057	(−0.208, 0.094)	−0.056	(−0.186, 0.053)	***0.132*** [a]	(0.069, 0.191)
Hammond's Flycatcher	−0.049	(−0.368, 0.246)	***−0.658*** [a]	(−0.986, −0.298)	–	–
Dusky Flycatcher	***−0.148*** [a]	(−0.202, −0.097)	–	–	***0.184*** [a]	(0.132, 0.241)
Pacific-slope Flycatcher	–	–	–	–	***0.313*** [a]	(0.120, 0.490)
Cassin's Vireo	−0.035	(−0.424, 0.368)	***−0.482*** [a]	(−0.812, −0.174)	***0.196*** [a]	(0.100, 0.287)
Warbling Vireo	–	–	–	–	***0.294*** [a]	(0.217, 0.372)
Steller's Jay	–	–	–	–	***0.107*** [a]	(0.064, 0.151)
Clark's Nutcracker	***−0.156*** [a]	(−0.226, −0.091)	***0.100*** [a]	(0.061, 0.140)	***0.218*** [a]	(0.139, 0.297)
Common Raven	***−0.617*** [a]	(−0.906, −0.372)	0.153	(−0.016, 0.290)	***0.224*** [a]	(0.120, 0.337)

Table A9-2 (continued). Estimates of linear and nonlinear effects of precipitation-as-snow (β_{PAS} and β_{PAS}^2) and linear effects of mean spring temperature (β_{MST}), three of several covariates in hierarchical models of avian population density based on breeding-season point-count data collected annually during 2011–2014 and 2016–2019 in Sequoia and Kings Canyon National Parks and Yosemite National Park. The 62 species analyzed are listed in taxonomic order. Each covariate represents a standardized climatic anomaly (relative to 1981–2010 normals), lagged by one year to model the demographic response to conditions in the previous breeding season. For each β with asterisk (also shown in bold italics), the 95% credible interval (CRI) on the mean did not overlap zero, indicating strong support for the effect. Missing values appear where these effects were removed from models to improve fit or promote the convergence of other parameter estimates.

	β_{PAS}		β_{PAS}^2		β_{MST}	
Species	**Mean**	**95% CRI**	**Mean**	**95% CRI**	**Mean**	**95% CRI**
Mountain Chickadee	***−0.119*** [a]	(−0.164, −0.075)	−0.008	(−0.033, 0.019)	***0.056*** [a]	(0.014, 0.098)
Wrentit	0.041	(−0.634, 0.594)	–	–	***0.285*** [a]	(0.096, 0.470)
Golden-crowned Kinglet	***−0.177*** [a]	(−0.300, −0.057)	0.057	(−0.016, 0.127)	***0.198*** [a]	(0.133, 0.259)
Ruby-crowned Kinglet	***−0.281*** [a]	(−0.420, −0.143)	–	–	–	–
Red-breasted Nuthatch	***−0.169*** [a]	(−0.245, −0.094)	–	–	***0.104*** [a]	(0.059, 0.151)
White-breasted Nuthatch	–	–	–	–	***0.363*** [a]	(0.216, 0.509)
Brown Creeper	***−0.173*** [a]	(−0.275, −0.070)	***0.055*** [a]	(0.001, 0.109)	***0.220*** [a]	(0.153, 0.286)
Rock Wren	***−0.218*** [a]	(−0.360, −0.090)	–	–	***0.403*** [a]	(0.259, 0.569)
Canyon Wren	–	–	–	–	–	–
House Wren	–	–	–	–	***0.234*** [a]	(0.048, 0.405)
Pacific Wren	–	–	–	–	–	–
Bewick's Wren	–	–	–	–	0.300	(−0.064, 0.686)
Mountain Bluebird	–	–	–	–	–	–
Townsend's Solitaire	−0.091	(−0.203, 0.014)	–	–	−0.052	(−0.159, 0.049)
Hermit Thrush	***−0.296*** [a]	(−0.370, −0.221)	***0.086*** [a]	(0.046, 0.127)	***0.199*** [a]	(0.121, 0.279)
American Robin	***−0.221*** [a]	(−0.307, −0.132)	***0.075*** [a]	(0.031, 0.118)	–	–
American Pipit	***−0.526*** [a]	(−0.738, −0.328)	–	–	0.108	(−0.085, 0.302)
Gray-crowned Rosy-Finch	***−0.324*** [a]	(−0.491, −0.148)	***0.335*** [a]	(0.206, 0.460)	−0.151	(−0.339, 0.043)
Purple Finch	***0.263*** [a]	(0.011, 0.498)	–	–	–	–
Cassin's Finch	***−0.160*** [a]	(−0.211, −0.107)	–	–	***0.247*** [a]	(0.182, 0.313)
Pine Siskin	–	–	–	–	***0.344*** [a]	(0.251, 0.439)
Chipping Sparrow	***−0.242*** [a]	(−0.406, −0.069)	***0.128*** [a]	(0.046, 0.213)	***0.367*** [a]	(0.213, 0.512)

Table A9-2 (continued). Estimates of linear and nonlinear effects of precipitation-as-snow (β_{PAS} and β_{PAS}^2) and linear effects of mean spring temperature (β_{MST}), three of several covariates in hierarchical models of avian population density based on breeding-season point-count data collected annually during 2011–2014 and 2016–2019 in Sequoia and Kings Canyon National Parks and Yosemite National Park. The 62 species analyzed are listed in taxonomic order. Each covariate represents a standardized climatic anomaly (relative to 1981–2010 normals), lagged by one year to model the demographic response to conditions in the previous breeding season. For each β with asterisk (also shown in bold italics), the 95% credible interval (CRI) on the mean did not overlap zero, indicating strong support for the effect. Missing values appear where these effects were removed from models to improve fit or promote the convergence of other parameter estimates.

	β_{PAS}		β_{PAS}^2		β_{MST}	
Species	**Mean**	**95% CRI**	**Mean**	**95% CRI**	**Mean**	**95% CRI**
Fox Sparrow	0.023	(−0.076, 0.127)	***−0.090*** [a]	(−0.167, −0.022)	***0.085*** [a]	(0.026, 0.143)
Dark-eyed Junco	***−0.098*** [a]	(−0.140, −0.057)	***0.028*** [a]	(0.005, 0.049)	0.035	(−0.001, 0.070)
White-crowned Sparrow	***−0.242*** [a]	(−0.363, −0.123)	***0.098*** [a]	(0.017, 0.183)	−0.100	(−0.236, 0.034)
Song Sparrow	–	–	–	–	–	–
Lincoln's Sparrow	***−0.309*** [a]	(−0.499, −0.118)	***0.131*** [a]	(0.016, 0.256)	−0.078	(−0.230, 0.080)
Green-tailed Towhee	***−0.181*** [a]	(−0.344, −0.018)	0.070	(−0.037, 0.178)	***0.582*** [a]	(0.439, 0.728)
Spotted Towhee	–	–	–	–	0.027	(−0.048, 0.104)
Red-winged Blackbird	0.040	(−0.199, 0.266)	–	–	0.035	(−0.140, 0.202)
Orange-crowned Warbler	–	–	–	–	–	–
Nashville Warbler	***−0.208*** [a]	(−0.310, −0.099)	–	–	***0.096*** [a]	(0.032, 0.161)
MacGillivray's Warbler	***−0.364*** [a]	(−0.518, −0.208)	−0.004	(−0.115, 0.104)	***0.308*** [a]	(0.235, 0.380)
Yellow Warbler	0.118	(−0.482, 0.759)	−0.099	(−0.531, 0.206)	0.121	(−0.118, 0.368)
Yellow-rumped Warbler	***−0.073*** [a]	(−0.113, −0.034)	–	–	***0.147*** [a]	(0.108, 0.186)
Black-throated Gray Warbler	–	–	–	–	***0.361*** [a]	(0.256, 0.470)
Hermit Warbler	−0.199	(−0.498, 0.099)	***−0.329*** [a]	(−0.604, −0.032)	***0.116*** [a]	(0.040, 0.187)
Wilson's Warbler	−0.085	(−0.250, 0.084)	−0.086	(−0.210, 0.032)	***0.254*** [a]	(0.114, 0.399)
Western Tanager	***−0.282*** [a]	(−0.383, −0.183)	–	–	***0.150*** [a]	(0.105, 0.195)
Black-headed Grosbeak	−0.118	(−0.477, 0.229)	−0.153	(−0.436, 0.189)	***0.104*** [a]	(0.040, 0.175)
Lazuli Bunting	***−0.375*** [a]	(−0.647, −0.116)	0.048	(−0.222, 0.262)	***0.445*** [a]	(0.304, 0.585)

Appendix 10. Parameter estimates: availability and detection

Probabilities of availability for detection and metrics of fit are presented for Devils Postpile National Monument (Table A10-1) and for Sequoia and Kings Canyon National Parks and Yosemite National Park (Table A10-2).

Table A10-1. Probabilities of availability for detection (p_a) and detection (p_d), and metrics of fit (Bayesian p-values for sub-models of availability and detection) from hierarchical models of breeding-season avian point-count data collected annually during 2011–2014 and 2016–2019 in Devils Postpile National Monument (DEPO). The 25 species analyzed in DEPO are listed in taxonomic order.

	p_a		p_d		Bayesian p-value	
Species	**mean**	**95% CRI**	**mean**	**95% CRI**	p_a	p_d
Mountain Quail	0.943	(0.871, 0.981)	0.198	(0.159, 0.255)	0.497	0.638
Hairy Woodpecker	0.930	(0.815, 0.981)	0.281	(0.207, 0.388)	0.503	0.395
Northern Flicker	0.890	(0.652, 0.980)	0.680	(0.442, 0.907)	0.495	0.439
Olive-sided Flycatcher	0.986	(0.968, 0.995)	0.686	(0.537, 0.897)	0.528	0.716
Western Wood-Pewee	0.993	(0.986, 0.997)	0.401	(0.343, 0.469)	0.518	0.761
Dusky Flycatcher	0.974	(0.936, 0.992)	0.247	(0.191, 0.324)	0.510	0.831
Warbling Vireo	0.985	(0.963, 0.996)	0.329	(0.256, 0.424)	0.527	0.857
Steller's Jay	0.942	(0.896, 0.970)	0.403	(0.337, 0.485)	0.488	0.401
Clark's Nutcracker	0.961	(0.874, 0.995)	0.463	(0.281, 0.708)	0.509	0.238
Mountain Chickadee	0.964	(0.939, 0.980)	0.325	(0.274, 0.389)	0.512	0.518
Golden-crowned Kinglet	0.902	(0.703, 0.982)	0.375	(0.267, 0.530)	0.522	0.532
Red-breasted Nuthatch	0.910	(0.792, 0.970)	0.429	(0.321, 0.581)	0.502	0.606
Brown Creeper	0.946	(0.841, 0.989)	0.314	(0.219, 0.476)	0.504	0.448
House Wren	0.932	(0.800, 0.988)	0.402	(0.289, 0.565)	0.511	0.394
Townsend's Solitaire	0.982	(0.935, 0.999)	0.762	(0.452, 0.964)	0.679	0.593
American Robin	0.933	(0.859, 0.974)	0.492	(0.378, 0.651)	0.493	0.502
Cassin's Finch	0.952	(0.905, 0.980)	0.604	(0.481, 0.772)	0.535	0.613
Fox Sparrow	0.996	(0.993, 0.998)	0.402	(0.356, 0.454)	0.504	0.860
Dark-eyed Junco	0.973	(0.955, 0.985)	0.316	(0.277, 0.361)	0.499	0.582
Song Sparrow	0.884	(0.660, 0.974)	0.700	(0.424, 0.949)	0.557	0.587
Green-tailed Towhee	0.991	(0.978, 0.998)	0.505	(0.384, 0.679)	0.549	0.740
MacGillivray's Warbler	0.970	(0.918, 0.993)	0.320	(0.237, 0.443)	0.484	0.500
Yellow-rumped Warbler	0.971	(0.949, 0.985)	0.432	(0.361, 0.520)	0.525	0.640

Table A10-1 (continued). Probabilities of availability for detection (p_a) and detection (p_d), and metrics of fit (Bayesian p-values for sub-models of availability and detection) from hierarchical models of breeding-season avian point-count data collected annually during 2011–2014 and 2016–2019 in Devils Postpile National Monument (DEPO). The 25 species analyzed in DEPO are listed in taxonomic order.

	p_a		p_d		Bayesian p-value	
Species	**mean**	**95% CRI**	**mean**	**95% CRI**	p_a	p_d
Wilson's Warbler	0.966	(0.897, 0.994)	0.485	(0.327, 0.795)	0.527	0.446
Western Tanager	0.978	(0.954, 0.992)	0.419	(0.338, 0.527)	0.526	0.618

Table A10-2. Probabilities of availability for detection (p_a) and detection (p_d), and metrics of fit (Bayesian p-values for sub-models of availability and detection) from hierarchical models of breeding-season avian point-count data collected annually during 2011–2014 and 2016–2019 in Sequoia and Kings Canyon National Parks and Yosemite National Park. The 62 species analyzed across these parks are listed in taxonomic order.

	p_a		p_d		Bayesian p-value	
Species	**mean**	**95% CRI**	**mean**	**95% CRI**	p_a	p_d
Mountain Quail	0.979	(0.967, 0.988)	0.210	(0.186, 0.242)	0.498	0.577
Sooty Grouse	0.971	(0.946, 0.987)	0.215	(0.171, 0.273)	0.508	0.389
Anna's Hummingbird	0.658	(0.199, 0.885)	0.227	(0.166, 0.310)	0.496	0.599
Rufous Hummingbird	0.223	(0.158, 0.314)	0.246	(0.195, 0.311)	0.528	0.365
Acorn Woodpecker	0.945	(0.836, 0.988)	0.305	(0.254, 0.370)	0.492	0.501
Williamson's Sapsucker	0.908	(0.837, 0.951)	0.324	(0.266, 0.396)	0.489	0.456
Red-breasted Sapsucker	0.894	(0.837, 0.936)	0.242	(0.200, 0.294)	0.510	0.418
Hairy Woodpecker	0.924	(0.890, 0.950)	0.331	(0.287, 0.386)	0.501	0.505
White-headed Woodpecker	0.891	(0.820, 0.942)	0.315	(0.272, 0.363)	0.480	0.625
Northern Flicker	0.886	(0.852, 0.914)	0.269	(0.242, 0.299)	0.518	0.645
Pileated Woodpecker	0.893	(0.770, 0.959)	0.173	(0.153, 0.198)	0.506	0.740
Olive-sided Flycatcher	0.970	(0.952, 0.982)	0.163	(0.144, 0.186)	0.501	0.519
Western Wood-Pewee	0.983	(0.977, 0.988)	0.401	(0.360, 0.445)	0.527	0.552
Hammond's Flycatcher	0.952	(0.892, 0.981)	0.289	(0.242, 0.347)	0.483	0.441
Dusky Flycatcher	0.978	(0.972, 0.982)	0.354	(0.319, 0.394)	0.523	0.859
Pacific-slope Flycatcher	0.962	(0.940, 0.979)	0.395	(0.332, 0.473)	0.506	0.523
Cassin's Vireo	0.938	(0.894, 0.969)	0.360	(0.317, 0.410)	0.499	0.410
Warbling Vireo	0.980	(0.974, 0.985)	0.368	(0.321, 0.423)	0.516	0.373
Steller's Jay	0.966	(0.959, 0.972)	0.302	(0.276, 0.331)	0.495	0.112
Clark's Nutcracker	0.950	(0.928, 0.967)	0.373	(0.336, 0.412)	0.436	0.186
Common Raven	0.643	(0.466, 0.848)	0.138	(0.120, 0.161)	0.476	0.384
Mountain Chickadee	0.970	(0.965, 0.974)	0.433	(0.401, 0.466)	0.465	0.101
Wrentit	0.956	(0.921, 0.978)	0.279	(0.214, 0.359)	0.503	0.472
Golden-crowned Kinglet	0.984	(0.980, 0.988)	0.396	(0.349, 0.449)	0.522	0.717
Ruby-crowned Kinglet	0.975	(0.954, 0.989)	0.481	(0.371, 0.634)	0.488	0.285
Red-breasted Nuthatch	0.978	(0.971, 0.983)	0.394	(0.352, 0.442)	0.528	0.901
White-breasted Nuthatch	0.922	(0.879, 0.954)	0.338	(0.287, 0.400)	0.484	0.402

Table A10-2 (continued). Probabilities of availability for detection (p_a) and detection (p_d), and metrics of fit (Bayesian p-values for sub-models of availability and detection) from hierarchical models of breeding-season avian point-count data collected annually during 2011–2014 and 2016–2019 in Sequoia and Kings Canyon National Parks and Yosemite National Park. The 62 species analyzed across these parks are listed in taxonomic order.

	p_a		p_d		Bayesian p-value	
Species	**mean**	**95% CRI**	**mean**	**95% CRI**	p_a	p_d
Brown Creeper	0.943	(0.928, 0.955)	0.363	(0.325, 0.404)	0.519	0.621
Rock Wren	0.952	(0.922, 0.973)	0.289	(0.234, 0.360)	0.484	0.285
Canyon Wren	0.970	(0.928, 0.991)	0.301	(0.238, 0.379)	0.496	0.632
House Wren	0.932	(0.896, 0.961)	0.295	(0.243, 0.360)	0.492	0.471
Pacific Wren	0.981	(0.963, 0.991)	0.422	(0.341, 0.527)	0.500	0.454
Bewick's Wren	0.985	(0.959, 0.997)	0.209	(0.150, 0.288)	0.527	0.540
Mountain Bluebird	0.901	(0.808, 0.955)	0.181	(0.152, 0.217)	0.474	0.216
Townsend's Solitaire	0.945	(0.922, 0.962)	0.284	(0.249, 0.327)	0.505	0.491
Hermit Thrush	0.980	(0.972, 0.986)	0.365	(0.325, 0.410)	0.492	0.312
American Robin	0.946	(0.933, 0.957)	0.239	(0.219, 0.260)	0.453	0.214
American Pipit	0.971	(0.949, 0.985)	0.351	(0.296, 0.417)	0.498	0.275
Gray-crowned Rosy-inch	0.717	(0.613, 0.811)	0.222	(0.181, 0.276)	0.384	0.091
Purple Finch	0.946	(0.915, 0.968)	0.377	(0.308, 0.466)	0.482	0.257
Cassin's Finch	0.945	(0.932, 0.956)	0.376	(0.338, 0.419)	0.476	0.123
Pine Siskin	0.879	(0.833, 0.913)	0.353	(0.291, 0.421)	0.338	0.034
Chipping Sparrow	0.958	(0.932, 0.977)	0.421	(0.337, 0.516)	0.473	0.399
Fox Sparrow	0.981	(0.977, 0.985)	0.233	(0.209, 0.261)	0.490	0.468
Dark-eyed Junco	0.956	(0.950, 0.962)	0.312	(0.292, 0.333)	0.468	0.141
White-crowned Sparrow	0.914	(0.834, 0.965)	0.188	(0.164, 0.218)	0.479	0.490
Song Sparrow	0.964	(0.940, 0.981)	0.324	(0.262, 0.397)	0.503	0.485
Lincoln's Sparrow	0.971	(0.953, 0.984)	0.192	(0.162, 0.228)	0.503	0.541
Green-tailed Towhee	0.950	(0.928, 0.967)	0.280	(0.235, 0.335)	0.483	0.185
Spotted Towhee	0.974	(0.965, 0.981)	0.300	(0.264, 0.344)	0.502	0.669
Red-winged Blackbird	0.987	(0.976, 0.994)	0.636	(0.512, 0.763)	0.508	0.517
Orange-crowned Warbler	0.805	(0.604, 0.940)	0.224	(0.160, 0.311)	0.466	0.439
Nashville Warbler	0.981	(0.975, 0.986)	0.559	(0.493, 0.627)	0.476	0.260
MacGillivray's Warbler	0.968	(0.955, 0.977)	0.377	(0.332, 0.427)	0.499	0.205

Table A10-2 (continued). Probabilities of availability for detection (p_a) and detection (p_d), and metrics of fit (Bayesian p-values for sub-models of availability and detection) from hierarchical models of breeding-season avian point-count data collected annually during 2011–2014 and 2016–2019 in Sequoia and Kings Canyon National Parks and Yosemite National Park. The 62 species analyzed across these parks are listed in taxonomic order.

	p_a		p_d		Bayesian p-value	
Species	**mean**	**95% CRI**	**mean**	**95% CRI**	p_a	p_d
Yellow Warbler	0.976	(0.946, 0.992)	0.398	(0.278, 0.579)	0.507	0.617
Yellow-rumped Warbler	0.973	(0.969, 0.977)	0.383	(0.350, 0.416)	0.509	0.560
Black-throated Gray Warbler	0.920	(0.853, 0.966)	0.295	(0.252, 0.348)	0.493	0.391
Hermit Warbler	0.851	(0.748, 0.937)	0.304	(0.269, 0.343)	0.432	0.285
Wilson's Warbler	0.959	(0.938, 0.975)	0.322	(0.268, 0.388)	0.500	0.447
Western Tanager	0.976	(0.968, 0.983)	0.414	(0.370, 0.464)	0.498	0.490
Black-headed Grosbeak	0.918	(0.865, 0.960)	0.250	(0.226, 0.279)	0.460	0.681
Lazuli Bunting	0.977	(0.959, 0.988)	0.301	(0.236, 0.380)	0.494	0.189

Appendix 11. Parameter estimates: effects of survey timing and habitat conditions on detection

Table A11-1. Effects of day (β_{day}) and hour (β_{hour}) on bird availability for detection, and effects of cover (β_{cover}) and noise (β_{noise}) on bird detection in hierarchical models of avian population density based on breeding-season point counts conducted annually across Sequoia and Kings Canyon National Parks and Yosemite National Park during 2011–2014 and 2016–2019. For each β with asterisk (also shown in bold italics), the 95% credible interval (CRI) on the mean did not overlap zero, indicating strong support for the effect. Missing values appear where these effects were removed from models to improve fit or promote the convergence of other parameter estimates. The 62 species analyzed across these parks are listed in taxonomic order. Species codes appear in Table 4 of the main text and align with species names in Table A10-2.

	β_{day}		β_{hour}		β_{cover}		β_{noise}	
Species Code	**Mean**	**95% CRI**	**Mean**	**95% CRI**	**Mean**	**95% CRI**	**Mean**	**95% CRI**
MOUQ	0.024	(−0.060, 0.114)	–	–	***−0.024*** [a]	(−0.038, −0.010)	***−0.059*** [a]	(−0.074, −0.044)
SOGR	–	–	–	–	–	–	***−0.102*** [a]	(−0.148, −0.059)
ANHU	–	–	–	–	***−0.076*** [a]	(−0.122, −0.035)	–	–
RUHU	***−1.313*** [a]	(−1.594, −1.034)	***0.205*** [a]	(0.036, 0.374)	–	–	−0.046	(−0.100, 0.010)
ACWO	0.009	(−0.293, 0.337)	0.012	(−0.101, 0.124)	–	–	–	–
WISA	−0.006	(−0.209, 0.169)	0.035	(−0.099, 0.168)	0.020	(−0.025, 0.064)	***−0.189*** [a]	(−0.244, −0.140)
RBSA	−0.021	(−0.147, 0.106)	0.081	(−0.035, 0.195)	***−0.035*** [a]	(−0.072, −0.002)	***−0.101*** [a]	(−0.139, −0.065)
HAWO	0.017	(−0.071, 0.110)	–	–	0.001	(−0.027, 0.028)	***−0.108*** [a]	(−0.134, −0.083)
WHWO	***0.144*** [a]	(0.006, 0.283)	0.069	(−0.010, 0.152)	–	–	***−0.119*** [a]	(−0.146, −0.092)
NOFL	−0.033	(−0.100, 0.035)	–	–	−0.004	(−0.024, 0.017)	***−0.095*** [a]	(−0.114, −0.075)
PIWO	0.080	(−0.110, 0.289)	0.026	(−0.117, 0.190)	0.015	(−0.014, 0.044)	***−0.097*** [a]	(−0.129, −0.066)
OSFL	***0.134*** [a]	(0.038, 0.235)	–	–	−0.016	(−0.035, 0.003)	***−0.065*** [a]	(−0.085, −0.045)
WEWP	−0.039	(−0.097, 0.020)	0.005	(−0.036, 0.044)	−0.002	(−0.023, 0.019)	***−0.073*** [a]	(−0.092, −0.053)
HAFL	0.117	(−0.022, 0.288)	–	–	–	–	***−0.118*** [a]	(−0.162, −0.077)

Table A11-1 (continued). Effects of day (β_{day}) and hour (β_{hour}) on bird availability for detection, and effects of cover (β_{cover}) and noise (β_{noise}) on bird detection in hierarchical models of avian population density based on breeding-season point counts conducted annually across Sequoia and Kings Canyon National Parks and Yosemite National Park during 2011–2014 and 2016–2019. For each β with asterisk (also shown in bold italics), the 95% credible interval (CRI) on the mean did not overlap zero, indicating strong support for the effect. Missing values appear where these effects were removed from models to improve fit or promote the convergence of other parameter estimates. The 62 species analyzed across these parks are listed in taxonomic order. Species codes appear in Table 4 of the main text and align with species names in Table A10-2.

	β_{day}		β_{hour}		β_{cover}		β_{noise}	
Species Code	**Mean**	**95% CRI**	**Mean**	**95% CRI**	**Mean**	**95% CRI**	**Mean**	**95% CRI**
DUFL	–	–	0.036	(−0.003, 0.075)	***−0.023*** [a]	(−0.037, −0.010)	***−0.080*** [a]	(−0.095, −0.065)
PSFL	–	–	–	–	–	–	–	–
CAVI	***0.179*** [a]	(0.050, 0.310)	−0.001	(−0.062, 0.060)	***0.035*** [a]	(0.008, 0.061)	***−0.062*** [a]	(−0.089, −0.036)
WAVI	–	–	0.031	(−0.015, 0.077)	0.013	(−0.010, 0.036)	***−0.058*** [a]	(−0.078, −0.037)
STJA	***−0.054*** [a]	(−0.094, −0.013)	–	–	–	–	***−0.048*** [a]	(−0.059, −0.038)
CLNU	***−0.089*** [a]	(−0.173, −0.009)	–	–	−0.007	(−0.025, 0.011)	***−0.062*** [a]	(−0.082, −0.042)
CORA	***0.419*** [a]	(0.146, 0.645)	0.058	(−0.046, 0.164)	−0.009	(−0.036, 0.017)	***−0.052*** [a]	(−0.073, −0.031)
MOCH	***−0.037*** [a]	(−0.064, −0.009)	***0.064*** [a]	(0.038, 0.090)	–	–	***−0.088*** [a]	(−0.099, −0.076)
WREN	–	–	–	–	–	–	−0.049	(−0.108, 0.010)
GCKI	–	–	−0.019	(−0.058, 0.020)	***0.049*** [a]	(0.024, 0.073)	***−0.053*** [a]	(−0.070, −0.035)
RCKI	–	–	–	–	–	–	0.001	(−0.069, 0.074)
RBNU	***0.058*** [a]	(0.014, 0.104)	–	–	–	–	***−0.099*** [a]	(−0.115, −0.084)
WBNU	–	–	–	–	–	–	–	–
BRCR	–	–	***0.119*** [a]	(0.071, 0.168)	***0.051*** [a]	(0.032, 0.070)	***−0.059*** [a]	(−0.076, −0.042)
ROWR	–	–	–	–	–	–	–	–
CANW	0.112	(−0.064, 0.318)	–	–	–	–	–	–
HOWR	–	–	–	–	–	–	***−0.116*** [a]	(−0.161, −0.074)

Table A11-1 (continued). Effects of day (β_{day}) and hour (β_{hour}) on bird availability for detection, and effects of cover (β_{cover}) and noise (β_{noise}) on bird detection in hierarchical models of avian population density based on breeding-season point counts conducted annually across Sequoia and Kings Canyon National Parks and Yosemite National Park during 2011–2014 and 2016–2019. For each β with asterisk (also shown in bold italics), the 95% credible interval (CRI) on the mean did not overlap zero, indicating strong support for the effect. Missing values appear where these effects were removed from models to improve fit or promote the convergence of other parameter estimates. The 62 species analyzed across these parks are listed in taxonomic order. Species codes appear in Table 4 of the main text and align with species names in Table A10-2.

	β_{day}		β_{hour}		β_{cover}		β_{noise}	
Species Code	**Mean**	**95% CRI**	**Mean**	**95% CRI**	**Mean**	**95% CRI**	**Mean**	**95% CRI**
PAWR	–	–	–	–	–	–	–	–
BEWR	0.070	(−0.162, 0.309)	0.086	(−0.092, 0.262)	–	–	–	–
MOBL	–	–	–	–	–	–	***−0.097*** [a]	(−0.144, −0.051)
TOSO	0.017	(−0.069, 0.106)	–	–	0.009	(−0.014, 0.031)	***−0.078*** [a]	(−0.102, −0.055)
HETH	−0.056	(−0.117, 0.003)	–	–	0.010	(−0.008, 0.028)	***−0.077*** [a]	(−0.096, −0.058)
AMRO	–	–	***0.085*** [a]	(0.043, 0.130)	0.011	(−0.002, 0.024)	***−0.040*** [a]	(−0.052, −0.028)
AMPI	–	–	–	–	–	–	***0.054*** [a]	(0.000, 0.118)
GCRF	***−0.339*** [a]	(−0.483, −0.196)	–	–	–	–	–	–
PUFI	–	–	–	–	–	–	–	–
CAFI	–	–	0.027	(−0.019, 0.072)	−0.009	(−0.025, 0.006)	***−0.070*** [a]	(−0.088, −0.052)
PISI	***0.119*** [a]	(0.019, 0.222)	–	–	−0.005	(−0.032, 0.021)	***−0.091*** [a]	(−0.119, −0.063)
CHSP	–	–	0.062	(−0.034, 0.162)	−0.006	(−0.046, 0.033)	***−0.088*** [a]	(−0.140, −0.039)
FOSP	0.020	(−0.029, 0.070)	−0.009	(−0.042, 0.024)	−0.003	(−0.016, 0.008)	***−0.064*** [a]	(−0.078, −0.051)
DEJU	−0.022	(−0.048, 0.004)	***0.053*** [a]	(0.028, 0.077)	–	–	***−0.036*** [a]	(−0.044, −0.028)
WCSP	***−0.220*** [a]	(−0.405, −0.046)	–	–	***−0.039*** [a]	(−0.060, −0.019)	***−0.036*** [a]	(−0.058, −0.014)
SOSP	–	–	–	–	0.011	(−0.040, 0.056)	−0.040	(−0.088, 0.008)
LISP	–	–	0.015	(−0.077, 0.109)	−0.006	(−0.034, 0.021)	***−0.031*** [a]	(−0.061, −0.001)

Table A11-1 (continued). Effects of day (β_{day}) and hour (β_{hour}) on bird availability for detection, and effects of cover (β_{cover}) and noise (β_{noise}) on bird detection in hierarchical models of avian population density based on breeding-season point counts conducted annually across Sequoia and Kings Canyon National Parks and Yosemite National Park during 2011–2014 and 2016–2019. For each β with asterisk (also shown in bold italics), the 95% credible interval (CRI) on the mean did not overlap zero, indicating strong support for the effect. Missing values appear where these effects were removed from models to improve fit or promote the convergence of other parameter estimates. The 62 species analyzed across these parks are listed in taxonomic order. Species codes appear in Table 4 of the main text and align with species names in Table A10-2.

	β_{day}		β_{hour}		β_{cover}		β_{noise}	
Species Code	**Mean**	**95% CRI**	**Mean**	**95% CRI**	**Mean**	**95% CRI**	**Mean**	**95% CRI**
GTTO	−0.053	(−0.170, 0.063)	0.054	(−0.034, 0.141)	−0.018	(−0.043, 0.006)	***−0.095*** [a]	(−0.123, −0.067)
SPTO	–	–	–	–	−0.014	(−0.035, 0.007)	***−0.078*** [a]	(−0.104, −0.053)
RWBL	–	–	–	–	–	–	–	–
OCWA	0.304	(−0.092, 0.641)	−0.159	(−0.380, 0.054)	–	–	***−0.101*** [a]	(−0.182, −0.027)
NAWA	***0.064*** [a]	(0.009, 0.123)	***0.051*** [a]	(0.010, 0.091)	−0.005	(−0.030, 0.018)	***−0.054*** [a]	(−0.080, −0.028)
MGWA	0.059	(−0.005, 0.123)	–	–	0.020	(−0.002, 0.042)	***−0.067*** [a]	(−0.088, −0.046)
YEWA	–	–	–	–	–	–	–	–
YRWA	–	–	–	–	***0.037*** [a]	(0.026, 0.048)	***−0.057*** [a]	(−0.068, −0.047)
BTYW	***0.180*** [a]	(0.002, 0.358)	–	–	−0.004	(−0.029, 0.020)	***−0.035*** [a]	(−0.065, −0.004)
HEWA	***0.365*** [a]	(0.193, 0.524)	–	–	***0.053*** [a]	(0.026, 0.080)	***−0.045*** [a]	(−0.066, −0.025)
WIWA	−0.111	(−0.236, 0.012)	–	–	***−0.054*** [a]	(−0.090, −0.020)	0.031	(−0.002, 0.066)
WETA	0.020	(−0.033, 0.075)	***0.082*** [a]	(0.050, 0.115)	–	–	***−0.075*** [a]	(−0.090, −0.062)
BHGR	***0.253*** [a]	(0.119, 0.381)	–	–	***−0.027*** [a]	(−0.043, −0.012)	***−0.050*** [a]	(−0.065, −0.035)
LAZB	0.071	(−0.031, 0.176)	***0.075*** [a]	(0.002, 0.146)	−0.005	(−0.033, 0.023)	***−0.057*** [a]	(−0.086, −0.027)

Appendix 12. Parameter estimates: detection distance

Detection distance parameters by species are presented for Devils Postpile National Monument (Table A12-1) and for Sequoia and Kings Canyon National Parks and Yosemite National Park (Table A12-2).

Table A12-1. Detection-distance parameters by species in Devils Postpile National Monument (DEPO), including the percent of recorded distances discarded (D%) from the tail of the observed detection-distance distribution prior to fitting a half-normal density to the data, the maximum detection distance (d_{max}) in the remaining sample, the effective area (Area) over which density was estimated around each point-count station, and the fitted estimate (mean and 95% credible interval) of the shape parameter of the half-normal detection-distance function ($\sigma_{half\text{-}norm}$). The 25 species analyzed in DEPO are listed in taxonomic order.

				$\sigma_{half\text{-}norm}$	
Species	**D%**	**d_{max} (m)**	**Area (ha)**	**Mean**	**95% CRI**
Mountain Quail	10.11	261	21.4	84	(75, 95)
Hairy Woodpecker	9.68	114	4.1	43	(37, 52)
Northern Flicker	10.00	122	4.7	100	(58, 187)
Olive-sided Flycatcher	9.52	110	3.8	87	(62, 159)
Western Wood-Pewee	7.72	91	2.6	42	(38, 48)
Dusky Flycatcher	5.26	81	2.1	29	(25, 34)
Warbling Vireo	10.19	80	2.0	33	(29, 39)
Steller's Jay	10.05	106	3.5	50	(44, 57)
Clark's Nutcracker	10.26	135	5.7	83	(51, 174)
Mountain Chickadee	9.96	80	2.0	33	(30, 38)
Golden-crowned Kinglet	10.81	51	0.8	21	(17, 28)
Red-breasted Nuthatch	9.76	104	3.4	51	(42, 65)
Brown Creeper	10.64	60	1.1	24	(20, 33)
House Wren	9.30	64	1.3	28	(22, 38)
Townsend's Solitaire	8.57	75	1.8	89	(37, 190)
American Robin	9.62	82	2.1	44	(36, 58)
Cassin's Finch	14.07	74	1.7	48	(38, 68)
Fox Sparrow	13.07	81	2.1	38	(35, 42)
Dark-eyed Junco	9.63	68	1.5	28	(26, 30)
Song Sparrow	8.70	88	2.4	83	(42, 186)
Green-tailed Towhee	9.91	68	1.5	38	(30, 53)

Table A12-1 (continued). Detection-distance parameters by species in Devils Postpile National Monument (DEPO), including the percent of recorded distances discarded (D%) from the tail of the observed detection-distance distribution prior to fitting a half-normal density to the data, the maximum detection distance (d_{max}) in the remaining sample, the effective area (Area) over which density was estimated around each point-count station, and the fitted estimate (mean and 95% credible interval) of the shape parameter of the half-normal detection-distance function ($\sigma_{half\text{-}norm}$). The 25 species analyzed in DEPO are listed in taxonomic order.

				$\sigma_{half\text{-}norm}$	
Species	**D%**	**d_{max} (m)**	**Area (ha)**	**Mean**	**95% CRI**
MacGillivray's Warbler	10.29	86	2.3	36	(29, 46)
Yellow-rumped Warbler	8.70	67	1.4	34	(29, 41)
Wilson's Warbler	9.80	60	1.1	34	(24, 64)
Western Tanager	10.20	89	2.5	42	(37, 51)

Table A12-2. Detection-distance parameters by species in Sequoia and Kings Canyon National Parks and Yosemite National Park, including the percent of recorded distances discarded (D%) from the tail of the observed detection-distance distribution prior to fitting a half-normal density to the data, the maximum detection distance (d_{max}) in the remaining sample, the effective area (Area) over which density was estimated around each point-count station, and the fitted estimate (mean and 95% credible interval) of the shape parameter of the half-normal detection-distance function ($\sigma_{half\text{-}norm}$). The 62 species analyzed across these parks are listed in taxonomic order.

				$\sigma_{half\text{-}norm}$	
Species	**D%**	**d_{max} (m)**	**Area (ha)**	**Mean**	**95% CRI**
Mountain Quail	5.01	346	37.6	111	(103, 120)
Sooty Grouse	9.94	183	10.5	59	(52, 68)
Anna's Hummingbird	11.80	36	0.4	12	(10, 16)
Rufous Hummingbird	9.91	24	0.2	8	(8, 10)
Acorn Woodpecker	4.03	136	5.8	54	(48, 62)
Williamson's Sapsucker	9.93	117	4.3	48	(42, 56)
Red-breasted Sapsucker	4.85	130	5.3	45	(40, 51)
Hairy Woodpecker	9.90	101	3.2	42	(38, 47)
White-headed Woodpecker	9.89	99	3.1	40	(36, 44)
Northern Flicker	9.82	152	7.3	56	(53, 60)
Pileated Woodpecker	9.91	229	16.5	68	(64, 73)
Olive-sided Flycatcher	5.02	199	12.4	58	(54, 61)
Western Wood-Pewee	9.81	106	3.5	50	(47, 55)
Hammond's Flycatcher	4.96	77	1.9	29	(26, 33)
Dusky Flycatcher	9.76	74	1.7	32	(30, 35)
Pacific-slope Flycatcher	5.68	80	2.0	37	(33, 44)
Cassin's Vireo	4.76	89	2.5	39	(36, 43)
Warbling Vireo	9.89	87	2.4	40	(36, 44)
Steller's Jay	9.81	136	5.8	54	(51, 57)
Clark's Nutcracker	18.87	147	6.8	66	(62, 71)
Common Raven	5.07	270	22.9	74	(70, 79)
Mountain Chickadee	16.45	72	1.6	36	(34, 39)
Wrentit	10.14	146	6.7	55	(46, 67)
Golden-crowned Kinglet	9.90	45	0.6	22	(19, 24)
Ruby-crowned Kinglet	9.69	81	2.1	58	(37, 140)

Table A12-2 (continued). Detection-distance parameters by species in Sequoia and Kings Canyon National Parks and Yosemite National Park, including the percent of recorded distances discarded (D%) from the tail of the observed detection-distance distribution prior to fitting a half-normal density to the data, the maximum detection distance (d_{max}) in the remaining sample, the effective area (Area) over which density was estimated around each point-count station, and the fitted estimate (mean and 95% credible interval) of the shape parameter of the half-normal detection-distance function ($\sigma_{half\text{-}norm}$). The 62 species analyzed across these parks are listed in taxonomic order.

				$\sigma_{half\text{-}norm}$	
Species	**D%**	**d_{max} (m)**	**Area (ha)**	**Mean**	**95% CRI**
Red-breasted Nuthatch	6.96	111	3.9	52	(48, 58)
White-breasted Nuthatch	4.82	109	3.7	46	(41, 52)
Brown Creeper	11.57	56	1.0	25	(23, 27)
Rock Wren	9.86	133	5.6	51	(45, 61)
Canyon Wren	8.80	180	10.2	70	(61, 81)
House Wren	9.84	74	1.7	29	(25, 33)
Pacific Wren	10.10	76	1.8	38	(32, 48)
Bewick's Wren	4.94	132	5.5	44	(34, 60)
Mountain Bluebird	9.66	125	4.9	38	(35, 42)
Townsend's Solitaire	4.92	147	6.8	55	(51, 60)
Hermit Thrush	10.83	137	5.9	61	(56, 66)
American Robin	5.00	119	4.4	41	(39, 43)
American Pipit	9.76	92	2.7	40	(36, 45)
Gray-crowned Rosy-Finch	4.99	135	5.7	45	(40, 51)
Purple Finch	10.09	89	2.5	42	(35, 52)
Cassin's Finch	8.86	89	2.5	40	(37, 44)
Pine Siskin	9.86	61	1.2	28	(24, 34)
Chipping Sparrow	4.60	89	2.5	52	(38, 78)
Fox Sparrow	5.00	123	4.8	42	(39, 45)
Dark-eyed Junco	9.64	71	1.6	29	(28, 30)
White-crowned Sparrow	5.06	163	8.3	50	(47, 54)
Song Sparrow	4.95	117	4.3	48	(42, 56)
Lincoln's Sparrow	5.01	141	6.2	44	(40, 48)
Green-tailed Towhee	5.00	103	3.3	39	(35, 44)
Spotted Towhee	5.83	90	2.5	35	(32, 39)

Table A12-2 (continued). Detection-distance parameters by species in Sequoia and Kings Canyon National Parks and Yosemite National Park, including the percent of recorded distances discarded (D%) from the tail of the observed detection-distance distribution prior to fitting a half-normal density to the data, the maximum detection distance (d_{max}) in the remaining sample, the effective area (Area) over which density was estimated around each point-count station, and the fitted estimate (mean and 95% credible interval) of the shape parameter of the half-normal detection-distance function ($\sigma_{half\text{-}norm}$). The 62 species analyzed across these parks are listed in taxonomic order.

				$\sigma_{half\text{-}norm}$	
Species	**D%**	**d_{max} (m)**	**Area (ha)**	**Mean**	**95% CRI**
Red-winged Blackbird	14.58	116	4.2	124	(69, 308)
Orange-crowned Warbler	6.86	88	2.4	29	(23, 38)
Nashville Warbler	21.65	62	1.2	44	(36, 55)
MacGillivray's Warbler	9.99	75	1.8	34	(31, 38)
Yellow Warbler	9.82	86	2.3	45	(32, 102)
Yellow-rumped Warbler	9.95	77	1.9	36	(33, 38)
Black-throated Gray Warbler	4.85	95	2.8	37	(33, 41)
Hermit Warbler	5.01	92	2.7	36	(33, 39)
Wilson's Warbler	9.98	71	1.6	30	(26, 34)
Western Tanager	10.00	99	3.1	49	(45, 54)
Black-headed Grosbeak	4.95	130	5.3	46	(44, 49)
Lazuli Bunting	11.05	90	2.5	37	(30, 48)

Appendix 13. Breeding Bird Survey trend estimates for species trending in the Sierra Nevada Network

Population growth estimates based on Breeding Bird Survey data are presented in Tables A13-1 (for comparison with species showing negative growth in the current study) and A13-2 (for comparison with species showing positive growth in the current study).

Table A13-1. Independent estimates of population growth based on Breeding Bird Survey (BBS) data, for species with *negative* population growth ($\lambda_G < 1$ in Appendix 5) in the current study of Sequoia and Kings Canyon National Parks (SEKI) and Yosemite National Park (YOSE). BBS data were collected during 2011–2019 (Pardieck et al. 2020) and analyzed here using the smooth "slope" model from R package *bbsBayes* (Edwards and Smith 2021). Population growth metrics are presented here for Bird Conservation Region (BCR) 15, which encompasses SEKI and YOSE, and for the state of California, which encompasses BCR 15. Metrics presented are percent growth and "slope trend" over the focal period, where the latter explicitly integrates growth across 2011–2019, and is most similar to λ_G among the metrics available in *bbsBayes*. The proportion negative in each column indicates agreement between trends estimated from SIEN and BBS datasets.

Species code	Growth in BCR 15 (%)	Trend in BCR 15		Growth in California (%)	Trend in California	
		mean	95% CRI		mean	95% CRI
RBSA	−5.2	−0.664	(−1.677, 0.36)	12.7	1.500	(0.4, 3.285)
WEWP	−13.4	−1.777	(−2.265, −1.252)	−6.4	−0.825	(−1.206, −0.409)
STJA	−3.2	−0.406	(−0.969, 0.084)	0.8	0.099	(−0.179, 0.381)
WREN	−9.0	−1.2	(−2.273, −0.102)	−5.9	−0.8	(−1.158, −0.359)
GCRF	−4.1	−0.521	(−1.565, 0.574)	−3.3	−0.417	(−1.171, 0.328)
PUFI	−11.1	−1.461	(−2.281, −0.627)	−7.6	−0.979	(−1.54, −0.382)
PISI	−21.4	−2.965	(−4.576, −1.249)	−25.5	−3.605	(−4.507, −2.666)
FOSP	−7.9	−1.022	(−1.575, −0.441)	−5.4	−0.690	(−1.235, −0.06)
SPTO	0.2	0.023	(−0.553, 0.604)	0.0	0.004	(−0.25, 0.301)
OCWA	−8.9	−1.156	(−2.268, 0.067)	−4.3	−0.552	(−1.009, −0.026)
Proportion negative	*0.90*	*0.90*	*0.50*	*0.70*	*0.70*	*0.60*

Table A13-2. Independent estimates of population growth based on Breeding Bird Survey (BBS) data, for species with *positive* population growth ($\lambda_G > 1$ in Appendix 5) in the current study of Sequoia and Kings Canyon National Parks (SEKI) and Yosemite National Park (YOSE). BBS data were collected during 2011–2019 and analyzed here using the smooth "slope" model from R package *bbsBayes* (Edwards and Smith 2021). Population growth metrics are presented here for Bird Conservation Region (BCR) 15, which encompasses SEKI and YOSE, and for the state of California, which encompasses BCR 15. Metrics presented are percent growth and "slope trend" over the focal period, where the latter explicitly integrates growth across 2011–2019, and is most similar to λ_G among the metrics available in *bbsBayes*. The proportion positive in each column indicates agreement between trends estimated from SIEN and BBS datasets.

Species code	Growth in BCR 15 (%)	Trend in BCR 15		Growth in California (%)	Trend in California	
		mean	95% CRI		mean	95% CRI
MOUQ	−3.6	−0.461	(−1.473, 0.660)	−3.0	−0.374	(−1.107, 0.417)
HAWO	3.5	0.432	(−0.481, 1.352)	10.0	1.198	(0.628, 1.778)
DUFL	−3.3	−0.421	(−1.350, 0.447)	17.8	2.072	(1.053, 3.433)
CAVI	34.8	3.807	(2.991, 4.615)	23.1	2.628	(2.069, 3.239)
RBNU	2.8	0.345	(−0.384, 1.033)	6.4	0.773	(0.258, 1.293)
HOWR	−3.2	−0.400	(−1.402, 0.598)	1.8	0.229	(−0.341, 0.768)
TOSO	3.5	0.427	(−0.557, 1.479)	30.4	3.378	(2.007, 5.113)
AMRO	−11.8	−1.563	(−1.940, −1.177)	−1.2	−0.156	(−0.378, 0.086)
CAFI	−11.7	−1.545	(−2.718, −0.453)	12.0	1.429	(−0.011, 3.470)
DEJU	−2.9	−0.370	(−1.326, 0.577)	2.0	0.245	(−0.324, 0.789)
LISP	−1.2	−0.152	(−1.863, 1.667)	−1.7	−0.215	(−1.699, 1.396)
GTTO	−1.0	−0.129	(−0.933, 0.679)	5.2	0.638	(−0.424, 1.963)
BTYW	−11.2	−1.472	(−2.414, −0.520)	−6.3	−0.805	(−1.366, −0.239)
LAZB	36.2	3.934	(2.876, 5.006)	3.7	0.458	(−0.078, 1.013)
Proportion positive	*0.36*	*0.36*	*0.14*	*0.71*	*0.71*	*0.36*



Hairy Woodpecker population density during the breeding season appeared to double from 2011 to 2019 in Yosemite National Park. Photo by Doug Greenberg, Flickr, CC BY-NC 2.0.

The Department of the Interior protects and manages the nation's natural resources and cultural heritage; provides scientific and other information about those resources; and honors its special responsibilities to American Indians, Alaska Natives, and affiliated Island Communities.

NPS 963/181584, June 2022



Natural Resource Stewardship and Science
1201 Oakridge Drive, Suite 150
Fort Collins, CO 80525